PhD-FSTC-2015-12
The Faculty of Sciences, Technology and Communication

DISSERTATION

Defense held on 04/03/2015 in Luxembourg

to obtain the degree of

DOCTEUR DE L'UNIVERSITÉ DU LUXEMBOURG

EN *Informatique*

by

Roberto Piazza
Born on 20 April 1986 in Udine, (Italy)

TITLE OF THE DISSERTATION

On-ground Signal Processing Techniques Enabling Efficient Amplification of Multiple Carriers in Satellite Channels

Dissertation defense committee

Prof. Dr. Björn Ottersten, dissertation supervisor
Université du Luxembourg

Prof. Dr. Daniel Rönnow, Deputy Chairman
University of Gävle

Prof. Dr-Ing. Holger Voos, Chairman
Université du Luxembourg

Dr Bhavani Shankar M.R., Member
Université du Luxembourg

Prof. Dr. Alessandro Vanelli-Coralli, Member
University of Bologna

On-ground Signal Processing Techniques Enabling Efficient Amplification of Multiple Carriers in Satellite Channels

Roberto Piazza

January 5, 2015

Abstract

Satellite communication is facing the urgent need of improving data rate and efficiency to compete with the quality of service offered by terrestrial communication systems. An imminent gain, achievable without the need of upgrading current satellite technology, can be obtained by exploiting on-board multiple carrier operation at the transponder and using highly efficient modulation schemes. Sharing the on-board high power amplifier amongst carriers would reduce the flying hardware cost and weight. Further, multiple carrier operation would provide, to the on-ground transmitter, flexibility in the configuration of the parameters of the carriers waveforms. However, on-board multicarrier joint amplification is a critical operation as it brings severe non-linear distortion effects. This distortion becomes even more severe when high spectrally efficient modulation schemes are used. The inherent non-linearity of the amplifier results in an increased Adjacent Channel Interference and peak to average power ratio that degrade power and spectral efficiencies while offsetting other potential benefits. The current baseline configuration for multiple carrier requires to operate the on-board power amplifier in its linear region at the cost of poor on-board power efficiency and reduced output power.

In order to enable efficient on-board multiple carrier joint amplification, countermeasures techniques have to put in place. This Thesis describes several on-ground signal processing techniques that mitigate the interference and enable efficient joint on-board amplification. This includes transmitter techniques, as *Predistortion* and receiver techniques as *Equalization*. Predistortion operates a the transmitter to pre-compensate the liner and nonlinear channel distortion effects and to reduce the resulting receiver interference. We propose several multiple carrier predistortion methods performing joint data processing either based on *Memory Polynomial* or *Look -Up Table*. This includes the derivation advanced parameters estimation methods to provide robustness to receiver noise and improved performance. Further, distributed transmission scenario in which multiple gateway uplink to a single satellite transponder, are investigated and specific tailored predistortion schemes derived. Waveform or *Signal* predistortion is also considered and novel *Crest Factor Reduction* optimization methods devised. End receivers equalization is aimed to compensate the residual channel distortion and to adapt to the fast channel variations. We propose single carrier equalization techniques based on *Symbol* and *Fractionally Spaced Equalization* for multiple carrier satellite channel. Joint equalization of multiple carrier is also considered for professional applications and for the return link.

Acknowledgments

First of all, I would like to thank my supervisor Prof. Ottersten for giving me the opportunity to pursue my PhD with his group. His extraordinary support and guidance helped me facing all the challenges I encountered on the way. Special thanks goes to my co-supervisor Dr. Bhavani Shankar. Working side by side with him on both academic publication and projects was an invaluable experience for me. His contribution to my PhD is only marginally lower then mine. I would like also to thank my other co-supervisor Prof. Daniel Ronnow. In several occasions, he welcomed me at the University of Gavle, where he leads a fantastic group of people working in non-linear systems and related applications. The collaborations with him and his Ph.D. student Efrain Zenteno were fundamental for my research project.

Further, I want to thank all my colleagues and friends here at the SnT. This includes all members of the sigcom group with a special thanks to Dr. Dimitrios Christopoulos for his inspiring motivation and positive attitude. I would like also to thank the administrative team for their professionality and patience. A particular thanks to Isabelle Chesnay for her fundamental support in all the complicated AFR related procedures.

Finally, I want to thank my industrial advisor Frank Zimmer for supporting my relationship with SES TechCom and for his constant interest in my research work. This collaboration was always a reason of great motivation for me.

What is now proved was once only imagined.

WILLIAM BLAKE

Contents

List of Tables

List of Figures

List of Symbols

$\mathbb{E}$	Ensemble average
$()^*$	Hermitian
$()^T$	Transpose
$\mathbf{A}$	Matrices
$\mathbf{A}^\dagger$	Pseudo-inversion
$\mathbf{b}$	Column vectors
$\otimes$	Kronecker Product
$h(*)$	Function
$\mathbf{I}_K$	Identity matrix of dimension K

Acronyms

ACI	Adjacent Channel Interference. 21, 22, 26, 29–31, 39, 41, 49, 68, 107, 156
AGC	Automatic Gain Control. 28
APSK	Amplitude Shift Keying. 30
AWGN	Additive White Gaussian Noise. 30, 49, 140
BER	Bit Error Rate. 49
BGAN	Broadband Global Area Network. 157
CCI	Co-Channel Interference. 19
CFR	Crest Factor Reduction. 38, 74
DPD	Digital Pre-Distortion. 21, 32, 33, 35, 37, 38, 40, 47
DTH	Direct To Home. 19, 27, 39
DVB − S2	second generation standard for Digital Video Broadcasting over Satellite. 25, 27, 40, 46
DVB − S	Digital Video Broadcasting over Satellite. 25
EQ	Equalization. 21, 40
FEC	Forward Error Correction. 158
FIR	Finite Impulse Response. 28, 47
FSE	Fractionally Spaced Equalization. 40, 43
GEO	Geostationary. 109
GW	Gateway. 30, 40, 45, 47, 107, 142
HDTV	High Definition Television. 19
HPA	High Power Amplifier. 20–23, 27, 29, 30, 33–35, 46, 49, 107, 140
IBO	Input Back Off. 28
IMD	Inter Modulation Products. 22, 31, 46, 107
IMUX	Input Multiplexer. 27, 30, 39
IRD	Integrated Receiver Decoder. 19, 27
ISI	Inter-Symbol Interference. 20, 26, 29–31, 33, 39, 49, 68, 159
L − TWTA	Linearized Traveling Wave Tube Amplifier. 28, 46
LASSO	Least Absolute Shrinkage and Selection Operator. 133, 143
LMS	Least Mean Squares. 49
LUT	Look-Up Table. 26, 33–38, 68
MIMO	Multi Input Multi Output. 35
MMSE	Minimum Mean Square Error. 39, 136

MP	Memory Polynomial. 26
OBO	Output Back Off. 22, 29, 46, 49
OMUX	Output Multiplexer. 27, 30, 39
PAPR	Peak to Average Power Ratio. 37, 38, 94
RF	Radio Frequency. 35
RLS	Recursive Least Squares. 49, 65, 137
RRC	Root Raised Cosine. 158
SINR	Signal-to-Interference plus Noise ratio. 22, 69
SNR	Signal-to-Noise ratio. 22
SSPA	Solid State Power Amplifier. 156, 158
TD	Total Degradation. 49
TWTA	Traveling Wave Tube Amplifier. 28, 29, 46
UHDTV	Ultra High Definition Television. 19
UT	User Terminal. 19, 41, 109, 133, 136, 142, 156

Chapter 1

Introduction

1.1 Motivation

Historically, satellite telecommunication systems have been successful in providing wide coverage and connectivity everywhere. In recent years, there is an increasing demand for higher data rates and bandwidth efficiency. Many emerging applications and services are pushing satellite communications to provide higher bandwidth: on one hand we have high data rate broadcasting applications, such as High Definition Television (HDTV) and Ultra High Definition Television (UHDTV); On the other, broadband internet applications for communities and bi-directional professional networks [2]. Further, the fifth generation of wireless system (5G) foresees a possible total integration of satellite and terrestrial networks [3]. A recent example of this trend is Viasat-1 that reaches a total throughput of 140 Gbps being the highest capacity broadcast satellite ever launched [4].

In satellite broadcast systems, the data stream goes from the transmitter to the end receivers through the forward link, where we have, in general, three actors: the gateways, the satellite transponders and the end-receivers. The gateways collect the data and transmit the signal to one or more satellites. Each satellite transponder receives the data signal from one or more gateways and it then redirects the signal to the ground receivers. In widespread Direct To Home (DTH) services, the end receivers are fixed Integrated Receiver Decoder (IRD) for mostly TV applications. Figure 1.1 shows a general satellite communication scenario where different applications are depicted.

Multi-beam satellite systems enable improved spectral efficiency at the expense of increased on board hardware complexity [5]. Instead of having a single beam with a very large coverage, the multi-beam systems have many small beams with a smaller coverage. Each narrow beam provides higher antenna gain and it is capable of delivering higher spectral efficiency to the User Terminal (UT)s. However, each beam requires additional on-board hardware including dedicated filters, power amplifiers and antennas. Ground receivers can suffer Co-Channel Interference (CCI) from adjacent beams due to the overlapping areas at the beam boundary. However, CCI is avoided employing different frequencies in adjacent beams (kindly refer to Fig. 1.2). While different frequencies are assigned to adjacent beams, the same frequencies can be used in not adjacent

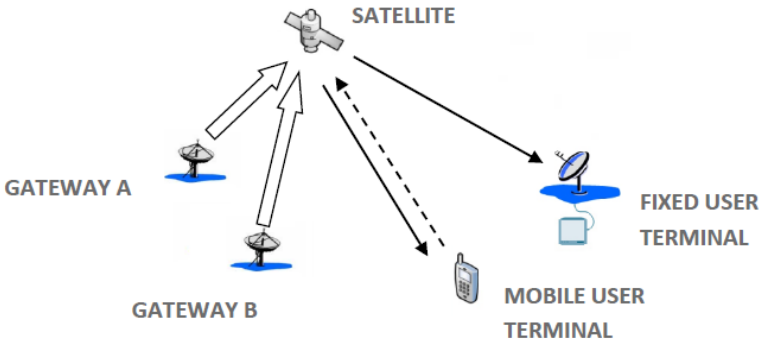

Figure 1.1: General Satellite Communication Scenario

beams.

Current multi beam systems can have as many as 150 beams resulting in high transponder complexity, weight and cost. One possible way forward to enable higher throughput satellite systems, is to improve the efficiency of the on-board hardware usage. This can be achieved by sharing on-board hardware resources. Different carriers can share the same High Power Amplifier (HPA) reducing the total number of required on-board HPAs. Further, sharing the on-board amplifier amongst different carriers allows the on-ground transmitter the flexibility to reconfigure the uplinked multiple carrier signal in terms of number of carriers, carriers spacing and bandwidth.

Transparent payloads, where the uplink data is mainly amplified and forwarded to users, are by far the most common telecom satellite architectures due to their competitive cost and technological flexibility. On the other hand, in regenerative transponders, on-board processing is permitted enabling improved performance at the expense of increased payload cost and complexity, higher power consumption and reduced upgrade capability [5]. In regenerative transponders the uplinked signal is decoded and re-modulated for downlink. In fact, the signal processing carried out on the ground can be updated with technological advancements in the course of the lifetime of the satellite.

To ensure that the on-board amplification is power-efficient, the HPA is operated close to the saturation point. Power saturation , while being a natural effect related to the limited available power, is inherently non-linear. In fact, while in the linear region the output power grows linearly with respect to the input power, close to the saturation region this linear relationship does not hold anymore. Therefore, the on-board HPAs suffer from non-linear effects when driven close to saturation leading to undesired distortion of the amplified signal. Typically, the combination of HPA non-linearity with the on-board channelizing filters, introduces non-linear Inter-Symbol Interference (ISI) [6] and out of band interference.

However, the non-linear effects become even more prominent when multiple carriers are amplified using a single HPA. This leads to spurious terms arising

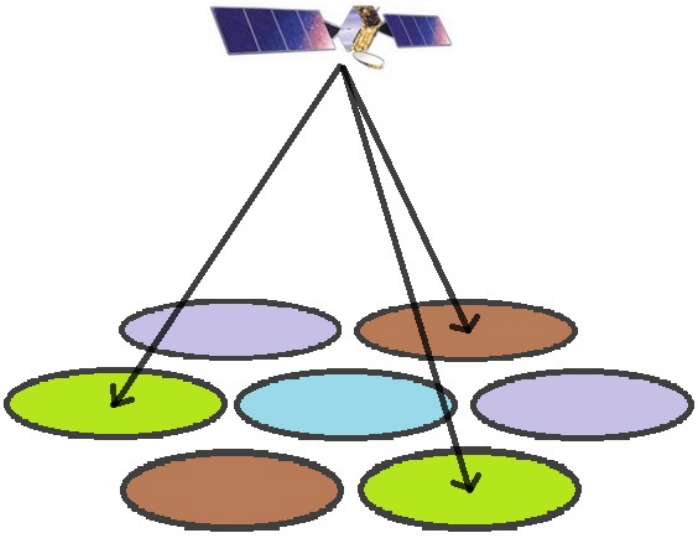

Figure 1.2: Multibeam satellite system representation where each color represents a different carrier frequency

due to the inter-modulation products caused by the HPA non-linearity [1]. A large guard-band between the carriers may be needed in order to avoid inter-modulation products or Adjacent Channel Interference (ACI). Additionally, use of multiple carriers leads to the well-known high peak to average power ratios, and this increases the back-off used in the power amplification, leading to loss in amplification efficiency. These effects are manifested as spectrum-inefficient frequency carrier segregation and power loss depending on the spectral efficiencies of the individual carriers.

An improvement in power and spectral efficiencies warrants the development of *on-ground* mitigation techniques including Digital Pre-Distortion (DPD) at transmitter and Equalization (EQ) at receiver. The goal to enable higher the usage of higher order modulations with efficient code rate, reducing the carrier spacing and increase the efficiency of the on-board amplifier.

1.2 Problem Definition

In this thesis work we focus on the optimization of two fundamental parameters of the satellite communication system: On one hand, we have the transmission spectral efficiency; on the other hand the on-board HPA power efficiency. Spectral efficiency is defined as the ration between the transmitted bit rate and the available transponder bandwidth described by the equation,

$$S_{eff} = \frac{R}{W_T} \tag{1.1}$$

where R is the total transmitted information rate in bit per seconds and W_T is the available transponder bandwidth in Hz. The on-board HPA power efficiency

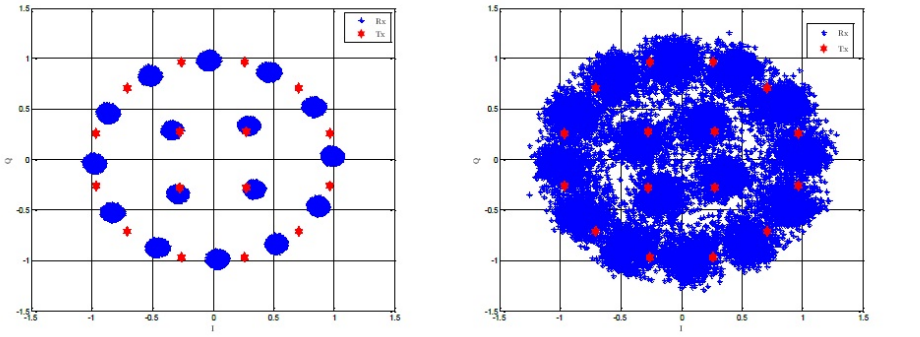

u

Figure 1.3: Scatter plots corresponding to single carrier (left) and multicarrier (right) signals.

is the ratio between the saturation power and the signal output power. This is usually defined in dB as Output Back Off (OBO),

$$OBO = 10\log_{10}(\frac{P_{out}}{P_{sat}}) \tag{1.2}$$

where $P_{sat}$is the nominal amplifier saturation power and P_{out} is the amplified signal power.

It is desirable to maximize the on board power efficiency we have to operate the HPA closer and closer to the saturation where the distortion effects are more prominent. The distortion results are particularly severe when the amplifier is operated in multiple carrier mode due to the generated Inter Modulation Products (IMD) [1] (kindly refer to Fig. 1.3). This determines a tight trade off between power and spectral efficiency.

Spectral efficiency is directly penalized by the generated non-linear interference that reduces the receiver Signal-to-Interference plus Noise ratio (SINR) limiting the applicability of spectrally efficient modulations and codes. Further, high order modulations are inherently penalized due to their higher peak to average power ratio resulting in even higher interference level. When the HPA is operated in multiple carrier mode, and in order to reduce the ACI level, a significant guard band level has to be introduced between the uplinked carriers. These spectral holes further reduce the spectral efficiency with respect to the available transponder bandwidth.

The overall satellite transponder power is only provided by the installed solar panels. This makes on-board power a scarce resource that has to be carefully managed. Further, wasted power transforms in heat that has to be eliminated with sophisticated heat sink technology. On-board power amplifiers have a major impact on the overall satellite power efficiency requiring special attention. More, a low HPA power efficiency corresponds to a lower transmitted power that might not satisfy the required receiver Signal-to-Noise ratio (SNR).

Figure 1.4 shows the SINR trend of a single and multiple carrier transponder with respect to the selected power efficiency. From Fig. 1.4 we observe that the single carrier application can achieve much higher SINR level compared to the multiple carrier case. Further, as discussed above, SINR is in general penalized

by the strong interference level when the HPA is driven close to saturation and again when the amplifier is operated in the linear region due to the reduced output power and the consequent loss in signal to noise ratio.

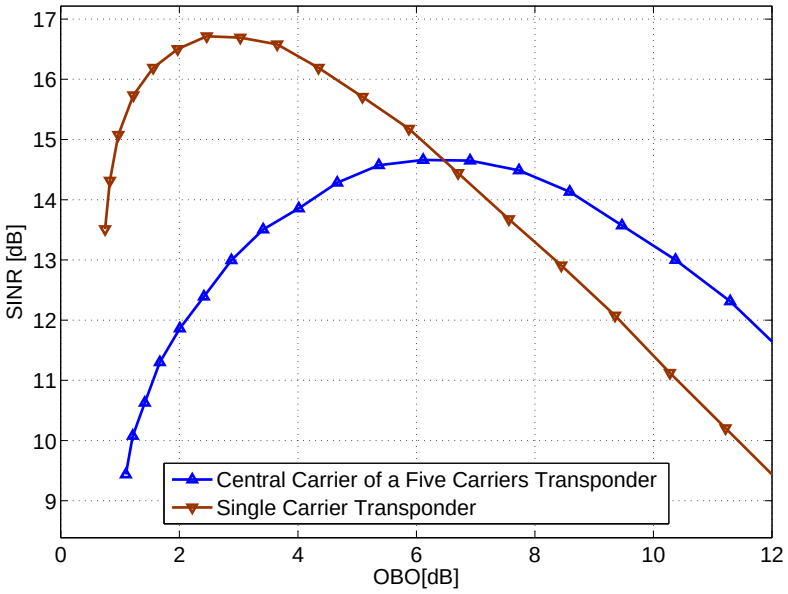

Figure 1.4: Signal to interference plus noise ratio with respect the HPA OBO for the single and multiple carrier transponder.

In conclusion, efficient on-board amplification of multiple carriers results in strong non-linear interference while inefficient power amplification is unacceptable from the system point of view nor from a commutation link budget point of view. Thus, in order to enable efficient on-board multiple carrier amplification, specific counter measures techniques have to be defined.

Counter measures techniques can be implemented on-board the satellite or on-ground. However, transparent satellite transponder technology, where the up-linked signal is mostly filtered and amplified, is by far the most common satellite transponder architecture. In fact, on-board digital processing requires signal down conversion and sampling resulting in higher complexity, higher power requirements and in general decreases the satellite mission life-time. Given these system level constraints we only consider on-ground counter measures techniques namely predistortion at the transmitter and equalization at the receiver.

With predistortion we refer to the class of signal processing transmitter techniques aimed to pre-compensate the channel distortion effects. In order to pre-compensate the channel non-linear effects, predistortion implements an equivalent channel pre-inverse function. This is usually obtained resorting to some non-linear function often including memory effects. On the other hand, as equalization we generally refer to a class of receiver techniques aimed to reconstruct the original transmitted signal eliminating the residual channel distortions.

1.3 Thesis Outline

All the work of this thesis relates to satellite communication and digital signal processing techniques for mitigating channel non-linear distortion.

Chapter 2 In this chapter we provide a detailed overview of the thesis work. The chapter includes the definition of the satellite communication models, the analytic description of the channel distortion and a brief presentation of the proposed countermeasures techniques. In the final part of the chapter we detail the contributions of this Thesis with respect to the state of the art.

Chapter 3 In this chapter we present several on-ground transmitter solutions to counteract the distortion effects of a multiple carrier satellite channel.

Chapter 4 Building on Chapter 3, we provide advanced estimation techniques to improve the performance of the proposed data and signal predistortion.

Chapter 5 As a generalization of the multiple carrier predistortion for single gateway application considered in Chapter 3, we here consider multi-gateway transmission where carriers are independently uplinked toward the same satellite from different gateways. For this distributed scenario, we propose several on-ground transmitter techniques providing a complexity versus performance trade-off.

Chapter 6 In this chapter we consider receiver equalization techniques for the multiple carrier satellite channel.

Chapter 7 This chapter contains final conclusions and describes some directions for future research.

Chapter 2

Distortion Countermeasure Techniques for Multicarrier Satellite Channels

2.1 Introduction

Driven by multimedia applications and other personal services, there has been an increase in the demand for higher data rates by consumers. In addition to enhancing throughput per user, communication systems are also being geared towards providing ubiquitous connectivity. Several societal benefits can be derived from having access to broadband connection [7] and the Digital Agenda drafted by the European Commission aims at providing 50% of the households with a broadband connectivity (over 100 Mbps) by 2020 [3]. Towards meeting the increased capacity and connectivity goals, and thereby serving the agenda in [3], terrestrial communication systems have evolved from first generation networks to the fourth generation (4G) under deployment providing enhanced data, voice and multimedia services to fixed and mobile customers. Like their terrestrial counterparts, satellite systems have seen a number of technological advances to cope with the increased demand [5]. These include changes to the payload architecture and the communication methodology. Transition from single beam to multiple beam systems is evidence of the former. Multibeam systems, similar to the cellular systems, allow for increased capacity through frequency reuse and exhibit flexibility in terms of resource allocation, coverage, connectivity and routing [5]. High throughput satellites have multiple spot beam coverage: recent examples of this trend include Viasat-1 that reaches a total throughput of 134 Gbps [4] and Ka-SAT that provides in excess of 90 Gbps with 82 spot beams [8]. While advanced payload architectures are being sought, a clear strategy towards reducing the mission costs and providing the end users with an economical solution is being pursued by the operators. Further, advances in technology from Digital Video Broadcasting over Satellite ($\mathrm{DVB-S}$) to second generation standard for Digital Video Broadcasting over Satellite ($\mathrm{DVB-S2}$) [9] to the newly formulated DVB-S2x [10], indicate the importance of employing the state-of-the-art transmitter and receiver-based

digital processing techniques to address the traffic growth and remain competitive. The recurring phenomena in these advances has been the constant search for spectrally efficient transmissions; itâĂŹs worth mentioning here that the time frequency packing techniques [11, 12] have been shown to be promising in the multicarrier per transponder scenario.

An application of the use of transmitter and receiver techniques for reducing the mission costs emerges in the context of amplification of multiple satellite carriers using a single on-board amplifier. With the development of wideband amplifiers, joint amplification clearly allows reduction of the payload mass in comparison to the traditional single amplifier per link case. The resulting sharing of satellite real estate among many links reduces the mission cost and also provides a degree of flexibility.

However, efficient amplification is, typically, a non-linear operation and joint amplification leads to spurious inter-modulation products. This coupled with the on-board filtering leads to distortions caused by symbols from other carriers (ACI) or from the same carrier itself (ISI). These distortions can cause severe degradation in the link performance, more so for higher order (spectrally efficient) modulations. In the absence of compensation techniques, either a large guard-band between the carriers is used and/ or the amplifier is operated in a linear region.

The former results in an inefficient frequency carrier segregation, while the latter translates into a power efficiency loss compared to single carrier operations depending on the spectral efficiencies of the individual carriers. Towards exploiting benefits of joint amplification in full, several studies have been recently pursued towards development of mitigation techniques. These techniques would be implemented on ground so as to provide the up-gradation flexibility while keeping the payload intact. The techniques at the transmitter is termed as Pre-distortion while those at the receiver are known as Equalization in literature.

Mitigation techniques based on Volterra series [13], [14] or look-up tables (LUT) [6] have been proposed in satellite literature and the resulting gains are promising [6, 15]. Further, literature on terrestrial systems describes a variety of mitigation algorithms based on memory polynomials [16], orthogonal polynomials [17, 18] and Look-Up Table (LUT) [19] for single carrier operations. However, these methods are not suited for the multicarrier scenario since they do not cater to ACI reduction.

Volterra analysis for non-linear satellite channels is developed for two carriers in [20] and extended to multiple carriers in [1]. Different joint data equalization schemes based on Volterra series are then pursued. However, due to compatibility issues, complexity considerations and access restrictions to data on different carriers, the receiver can demodulate only its intended carrier, thereby ruling out joint equalization. On the contrary, the gateway has access to data on all carriers, allowing the implementation of a joint predistortion technique to precompensate for ACI and ISI. A dual carrier channel signal predistortion based on Memory Polynomial (MP) [16] is provided in [21] for terrestrial application.

This chapter will describe the multicarrier scenario and the related non-linear impairments. Further, a brief overview on the developed countermeasures techniques is provided.

2.2 Joint Amplification of Multiple Carriers

The scenario envisaged includes a gateway uplinking many carriers that are amplified by a single on-board HPA. To make the scenario concrete, each carrier can be considered similar to the well-known DVB − S2 waveform in the standard Ka-band [5]; for e.g., each could represent a time division multiplexed carrier carrying broadband data content. Driven by their commercial attractiveness, we consider transparent satellites in the current application. Such satellites receive the data signal from one or more gateways and then redirect it to the ground receivers after requisite frequency translation and amplification. In widespread DTH services, the end receivers are generally IRD. Typically, these receivers decode only a particular carrier: this stems from complexity considerations and access restrictions. In the short-to-medium term perspective, an attractive strategy would be the continued use of such receivers capable of decoding single carrier. Further, as will be detailed later, effective compensation techniques need to process the carriers jointly. These warrant that bulk of the mitigation takes place at the gateway. Thus multicarrier pre-distortion would take a central theme and can be construed as heralding âĂIJcooperationâĂİ among different links âĂIJfor common goodâĂİ. On the other hand, single carrier equalization techniques are put in place to mitigate residual non-linearities arising out of non-ideal transmitter compensation and variations in transponder characteristics due to ageing and thermal effects. In line with the motivation for single carrier receivers, the complexity of the equalization schemes are kept at a minimum. Central to the design of such a system is to model the underlying channel and associated distortions, a task that will be pursued next.

2.2.1 Composite Model of a Satellite Channel

The typical satellite transponder model of the path between the transmitter and the receiver in a transparent satellite communication is shown in Figure 2.1. The involved entities are the

- Input Multiplexer (IMUX) filter
- HPA
- Output Multiplexer (OMUX) filter

To focus on the distortions caused by these components, we assume that other components (like frequency translators) do not induce any loss. Finally, we assume that the link from the gateway to the satellite is ideal.

IMUX and OMUX filters

IMUX filters are used to reject out-of-band signals and noise from entering the satellite (feeder) uplink chain. On the other hand, the OMUX filter eliminates the out-of-band spectra caused by the HPA non-linear amplification. It should be noted that these filters have a relatively low insertion loss. The typical amplitude and group delay response of the IMUX/ OMUX filters are depicted in Figure 2.2 and extracted from [9]. While the pass-band gain is nearly constant, there can be appreciable variations in the group delay at the edge of the bands. These analogue wideband filters are approximated as Finite Impulse Response (FIR) filters.

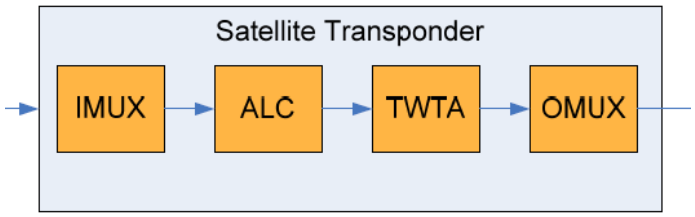

Figure 2.1: A Simplified Satellite Transponder Architecture

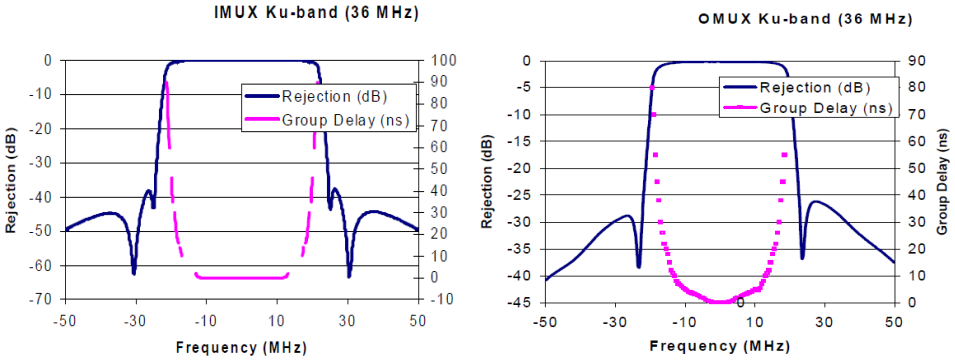

Figure 2.2: Typical input (left figure) and output (right figure) MUX filters response

High Power Amplifiers

The on-board amplifiers are usually implemented as Traveling Wave Tube Amplifier (TWTA). Tube wave amplifiers are wideband amplifier whose response can be assumed to be static (memory-less) with good approximation [22]. Commonly, the baseband amplifier response is static and defined by means of two AM/AM and AM/PM characteristics. The AM/AM function relates the input signal amplitude ρ with the output signal amplitude $A(\rho)$, while the AM/PM responses defines the amplifier phase response as a function of the input signal amplitude as $\theta_{out} = \theta + \phi(\rho)$, where θ is the input signal phase. Typical characteristic of a TWTA amplifier, extracted from [9], is shown in Fig. 2.3 together with a linearized version of the same (Linearized Traveling Wave Tube Amplifier (L – TWTA)).

The Automatic Gain Control (AGC) block amplifies the input signal accordingly to the set input back off (IBO). Further, the Input Back Off (IBO) is defined as $IBO = -10\log\left(\frac{<|v_{in}(t)|^2>}{P_{sat}^{in}}\right)$, where $< |v_{in}(t)|^2 >$ is the average input power to the amplifier and P_{sat}^{in} is the input power corresponding to the amplifier saturation point (for other amplifier technologies this can correspond to the -1 dB compression point). Similarly the OBO is defined as

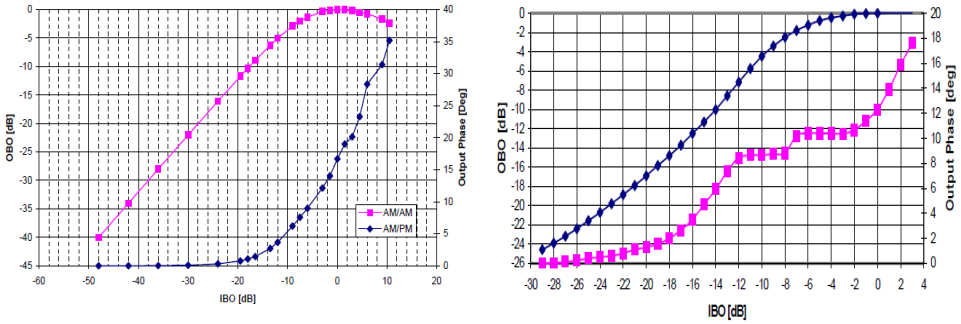

Figure 2.3: A Typical Traveling Tube Wave Amplifier Characteristic (left figure) and Linearized -TWTA response (right figure)

$OBO = -10\log\left(\frac{<|v_{out}(t)|^2>}{P_{sat}^{out}}\right)$, with $|v_{out}(t)|^2$ being the average output power of the amplifier and P_{sat}^{out} is the saturation output power.

A well-known mathematical model for TWTA is the Saleh model [23]. Under this model, an input signal with an amplitude ρ and phase θ results in HPA output, $A(\rho)e^{j(\theta+\phi(\rho))}$. Here $A(\rho)$ determines the AM/ AM characteristic while $\phi(\rho)$ denotes the AM/ PM characteristic as,

$$A(\rho) = \frac{\alpha_a \rho}{\beta_a \rho^2 + 1} \tag{2.1}$$
$$\phi(\rho) = \frac{\alpha_p \rho^2}{\beta_p \rho^2 + 1}$$

where $\alpha_a, \alpha_p, \beta_a, \beta_p$ are the model parameters.

2.3 Non-linear Interference and Modelling

The transponder of Fig. 2.1 with the characteristics presented above, can be abstracted as a non-linear channel with memory; HPA is the cause of non-linearity and the filters contribute to the memory. Such a channel leads to the following distortions [22]:

- Constellation Warping caused by memoryless non-linearity;
- Clustering caused by ISI: First order ISI is due to linear memory while higher order due to non-linearity coupled with the filters. It should be noted that ISI does not arise from adjacent carriers;
- Clustering caused by ACI due to non-linearity;

Figure 2.4 depicts a multicarrier satellite channel block diagram. Referring to Fig. 2.4, a Gateway (GW) is uplinking M independent carriers. The modulated symbol $u_m(n)$ is relative to the mth carrier and is draw from an Amplitude Shift Keying (APSK) modulation scheme [9]. In a typical mutlicarrier scenario [1],

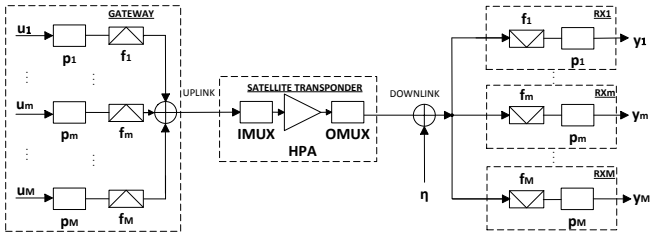

Figure 2.4: Multicarrier Non-linear Satellite Channel Model

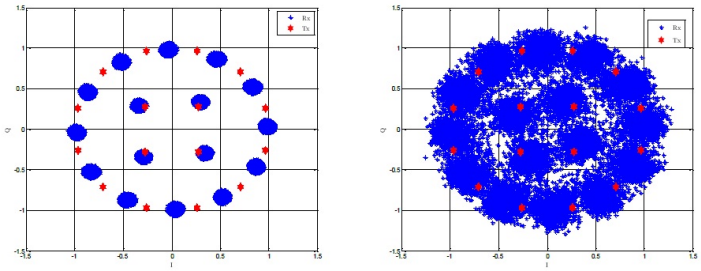

Figure 2.5: Scatter plots corresponding to Single carrier (left) and Multicarrier (right) signals

the carrier are equally spaced in frequency of Δf. The channel includes a wideband satellite transponder that hosts all the uplinked carriers. In particular the multicarrier signal is jointly filtered by a wide band IMUX filter, amplified by the on-board HPA and output filtered by the OMUX filter. The uplink channel is assumed to be ideal and noiseless while the downlink is Additive White Gaussian Noise (AWGN).

Such a satellite channel can be modeled as a *non-linear system with memory* leading to constellation warping, ISI and ACI. Strong non-linear adjacent channel interference is generated by the intermodulation products relative to the different carriers. The effects of this, are depicted in Figure 2.5 where the scatter plot of the received 16 APSK symbols on the central carrier of a three carrier system is presented (on the right). The corresponding effect for the single carrier is also shown (on the left) to highlight the dominant effect of ACI.

2.3.1 Volterra Analysis

In order to investigate the nature of the non-linear distortion of the satellite channel we consider Volterra theory [24] to model the channel. Baseband Volterra analysis for multiple carrier satellite channel is provided in [1].

In Fig 2.4, the mth modulated carrier stream, u_m is pulse shaped, upconverted to a center frequency f_m and uplinked to the satellite transponder. The

composite signal at the input of the satellite transponder is

$$s(t) = \sum_m \sum_n u_m(n) p_m(t - nT_s - \epsilon_m T_s) e^{j(2\pi f_m t + \phi_m)}, \tag{2.2}$$

where $u_m(n)$ is the nth symbol uplinked by the mth carrier, $p_m(\cdot)$ is the pulse shaping function, T_s is the symbol period, ϵ_m is the delay relevant to the mth carrier, f_m denotes the uplink center frequency of the mth carrier and ϕ_m the corresponding phase. The carriers are assumed to have similar baudrates R_s and roll-off ρ while being equally spaced in frequency with a separation of $\Delta f = R_s(1 + \rho)$.

We can express the sampled received symbols for the mth carrier at the nth sampling instance by means of the baseband Volterra discrete model [1] here limited to the third polynomial degree for convenience,

$$\begin{aligned} y_m(n) = & \sum_p \sum_{k=0}^{K_1} h^{(1)}_{p,m}(k) u_p(n-k) + \\ & \sum_{(p_1,p_2,p_3)\in\Omega_{m,3}} \sum_{k_1,k_2,k_3=0}^{K_3} h^{(3)}_{p_1,p_2,p_3,m}(k_1,k_2,k_3) u_{p_1}(n-k_1), \\ & u_{p_2}(n-k_2) u_{p_3}(n-k_3)^* e^{j2\pi(f_{p_1}+f_{p_2}-f_{p_3}-f_m)nT_s} + \eta_m(n). \end{aligned} \tag{2.3}$$

$\{h^{(p)}_*(\cdot)\}$ are the pth order Volterra kernel coefficients, $u_p(n)$ is the transmitted symbol on carrier p at time n and $\eta_m(n)$ is the receiver noise on carrier m at nth instance and $\Omega_{m,d}$ is the set of considered inter-modulation products for the d th degree and the mth carrier. In (5.3), we can identify in-band distortion terms as those intermodulation terms for which it holds $f_{m_1} + f_{m_2} - f_{m_3} - f_m = 0$ [1]. Those include the total in-band ACI and ISI. Referring to (5.3), we can identify as the strictly ISI terms as those elements for which $m_1 = m_2 = m_3 = m$. Table 2.1 provides the third degree frequency-centered IMD $\Omega_{m,3}$ derived in [1] for the three and five carriers scenarios, respectively. Often, for complexity reason, when modeling a multi-carrier satellite channel, only the in-band distortion terms are considered. However, not centered frequency inter-modulation terms can also be considered as they are showed to significantly contribute to the accuracy of the model [1].

2.3.2 Counter measures

It is clear from the earlier discussions that linear and non-linear interference needs to be mitigated to have any meaningful communication. The focus here is on a transparent analogue payload and hence the on-board processing is ruled out. Thus, on-ground techniques are considered at the transmitter and the receiver. The counter measures include a multiple carrier predistorter at the gateway and a single carrier equalizer at the user terminal. The various counter measures will now be briefly presented and then detailed in the following chapters.

Table 2.1: Frequency Centered IMD [1]: (a) Three Carrier Channel In-band Terms, (b) Five Carriers Channel In-band Terms

(A)

$\Omega_{1,3}$	$\Omega_{2,3}$	$\Omega_{3,3}$
[111]	[121]	[131]
[122]	[132]	[221]
[133]	[222]	[232]
[223]	[233]	[333]

(B)

$\Omega_{1,3}$	$\Omega_{2,3}$	$\Omega_{3,3}$	$\Omega_{4,3}$	$\Omega_{5,3}$
[111]	[121]	[131]	[141]	[151]
[122]	[132]	[142]	[152]	[241]
[133]	[143]	[153]	[231]	[252]
[144]	[154]	[221]	[242]	[331]
[155]	[222]	[232]	[253]	[342]
[223]	[233]	[243]	[332]	[353]
[234]	[244]	[254]	[343]	[443]
[245]	[255]	[333]	[354]	[454]
[335]	[334]	[344]	[444]	[555]
[-]	[345]	[355]	[455]	[-]
[-]	[-]	[445]	[-]	[-]

2.4 Multiple Carrier Predistortion

In this section we present the most relevant state of the art for predistortion in multiple carrier applications. Further, the related specific contributions of this thesis are briefly described.

Pre-distortion techniques can be historically classified based on a number of criteria. They include:

- Analogue and Digital Pre-distortion: This classification is based on the domain of the input signal to the predistorter and the underlying implementation (either analog or in the digital domain [22]).
- Signal and Data Pre-distortion: Signal pre-distortion involves applying DPD to the baseband signal after pulse shaping [16,25]. Data pre-distortion, as the name suggests, will operate on the constellation symbols prior to any pulse shaping [6, 19];
- Model based [26, 27] and Look-up-Table based [6, 28] pre-distortion: The model based pre-distortion techniques describe the predistorter as a mathematical function of the input signal;

Further, regarding specifically satellite communication, we also have to distinguish *on-ground* and *on-board* processing [22].

In the following section we summarize Signal and Data Pre-distortion and Model based and Look-Up Table based Predistortion. Each topic is introduced recalling the fundamental state of the art and than followed by a summary of the corresponding main thesis contributions.

In this thesis work we mostly focus on digital data predistortion for multicarrier satellite channels. A broad plethora of multiple carrier techniques for

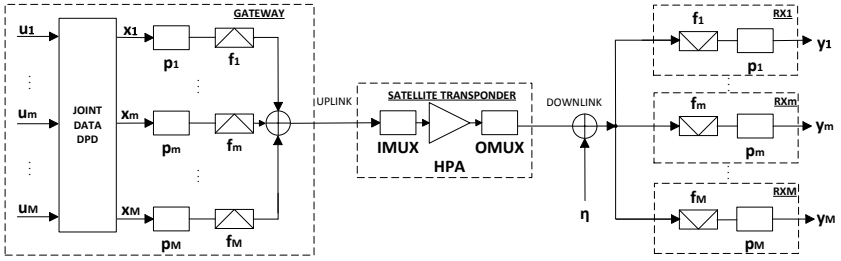

Figure 2.6: Block Diagram of Data Predistortion.

predistortion is provided in Chapter 3. This includes several model based and look-up table based data predistortion techniques [29–32]. In section 4.2, we propose advanced estimation and clipping techniques for multiple carrier signal predistortion. Multicarrier predistortion is also considered in Chapter 5 for a distributed scenario where multiple gateway share a single transponder HPA [33].

2.4.1 State of The Art

Data Predistortion

As discussed earlier, the data pre-distorter operates on the baseband data symbols and is depicted in Figure 2.6. It modifies the transmitted constellation in such a way that, after linear filtering and non-linear processing in the downlink, the average of the received samples at the detector would match the desired signal constellation [22].

While single carrier data DPD is explored in literature [6, 19], multicarrier data DPD has not been considered in the literature before. In general, single carrier data predistortion aims to reduce the warping and clustering effects on the received constellation symbols. Warping is directly related to the static non-linear distortion of the HPA, while clustering is the result of ISI. Data predistortion is defined as a non-linear map, with or without memory that relates a sequence of channel input symbols to a predistorted symbol as,

$$x(n) = f(u(n), \cdots, u(n-K)) \tag{2.4}$$

where u(n) is the nth channel intended input symbol, K is the predistorter memory and $x(n)$ is the predistorted symbol input to the channel.

The identification and implementation of the map $f(\cdot)$ is key to the predistortion performance. In particular, [6] proposes two on-ground predistortion schemes for non-linear satellite channels, namely *static* and *dynamic* predistortion. *Static* predistortion is designed to compensate only for warping effects while dynamic predistoriton includes memory and compensates for clustering as well. Both approaches are LUT-based and parameters estimation is implemented usign a iterative numerical method [19].

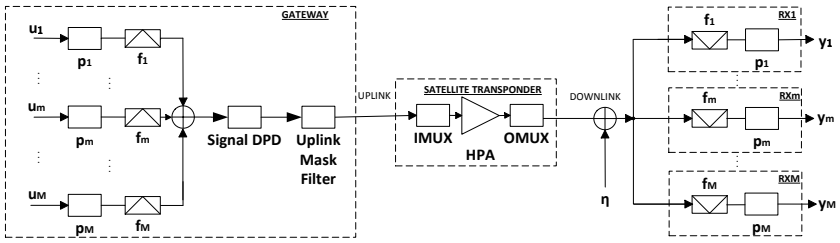

Figure 2.7: Block Diagram of Signal Predistortion.

Signal Predistortion

Signal (or waveform) pre-distorter generates a signal that compensates for the non-linearities introduced by the RF module without accessing the underlying original data symbol sequence.

Traditional signal predistortion operates on the signal after pulse shaping, and it is equivalently applyed to single or multiple carriers signals as depicted in Figure 2.7. Several works on signal pre-distortion are available in literature and include, for e.g., [16, 18, 26] and more recently [17, 25, 34–36].

Since signal pre-distortion can operate on the multicarrier signal, it is has the advantage that it can be used to generate signals with higher bandwidths. Referring to (2.2) and Figure 2.7, signal predistortion operates on the multicarrier basedband signal $s(t)$ as,

$$z(nT_o) = f(s(nT_o), s((n-1)T_o), \cdots, s((n-K)T_o)) \tag{2.5}$$

where f is the non-linear function, $s(nT_o)$ is the sampled original multicarrier baseband signal, T_o is the oversampling period and K is the memory depth. Notice that in general f can be either a model based function, such as a polynomials, or a LUT based function. For implementation reasons, the latter approach is common when memory can be neglected ($K = 0$).

A HPA that is described by a p^{th} order non-linearity, will need a pre-distorted signal with bandwidth p times the signal bandwidth. Further, the design of the signal predistorter is agnostic to the number of carriers as it operates on the superposed signal. While signal pre-distortion offers various advantages, it has the following system level implications

- (1) The bandwidth of the uplinked signal is no longer similar to the âĂIJunpre-distortedâĂİ signal. This suggests violation of the stringent requirements on the uplink unless additional processing is implemented. This could be simply achieved by applying an uplink mask filter after predistortion as showed in Fig. 2.7;

- (2) The computations are performed on the superposed signal. At first, the bandwidth of such a signal is more than that of the constituent single carrier system. Further, such a signal is typically oversampled. Hence the processing (including Digital-to-Analog converters) is performed at a rate many times larger than the symbol rate. As an example, if there are 3

closely spaced carriers, each of bandwidth 40 MHz, and the superposed signal is oversampled 10 times (say), then the processing needs to be performed at 1.2 GHz, while data DPD works at 40 MHz

Several signal pre-distortion studies have been performed towards overcoming the aforesaid shortcomings in the multicarrier scenario [21, 37]. HPAs operated in concurrent dual band mode are now being introduced in terrestrial telecommunication. In this case two or more RF signals are amplified by the HPA simultaneously; the frequency separation is in this case large compared to the signal bandwidth. Two or more baseband signals are up-converted to Radio Frequency (RF). DPD of concurrent band HPAs were reported in [37] where memory polynomials were used. An important difference to single carrier DPD is that cross-talk terms must be included in the DPD algorithm. A similar algorithm has also been used for DPD of Multi Input Multi Output (MIMO) transmitters with cross talk effects [21]. Parameter efficient algorithms like separable functions and orthonormal basis functions have not been formulated for multiple carriers, to the best of our knowledge.

Similarly to the block diagram presented in Fig. 2.7, in [25] and [36], an additional bandpass filtering is performed after the DPD to satisfy the mask. However, with such modified architectures or additional processing, the advantages of the signal pre-distortion can be curtailed with its optimality possibly compromised.

Model Based DPD

Digital predistortion algorithms are commonly separated into model based algorithms and look-up-table based ones [22]. This subdivision applies to both data and signal predistortion approaches. Model based predistortion is based on non linear functions, usually polynomials, whose coefficients have to be determined. On the other hand, LUT -based predistortion implements a complete map between the input and the predistorter output that has to be fully determined.

In model based algorithms for signal predistortion, the non-linear dynamic transfer function of the HPA (or non-linear channels) is derived. The derivation can be made by determining the systemâĂŹs non-linear dynamic transfer function and then inverting it, using the p^{th} order inverse theory. A non-linear dynamic system with memory can be described using a Volterra model; a systemâĂŹs inverse is also a non-linear dynamic system and can, therefore be described by a Volterra model. Thus, a Volterra model is a natural choice for a DPD [24, 26]. However, the Volterra series converges slowly, and hence in practice various reduced Volterra models are used; these include memory polynomial based predistorters [16, 27], generalized memory polynomials [38] and orthogonal polynomial based predistorters [18]. Other model based DPD algorithms âĂŞ with properties as the Volterra series âĂŞ have been formulated using orthonormal basis functions [17].

Identification of Model Parameters

Central to the performance of the given predistorter model is the ability to estimate the coefficients with high fidelity [39]. Estimation of model coefficients relies on training. Training for the predistorter coefficients requires feedback

from at least one receiver. This can be obtained either from a high fidelity simulation or during on-line operation. The feedback signal is used in combination with the corresponding transmitted signal to identify the predistorter as channel inverse function. There are two main approaches to train the predistorter coefficient: using indirect [26, 27] or direct learning [40].

The well-known indirect estimation of the parameters leads to a post-channel inverse function as predistorter [16]. This method is based on the fundamental p^{th} order theorem that states that the post inverse and pre inverse of a non-linear dynamic system are identical and that the non-linear order (p) of the systemâĂŹs inverse is the same as the non-linear order of the system itself. The post inverse estimation problem can be solved resorting to standard least squares techniques without requiring adaptive closed loop processing [16, 39].

On the other hand, direct learning follows a different approach in which the predistorter coefficients are estimated iteratively toward directly reducing the receiver interference [40]. The optimization method implements a least squares minimization of the receiver signal error and it requires complex partial derivatives and the estimation of the channel parameters. This approach results in higher complexity but with improved performance compared to the indirect one especially in presence of receiver noise [39].

However, direct learning as proposed in [40] cannot be applied to multiple carrier systems calling for a novel formulation to be derived. In this thesis we propose optimization methods for estimating the predistorter coefficients for multicarrier satellite systems [41]. Further, our optimization method devised in [41] is general and can also be used to generate a Look-Up Table (LUT) based multicarrier predistortion solution [32].

Look Up Table based DPD

Unlike model based techniques, LUT- based solutions do not require any complex processing to compute the pre-distorted symbols on-line. This enhances the attractiveness of LUT based pre-distortion in real time applications.

LUT based signal predistortion is very common in practical applications due to its low on-line processing complexity that allows wideband processing seamlessly. In most applications, LUT based signal predistortion is implemented as a memoryless non-linear function [28], often combined with a separate linear filtering operation to partially compensate memory effects [42] while still keeping the complexity low. More complex solutions include directly the memory effects in the LUT resulting in larger multidimensional tables [43, 44].

Regarding LUT-based data predistortion, for each nominal constellation point, a pre-distorted one is determined, that gives the nominal one, after the non-linear channel. Single carrier LUT pre-distortion has been well studied in literature. In [19], LUT is computed iteratively by a numerical method that requires lengthy closed loop operation.

2.4.2 Problems Addressed In the Thesis

Multiple Carrier Model-based Data DPD

Multiple carrier data predistortion can be constructed as a coding technique, wherein dependency between different symbols are introduced. However, unlike

traditional coding, input and output symbols are not from the same constellation and the symbol rate is unchanged.

While the distortion depends on the multicarrier signal, obtained by superposing the different carriers, data DPD works on a stream by stream basis as

$$x_m(n) = f_m(\mathbf{u}_1, \cdots, \mathbf{u}_M) \tag{2.6}$$

where f_m is the non-linear data predistortion function relative to the mth carrier, $\mathbf{u}_m = [u_m(n), \cdots, u_m(n-K)]^T$, and $u_m(n)$ is the nth intended transmitted symbols for the mth carrier, and K the predistorter function memory depth.

Further, the presence of the pulse shaper tends to constrain the flexibility of data DPD and hints at a non-ideal positioning of the data predistorter. This shortcoming is more than offset by the two features of the data DPD:

- (1) The operations are performed prior to pulse shaping filter and there is no bandwidth expansion compared to the no DPD case. Hence the spectrum of the pre-distorted signal meets the regulations imposed on the uplink without additional processing.
- (2) The computations are performed at the symbol rate allowing for the use of existing technology. This can be implemented either with on line model based processing (i.e. complex polynomial functions) or using efficient LUT.

In this thesis we propose several on-ground techniques for single gateway multiple carrier data predistortion. These contributions are presented in chapter 3. Our first work on multiple carrier data predistortion is [29] where joint data pre-distortion based on memory polynomials is considered. Performance of the designed DPD is studied under different channel configurations with the results being reported in [30]. Using an approach similar to [29], in [31] we propose orthogonal basis function for reduced complexity multicarrier pre-distortion.

Further, concerning the identification of parameters for multiple carrier predistortion, in this thesis we propose a novel optimization method based on the direct learning approach for estimating the predistorter coefficients for multicarrier satellite systems [41]. The method relies on the multiple carrier polynomials model for proposed in [1,29] and builds on the direct learning algorithms of [40]. This contribution is presented in section 4.1.

Finally, building on the devised multiple carrier techniques, we proposed novel distributed predistortion methods for multiple gateway applications to enable on-board efficient multiple carrier operation. This contribution includes the analytical derivation of the distributed predistortion models, derivation of robust customized parameters estimation methods and the evaluation of synchronization non-idealities related to the distributed nature of the problem. This contribution is presented in 5.

Advanced Signal Predistortion

Very large Peak to Average Power Ratio (PAPR) values, typical of multicarrier signals, force a substantial component of the signal input distribution beyond the amplifier saturation point. This effect introduces unwantced strong distortion that cannot be compensated with predistortion. Toward mitigating distortion effects, several PAPR reduction methods have been proposed for multicarrier

systems [45]. Amongst all, clipping and filtering can provide significant PAPR reduction with minor interference generation (clipping noise) [46]. Clipping of the signal is in general referred as Crest Factor Reduction (CFR). Further, the combination of PAPR reduction and signal predistortion has also been widely considered in literature. Several works propose a scheme in which PAPR reduction precedes predistortion [47, 48], while in [49] it is proposed a scheme where predistortion is followed by PAPR reduction. A different approach was recently proposed in [50], that presents a method to include PAPR control as a constraint in the estimation of the predistortion parameters.

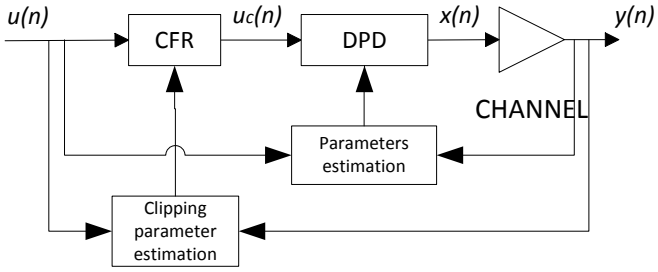

Figure 2.8: Combined Optimization Function Block Diagram

Figure 2.8 depicts the considered transmitter block diagram including the two iterative optimization processes. In this thesis, we propose a transmitter architecture in which the CFR block precedes the DPD block and we derive novel optimization algorithms to determine the optimal CFR and predistortion parameters toward reducing the interference at the receiver [51]. This contribution is presented in chapter 4.2.

Multiple Carrier Look-Up Table based DPD

In [52] we propose single carrier data predistortion for satellite channels in which the computation of table entries based on an ad hoc numerical technique for channel inversion. Notice that a LUT dealing with a K- ary constellation and a channel memory of L leads to a K^L sized table. This work is presented in the Appendix.

In [32] we propose a LUT for multicarrier operations focusing only on memoryless systems (kindly refer to section 3.3). Unlike the iterative approach in single carrier case, an analytical approach is pursued to estimate the entries of this table. An interesting aspect of this study is that it exploits non-linear channel modeling to generate a LUT. Further, the models induce symmetry which are further exploited to reduce the complexity. This becomes essential, since even without channel memory, a K-ary constellation on each of the M carriers leads to a M^K sized table. The table becomes even larger when memory is considered resulting in a M^{KL} entries table, where L is the double-side memory depth. Performance of the LUT is better compared to model based predistorters for lower number of carriers, while the gains are diminished for higher number

of carriers. This can be attributed to the enlarged size of the LUT which poses issues with its generation.

2.5 Equalization: State of the Art and Thesis Contribution

Since a pre-distortion technique cannot compensate the non-linearity perfectly, the residual uncompensated distortions warrant receiver processing, or equalization, for further performance improvement. There exist a rich literature on equalization of single carrier transmissions [22]; these include the optimal and various sub-optimal architectures, linear and non-linear structures, receivers based on the turbo principle and those working on a higher sampling rate. The receivers could also be training based or blind. Recent papers [14], [53] deal with detection techniques for non-linear channels. Further, for professional application or for return channel application, we consider multicarrier receiver equalization. Multicarrier receiver equalization for non-linear satellite channel was first proposed in [1, 20] using a Turbo Volterra architecture to iteratively cancel the channel ISI and ACI at the receiver.

2.5.1 Symbol And Fractionally Spaced Equalization

Low complexity single carrier receivers are by far the most suitable solution for common commercial DTH receivers. The input to the equalizer is typically sampled at the symbol rate and linearly processed to minimize the receiver mean square error (Minimum Mean Square Error (MMSE) equalization). Such an architecture is optimal when the signal encounters constant group-delay. However, it is well known that such receivers are not optimal when the signal path encounters filters with non-constant group delay [54, 55]. The representative characteristics of IMUX/ OMUX filters illustrated in Figure 2.2 indicate the varying group delay near the band edges. Towards enhancing the spectral efficiency, carrier rate optimizations are undertaken to fully utilize the transponder bandwidth. In such scenarios, non-constant group delay affects transmitted waveform resulting in sub-optimal sampling instance that can have an impact on performance. Further, acquiring accurate timing information can be cumbersome is such systems due to residual distortions (even after application of pre-distortion). Incorrect sampling can result in large performance penalties. While the optimal sampling instance in a controlled simulation environment can be easily obtained, it may not be the case in real time implementation.

A symbol synchronous equalizer, while being simple to implement, may not necessarily provide for the optimal linear filter [54]. Towards improving the performance, receivers working at a rate higher than the symbol rate have been considered. Such receivers, referred to as the Fractionally Spaced Equalization (FSE), are shown to provide enhanced performance by effectively compensating for the group delay distortions [54] (kindly refer to Fig. 2.9). In particular, when having sufficient taps, an FSE can be considered as implementing an analogue filter that is insensitive to timing offsets. The use of an FSE in satellites was initially considered in [55] for use on transmit and receive links. The FSE structure was linear and it was shown to reduce the effect of group delay on both the links. In [56], the use of FSE in non-linear satellite channels with a

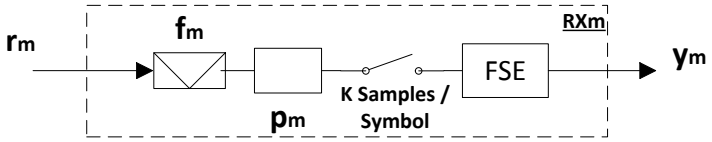

Figure 2.9: General Fractionally Spaced Equalizer Block Diagram

single carrier has been considered. In particular, [56] proposed an architecture comprising a FSE followed by a non-linear Volterra equalizer. Adaptation of FSE and Volterra equalizers were provided. Such a receiver was shown to perform better than symbol spaced equalizers because of its ability to emulate the optimal receiver filter-bank. Use of fractionally spaced equalizer (referred to as enhanced receiver) has been considered to maximize the spectral efficiency in the context of time frequency packing applied to the next generation DVB − S2 systems [57].

In this thesis we investigate both symbol spaced [29, 30] and fractionally spaced [58] single carrier equalization for multicarrier satellite channel. Further, we propose advanced de-mapping techniques to improve the receiver decoding performance [58].

2.5.2 Multicarrier Equalization

In common broadcast application systems the GW has access to all carriers while the user terminal can decode only one carrier. This scenario allows joint processing of all carriers at the GW which enables multicarrier DPD [29] for interference mitigation. However, in other scenarios, such as professional applications or return link, joint processing of all carriers can still be envisaged enabling the use of multicarrier EQ techniques as described in [1, 20] (kindly refer to Fig. 2.10).

Multicarrier equalization for non-linear satellite channels was first introduced in [20] for a dual carrier channel. In [20] the authors design and compare two different kinds of equalization techniques: A Volterra equalizer implementing the channel inverse function and a interference canceler based on the channel function identification. Results show that the interference canceler slightly outperform the multicarrier equalization approach. In [1] the interference cancellation method is further extended to a Turbo Volterra architecture designed for a general arbitrary number of carriers.

In this thesis we consider two different scenarios where joint equalization is applicable: on one hand, we have a multicarrier forward link for professional applications where the UT is decoding all the carriers; on the other, we consider a multicarrier return link application where all the carriers are jointly decoded by the receiving gateway.

In the first scenario we propose a data-level low complexity multicarrier equalization for non-linear satellite channels [59]. Complexity reduction is ob-

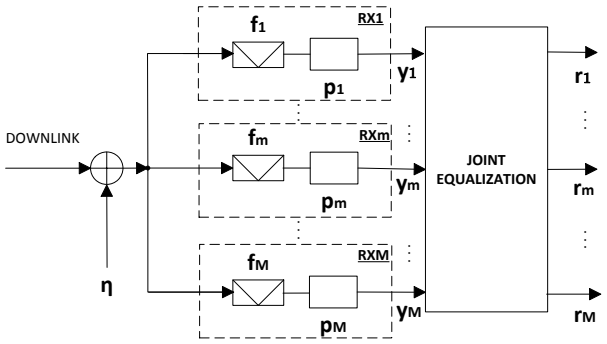

Figure 2.10: Joint Multicarrier Equalization Block Diagram

tained by systematically reducing the multicarrier Volterra basis functions set using the LASSO (least absolute shrinkage and selection operator), algorithm [60]. Regarding the second scenario, we propose a tailored multiple carrier equalization method at the gateway [61] to adapt to the specific channel characteristics in which non-linear ACI is not present.

2.6 Thesis Contributions

In the following, a brief summary of the chapters is presented together with the relevant contributions with respect to the prior literature. Further, for each chapter, the relevant published papers are listed

Chapter 2 Distortion Countermeasures Techniques for Multicarrier Satellite Channels:

In this chapter we provide a detailed overview of the thesis work. The chapter includes the definition of the satellite communication models, the analytic description of the channel distortion and a brief presentation of the proposed counter measures techniques. The main contribution of this chapter is the analysis and analytical modeling of the multiple carriers satellite channel based on [1]. The content of this chapter is mostly based on a published book chapter,

[A]Bhavani Shankar M. R, Roberto Piazza, Stefano Cioni, "On-ground Signal Processing Techniques Enabling Efficient Amplification of Multiple Carriers", in Cooperative and Cognitive Satellite Systems, Elsevier, Editors: Symeon Chatzinotas, Bjorn Ottersten and Riccardo de Gaudenzi.

Chapter 3 Multiple Carrier Predistortion Techniques:

In this chapter we present several on-ground transmitter solutions to counteract the distortion effects of a multiple carrier satellite channel. Data

predistortion operates jointly on the transmitted symbols while signal predistortion is directly applied to the baseband multicarrier signal waveform. As multicarrier data predistortion , we propose polynomials and Look-Up Table based solutions. Firstly, we introduce multiple carrier data predistortion, while in previous works, data predistortion was only developed for single carrier applications [6,19,22]. Further, we elaborate two approaches to multiple carriers data predistortion as model based data predistortion and look-up table based data predistortion.

The main contributions of this chapter have been published as

[B]R. Piazza, B. Shankar, E. Zenteno, D. Rönnow; J. Grotz, F. Zimmer, M. Grasslin, F. Heckmann, S. Cioni, "Multicarrier Digital Predistortion/ Equalization Techniques for Non-linear Satellite Channels", in Proc. 30th AIAA Intern.Commun. Satellite Syst. Conference, 2012.

[C]R. Piazza, S. Bhavani, B. Ottersten, "Data Predistortion for Multicarrier Satellite Channels using Orthogonal Memory polynomials", in International Workshop on Signal Processing Advances for Wireless Communication, June 16, 2013.

[D] R. Piazza, S. Bhavani, B. Ottersten, "Multicarrier LUT-based Data Predistortion for Non-linear Satellite Channels", in International Conference on Communication, 2014.

[E]R. Piazza, S. Bhavani, E. Zenteno, D. Rönnow, K. Liolis, F. Zimmer, M. Grasslin, T. Berheide, S. Cioni, "Sensitivity Analysis of Multicarrier Digital Pre-distortion/ Equalization Techniques for Non-linear Satellite Channels", in Proc. 31th AIAA Intern. Commun. Satellite Syst. Conference, 2014.

Chapter 4 Improved Estimation Techniques for Multicarrier Predistortion:

Building on Chapter 3, we provide novel parameter estimation methods to improve the performance of the proposed data and signal predistortion techniques. Performance improvement is enabled by applying novel enhanced parameter estimation methods based on the direct leaning paradigm. Further, an optimization method for crest factor reduction is discussed and evaluated in combination with signal predistortion. The main contributions of this chapter with respect of the prior literature are the followings:

- Derivation of novel estimation methods for multiple carrier data predistortion
- Derivation of improved estimation methods for signal predistortion
- Derivation of novel estimation methods for crest factor reduction

The results of this chapter have been submitted and published as

[F]R. Piazza, S. Bhavani, B. Ottersten, "Data Predistortion for Multicarrier Satellite Channels Based on Direct Learning", In IEEE Transaction on Signal Processing, 2014.

[G]R. Piazza, S. Bhavani, B. Ottersten,"Generalized Direct Volterra Predistortion with Adaptive Crest Factor Reduction ControlâĂİ , 2014.

Chapter 5 Distributed Multiple Carrier Predistortion:

As a generalization of the multicarrier predistortion for single gateway application considered in Chapter 3, we here consider multi-gateway transmission where carriers are independently uplinked toward the same satellite from different gateways. For this distributed scenario, we propose several on-ground transmitter techniques providing a complexity versus performance trade-off. The main contribution of this chapter with respect to the prior literature includes the analysis of the multi gateway scenario and a proposed distributed data predistortion method. The content of this chapter has been published as,

[H]R. Piazza, S. Bhavani, B. Ottersten, "Multi-gateway Data Predistortion for Non-linear Satellite Channels", Submitted in IEEE Transaction on Communication, 2014.

Chapter 6 Equalization Techniques:

In this chapter we consider receiver equalization techniques for the multiple carrier satellite channel. Advanced single carrier techniques are proposed for end users applications while multiple carrier equalization techniques are considered for professional applications as well as for satellite return channel. The main contributions of this chapter with respect to prior literature includes:

- Single carrier FSE performance evaluation in multiple carrier non-linear satellite channels
- A non-linear de-mapping method for non-linear channels
- Joint multiple carrier data equalization for satellite return channel

The main contributions have been published in,

[I]R. Piazza, B. Shankar, M. Grasslin, T. Berheide, S. Cioni, "Performance Analysis of Fractionally Spaced Equalization in Non-linear Multicarrier Satellite Channels", in Proc. 32th AIAA Intern. Commun. Satellite Syst. Conference, 2014.

[L]E. Zenteno, R. Piazza, B. Shankar, D. Rönnow, B. Ottersten "Low Complexity Predistortion and Equalization in Nonlinear Multicarrier Satellite Communications", Submitted in EURASIP Journal on advances in Signal Processing, 2014.

[M]R. Piazza, B. Shankar, B. Ottersten, "Carrier Rate Optimization on the Return Link of Interactive Mobile Satellite Networks", In European Wireless 2014.

Chapter 7 Conclusion: contains final conclusions and describes future work.

Appendix A This Appendix contains a separate work on single carrier data predistortion which is been published as,

[N]R. Piazza, S. Bhavani, B. Ottersten, "Non-parametric data predistortion for non-linear channels with memory", in International Conference on Acoustics, Speech, and Signal Processing , 2013.

Chapter 3

Multiple Carrier Predistortion Techniques

In this chapter we present several transmitter techniques implementing data predistortion for multiple carrier satellite channels. The underlying basic idea is to jointly process the transmitted symbols from all carriers toward counteracting the channel distortion effects and hence improve power and spectral efficiency.

This chapter presents three different approaches to multiple carrier data predistortion based on:

- Polynomials
- Orthogonal polynomial
- Look-Up Table

All methods are applicable to a single GW scenario and are characterized by joint symbol-rate processing performed on the intended transmitted symbols prior to signal shaping.

3.1 Memory Polynomials Data Predistortion

3.1.1 Introduction

Memory polynomials predistortion is an established methodology for single carrier signal predistortion [16, 26, 27, 38].

A non-linear system with memory can be modeled as a Volterra system that corresponds to a polynomial function that includes cross memory terms [24]. This modeling approach is related to the basic application of the Taylor principle for which every continuous function can be equivalently described with a polynomial expansion. The polynomial model is then extended with memory terms. Finally, the base band model has to include conjugate operations to account for in-band and out-of-band interference [62]. The same modeling approach, can be equivalently applied to the non-linear channel as well as to the predistorter.

Memory polynomials based predistortion for multiple carrier amplification has been partially addressed in [21] for a terrestrial application where a multicarrier signal predistortion model is introduced to compensate distortion effects in an HPA operated in dual carrier mode. Multicarrier memory polynomials for data predistortion have been first introduced in [29] as a low complexity solution to pre-compensate IMD in multicarrier satellite channels. In the following sections we present the contributions of [29, 30, 59] where memory polynomial data predistortion for multiple carrier satellite channels has been proposed and evaluated.

3.1.2 Scenarios

As discussed in Chapter 2, recently launched wideband satellite transponders perform joint filtering and amplification of multiple carrier signals and the trend is envisaged for future systems as well. In such applications, different carriers are usually independent and dedicated to different user terminals or applications. Joint on-board filtering and amplification of the stream of carriers, allows significant savings in hardware complexity and weight. Improved spectral and power efficiencies of this setting motivates the target scenario where a satellite broadcast transmission from a single gateway to many receivers with a transparent satellite transponder is considered. Each carrier channel is assumed to be compliant with $DVB-S2$ standard. Present multicarrier transponders have typical bandwidths of 33 and 72 MHz, carrier throughputs varying from 10MSps to 45 MSps and an $L-TWTA$ with typical OBO in the range of 2.9 to 4.5 dB.

From a system perspective, the predistortion needs be designed under the assumption of full knowledge of the channel characteristics in terms of filters, amplifiers etc at the gateway prior to launch and only sporadic data on a loop back signal will be assumed available. Possible feedback from the receivers (dedicated receivers stations) can be considered available, at regular intervals, for channel reconfiguration. Concerning user terminals equalization, although the on-board joint amplification of multiple carriers can often occur, most of the current user receivers usually support demodulation and decoding only for a single carrier signal. The compensation of possible channel variations, e.g. TWTA parameters drift, will be delegated to the end receiversâĂŹ that have to track fast channel variations. Receiver equalization technique will be discussed in detail in Chapter 6.

3.1.3 Channel Model

The typical model of the path between the transmitter and the receiver in a transparent satellite communication is described in Section 2.2.1. The signals from the GW are channelized to the satellite HPA through the IMUX filter whose amplitude and group delay response is depicted in Fig. 2.2 in Section 2.2.1. This wideband filter can be approximated as a linear system with memory (FIR filter) whose parameters are obtained from the response. Further, the TWTAs used in Ku-band can be assumed to have a transfer characteristic largely independent of the frequency. Such memoryless systems are characterized by the AM/AM and AM/ PM curves depicted in Fig. 2.3 in Section 2.2.1.

3.1.4 Joint Data Predistortion Based on Memory Polynomials

DPD, introduced at the GW, aims to mitigate the channel interference and to increase power efficiency. Joint carrier processing allows pre-cancellation of the relevant interferences generated by the intermodulation products. Further, processing is performed at the data level, prior to pulse shaping, in order to avoid signal spectral regrowth on the uplink channel (cf. to Fig. 3.1).

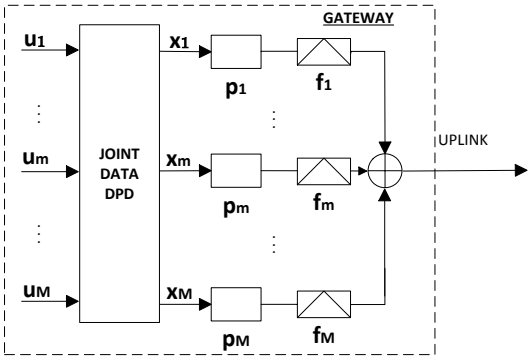

Figure 3.1: Joint multicarrier DPD. The M carriers are processed simultaneously at the GW.

Recalling the P-th oder inverse theory [24], the pre-distorter function shall approximate the inverse channel, which is also non-linear and dynamic, and hence can be described as a Volterra series. As a consequence, the predistorter model can be described as:

$$x_i(n) = \phi_i(\mathbf{u}_K(n))^T \mathbf{w}_i, \tag{3.1}$$

where $i = 1, \ldots, M$, M is the total number of carriers, $\mathbf{w}_i$ is the $\sum_{p=1}^{P} M^p(K+1)^p \times 1$ parameter vector of the predistorter and ϕ_i the vector of the non-linear input combination and K is the single-side memory depth. We can define

$$\mathbf{u}(n) = [u_1(n), \ldots, u_M(n)]^T, \tag{3.2}$$

$$\mathbf{u}_K(n) = [\mathbf{u}^T(n-K), \ldots, \mathbf{u}^T(n+K)]^T. \tag{3.3}$$

Further, the entries of vector ϕ_i are the Volterra basis $\phi^{\{d\}}_{k_1,\ldots,k_d/m_1,\ldots,m_d}$ defined as:

$$\phi^{\{d\}}_{k_1,\ldots,k_d/m_1,\ldots,m_d}(\mathbf{u}(n)) = \prod_{j=1}^{(d+1)/2} u_{m_j}(n-k_j) \prod_{j=(d+1)/2+1}^{d} u^*_{m_j}(n-k_j). \tag{3.4}$$

For each non-linear order we stack terms relative to all carrier combination together with memory combinations in the vector

$$\phi^{\{d\}}_i(\mathbf{u}_K(n)) = [\{\phi^{\{d\}}_{k_1,\ldots,k_d/m_1,\ldots,m_d}(\mathbf{u}(n))\}] \ \forall i_j \in (1, M), \forall m_j \in (-K, K). \tag{3.5}$$

Finally, we augment vectors of different non-linear orders obtaining

$$\phi_i(\mathbf{u}_K(n)) = [\{\phi_i^{\{d\}}(\mathbf{u}_K(n))\}] \; \forall d \in (1, P), \tag{3.6}$$

with $\phi_i^{\{d\}}(\mathbf{u}_K(n))$ a $\sum_{p=1}^{P} M^p(2K+1)^p \times 1$ vector. Notice that for simplifyin the notiation we have her e assumed that memory depth K is the same for every polynomial degree d while in reality K_d should be considered. Identification of the parameters $\mathbf{w}_i$ is made such that the predistorter function resembles the channel post-inverse. This can be achieved using the indirect learning architecture [63] in which case the inverse is estimated from the input and output signals. A detailed description of the parameters identification method is provided in the sequel.

Channel Inverse Parameters Identification

Referring to Fig. 3.1, the aim is to estimate $\mathbf{w}_i$ such that $E[||u_i(n) - r_i(n)||^2]$ is minimized for each $i \in (1, \ldots, K)$. This is a standard least squares problem of the identification of the channel post-inverse function described as

$$u_i(n) = \phi_i(\mathbf{y}(n))^T \mathbf{w}_i \tag{3.7}$$

leading to the $||u_i(n) - r_i(n)||^2 = 0$. Given a dedicated training sequence providing N samples of transmitter and received symbols, u_i and $\mathbf{y}$ respectively, we can stack the quantities

$$\mathbf{s}_i = [u_i(0) \ldots u_i(N-1)]^T \tag{3.8}$$

$$\mathbf{\Phi}_i = \begin{bmatrix} {\phi_i}^T(\mathbf{y}(0)) \\ \vdots \\ {\phi_i}^T(\mathbf{y}(N-1)) \end{bmatrix} \tag{3.9}$$

such as we obtain $\mathbf{s}_i \approx \mathbf{\Phi}_i \mathbf{w}_i$. The least squares solution for $\mathbf{w}_i$ is then already provided [64]

$$\mathbf{w}_i = (\mathbf{\Phi}_i^H \mathbf{\Phi}_i)^{-1} \mathbf{\Phi}_i^H \mathbf{s}_i. \tag{3.10}$$

Complexity

Regarding the complexity of the presented multiple carrier data predistortion method we have to distinguish between the *On-line* processing complexity and the *Off-line* complexity. On-line processing complexity is dictated by the performed complex polynomial operations and it depends on the selected polynomial model degree and memory depth and number of carriers. In general we have to compute M non linear combination vector ϕ_i for a total of $\sum_{p=1}^{P} M^p(2K+1)^p$ computed terms and then perform K linear multiplication $x_i(n) = \phi_i(\mathbf{u}_K(n))^T \mathbf{w}_i$. Notice that the processing is performed at the symbols rate R_s.

Off-line processing is related to the estimation of the predistorter parameters $\mathbf{w}_i$ and has a complexity order of $O(NK^2P^2)$ where the critical operation is the matrix inversion (kindly refer to (3.10)). Notice that the inversion can alternately be implemented by using standard Least Mean Squares (LMS) or Recursive Least Squares (RLS) techniques [1, 20].

3.1.5 Performance Evaluation

Figure of Merit

Performance of each channel is evaluated by means of the Total Degradation (TD) [6] defined as,

$$TD_{BER} = E_s/N_{0_{NL}} - E_s/N_{0_{AWGN}} + OBO. \tag{3.11}$$

Here, $[E_s/N_0]_{NL}$ is the signal to noise ratio needed in the considered non-linear channel to achieve the target Bit Error Rate (BER) for the specific modulation and code scheme, while $E_s/N_{0_{AWGN}}$ is the signal to noise ratio achieving the same target BER with an identical transmission scheme but with a linear AWGN single carrier channel and, finally, OBO is a measure of the on-board HPA power efficiency. The total degradation results in a convex function of the output back-off providing for the optimal amplifier operating point.

Numerical Results

In Figure 3.2, we present results for a three carrier channel where we implement the multiple carrier data predistortion described in section 3.1.4. Results for the central and one of the external carriers is presented due to the symmetric placement of carriers. The central carrier is largely affected by adjacent channel interference while the external carriers experience non-constant group delay of the filters. As expected, performance of the central carrier is in general worse than the external ones. Clearly digital pre-distortion is shown to be effective in reducing the TD, in both the internal as well as external channels by about $0.5 - 0.8$ dB.

A four carrier experiment is reported in Figure 3.3. Inner and outer carriers, in pairs, have similar performance. In this very tight scenario where the number of intermodulation products is very high, pre-distortion is even more effective providing very significant gain reducing the total degradation of about $1.0 - 1.5$dB and improving power efficiency (optimum OBO) of about 2 dB.

This section presents a novel framework for generating and applying memory polynomials as a data predistortion technique for multiple carriers satellite channels. This technique provides for a mitigation of ACI and ISI at the symbols level thereby improving decoding performance and hence the resulting TD. In the following section we propose a variation of the presented memory polynomial multiple carrier predistorton based on orthogonal basis to reduce parameters estimation complexity.

3.2 Orthogonal Memory Polynomials Data Predistortion

3.2.1 Introduction

Orthogonal polynomials were developed to improve the accuracy of kernel estimation in the single carrier case [18]. These polynomials are orthogonal in statistical sense when restricted to the memoryless terms [18]. In this section we present the contribution of [31], where we propose the use of orthogonal memory polynomials for multicarrier predistortion. A novel systematic approach for

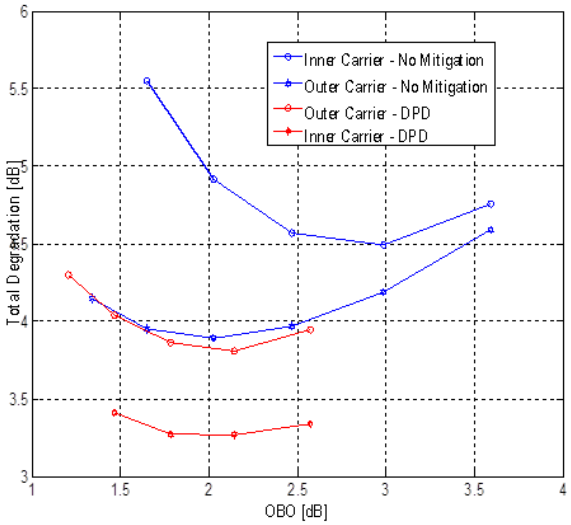

Figure 3.2: Total degradation versus aggregate OBO in a three- carrier scenario using 16 APSK Â" in each channel 10Mbaud each channel, $\rho = 0.2$, interpolated LUT for TWTA, 10% overlap among carriers.

generating orthogonal MP exploiting data from all carriers is devised. This approach ensures the orthogonality of polynomials in the statistical sense [18] without any restrictions. The salient features of the new multicarrier orthogonal MP are highlighted and their implications on system design are described. Of particular interest are reduced complexity and modularity: simpler estimation of polynomial co-efficients reduces complexity and the ability to increase the degree/ memory of the predistorter without altering the already computed coefficients imparts scalability.

3.2.2 Joint Multicarrier Amplification

Multicarrier Satellite System

- Scenario: The considered multicarrier satellite system involves broadcasting in Ku-band from a geostationary satellite to fixed terminals. A single gateway transmitting independent carriers is assumed and each carrier could correspond to a different service or an application. The user terminal is assumed to be a legacy receiver (e.g. a commercial TV decoder) capable of demodulating and decoding a single carrier, unlike in [1, 20]. This requirement arises from compatibility constraints, complexity considerations and access restrictions. Such single carrier user-terminals cannot compensate for ACI [20, 29]. On the other hand, the predistorter at the gateway is assumed to have information about all the channels; this can be exploited to mitigate ACI.

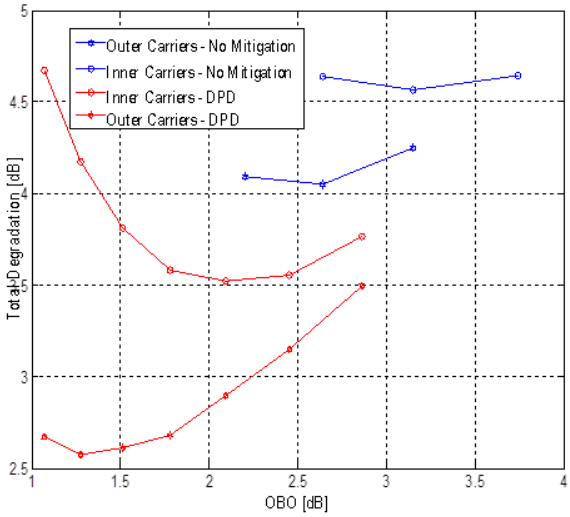

Figure 3.3: Total degradation versus aggregate OBO in a three- carrier scenario using 16 APSK Â" in each channel 10Mbaud each channel, = 0.2, interpolated LUT for TWTA, 10% overlap among carriers

- Channel: Figure 3.4 illustrates a baseband model for the considered system. This model differs from [1] only in the choice of the mitigation technique. The filters, $\{p_i\}$, which add memory effects, represent a cascade of pulse shaping and on-board channelizing filters. TWTAs (Traveling Wave Tube Amplifier) constitute the commercially used on-board HPA; their characteristic is intrinsically non-linear and can be assumed to be frequency independent. Such a memoryless system is characterized by the AM/AM and AM/PM curves [6] and the Saleh model [23] is widely used to parameterize them. To focus on the HPA impairments, we assume an ideal uplink and an AWGN channel for the downlink.

- Data Predistortion Unlike in terrestrial scenarios [16, 21], the predistorter and HPA are not co-located due to payload constraints and the need for flexibility. Hence, the predistorter output has to adhere to strict regulations on out-of-band emissions for the uplink. Since a traditional signal level predistorter [16, 22] causes spectral regrowth, we implement a data predistorter preceding the pulse shaping filter and operating jointly on multiple carrier data. Clearly, such a DPD does not cause spectral enlargement and is preferred for satellite uplink [6].

Data Predistortion Techniques

Unlike the typical single carrier channels, the considered system is characterized by strong ACI that dominates ISI and the same is well documented in [1, 29]. Central to developing a model based predistortion technique is the ability to parameterize the channel. The channel, essentially a non-linear system with

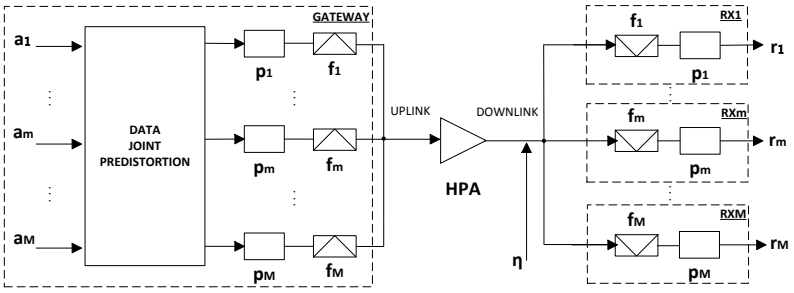

Figure 3.4: Multicarrier Channel Model

$$y_{m,V}^{(p)}(n) = \sum_{(m_1,\ldots m_p)\in\Omega_{m,p}} \sum_{k_1=-K_{m_1}^{(p)}}^{K_{m_1}^{(p)}} \cdots \sum_{k_p=-K_{m_p}^{(p)}}^{K_{m_p}^{(p)}} \tag{3.13}$$
$$g_{m_1,m_2,\ldots,m_p,m}(\{k_l\}_{l=1}^{p}) \prod_{s=1}^{\frac{p+1}{2}} a_{m_s}(n-k_s) \prod_{s=\frac{p+3}{2}}^{p} a_{m_s}^{*}(n-k_s)$$

memory can be completely described using the discrete Volterra series as detailed in [1]. The Volterra analysis then forms the basis for the predistorter design.

- Volterra DPD: In [1], the derived Volterra series is used towards devising an equalizer. Exploiting the fact that the post-inverse and pre-inverse are ideally the same [24], such an equalizer can also be used as a discrete Volterra multicarrier DPD. In general, the Volterra DPD has infinite order and memory; it is truncated to third or fifth degree for ease of implementation resulting in the output, $y_m(n)$, with

$$y_m(n) = y_{m,V}^{(1)}(n) + y_{m,V}^{(3)}(n) + y_{m,V}^{(5)}(n) + \eta_m(n)$$
$$y_m^{(1)}(n) = \sum_{m_1=1}^{M_c} \sum_{k=-K_{m_1}^{(1)}}^{K_{m_1}^{(1)}} g_{m_1,m}^{(1)}(k) a_{m_1}(n-k) \tag{3.12}$$

  where $y_m^{(p)}(n)$ denotes the pth degree Volterra term (the general expression is given in (3.13), top of the next page). M_c is the number of carriers, $K_m^{(p)}$ denotes memory for the pth degree term for carrier m, $\{g_*^{(p)}(\cdot)\}$ are the pth degree Volterra kernel coefficients, $a_m(n)$ and $\eta_m(n)$, respectively, are the data symbols and receiver noise on carrier m at instance n.

  The simplified DPD of (3.13) uses only those non-linear terms that produce in-band ISI and ACI. In this section, we define $\Omega_{m,D}$ as the set of carriers $(m_1, \ldots, m_D)$ causing in-band distortions to carrier m due to the

non-linear terms of degree D. The sets $\Omega_{m,D}$ for many significant scenarios are summarized in [1]. Volterra predistortion of degree D requires $O(K^{D+1}), K = max_m\{K_m^{(D)}\}$.

- Memory Polynomial DPD (MP-DPD): Volterra DPD predistorter is highly complex due to a large number of cross memory terms involved (even after confining the terms to Ω_*). This invariably leads to estimation inaccuracies of $\{g_*^{(p)}(\cdot)\}$ based on training . On the other hand, low complexity multicarrier MP-DPD has been derived in [29] developing on their application to single carrier scenarios. The output of a MP-DPD, $y_m(\cdot)$, takes the form,

$$y_m(n) = \sum_{w=1}^{W}\sum_{k=-K_w}^{K_w} h_{w,m}(k)\Phi_{m,w,k}(\mathbf{a}(n)) \tag{3.14}$$

where $\{\Phi_{m,w,k}(\cdot)\}$ constitutes the standard multicarrier memory polynomial bases described in [29], $\{h_{w,m}(\cdot)\}$ are the kernel coefficients and $\mathbf{a}(n) = [a_1(n), \ldots, a_{M_c}(n)]$. Table 3.1 details $\Phi_{m,w,k}(\cdot)$ for cross terms up to the fifth degree and memory depth $2K_w$. Complexity of MP-DPD of degree D is $O(KD), K = max_w\{K_w\}$ compared to $O(K^{D+1})$ of Volterra DPD. We now describe a novel DPD based on multicarrier Orthogonal memory polynomials that allows for faster kernel estimation.

3.2.3 Orthogonal Memory Polynomials Based Data Predistorter

Orthogonal polynomials were introduced in [18] as a signal predistortion mechanism to reduce inaccuracies in estimation of kernel coefficients and hence improve out-of-band emissions. While out-of-band emission is not an issue here, as will be shown in the sequel, these polynomials exhibit interesting properties that warrant their use in the multicarrier scenario.

Basis representation of the predistortion function

Let $\{\psi_{m,w,k}(\cdot)\}, m \in [1, M_c], w \in [1, W], k \in [-K_w, K_w]$ denote the set of basis functions and denote, $\psi_{m,i,k}(\mathbf{a}(n)) = \psi_{m,i,k}(a_1(n-k), \ldots, a_{M_c}(n-k))$. Motivated by their form in [18], a novel multicarrier data predistorter based on orthogonal polynomials is defined similar to (3.14) as,

$$y_m(n) = \textstyle\sum_{w=1}^{W}\sum_{k=-K_w}^{K_w} h_{w,m}(k)\psi_{m,w,k}(\mathbf{a}(n))\forall\ m, \tag{3.15}$$

where $y_m(n)$ is the predistorter output for the mth carrier at the nth instance and $\{h_{w,m}(k)\}$ are the kernel coefficients. Note that predistorted output for mth carrier depends on symbols from other carriers and utilizes a memory depth of $2K_w$ for each polynomial term w. Similar to [18], these basis functions are constrained to satisfy statistical orthonormality as defined below,

$$\begin{aligned} &< \psi_{m,i,k}(\mathbf{r}), \psi_{m,j,l}(\mathbf{r}) >= \mathbb{E}\{\psi_{m,i,k}(\mathbf{r}(n))[\psi_{m,j,l}(\mathbf{r}(n))]^*\}, \\ &< \psi_{m,i,k}(\mathbf{r}), \psi_{m,j,l}(\mathbf{r}) >= \begin{cases} 0 & \forall j \neq i, k \neq l \\ 1 & i = j, k = l \end{cases} \end{aligned} \tag{3.16}$$

Table 3.1: Standard Multicarrier Memory Polynomial Basis

	$\Phi_{m,w,k}(\mathbf{a}(n)), \quad k \in [-K_w, K_w]$
Linear terms	$a_w(n-k)$
3^{rd} degree terms	$\begin{cases} a^*_{m_3}(n-k)\prod_{i=1}^{2} a_{m_i}(n-k) \\ (m_1,m_2,m_3) \in \Omega_{m,3} \end{cases}$
5^{th} degree terms	$\begin{cases} \prod_{i=1}^{3} a_{m_i}(n-k)\prod_{i=4}^{5} a^*_{m_i}(n-k) \\ (m_1,m_2,m_3,m_4,m_5) \in \Omega_{m,5} \end{cases}$

where $r_m(n)$ is the received signal on carrier m at instance n, $\psi_{m,i,k}(\mathbf{r}(n)) = \psi_{m,i,k}(r_1(n-k),\ldots,r_{M_c}(n-k))$ and the averaging is performed over the statistics of $\{r_m(\cdot)\}$.

Basis Orthogonalization

We now proceed with the construction of $\{\psi_{m,w,k}(\cdot)\}$ satisfying (3.16). The approach is two fold : (1) to choose a set of standard basis functions and (2) obtain an orthonormal set from these basis functions. With regards to the first requirement, motivated by [16,29], we choose the standard basis functions corresponding to the multicarrier MP as described in Table 3.1. With the standard basis defined, we use the Modified Gram Schmidt method for orthogonalization [65]. For the ease of comprehension, we present the procedure for $K_w = 0, \forall w$ and the same can be extended to any K_w. With $K_w = 0$, dropping subscript k and the input arguments of the bases for simplicity, the standard iterative Gram Schmidt [65] process for the generation of an orthonormal basis $\psi_{m,w}$ from a general basis $\Phi_{m,w}$ is defined in (3.17),

$$\begin{aligned} \Psi_{m,w} &= \Phi_{m,w} - \sum_{z=1}^{w-1} \frac{<\Phi_{m,w}, \Psi_{m,z}>}{<\Psi_{m,z}, \Psi_{m,z}>}\Psi_{m,z}, \\ \psi_{m,w} &= \frac{\Psi_{m,w}}{|\Psi_{m,w}|}. \end{aligned} \tag{3.17}$$

However, this process suffers from numerical instability and the Modified Gram Schmidt method overcomes this problem by computing each basis $\Psi_{m,w}$ as a sequence of recurrent inner products rather than a summation of inner products,

$$\begin{aligned} \Psi^{(1)}_{m,w} &= \Phi_{m,w} - \frac{<\Phi_{m,w}, \Psi_{m,1}>}{<\Psi_{m,1}, \Psi_{m,1}>}\Psi_{m,1} \\ \Psi^{(2)}_{m,w} &= \Psi^{(1)}_{m,w} - \frac{<\Psi^{(1)}_{m,w}, \Psi_{m,2}>}{<\Psi_{m,2}, \Psi_{m,2}>}\Psi_{m,2} \\ &\vdots \\ \Psi_{m,w} &= \Psi^{(w-2)}_{m,w} - \frac{<\Psi^{(w-2)}_{m,w}, \Psi_{m,w-1}>}{<\Psi_{m,w-1}, \Psi_{m,w-1}>}\Psi_{m,w-1}. \end{aligned} \tag{3.18}$$

In effect, the Modified Gram Schmidt procedure returns a vector of coefficients $c_{w,l}$ such that each orthonormal basis $\psi_{m,w}$, can be written as a linear combination of the standard basis functions: $\psi_{m,w} = \sum_{l=1}^{w} c_{w,l}\Phi_{m,l}$.

Having defined the functional form of the bases and an orthogonalization procedure, it remains to compute the various correlation coefficients, denoted using $< \cdot , \cdot >$ in (3.18), and estimate the kernel coefficients towards implementing (3.15).

Computing the Correlation Coefficients

We now compute the correlation coefficients so that the bases satisfy (3.16). In this work, no a priori assumption is made on the distribution of the received symbols. Training symbols are used and channel statistics are extracted from the corresponding noisy received data. We approximate the ensemble average by time average based on $r_m(n)$ as,

$$< \Phi_{m,i,k}(\mathbf{r}), \Psi_{m,j,l}(\mathbf{r}) > \approx \frac{\sum_{n=1}^{N_{tr}} \Phi_{m,i,k}(\mathbf{r}(n))[\Psi_{m,j,l}(\mathbf{r}(n)]^*}{N_{tr}} \tag{3.19}$$

In [18], a closed-form expression for polynomials is obtained for a single carrier and for a specific distribution of $\{r_1(n)\}$. Further, the orthogonality is satisfied for the memoryless terms. However, the construction provided above can be applied regardless of the polynomial degree, distribution of received symbols and channel characteristics. Further, the proposed construction imposes orthogonality both on the polynomial terms w as well as on the memory k of the orthogonal MP (kindly refer to (3.15)).

Kernel Estimation

It now remains to obtain the kernel coefficients $\{h_{w,m}(k)\}$. By virtue of being used for DPD, $\{h_{w,m}(k)\}$ model the inverse of the channel function. Thus $\{h_{w,m}(k)\}$ can be estimated using the received symbols by modeling predistortion as a post-inverse [24]. Typically, $\{h_{w,m}(k)\}$ are computed prior to launch by measuring the HPA characteristics and simulating the satellite transmission [6]. However, aging and temperature variations (diurnal variations as the satellite moves back and forth from the shadow of earth) changes the channel characteristics. This motivates a periodic, training based, estimation of $\{h_{w,m}(k)\}$ when the satellite is in operation using operator owned dedicated reference terminals capable of multicarrier demodulation. These terminals compute $\{h_{w,m}(k)\}$ and feed them back to the gateway.

Recalling the definition of $r_i(n), a_i(m)$ from earlier sections, the post-inverse takes a form similar to (3.15) with,

$$a_m(n) = \sum_{w=1}^{W} \sum_{k=-K_w}^{K_w} h_{w,m}(k)\psi_{m,w,k}(\mathbf{r}(n)) + \epsilon_m(n) \tag{3.20}$$

where $\mathbf{r}(n) = [r_1(n), \ldots, r_{M_c}(n)]$ and $\epsilon_m(n)$ is the modeling error. Stacking N_{tr} number of training symbols $\{a_m(n)\}$ into a vector $\mathbf{b}_m$ and letting $\mathbf{h}_m = [h_{1,m}(-K_1), \ldots, h_{1,m}(K_1), h_{2,m}(-K_2), \ldots, h_{W,m}(K_W)]^T$ we can write (3.20) as $\mathbf{b}_m = \mathbf{A}_m\mathbf{h}_m + \mathbf{e}_m$. Here, $\mathbf{e}_m$ is the stacked error vector, and $\mathbf{A}_m$ is a matrix whose pth row corresponds to the evaluation of $\{\psi_{m,w,k}()\}$ for the pth received symbol. Based on this relation, $\{h_{w,m}(k)\}$ are obtained by minimizing, $[\mathbf{A}_m\mathbf{h}_m - \mathbf{b}_m]^*[\mathbf{A}_m\mathbf{h}_m - \mathbf{b}_m]$, as,

$$\mathbf{h}_m = \mathbf{A}_m^{\dagger}\mathbf{b}_m, m \in [1, M_c]. \tag{3.21}$$

Equation (3.21) involves a complexity of $O(N_{tr}K^2W^2)$, $K = \max_w K_w$ and can be susceptible to ill conditioning of $\mathbf{A}_m$. The reduction in complexity estimation is described next.

Properties of Orthogonal Bases

- Low Complexity Kernel Estimation: The lth column of $\mathbf{A}_m$ corresponds to the evaluation of $\psi_{m,w_0,k_0}(\cdot)$ (for some w_0, k_0) on the N_{tr} symbols. From (3.19), it can be therefore deduced that the columns of $\mathbf{A}_m$ are orthonormal. In fact, $\mathbf{A}_m$ is the orthogonal component (computed using QR decomposition) of the regression matrix corresponding to MP. Due to orthonormality, (3.21) can be simplified as,

$$\mathbf{h}_m = \mathbf{A}_m^* \mathbf{b}_m. \tag{3.22}$$

  Equation (3.22) shows that estimation procedure is simplified to a large extent by use of orthogonal MP with the complexity being only $O(N_{tr}KW)$. This simplification leads to cheaper reference terminals.

- Modularity: An important manifestation of (3.22) is modularity; additional basis functions (in terms of degree and/ or memory) could be included and the kernel coefficients corresponding to these new functions can be found without altering those estimated already. This arises from the fact that adding a new basis appends a new column to $\mathbf{A}_m$. Now, referring to (3.22), the corresponding kernel coefficient can simply be found as the inner product of new column of $\mathbf{A}_m$ and $\mathbf{b}_m$. When reference receive terminals are used, this scalability allows for a reduction in the amount of feedback. Similarly, the number of basis functions can be reduced by merely nulling the appropriate kernel coefficients. This feature provides for a control of received signal quality by a simple alteration of the memory or degree of the predistorter.

3.2.4 Simulation Results

Performance Metric

We now illustrate the performance of the proposed predistorter. The traditional measure of performance for non-linear channels is the Total Degradation (TD) [6]. In this paragraph we instead use the Signal to Interference plus Noise Ratio (SINR) as the performance metric since it (i) does not involve bit error rate evaluations and is faster to compute and (ii) is compatible to TD in behavior. In particular, the SINR for carrier m would be $\rho_m = \frac{\mathbb{E}(|a_m(n)|^2)}{\mathbb{E}(|\alpha_m r_m(n) - a_m(n)|^2)}$, where $\alpha_m > 0$ effects an unit power normalization to the desired signal at the receiver (depends on the set amplification level). When the Input Backoff (IBO) increases, the non-linear interference reduces but the signal strength after amplification also reduces thereby increasing the relative noise level ($\alpha_m > 1$). Reducing IBO increases signal power compared to noise, but the non-linear interference also increases. These effects are well captured in the denominator of ρ_m. Hence, similar to TD, there exists an optimum IBO (or equivalently Output Backoff, OBO) at which ρ_m is maximized.

Set-up

Simulations have been carried out with two and three carriers ($M_c = 2, 3$) per HPA. Saleh model [23] is used to obtain the HPA characteristic with the same

Table 3.2: Simulation Parameters

Symbol rates, R_s in MBaud	8 ($M_c = 3$), 12 ($M_c = 2$)
Carrier frequency spacing, $\triangle f$	1.25 R_s
{DPD degree, DPD memory}	{5 (Table 3.1) , $K_w = 1, \forall w$ in eq. (3.15)}
Number of training symbols	3200 (A DVBS2 short frame)
Modulation	32 APSK
Filters, $\{p_i\}$	Root Raised Cosine, roll-off 0.25
Simulation Oversampling	38 ($M_c = 3$), 25 ($M_c = 2$)
E_s/N_o	20dB

parameters as in [1]. As in [1], the pilots are drawn from 32 APSK constellation (target modulation). For comparing with the proposed scheme (depicted as Orth. MP-DPD), a MP-DPD of Section 3.2.2 is designed [29]. For the current scenario, Volterra DPD is omitted due to its exponential complexity (kindly refer Section 3.2.2). Further the benchmark cases of No DPD (without any HPA non-linearity compensation at the receiver) and an ideal linear amplifier with normalized gain (denoted as AWGN channel) are also simulated.

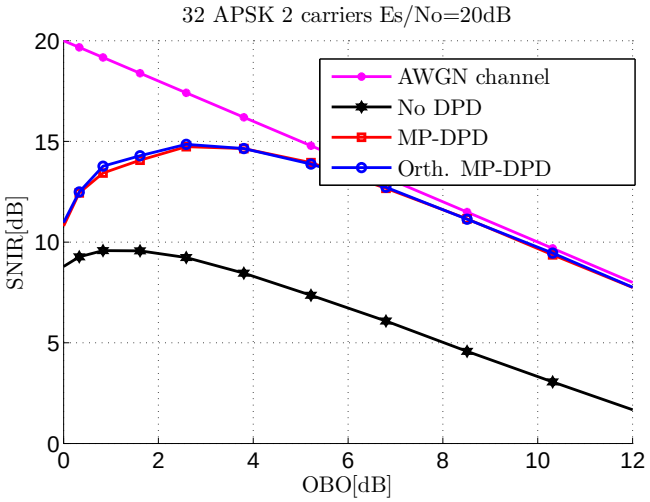

Figure 3.5: SINR performance of different DPDs : $M_c = 2$

Results

When $M_c = 2$, because of symmetry, both carriers have the same SINR and hence only one is depicted in Fig. 3.5. For $M_c = 3$, performance of the central carrier is impacted by strong ACI from the two external carriers. Hence the

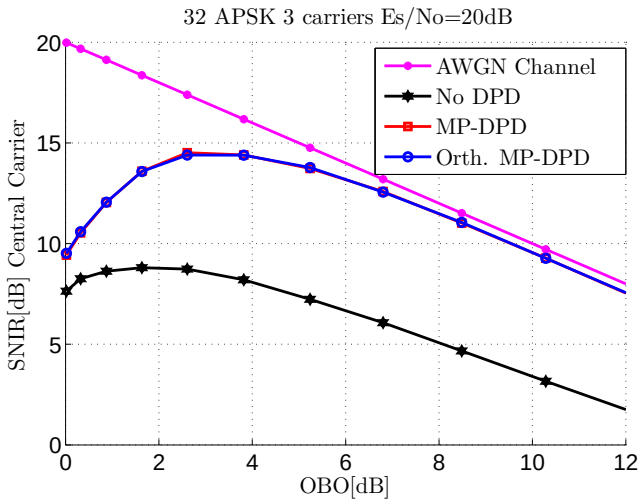

Figure 3.6: SINR performance of different DPDs : $M_c = 3$, (Central Carrier)

SINR of central carrier is shown in Fig. 3.6, while the performance of the external carriers are similar to Fig 3.5. Performance of the designed DPD is similar to MP-DPD for an identical order and memory depth, while providing the benefits outlined in Section 3.2.3. Comparing with the No DPD case, the use of predistortion effectively compensates the non-linear effects of the channel providing about 3 dB of gain in the region of high power efficiency (OBO $\approx$ 2.5 dB). Further, this SINR gain can also be translated into a power efficiency improvement: for a target SINR, the OBO can be significantly reduced by applying DPD. Comparing Fig. 3.5 and Fig. 3.6, we notice that a higher number of carriers introduces greater ACI, thereby reducing the absolute SINR. As a consequence of this, increasing M_c gradually moves the optimum OBO, corresponding to the maximum SINR, towards the linear region of the amplifier. As expected, the DPD performance approaches the linear amplification case for high OBO (small difference being due to the modeling/ estimation errors). The No DPD case asymptotically (in OBO) reaches the performance of the AWGN case, mainly due to the slow decay of the HPA phase with OBO [23]. This section presents a novel framework for generating and applying orthogonal memory polynomials as a predistortion technique when multiple carriers are amplified by a single HPA. This technique provides for mitigation of ACI and ISI thereby improving received SINR and power efficiency. Exploiting orthogonality reduces the complexity while resulting in a modular (scalable) implementation. These properties provide for a favorable comparison of the proposed technique with prior-art strongly motivating its use in future systems.

3.3 Look-Up Table based Data Predistortion

3.3.1 Introduction

Unlike polynomial based techniques, Look-up Table (LUT) based solutions do not require any complex processing to compute the predistorted symbols on-

line. This enhances the attractiveness of LUT based predistortion in real time applications. Single carrier LUT data predistortion has been well studied in literature. In [6, 19], LUT is computed iteratively by a numerical method that requires lengthy closed loop operation of the channel. In [52], computation of table entries relies on an *ad hoc* numerical technique for channel inversion.

In this section we present a novel method for multicarrier predistortion based on LUT we proposed in [32]. Differently from [6,19,52], we develop an analytical approach toward LUT generation. Exploiting the channel model, LUT generation is formulated as a minimization problem and is solved using recursive least squares (RLS) algorithm. In addition, we propose a novel method to reduce LUT computational complexity by identifying a property inherent in baseband non-linear system modelling. This leads to a computation reduction by about an order of magnitude. From an exhaustive search of prior-art, predistortion based on polynomial model seems to be the only available transmitter technique for multiple carrier non-linear channels [29, 31]. Hence, despite the different nature of the two solutions, polynomial predistortion has then been selected for performance comparison. It will be shown later in the section that the proposed technique provides gains over [29, 31] further enhancing its candidature for use in future applications.

3.3.2 Multicarrier Satellite Channel with Joint Power Amplification

In this section, we describe the scenario involving multicarrier non-linear satellite channel and the associated impairments.

System Scenario

A multichannel broadcast application from GEO satellites to fixed terminals is considered in this study. Each channel corresponds to a carrier and provides an independent service to the receivers. A typical example of a channel application is direct to home services (DTH) implementing DVB-S2 standard. Further, all the carriers are uplinked to the satellite transponder through a single gateway. The single transponder HPA is operated in multicarrier mode in order to reduce satellite weight and hardware cost [29]. Ground user terminals (UT) are assumed to decode information on a single carrier signal like in most commercial applications such as TV broadcasting. Reference user terminals can provide feedback to the gateway for configuration and calibration of transmission parameters.

Channel Model

The multicarrier satellite channel model is illustrated in Fig. 3.7 and has a configuration corresponding to [1]. With the amplifier itself being frequency non-selective and on-board filtering effects considered negligible. The latter assertion arises from the assumption that all carriers are within the filters bandwidth where amplitude in constant and phase is linear in frequency. At the gateway (GW) station M input carriers $\{u_m\}$ are first jointly predistorted with a LUT; the predistorted symbols $\{x_m\}$ are then uplinked to the satellite transponder.

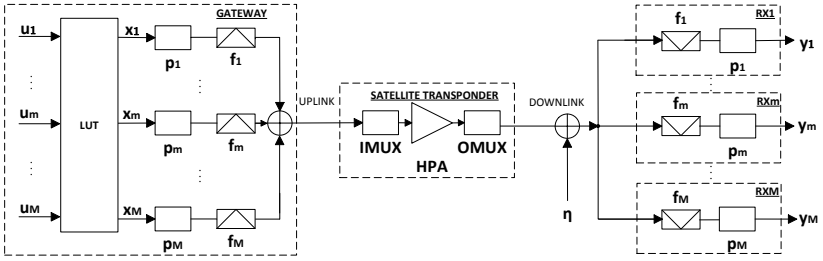

Figure 3.7: Multicarrier Channel Model

The memoryless amplifier is a Saleh model [23] with AM/AM and AM/PM characteristics as in [1, 20]: $A(r) = \frac{2r}{1+r^2}; \Phi(r) = \frac{\pi}{6}\frac{r^2}{1+r^2}$. Each downlinked carrier is then decoded by a UT receiver.

In the chosen scenario, ISI is negligible compared to ACI [29] and hence we consider a memoryless channel model. Further, avoiding the elaborate formulation of [1], we write the channel function in a compact way using the Kronecker product

$$\mathbf{y}(n) = \mathbf{G}_1\mathbf{x}(n) + \mathbf{G}_3\mathbf{x}(n) \otimes \mathbf{x}(n) \otimes \mathbf{x}(n)^* + \eta(n) \tag{3.23}$$

where $\mathbf{x}(n) = [x_1(n) \dots x_M(n)]^T$ with $x_m(n)$ the predistorted symbol on carrier m at instance n and $\mathbf{y}(n) = [y_1(n) \dots y_M(n)]^T$ with $y_m(n)$ being the corresponding received signal on carrier m_{th}. $\mathbf{G}_1$ is an $M \times M$ matrix comprising coefficients of linear terms and $\mathbf{G}_3$ is an $M \times M^3$ matrix of coefficients corresponding to the third degree terms in the Volterra expansion [66]. Moreover, similar to [1] the non-linear polynomial expansion has been limited to third degree in (3.23). For equally spaced carriers, we can identify those product terms in the multicarrier Volterra expansion that generate in-band interference [1]. These terms are selected by the matrix $\mathbf{G}_3$ in (3.23). Terms that are not in-band or redundant are nulled by zero entries in the matrix. In Table C.1, we provide the third degree in-band terms for a two and three carrier channel. Each index vector $[k_1\ k_2\ k_3]$ refers to the polynomial term $x_{k_1}x_{k_2}x^*_{k_3}$.

Table 3.3: Frequency Centered: (a) Two Carrier Channel In-band Terms, (b)Three Carriers Channel In-band Terms

(A)

$m=1$	$m=2$
[111]	[211]
[122]	[222]

(B)

$m=1$	$m=2$	$m=3$
[111]	[121]	[131]
[122]	[132]	[221]
[133]	[222]	[232]
[223]	[233]	[333]

Notice that (3.23) can be easily generalized to any memory depth P greater than zero simply substituting $\mathbf{x}(n)$ with $\mathbf{x}_P(n) = [\mathbf{x}(n-P)^T \dots, \mathbf{x}(n)^T, \dots \mathbf{x}(n+$

$P)^T]^T$.

3.3.3 Multicarrier LUT-based Data Predistortion

The approach to obtain a LUT is three fold: First the LUT generation is posed as a minimization problem, the key inputs to the minimization problem $\mathbf{G}_1$and $\mathbf{G}_3$ are estimated and finally, algorithms to solve the minimization problem are obtained by exploiting the channel model. Moreover, a method to reduce the required number of LUT entries to be computed is also devised.

LUT as Point-wise Channel Pre-inversion

As depicted in Fig. 3.7, the LUT maps input symbols $\{u_m(n)\}$ to predistorter symbols $\{x_m(n)\}$ at each instance. Dropping time index and defining $\mathbf{u} = [u_1 \dots u_M]^T$ and $\mathbf{x} = [x_1 \dots x_M]^T$, the LUT is the map defining $\mathbf{u} \mapsto \mathbf{x}$. Given the relation in (3.23) we can define a cost function representing the deviation of the channel output $\mathbf{y}$ with respect to the desired data vector $\mathbf{u}$ as

$$C_{\mathbf{u}}(\mathbf{x}) = E[||\mathbf{u} - (\mathbf{G}_1\mathbf{x} + \mathbf{G}_3\mathbf{x} \otimes \mathbf{x} \otimes \mathbf{x}^*))||^2]. \tag{3.24}$$

For each input data vector $\mathbf{u}$, we have to find the specific predistorted vector $\mathbf{x}$ that minimizes the corresponding cost $C_{\mathbf{u}}$,

$$\mathbf{x} = \arg\min_{\mathbf{x}}\{C_{\mathbf{u}}(\mathbf{x})\}. \tag{3.25}$$

Note that the minimization explicitly uses the channel model. Further, we implicitly assume the dependence of $\mathbf{x}$ on $\mathbf{u}$ in (3.25) without invoking additional notation for ease of comprehension.

Channel Estimation

Key to solving (3.25) is the knowledge of the channel parameters $\mathbf{G}_1$and $\mathbf{G}_3$. We now describe briefly the channel estimation based on training symbols. Channel parameter estimation can be solved as a standard least squares problem given N training symbols. Assuming the channel parameters to be time-invariant, the training does not need closed loop operation but just a single transmission and feedback. For each channel output $y_m(n)$, we can write,

$$y_m(n) = \mathbf{x}(n)^T\mathbf{g}_m^{(1)} + \phi_m(\mathbf{x}(n))^T\mathbf{g}_m^{(3)}, \tag{3.26}$$

where $\phi_m(\cdot)$ column vector with entries in the form $x_{k_1}x_{k_2}x_{k_3}^*$ where $[k_1\ k_2\ k_3]$ are the specific in-band terms for carrier m (refer to Table C.1), while $\mathbf{g}_m^{(p)}$ is the column vector of coefficients relative to degree p. Given a training sequence of N symbols we can write,

$$\begin{aligned} \mathbf{g}_m = (\mathbf{\Phi}_m^H\mathbf{\Phi}_m)^{-1}\mathbf{\Phi}_m^H\mathbf{y}_m, \quad \text{where} \\ \mathbf{y}_m = [y_m(0) \dots y_m(N-1)]^T, \\ \mathbf{\Phi}_m = [\phi_m(\mathbf{x}(0)), \dots, \phi_m(\mathbf{x}(N-1))]^T, \\ \mathbf{g}_m = [{\mathbf{g}_m^{(1)}}^T {\mathbf{g}_m^{(3)}}^T]^T. \end{aligned} \tag{3.27}$$

Given the estimated vectors $\mathbf{g}_m \forall m$ we can determine the matrices $\mathbf{G}_1$ and $\mathbf{G}_3$ of (3.23)

$$\mathbf{G}_1 = [\mathbf{g}_1^{(1)}, \ldots, \mathbf{g}_M^{(1)}]^T \tag{3.28}$$

$$\tilde{\mathbf{G}}_3 = [\mathbf{g}_1^{(3)}, \ldots, \mathbf{g}_M^{(3)}]^T \tag{3.29}$$

where $\tilde{\mathbf{G}}_3$ contains all the non zero entries of matrix $\mathbf{G}_3$. The position of the non-zero elements $\mathbf{G}_3$ are determined by the in-band intermodulation terms generated by the vector $\mathbf{x}(n) \otimes \mathbf{x}(n) \otimes \mathbf{x}(n)^*$ (kindly refer to Table C.1).

Look-up Table Construction

After estimation of channel parameters, we proceed to the description of the off-line procedure for computation of the entries. We now provide an iterative solution to the minimization problem defined in (3.25). Having K_m as the modulation order applied the m^{th} carrier and M as the total number of carriers, we define the input set of the LUT as S_M with dimension $d_m = \prod_{m=1}^{M} K_m$ such as $\mathbf{u} \in S_M$. The outcome of the procedure is a LUT that maps each desired channel input data symbols $\mathbf{u} \in S_M$, to a vector $\mathbf{x}$ so that $C_{\mathbf{u}}(\mathbf{x})$ in (3.25) is minimized. Further, in order to reduce processing time to build the complete LUT, we implement a recursive least square algorithm (RLS). Toward this, we define the cost function at the j^{th} iteration as $C_{\mathbf{u}}^{RLS}(j) = \sum_{i=1}^{j} \lambda^{j-i} ||\mathbf{e}^{(i)}||^2$ with $\mathbf{e}^{(i)} = \mathbf{u} - \mathbf{y}^{(i)}$ and

$$\mathbf{y}^{(i)} = \mathbf{G}_1 \mathbf{x}^{(i)} + \mathbf{G}_3 \mathbf{x}^{(i)} \otimes \mathbf{x}^{(i)} \otimes \mathbf{x}^{(i)^*}. \tag{3.30}$$

Notice that at each iteration, the error is computed with respect to a fixed vector $\mathbf{u} \in S_M$. Based on (3.23) and the rules for partial differentiation for complex variables defined in [67], we derive,

$$\frac{\partial \mathbf{y}^{(i)}}{\partial \mathbf{x}} = \mathbf{G}_1 + \mathbf{G}_3 \ (\mathbf{I}_M \otimes \mathbf{x}^{(i)} + \mathbf{x}^{(i)} \otimes \mathbf{I}_M) \otimes \mathbf{x}^{(i)^*}. \tag{3.31}$$

Notice that, the multicarrier channel formulation in (3.23) and the derived gradient in (4.62) are introduced in this work for the first time in the context of satellite communications. Towards defining the RLS algorithm, we consider:

$$\frac{\partial C_{\mathbf{u}}^{RLS}(j)}{\partial \mathbf{x}} = -2 \sum_{i=1}^{j} \lambda^{n-i} \frac{\partial \mathbf{y}^{(i)}}{\partial \mathbf{x}}^T \mathbf{e}^{(i)^*} = \mathbf{0}. \tag{3.32}$$

Based on the derivation in [40], to obtain a standard RLS formulation, we have to approximate

$$\mathbf{e}^{(i)} \approx \mathbf{u} - \frac{\partial \mathbf{y}^{(i)}}{\partial \mathbf{x}} \mathbf{x}^{(i)}. \tag{3.33}$$

Rearranging (3.32) and using (3.33) results in

$$\mathbf{R}(j) \ \mathbf{x} = \mathbf{r}(j), \tag{3.34}$$

$$\mathbf{R}(j) = \sum_{i=1}^{j} \lambda^{j-i} \frac{\partial \mathbf{y}^{(i)}}{\partial \mathbf{x}}^H \frac{\partial \mathbf{y}^{(i)}}{\partial \mathbf{x}}, \tag{3.35}$$

$$\mathbf{r}(j) = \sum_{i=1}^{j} \lambda^{n-i} \frac{\partial \mathbf{y}^{(i)}}{\partial \mathbf{x}}^{H} \mathbf{u}. \tag{3.36}$$

The resulting $M \times M$ gain matrix $\mathbf{K}(j)$ is given by

$$\mathbf{K}(j) = \lambda^{-1}\mathbf{P}(n-1)\frac{\partial \mathbf{y}^{(j)}}{\partial \mathbf{x}} \tag{3.37}$$
$$(I + \lambda^{-1}\frac{\partial \mathbf{y}^{(j)}}{\partial \mathbf{x}}^{H} \mathbf{P}(n-1)\frac{\partial \mathbf{y}^{(j)}}{\partial \mathbf{x}})^{-1}$$

where $\mathbf{P}(j)$ takes the form of:

$$\mathbf{P}(j) = \lambda^{-1}(\mathbf{P}(j-1) - \mathbf{K}(j)\frac{\partial \mathbf{y}^{(j)}}{\partial \mathbf{x}}^{H} \mathbf{P}(j-1)). \tag{3.38}$$

The final update equation can be defined

$$\mathbf{x}^{(j+1)} = \mathbf{x}^{(j)} + \mu\mathbf{K}(j)\mathbf{e}^{(j)}. \tag{3.39}$$

where $\mathbf{P}(0) = \mathbf{I}_M$ and $\mathbf{x}^{(0)} = \mathbf{0}$. On the other hand, μ and λ depend on the problem settings and are tuned during simulation to guarantee convergence (kindly refer to section 3.3.4).

LUT Complexity Reduction

The total LUT size is $d_m = \prod_{m=1}^{M} K_m$ and each table entry has to be computed using the RLS algorithm described in Section 3.3.3, resulting in very high complexity. However, this complexity can be considerably reduced exploiting Volterra theory for non-linear systems [24]. The LUT is a non-linear base-band function of the input $\mathbf{u} \in S_M$ that can be generally written as $\mathbf{x} = h(\mathbf{u})$. As a consequence of this observation, $h(\mathbf{u})$ can be completely described by an infinite polynomial expansion of the input vector $\mathbf{u}$

$$h(\mathbf{u}) = \sum_{p=1}^{\infty} \mathbf{H}_{2p-1}\mathbf{u}^{(p)} \otimes [\mathbf{u}^{(p-1)}]^{*} \tag{3.40}$$

where $\mathbf{H}_{2p-1}$ is an $M \times M^{2d-1}$ predistortion matrix and $\mathbf{u}^{(p)} = \mathbf{u} \otimes \cdots \otimes \mathbf{u}$. From the above we can easily identify the property

$$h(\mathbf{u}e^{j\theta}) = h(\mathbf{u})e^{j\theta}, \tag{3.41}$$

where $\mathbf{u} \in S_M$ and $\theta \in (0, 2\pi)$. We further define

$$\Lambda_{\mathbf{v}} = \{\mathbf{u} \in S_m | \exists \theta \in (0, 2\pi) : \ \mathbf{u} = \mathbf{v}e^{j\theta}.\} \tag{3.42}$$

It can be shown that either $\Lambda_{\mathbf{v}_i} = \Lambda_{\mathbf{v}_j}$ or $\Lambda_{\mathbf{v}_i} \cap \Lambda_{\mathbf{v}_j} = \{\}$. Thus $\{\Lambda_{\mathbf{v}_i}\}$ forms a partition of S_M. Given the solution $h(\mathbf{v})$ and exploiting property (3.41), for each element $\mathbf{u} \in \Lambda_{\mathbf{v}}$ we can compute $h(\mathbf{u}) = h(\mathbf{v})e^{j\theta}$. Therefore, we are only required to compute one vector value $h(\mathbf{v})$ for each identified partition $\Lambda_{\mathbf{v}}$.

For example, having constant M-ary PSK modulation in all carriers of order $K_m = K \ \forall m$, we obtain K^{M-1} partitions $\Lambda_{\mathbf{v}}$, reducing the number of required LUT entries to be computed from K^M to K^{M-1}. Complexity reductions of similar order can be obtained also for cases employing higher order modulations and mixed schemes. In the simulation results we provide the achieved complexity reductions for the considered scenarios (kindly refer to Section 3.3.4).

3.3.4 Simulation Results

In this section we numerically evaluate the performance gain of the proposed LUT predistortion technique with respect to multicarrier polynomial predistorter as described in [29, 31].

Figure of Merit

Performance of each channel m is evaluated by means of the Total Degradation (TD) [6] defined as,

$$TD|_{@BER} = \frac{E_s}{N_0}|_{NL} - \frac{E_s}{N_0}|_{AWGN} + OBO, \tag{3.43}$$

where $\frac{E_s}{N_0}|_{NL}$ is the signal to noise ratio needed in the considered non-linear channel to achieve the target bit error rate (BER) for the specific modulation and code scheme, $\frac{E_s}{N_0}|_{AWGN}$ is the signal to noise ratio achieving the same target BER with an identical transmission scheme but with a linear AWGN single carrier channel and, finally, the output back off (OBO) measures of the on-board HPA power efficiency. The Output back-off (OBO) is defined as $OBO = -10\log\frac{P_{out}}{P_{out}^{SAT}}$ where P_{out} and P_{out}^{SAT} are the output and saturated powers of the HPA, respectively. The total degradation results in a convex function of the output back-off providing for the optimal amplifier operating point.

System Parameters

The developed LUT technique is evaluated in three different scenarios with one, two and three carriers. The modulation scheme and code rate are selected from the DVB-S2 standard with amplitude phase shift keying (APSK) modulation and powerful low density parity check (LDPC) codes. Table 5.1 summarizes the channel settings.

Table 3.4: Simulation Parameters

Number of carriers	$M = 1, 2, 3$
Symbols rate , Roll Off	$R_s, \rho = 0.25$
Carrier frequency spacing, $\triangle f$	1.25 R_s
Modulation, Code	16 APSK, LDPC 2/3
Target BER	10^{-5}
Channel Estimation Noise	Es/No=12 dB
Training Symbols	15000

A training sequence is executed to estimate the channel parameters (refer to Section III.B) with a fixed channel noise level provided in Table 5.1. The parameters of the polynomial predistorter, implemented for comparison, are estimated using a training sequence with the same length and noise level.

Complexity and Convergence of LUT

Based on the simplification method provided in Section 3.3.3, we reduced the number of table entries that are required to be computed and the results are presented in Table 3.5.

Table 3.5: Computed Entries per Table

	$M=1$	$M=2$	$M=3$
Table Size	16	256	4096
Computed Entries	2	40	736

Each table entry is computed with the RLS algorithm provided in Section 3.3.3. The average squared error is defined as

$$e_M(j) = \frac{1}{l_M} \sum_{\mathbf{v} \in S_M} ||e^{(j)}||^2, \tag{3.44}$$

where l_m is the number of computed entries per table corresponding to the number of partitions $\Lambda_{\mathbf{v}}$. Convergence speed and residual error are dictated by parameters μ, λ and the number of iterations. RLS parameters for the considered cases are provided in Table 3.6.

Table 3.6: RLS Parameters

	$M=1$	$M=2$	$M=3$
Iterations	15000	15000	15000
μ	0.0075	0.005	0.005
λ	0.95	0.95	0.95

Convergence results are shown in Fig. 3.8 for each scenario Figure 3.8 shows the converge of the RLS algorithm to obtain the point-wise inversion of the channel function for different number or carriers M. Every curve is the result of the averaging of the run RLS algorithms in the number of the relevant table entries as 2, 40 and 736, respectively (kindly refer to (3.44) and Table 3.5). Figure 3.8 shows that the residual error increases with the number of carriers but similar convergence trend.

Performance Results

In this section we evaluate total degradation for the scenarios defined in Table 5.1. Figures 3.9,3.10 and 3.11 depict the TD for single, dual and triple carrier cases. In these plots we compare the performance for a channel without compensation (depicted as *No Compensation* in legend), multicarrier polynomial data DPD of [29, 31], a wideband signal predistorter similar to [16, 26] and the proposed LUT predistortion technique. Signal predistortion is applied on the multicarrier uplinked signal and it is defined as a memoryless complex polynomial function of degree 3. Considering M carriers with identical bandwidth $R_s(1+\rho)$ and an oversampling factor of K (typically $K=5$ to avoid

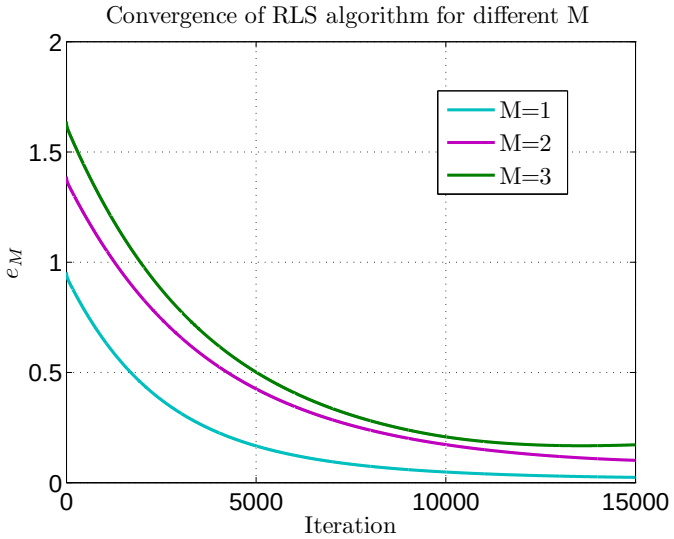

Figure 3.8: Convergence of RLS algorithm, Input Back-Off of 2.5 dB

aliasing caused by non-linear operations), signal predistortion requires a processing bandwidth of $KMR_s(1+\rho)$, while data predistortion only requires R_s. Further, signal predistoriton would cause spectral regrowth on the uplinked signal resulting in undesired out of band emission. For these reasons, performance comparison with signal predistortion is considered here for sake of completeness, although, as discussed in Section I, while its applicability is under consideration due to the aforementioned reasons.

As a benchmark case, we evaluated our novel technique for a single carrier scenario. In Fig. 3.9 the LUT-based predistortion gains more than 3 dB in the region of the minimum (OBO $\approx$ 0.9 dB) compared to the case when no compensation is applied. Moreover, about 1 dB is gained in the same region over the polynomial data DPD and about 0.5 dB over the signal predistortion solution.

In Fig. 3.10 we see the total degradation results for the dual carrier channel where only one carrier is shown for symmetry. In this case, the LUT-based predistortion gains more than 2 dB in the region of the minimum (OBO $\approx$ 1.4 dB) compared to the case when no compensation is applied. Moreover, about 1 dB is gained in the same region over the polynomial data DPD and about 0.5 dB over the signal predistortion technique. In general, for a given non-linear channel, the TD performance decreases as the number of carriers is increased.

In Fig. 3.11 we illustrate the TD for three carrier channel depicting one external carrier only (exploiting symmetry and denoted as (E)) and the internal carrier (denote as (I)). In this case, the LUT-based predistortion gains more than 1.5 dB in the region of the minimum (OBO $\approx$ 1.8 dB) compared to the case when no compensation is applied. Moverover, as shown in Fig. 3.11, gains can be gleaned over the polynomial solution and over signal predistortion. Notice that the overall gains obtained for this case by the LUT solution, are in line to the results provided in [1] for an identical channel configuration but using multicarrier iterative interference cancellation method at the receiver.

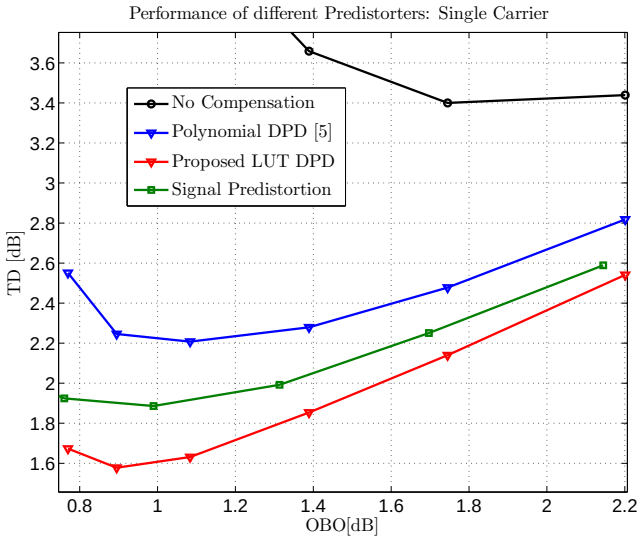

Figure 3.9: TD performance comparison: Single carrier case

In this section we presented a look up table based predistortion technique for multicarrier satellite channel. A novel analytical approach to estimate the entries of this table has been developed that exploits the structure of the channel modelling. Accordingly, a least squares minimization problem is formulated towards effecting the point-wise channel inversion. The predistorted symbols are obtained by solving this optimization problem using RLS. Moreover, a novel approach for LUT partitioning is presented leading to considerable complexity reduction in the computation of table entries. Performance is improved with respect to standard model based predistortion techniques, especially for a lower number of carriers. Moreover, polynomial based predistortion usually requires high complexity on-line processing while, the LUT solution is technologically more suitable for real time operation. This makes the proposed predistortion solution a good candidate for future multicarrier DVB-S2 based satellite communications.

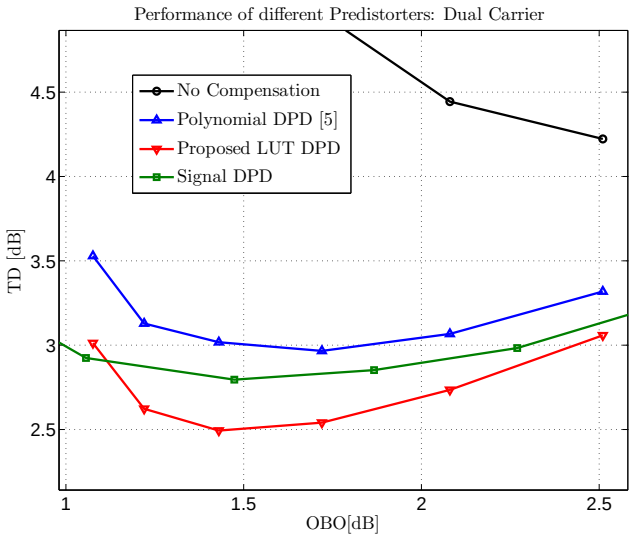

Figure 3.10: TD performance comparison: Dual carrier case, only one carrier presented

3.4 Comparisons and Conclusions

In this chapter we presented three innovative approaches to data predistortion for multiple carrier satellite systems: memory polynomial predistortion, orthogonal memory polynomial predistortion and LUT-based predistortion. All these techniques operate at the data level pre-canceling the generated ACI and ISI.

Memory polynomial data predistortion provides appreciable performance gain, is amenable to parameter adaptation and is applicable to any channel characteristics (in term of memory and non-linear degree). However it requires some on-line processing complexity for the computation of the polynomial terms. Orthogonal-based predistortion has similar characteristics in terms of performance and on-line complexity but requiring lower complexity for parameter estimation. Finally LUT-based predistortion provides improved performance in a quasi memory-less channel and low on-line operation complexity. However, it is not amenable for parameter adaptation to channel variations and channel memory effects are difficult to include due to the exponential complexity in the number of table entries to be estimated.

In order to have a complete picture on the presented techniques, we here compare the multiple carrier data predistortion based on polynomial functions and LUT-based predistortion with recently emerged signal predistortion techniques. As competitor techniques, we consider the signal predistortion for multiple carrier satellite channels proposed in [25] and the block-based signal predistortion proposed in [68].

In [25], signal predistortion based on memory polynomials functions is proposed and is applied on-ground to the uplinked multiple carrier signal. Uplink signal spectrum occupation is confined to adhere to regulations by applying an uplink filter mask. On the other hand, in [68] the same authors propose a differ-

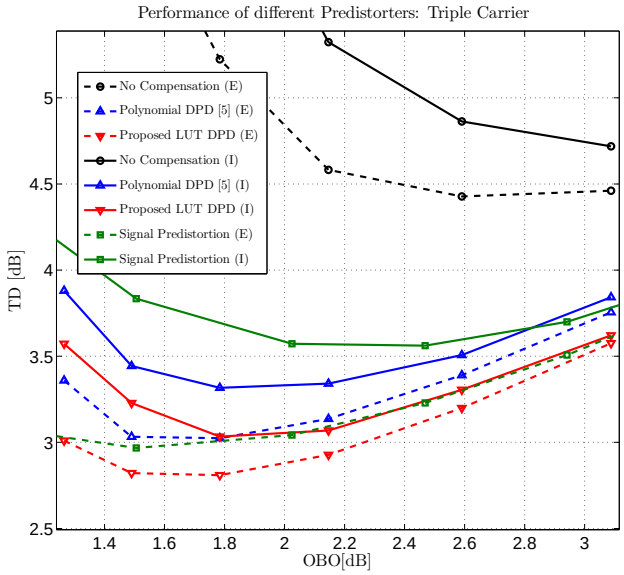

Figure 3.11: TD performance comparison: Three carriers case with external carrier (E) and internal Carrier (I)

ent implementation of [25] in which the predistortion is obtained by cascading two blocks: a memory-less LUT including the HPA inverse response; and a linear filter (FIR) to compensate for the channel memory effects. The filter is designed using a simple MSE approach to invert the channel IMUX and OMUX while neglecting the amplifier response. On the other hand, the memory-less LUT reproduces a one to one inversion of the AM/AM and AM/PM on-board amplifier response. Similarly to [25], the uplink signal spectrum is filtered prior to uplink in order to adhere regulations.

Performance is evaluated in terms of SINR (kindly refer to Fig. 3.12) with a chosen level of noise such that, $SNR = 20$ dB in absence of interference (only the central carrier is showed). This simple figure of merit provides an insight about the overall effects of generated interference on the link budget.

As reference channel model, we consider the three carrier satellite channel described in section 2.2.1 including IMUX, OMUX and the on-board power amplifier.

Fig. 3.12 presents a performance comparison between the following techniques as,

- *MC-DPD* as multiple carrier data predistortion as presented in section 3.1.4.
- *MC-LUT* as the memory-less multiple carrier data LUT presented in 3.3.3.
- *S-DPD* as the polynomial-based signal predistortion proposed of [25]
- *BLOCK-S-DPD* as the block based predistortion of [68]

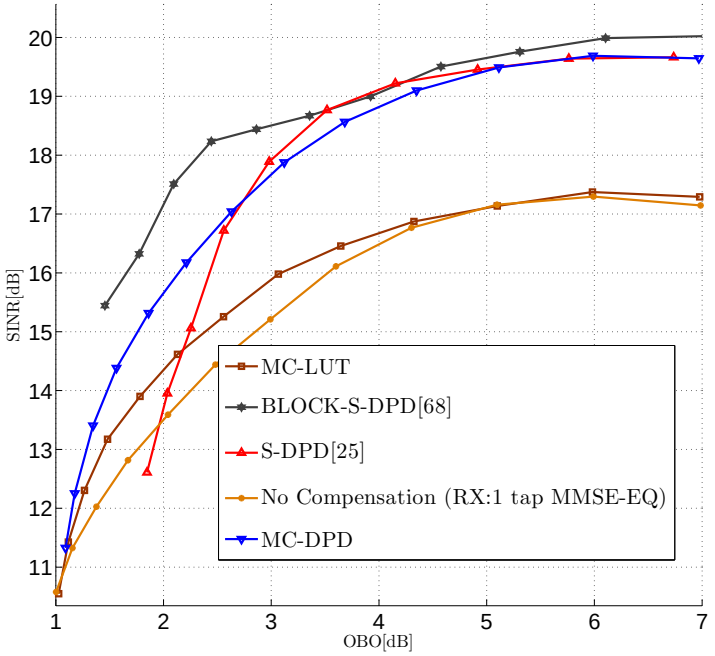

Figure 3.12: SINR Performa nce Comparison for Inner carrier in a Three Carrier Satellite Channel with modulation 16 APSK, $\rho = 0.2$, $\Delta f = 1.2R_s$

As discussed above, our proposed methods are compared with the wideband signal predistortion methods proposed in [25] and [68], respectively. Finally, the parameter estimation for all considered techniques is assumed to be noiseless. This aspect is key for the understanding of the results presented here with respect to the results presented in section 3.3.4 where a relatively high estimation noise was applied. Further, in section 3.3.4 the channel model does not include IMUX and OMUX filters resulting in negligible memory effects making the memory-less LUT-based predistortion a suitable approach matched to the channel characteristics.

The polynomial signal predistortion proposed in [25] provides performance similar to [68] in the high OBO region while it induces some performance degradation when the HPA is operated close to the saturation region. Multiple carrier data predistortion approaches the performance of signal predistortion techniques with only about 1 dB loss with respect to the method proposed in [68] in the low OBO region (2-3 dB). Further we notice that the LUT-based data predistortion is strongly penalized by the memory effects of the channel not included in the LUT model. In general, data predistortion techniques show a robust and stable performance behavioral when close to the HPA saturation region.

Table 3.7 provides a comprehensive comparison of the discussed techniques.

Notice that the on-line processing complexity of signal predistortion depends on the underlying implementation technology. The solution proposed in [25] includes memory polynomials requiring non-linear processing at an oversampled

Table 3.7: Performance and Complexity Comparison

	MC-DPD	MC-LUT	S-DPD [25]	BLOCK-S-DPD [68]
Estimation Complexity	Low/ Very Low	Very High	Low	Low
On-line Processing Complexity	Medium	Low	Very High	Medium
Adaptivity	Good	Poor	Good	Poor
Performance	Very Good	Good/Low	Very Good/Good	Very Good

rate with respect to the symbol rate of each carrier. On the other hand, the LUT implementation of [68] guarantees low on-line processing complexity but limiting the solution adaptivity to possible channel variations.

Multiple carrier data predistortion based on memory polynomials provides a good compromise between performance, adaptivity and complexity.

A final advantage of multiple carrier data predistortion with respect to standard signal predistortion techniques, is the possibility to integrate in a unique operation on one hand multiple carrier data predistortion aimed to cancel linear and non-linear ISI and ACI ; on the other, the transmitter pre-coding function for the compensation of adjacent beam interference enabling more efficient frequency usage schemes [69]. This aspect is briefly discussed in chapter 7 as future work.

Chapter 4

Improved Estimation Techniques for Multicarrier Predistortion

The performance of the predistortion function depends on the determination of the unknown parameters of the predistortion model. Recalling a general predistortion function (similar to (3.1) from section 3.1.4) we have,

$$x(n) = \phi(\mathbf{u}(n))^T \mathbf{w}, \tag{4.1}$$

where ϕ is the vector of linear and non-linear input combination and $\mathbf{w}$ is the parameters vector. Notice that the general predistortion function of (4.1) is linear in the parameters vector $\mathbf{w}$.

The parameters are traditionally estimated using the indirect estimation approach [26, 27] (kindly refer to Fig. 4.1).

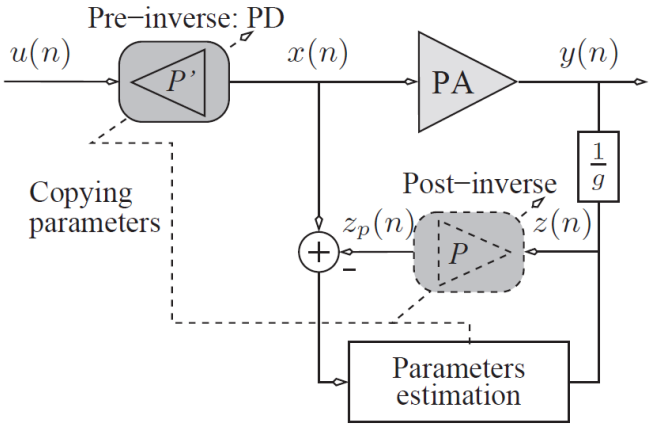

Figure 4.1: Indirect Learning Architecture

Accordingly to this method, the parameters are estimated such as the predistorter implements the channel post-inverse function. The learning architecture of Fig. 4.1 shows the estimation of the predistorter parameters in the lower branch; the channel output $y(n)$ is input to the predistorter (in the lower branch) whose coefficients are estimated such as the predistorter output resembles the channel input $x(n)$. The coefficients are then copied to the actual predistorter module. However, the optimality of this approach is not proven calling for the definition of other estimation methods to improve performance and robustness to noise. *Direct Estimation* of parameters for model based signal predistortion was proposed in [40] and critically evaluated in [39] (kindly refer to Fig. 4.2).

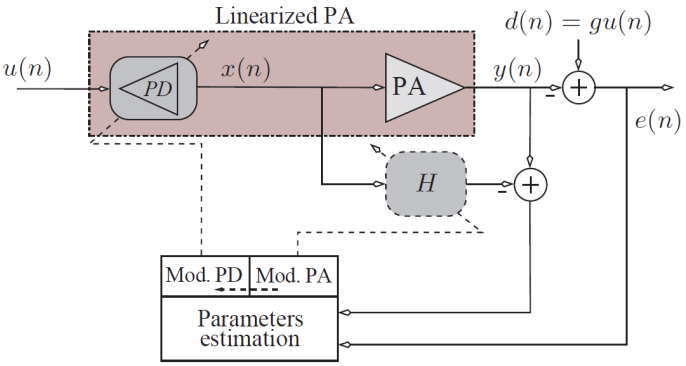

Figure 4.2: Direct Learning Architecture

As schematically illustrated in Fig. 4.2, for direct predistortion, the predistortion coefficients are directly estimated to reduce the channel output distortion implementing a so-called channel pre-inversion. In the following sections we propose advanced methods for predistortion parameter estimation under the general class of *Direct Learning*.

In the first section we consider the multiple carrier predistortion model presented in chapter 3.1.4 and we derive novel direct estimation methods. The focus of this first section is on data predistortion for multiple carriers. On the other hand, the second part of this chapter (kindly refer to section 4.2) investigates signal predistortion and proposes novel algorithms for direct learning and adaptive PAPR reduction techniques. Performance of the generalized signal predistortion in combination with CFR is evaluated for a multiple carrier satellite channel.

4.1 Multicarrier Data Predistortion Based on Direct Learning

4.1.1 Introduction

Key to the performance of the given predistorter is the ability to estimate the coefficients with high fidelity [39]. Two paradigms for the estimation of DPD

coefficients are explored in literature. The well known *indirect estimation* of the parameters leads to a post-channel inverse function as predistorter [16, 27]. This approach has a limited complexity but does not guarantee optimal performance with respect to the selected model [39]. On the other hand, the *direct estimation* method [40] leads to a predistorter function that resembles the channel pre-inverse function and provides better performance compared to indirect methods. Further, the direct method is shown to be robust to estimation noise [39], thereby easing the design requirements. While indirect methods have been considered for both single carrier and multicarrier scenarios [16], [29], the direct method has been considered only for single carrier scenario [40] where the parameter estimation is performed through the well known Recursive Least Squares (RLS) and Least Mean Squares (LMS) algorithms.

In this section we present our work [41] where we consider the direct estimation problem in the context of multicarrier satellite channels and present two novel optimization methods, namely Individual and Joint predistorter design, for estimation of predistorter parameters. The first method extends [40] by designing predistorters for each of the carriers individually, while a joint optimization of the predistorter parameters across carriers is undertaken in the latter method. Due to their formulation, these methods provide a complexity performance trade-off offering certain flexibility to the system designer. Building on the multicarrier Volterra model derived in [1] and the direct method estimation for single carrier provided in [40], we design novel adaptive multicarrier data predistortion mechanisms based on the low complexity memory polynomial model. Iterative algorithms are considered: RLS and LMS formulations for the parameter estimation have been derived and their convergence studied. Numerical evaluation of the techniques indicate a superior performance and robustness to noise of the proposed direct estimation compared to existing algorithms.

4.1.2 Multicarrier Satellite Channel with single on-board HPA

4.1.3 Scenario

A Ku-band ($12 - 18$ GHz) broadcasting application to fixed users employing a single Geostationary (GEO) satellite is considered. Further, a single GW is assumed to uplink multiple carriers to the GEO satellite where the composite signal will be processed by a single transponder. Each carrier provides an independent service; in a typical application different carriers could be relevant to different geographical location. Further, in common commercial applications such as TV broadcast, each UT can only decode its intended carrier.

System Model

In Fig. 5.2 we illustrate the overall multicarrier system model comprising a transmitting gateway, the satellite transponder and the on-ground receivers. The gateway performs the predistortion function and subsequently uplinks all the carriers. Let $u_m(n)$ be the modulated symbol on carrier m at the nth instance. The predistorted symbol of the mth carrier at the nth instance, denoted by $x_m(n)$, is obtained by jointly processing $\{u_m(n-k)\}_{m=1}^{M}$ with $-K < k < K$

where K indicates the (two sided) memory depth and M is number of carriers. Notice that if predistortion is not applied (no compensation) we simply have the identity $x_m(n) = u_m(n)\ \forall m, n$. The satellite transponder for multicarrier application includes wideband input and output multiplexing filters, namely IMUX and OMUX, and the HPA. The IMUX is used to eliminate out-of-band noise injection while OMUX is used to reduce out-of-band emission. The filter responses are extracted from [6], while we consider the well known Saleh model for the HPA [23]. The Saleh model is characterized by the AM/AM and AM/PM curves given by $A(r) = \frac{2r}{1+r^2}; \Phi(r) = \frac{\pi}{6}\frac{r^2}{1+r^2}$, respectively. Focusing on the non-linear impairments excited by the multicarrier application, we consider AWGN for the downlink. Since UT that can only decode its intended carrier, joint processing or multiple carriers cannot be supported by the receivers. Therefore, in order to target a realistic and commercially convenient scenario, in this study we do not consider any multi carrier equalization technique.

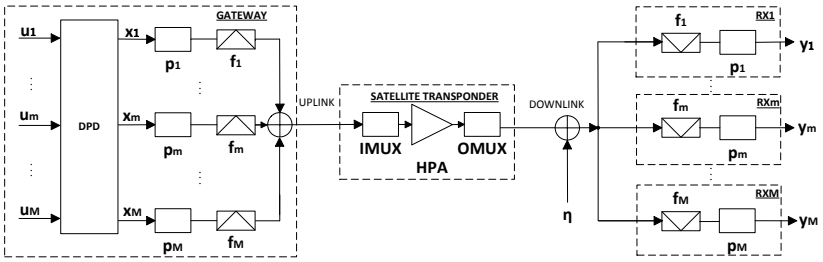

Figure 4.3: System model for a non-linear satellite channel with M carriers

Non-linear Channel Distortion Analysis

The aforementioned satellite channel can be modelled as a *non-linear system with memory* leading to constellation warping, ISI and ACI. The effect of these impairments are depicted in Figure 4.4 where the noiseless scatter plot of the 16 APSK modulated symbols received on the central carrier of a three carrier system is illustrated for the case of no compensation. The corresponding effect for the single carrier channel is also shown to highlight the significant increase of interference due to ACI and further motivate the need of specific countermeasures. Recalling that $u_m(n)$ is the modulated symbol on carrier m at time n, we define,

$$\mathbf{u}(n) = [u_1(n), \ldots, u_M(n)]^T, \tag{4.2}$$

$$\mathbf{u}_K(n) = [\mathbf{u}^T(n-K), \ldots \mathbf{u}^T(n+K)]^T, \tag{4.3}$$

where $\mathbf{u}(n)$ and $\mathbf{u}_K(n)$ are of drimensions $M \times 1$ and $(2K+1)M \times 1$ respectively. Here, $\mathbf{u}(n)$ is the vector of input symbols across M carriers at the instance n, while $\mathbf{u}_K(n)$ denotes a collection of $\mathbf{u}(n)$ for a specified time interval. We also define,

$$\mathbf{u}_K^{(d)}(n) = \underbrace{\mathbf{u}_K(n) \otimes \cdots \otimes \mathbf{u}_K(n)}_{\text{d times}}. \tag{4.4}$$

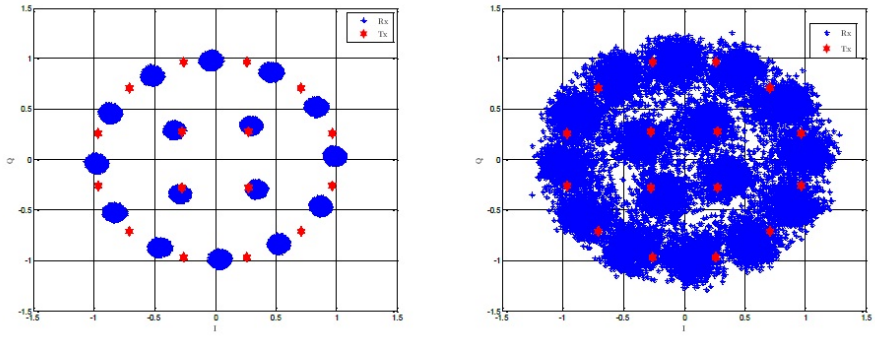

Figure 4.4: Scatter plots corresponding to single carrier (left) and multicarrier (right) signals for a five carrier noiseless non-linear satellite channel with Output Back Off (OBO)=3.6 dB

With these notations and considering a channel with no predistortion applied, we can express $y_m(n)$, the received symbols for the mth carrier at the nth sampling instance, using a general Volterra discrete time model [66] as

$$y_m(n) = y_m^{(1)}(n) + y_m^{(3)}(n) + y_m^{(5)}(n) + \ldots + \eta_m(n) \tag{4.5}$$

$$y_m^{(1)}(n) = \mathbf{g}_m^{(1)} \mathbf{u}_{K_1}{}^{(1)}(n) \tag{4.6}$$

$$y_m^{(3)}(n) = \mathbf{g}_m^{(3)} \mathbf{J}_m^{(3)} \mathbf{u}_{K_3}{}^{(2)}(n) \otimes [\mathbf{u}_{K_3}{}^{(1)}(n)]^* \tag{4.7}$$

$$y_m^{(5)}(n) = \mathbf{g}_m^{(5)} \mathbf{J}_m^{(5)} \mathbf{u}_{K_5}{}^{(3)}(n) \otimes [\mathbf{u}_{K_5}{}^{(2)}(n)]^*. \tag{4.8}$$

The row vectors $\mathbf{g}_m^{(p)}$ are the pth order Volterra kernel coefficients, $\eta_m(n)$ is the receiver noise on carrier m at nth instance and $\mathbf{J}_m^{(p)}$ is a selection matrix. In the complete Volterra representation, $\mathbf{J}_m^{(p)}$ corresponds to an identity matrix of dimension $((2K_p+1)M)^p$ where K_p is the (two sided) memory depth for degree p terms. However, such a representation has redundant terms like $u_1(n)u_2(n)u_3(n)^*$ and $u_2(n)u_1(n)u_3(n)^*$ and $\mathbf{J}_m^{(p)}$ can be used to eliminate redundant terms generated by the Kronecker products. In addition to providing a compact representation, $\mathbf{J}_m^{(p)}$ is used to select specific polynomial terms from the general model towards reducing the number of intermodulation products. In fact, the baseband model provided in (4.5) is valid only for intermodulation products that generate in-band distortion [1]. We define $\Omega_{m,d}$ as the set of intermodulation frequency products $(m_1, \ldots, m_d)$ of degree d that generate in band distortion to carrier m.

4.1.4 Memory Polynomial Predistortion and Channel Model

In this section, we define models used for the predistortion function and the non-linear channel. The channel model is described since it will be exploited in the estimation of the predistorter parameters.

Predistorter Model

We consider a memory polynomial model [29] for both the predistorter function and the channel model. This model is a special case of reduced complexity Volterra implementation where only the *diagonal* elements of the full model are considered. As documented in [1], the complexity of the Volterra model can be reduced by eliminating the kernel terms having negligible contribution (weight) while suffering only a minor loss in performance. In addition, to the best of authors' knowledge, a representation of the intermodulation products typical of the multicarrier non-linear channels [1] exists only for polynomial basis functions, thereby motivating their use.

The predistortion function is based on a complex polynomial function of the input symbols given by,

$$\phi^{\{d\}}_{m_1,\ldots,m_d}(\mathbf{u}(n)) = \prod_{j=1}^{(d+1)/2} u_{m_j}(n) \prod_{j=(d+1)/2+1}^{d} u^*_{m_j}(n), \tag{4.9}$$

where d is the polynomial degree and $(m_1,\ldots,m_d)$ are the selected product terms where each $m_i \in (1,\ldots,M)$. Recall that, for each carrier m and polynomial degree d, we have a specific set of in-band product terms enumerated in the set $\Omega_{m,d}$. This allows us to define,

$$\psi^{\{d\}}_m(\mathbf{u}(n)) = \{\phi^{\{d\}}_{m_1,\ldots,m_d}(\mathbf{u}(n))\}_{(m_1,\ldots,m_d)\in\Omega_{m,d}}, \tag{4.10}$$

as the $|\Omega_{m,d}| \times 1$ vector comprising polynomial function evaluations corresponding to the carrier combinations causing in-band distortion. We further define,

$$\chi^{\{d\}}_m = \Big[\Big[\psi^{\{d\}}_m(\mathbf{u}(n-K_d))\Big]^T, \Big[\psi^{\{d\}}_m(\mathbf{u}(n-K_d+1))\Big]^T, \ldots, \Big[\psi^{\{d\}}_m(\mathbf{u}(n+K_d))\Big]^T\Big]^T, \tag{4.11}$$

where $\chi^{\{d\}}_m$ is a $(2K_d+1)|\Omega_{m,d}| \times 1$ vector with (two sided) memory depth of K_d corresponding to degree d. Note that the memory depth is implicitly used for ease of notation. Finally we stack all the terms corresponding to different degrees as,

$$\phi_m(\mathbf{u}(n)) = \Big[\Big[\chi^{\{1\}}_m\Big]^T, \Big[\chi^{\{2\}}_m\Big]^T, \ldots, \Big[\chi^{\{p\}}_m\Big]^T\Big]^T, \tag{4.12}$$

where $\phi_m(\mathbf{u}(n))$ is now a $\sum_p (2K_p+1)|\Omega_{m,p}| \times 1$ dimensional vector.

Let $q_{m_1,\ldots,m_d}(k)$ denote the predistorter coefficient that will eventually weigh the basis function $\phi^{\{d\}}_{m_1,\ldots,m_d}(\cdot)$. Similar to (4.10), we first define,

$$\mathbf{q}^{\{d\}}_m(k) = \{q_{m_1,\ldots,m_d}(k)\}_{(m_1,\ldots,m_d)\in\Omega_{m,d}}, \tag{4.13}$$

to be a $|\Omega_{m,d}| \times 1$ coefficient vector corresponding to delay k. We further define,

$$\mathbf{z}^{\{d\}}_m = \Big[\Big[\mathbf{q}^{\{d\}}_m(-K_d)\Big]^T, \ldots, \Big[\mathbf{q}^{\{d\}}_m(K_d)\Big]^T\Big]^T, \tag{4.14}$$

where $\mathbf{z}_m^{\{d\}}$ is a $(2K_d+1)|\Omega_{m,d}|\times 1$ vector with K_d being the (two sided) memory depth of the predistorter function relative to degree d. We finally define the vector of predistorter coefficients for carrier m as,

$$\mathbf{w}_m = \left[\left[\mathbf{z}_m^{\{1\}}\right]^T, \ldots, \left[\mathbf{z}_m^{\{p\}}\right]^T\right]^T, \tag{4.15}$$

where $\mathbf{w}_m$ is a $\sum_p (2K_p+1)|\Omega_{m,p}| \times 1$ vector.

Having defined relevant quantities, the predistorter output $x_m(n)$ can now be defined similarly to [29] as an inner product between the non-linear input combination vector ϕ_m and the kernel coefficients $\mathbf{w}_m$,

$$x_m(n) = \mathbf{w}_m^T \left[\phi_m(\mathbf{u}(n))\right]. \tag{4.16}$$

A key aspect of the formulation is the linear dependence of $x_m(n)$ on $\mathbf{w}_m$, a fact that will be exploited later. The predistorted symbols $x_m(n)$ are then upsampled, filtered and transmitted through the non-linear channel. Towards further analysis, a channel model relating $\{x_m(n)\}$ to the output is needed; this is taken up next.

Reduced Complexity Channel Model

Rather than the full Volterra representation of (4.5), we select the memory polynomial function to model the channel. Such a model has the same form as the predistorter. This choice is motivated by the nature of the satellite channel where the memory effects are minor [29]. Such a simplification reduces the number of parameters, thereby simplifying the analysis and reducing the complexity of implementation. Further, such a choice provides a formulation that could be easily generalized to the complete Volterra model. Similar to (4.16), we can then express the output of the channel as,

$$y_m(n) = \mathbf{h}_m^T \left[\phi_m(\mathbf{x}(n))\right], \tag{4.17}$$

where $\phi_m(\cdot)$ now takes predistorted symbols, $\mathbf{x}(n) = [x_1(n) \ldots x_M(n)]^T$, as inputs and $\mathbf{h}_m$ denotes the channel co-efficients and are defined similarly to $\mathbf{w}_m$ in (4.15). With the channel model in place, we now briefly describe the estimation of the model parameters $\mathbf{h}_m$, which would be later used in the predistorter design.

Estimation of Channel Parameters

Given N samples of transmitted and received symbols, $\mathbf{x}(\cdot)$ and $y_m(\cdot)$ respectively, we consider minimizing, $\sum_{n=0}^{N-1} |y_m(n) - \mathbf{h}_m^T \left[\phi_m(\mathbf{x}(n))\right]|^2$. Towards this, we stack these quantities to obtain,

$$\mathbf{v}_m = [y_m(0), \ldots, y_m(N-1)]^T, \tag{4.18}$$

$$\mathbf{Z}_m = \begin{bmatrix} [\phi_m(\mathbf{x}(0))]^T \\ \vdots \\ [\phi_m(\mathbf{x}(N-1))]^T \end{bmatrix}, \tag{4.19}$$

so that the minimization reduces to $\|\mathbf{v}_m - \mathbf{Z}_m\mathbf{h}_m\|^2$. The least squares solution for $\mathbf{h}_m$ is then straightforward, leading to,

$$\mathbf{h}_m = (\mathbf{Z}_m^H\mathbf{Z}_m)^{-1}\mathbf{Z}_m^H\mathbf{v}_m. \tag{4.20}$$

Instead of the block implementation provided in (4.20), an iterative approach based on the RLS is considered similarly to [40]. Such an implementation will iteratively improve the estimate of $\mathbf{h}_m$ and will be exploited in the sequel for the estimation of predistorter parameters. Having determined the necessary quantities, we now proceed with the central theme of estimating $\{\mathbf{w}_m\}_m$.

- Estimation of Predistortion Parameters Two methodologies to estimate the predistorter parameters are prevalent in the literature. These are the *indirect* and *direct* methods [16], [40]. Typically predistortion design assumes a system where the receiver is capable of feeding back training data to the transmitter [6]. In the current work, we assume the presence of a dedicated multicarrier receiver connected to the GW and relaying the requisite data for the estimation of predistortion parameters. These special receivers are operator installed and are different from the standard user terminals. Indirect estimation is illustrated in

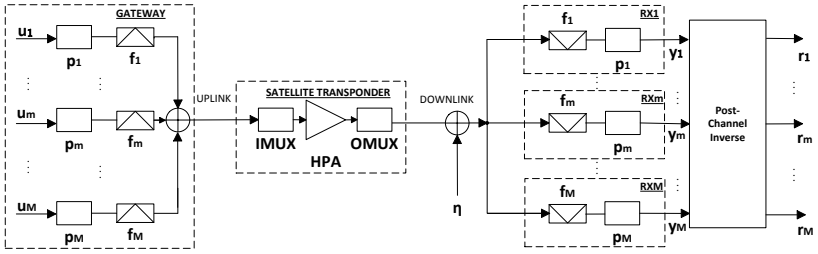

Figure 4.5: Multiple Carrier Post-inverse Channel Estimation Scheme

Fig. 4.5, where the post-inverse is modelled as $r_m(n) = \mathbf{w}_m^T[\phi_m(\mathbf{y}(n))]$. Note here that the arguments of $\phi_m(\cdot)$ are now the channel outputs, $\mathbf{y}(n) = [y_1(n), \ldots, y_M(n)]^T$. The methodology is to estimate $\mathbf{w}_m$ such that $E[|u_m(n) - r_m(n)|^2] \approx \frac{1}{N}\sum_{n=0}^{N-1}|u_m(n) - r_m(n)|^2$ is minimized for each $m \in (1, \ldots, M)$ and a given training sequence of length N. In other words, the channel inverse function with parameters $\mathbf{w}_m$ would process the channel output samples $\mathbf{y}(n)$ yielding, in the ideal case, the original input transmitted symbols $u_m(n)$. This is a standard Least Squares problem with a simple derivation and a low complexity implementation. Following the steps leading to the solution of $\mathbf{h}_m$ in (5.25), we can obtain

$$\mathbf{w}_m = (\mathbf{\Theta}_m^H\mathbf{\Theta}_m)^{-1}\mathbf{\Theta}_m^H\mathbf{s}_m \qquad \text{Indirect Method} \tag{4.21}$$

where $\mathbf{s}_m = [u_m(0), \ldots, u_m(N-1)]^T$ and $\mathbf{\Theta}$ is similar to $\mathbf{Z}$ in (4.18) with $\phi_m(\mathbf{x}(k))$ replaced by $\phi_m(\mathbf{y}(k))$. Kindly note in the current work, the indirect learning architecture, as proposed originally in [26] is not

implemented. Instead, similar to [16], we solve the post inverse LS estimation problem offline. It is important to point out that indirect estimation does not *directly* target the receiver error minimization defined as $E[|u_m(n) - y_m(n)|^2]$. However, it relies on the argument that the channel pre and post-inverses are equivalent. Such an argument has been proven in [24] for the single carrier case. The *direct* estimation method [40] overcomes this discrepancy and will be discussed in the following sections.

4.1.5 Direct Estimation

Problem Formulation

We now discuss a different approach for the estimation of $\mathbf{w}_m$ that *directly* targets the minimization of the interference at the receiver $e_m(n) = u_m(n) - y_m(n)$. While the formulation of the direct estimation is straight forward in the single carrier, the case is not so for multicarrier scenario (refer to Fig. 4.6). We consider the following interesting formulations,

- *M Individual* cost functions:
  - $E[C(\mathbf{w}_m(n))]$ with $C(\mathbf{w}_m(n)) = |e_m(n)|^2, m \in (1, \ldots, M)$
- *Joint* cost function:
  - $E[C(\mathbf{w}_1(n), \ldots, \mathbf{w}_M(n))]$ with $C(\mathbf{w}_1(n), \ldots, \mathbf{w}_M(n)) = \sum_{m=1}^{M} |e_m(n)|^2$

Individual estimation of predistortion parameters reduces to M distinct optimization processes, while *Joint* corresponds to a global optimization process. Further, minimizing each $E[C(\mathbf{w}_m(n))]$ separately is not equivalent to minimizing the global cost $E[C(\mathbf{w}_1(n), \ldots, \mathbf{w}_M(n))]$.

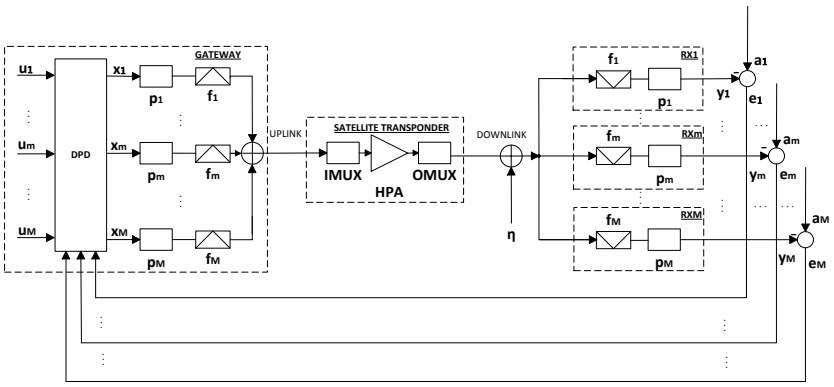

Figure 4.6: Multiple Carrier Pre-inverse Channel Estimation Scheme

Unlike the indirect approach, the direct estimation cannot be formulated as a standard least squares problem [40]. As a consequence, it can only be

implemented through iterative techniques. We now elaborate the iterative formulations for the direct estimation where the well known LMS and RLS are considered with some modifications.

Individual Predistorter Design

In this section, we develop first order techniques aimed at minimizing the error $E[|e_m(n)|^2]$, separately on each carrier, with respect to its corresponding predistortion coefficients $\mathbf{w}_m$ (kindly refer to Fig. 4.7). These algorithms ap-

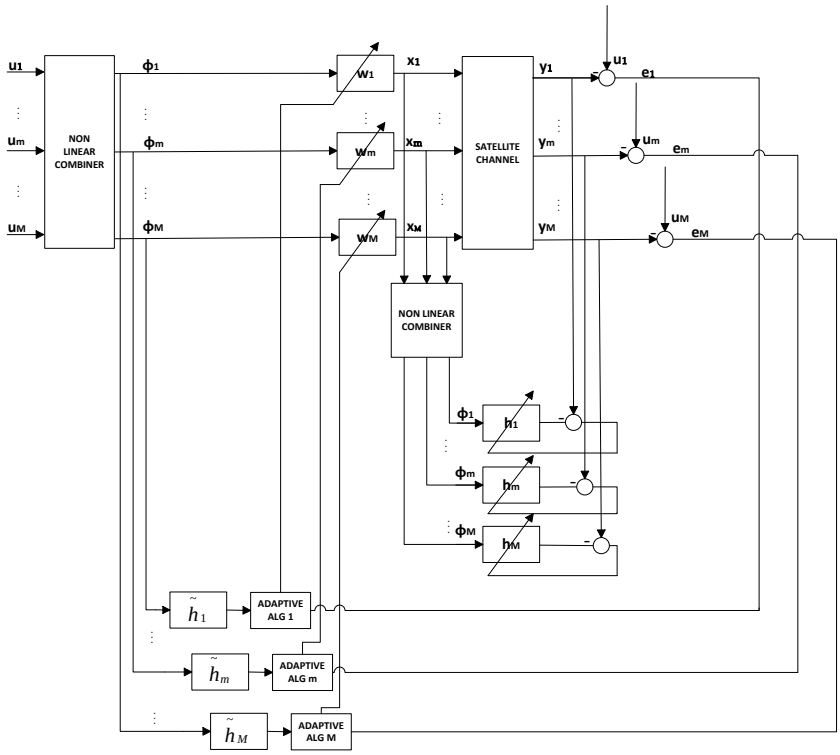

Figure 4.7: Functional scheme describing the individual direct estimation method

proximate $E[|e_m(n)|^2]$ and provide an iterative approach towards the solution. The simpler LMS algorithm is presented first followed by the RLS technique that yields superior performance at the cost of added complexity.

- LMS Formulation In the standard LMS algorithm, we consider the instantaneous error magnitude, $C_m(\mathbf{w}_m(n))$, as the cost function. Thus, in the pursued iterative optimization solution, the predistorter coefficients are updated as,

$$\mathbf{w}_m(n+1) = \mathbf{w}_m(n) + \frac{\mu}{2}\frac{\partial C_m(\mathbf{w}_m(n))}{\partial \mathbf{w}_m(n)}. \tag{4.22}$$

In (4.22), the iteration index is explicitly depicted and we will continue to do so when dealing with updates of the predistorter coefficients. Since $C_m(\mathbf{w}_m(n)) = |e_m(n)|^2$, (4.22) can be approximated to,

$$\mathbf{w}_m(n+1) = \mathbf{w}_m(n) + \mu e_m^*(n) \frac{\partial y_m(n)}{\partial \mathbf{w}_m(n)}. \tag{4.23}$$

Similarly to [40], we define the Instantaneous Equivalent Filter (IEF) relative to carrier m as,

$$\tilde{h}_m(n,l) = \frac{\partial y_m(n)}{\partial x_m(n-l)}. \tag{4.24}$$

The IEL can be analytically extracted using (4.17) as,

$$\tilde{h}_m(n,l) = \mathbf{h}_m^T \frac{\partial \phi_m(\mathbf{x}(n))}{\partial x_m(n-l)}, \tag{4.25}$$

where computation of the entries of $\frac{\partial \phi_m(\mathbf{x}(n))}{\partial x_m(n-l)}$ is based on the application of the partial differential rules defined in [67] to multicarrier complex polynomial functions (kindly refer to Appendix A.1). The gradient $\frac{\partial y_m(n)}{\partial \mathbf{w}_m(n)}$ can be expressed using the channel differentiability and the chain rule as,

$$\frac{\partial y_m(n)}{\partial \mathbf{w}_m(n)} = \sum_{l=-K}^{K} \tilde{h}_m(n,l) \frac{\partial x_m(n-l)}{\partial \mathbf{w}_m(n)}. \tag{4.26}$$

Recalling $x_m(n-l) = \mathbf{w}_m^T(n-l)\,[\phi_m(\mathbf{u}(n-l))]$ from (4.16), and approximating $\mathbf{w}_m(n) \approx \mathbf{w}_m(n-l)$ within memory range (similarly to [40]), we obtain,

$$\frac{\partial x_m(n-l)}{\partial \mathbf{w}_m(n)} \approx \phi_m(\mathbf{u}(n-l)). \tag{4.27}$$

Using (4.27) and (4.25) in (4.26), we have,

$$\frac{\partial y_m(n)}{\partial \mathbf{w}_m(n)} = \sum_{l=-K}^{K} \tilde{h}_m(n,l) \phi_m(\mathbf{u}(n-l)) \tag{4.28}$$

Equation (4.28) together with (4.23) provides the LMS step for the optimization. Notice that each vector $\mathbf{w}_m(n)$ is initialized such that the resulting predistortion functions simply correspond to $x_m(n) = u_m(n), \forall\, m$. As an example, if $K_d = 0, \forall d$ (no memory), then $\mathbf{w}_m(0)$ corresponds to the mth standard basis of dimension $\sum_p |\Omega_{m,p}| \times 1$.

- RLS Formulation For each carrier m, we now minimize $C_m(\mathbf{w}_m(n)) = \sum_{i=1}^{n} \lambda^{n-i} |e_m(i)|^2$ with respect to the corresponding $\mathbf{w}_m(n)$. The choice of the forgetting factor λ affects the performance and will be discussed in the simulation section. As a first step towards defining the RLS, we set,

$$-2 \sum_{i=1}^{n} \lambda^{n-i} \frac{\partial y_m(i)}{\partial \mathbf{w}_m(n)} e_m^*(i) = \mathbf{0}. \tag{4.29}$$

Similarly to [40], we use the weak non-linearity assumption to approximate the instantaneous channel output as,

$$y_m(n) \approx \sum_{l=-K}^{K} \tilde{h}_m(n,l) x_m(n-l). \tag{4.30}$$

Referring to Appendix A.2 and using (4.30), we arrive at the following standard formulation for (4.29),

$$\begin{aligned} \mathbf{R}_m(n)\mathbf{w}_m(n) &= \mathbf{r}_m(n), \quad \text{where} \\ \mathbf{R}_m(n) &= \sum_{i=1}^{n} \lambda^{n-i} \left[\frac{\partial y_m(i)}{\partial \mathbf{w}_m(n)}\right]^* \left[\frac{\partial y_m(i)}{\partial \mathbf{w}_m(n)}\right]^T, \\ \mathbf{r}_m(n) &= \sum_{i=1}^{n} \lambda^{n-i} \left[\frac{\partial y_m(i)}{\partial \mathbf{w}_m(n)}\right]^* \mathbf{u}_m(i). \end{aligned} \tag{4.31}$$

The formulation in (4.31) is amenable to a RLS implementation involving the following updates,

$$\mathbf{w}_m(n+1) = \mathbf{w}_m(n) + \mu \mathbf{k}_m(n) e_m(n), \tag{4.32}$$

where the gain vector $\mathbf{k}_m$ is obtained from,

$$\mathbf{k}_m(n) = \frac{\lambda^{-1}\mathbf{P}_m(n-1)\left[\frac{\partial y_m(n)}{\partial \mathbf{w}_m(n)}\right]}{1+\lambda^{-1}\left[\frac{\partial y_m(n)}{\partial \mathbf{w}_m(n)}\right]^H \mathbf{P}_m(n-1)\left[\frac{\partial y_m(n)}{\partial \mathbf{w}_m(n)}\right]}, \tag{4.33}$$

and the positive semidefinite matrix $\mathbf{P}_m$ satisfies the recursive relation,

$$\mathbf{P}_m(n) = \lambda^{-1}(\mathbf{P}_m(n-1) - \mathbf{k}_m(n)\left[\frac{\partial y_m(n)}{\partial \mathbf{w}_m(n)}\right]^H \mathbf{P}_m(n-1)). \tag{4.34}$$

Notice that, we choose $\mathbf{P}_m(0) = \mathbf{I}$ and $\mathbf{w}_m(n)$ is initialized as in Section 4.1.5. Further note that the evaluation of $\frac{\partial y_m(n)}{\partial \mathbf{w}_m(n)}$ follows from Section 4.1.5.

The individual estimation method results in M independent optimization processes to be run in parallel generating M predistortion coefficients vector $\{\mathbf{w}_m\}$. In the following section, we pursue a completely different approach where all predistortion parameters are estimated jointly towards achieving a global optimum.

Joint Predistorter Design

Each channel output $y_m(n)$ is a function of the predistorted symbols $\mathbf{x}(n)$ from all M input carriers as defined in (4.17). Intuitively, this calls for a joint estimation of the predistorter coefficients $\mathbf{w}_m$. In this section we develop first order techniques aimed to minimize the cost function $E[\sum_{m=1}^{M} |e_m(n)|^2]$ with respect to the predistortion coefficients of all the M carriers, compactly defined here as,

$$\mathbf{w} = [\mathbf{w}_1^T, \ldots, \mathbf{w}_M^T]^T. \tag{4.35}$$

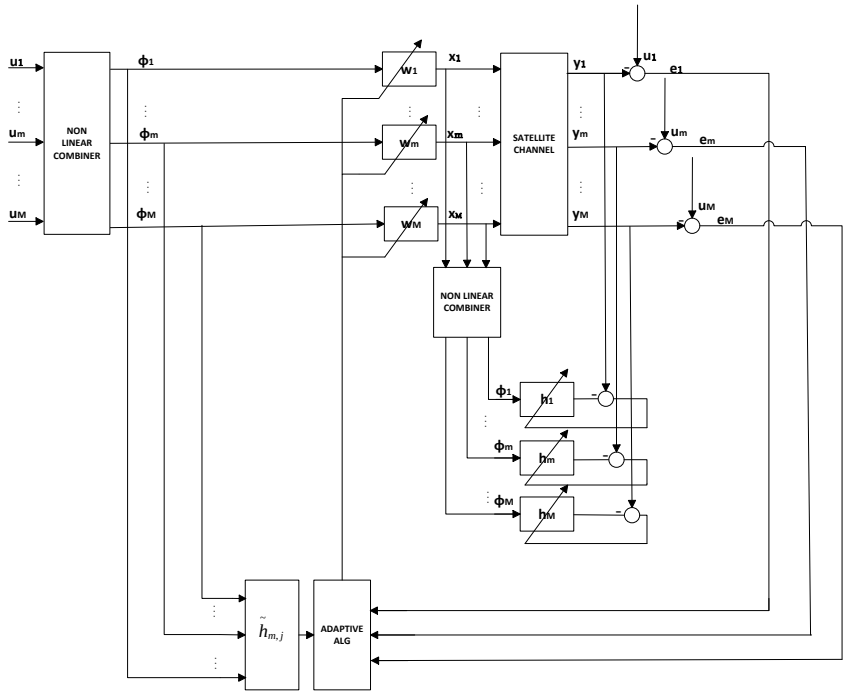

Figure 4.8: Functional scheme describing the joint direct estimation method

In Fig. 4.8 the scheme of the joint estimation method is illustrated. As mentioned earlier, joint estimation of $\{\mathbf{w}_m\}$ is not a generalization of the individual optimization method described in Section 4.1.5. The joint estimation methodology exploits the interdependence between channel outputs $y_m(n)$ and kernel coefficients $\mathbf{w}_i(n), i \neq m$. This results in an improved performance compared to the individual estimation, but at the cost of higher complexity.

- LMS Formulation The standard LMS formulation for this problem can be written similarly to (4.22). With $C(\mathbf{w}(n)) = \sum_{m=1}^{M} |e_m(n)|^2$, we use the update equation,

$$\mathbf{w}(n+1) = \mathbf{w}(n) + \mu \sum_{m=1}^{M} \frac{\partial y_m(n)}{\partial \mathbf{w}(n)} e_m^*(n). \tag{4.36}$$

  Based on form of $\mathbf{w}$ described in (4.35), we define the $\sum_m \sum_p (2K_p + 1)|\Omega_{m,p}| \times 1$ dimensional column vector $\frac{\partial y_m(n)}{\partial \mathbf{w}(n)}$ as,

$$\frac{\partial y_m(n)}{\partial \mathbf{w}(n)} = \left[\frac{\partial y_m(n)}{\partial \mathbf{w}_1(n)}^T \cdots \frac{\partial y_m(n)}{\partial \mathbf{w}_M(n)}^T \right]^T. \tag{4.37}$$

  Notice the complexity increase required for the computation of terms $\{\frac{\partial y_m(n)}{\partial \mathbf{w}(n)}\}_{m=1}^{M}$ in (4.37) compared to the individual LMS estimation in (4.23) where only terms $\{\frac{\partial y_m(n)}{\partial \mathbf{w}_m(n)}\}_{m=1}^{M}$ are required.

Similarly to [40], we define the Instantaneous Equivalent Filter (IEF) relative to carrier m with respect to carrier j as,

$$\tilde{h}_{m,j}(n,l) = \frac{\partial y_m(n)}{\partial x_j(n-l)}. \tag{4.38}$$

Note, that unlike in (4.24) of Section 4.1.5, we include here two subscripts for carrier m and j, respectively. Further, similar to (4.25), we have,

$$\tilde{h}_{m,j}(n,l) \quad = \quad \mathbf{h}_m^T \frac{\partial \phi_m(\mathbf{x}(n))}{\partial x_j(n-l)}. \tag{4.39}$$

In (4.39), the entries of $\frac{\partial \phi_m(\mathbf{x}(n))}{\partial x_j(n-l)}$ are computed based on the partial differential rules defined in [67] elaborated to the case of multicarrier complex polynomial functions (kindly refer to Appendix A.1). Each differential vector $\frac{\partial y_m(n)}{\partial \mathbf{w}_j(n)}$ in (4.37) can be expressed exploiting channel differentiability and the chain rule as,

$$\frac{\partial y_m(n)}{\partial \mathbf{w}_j(n)} = \sum_{l=-K}^{K} \tilde{h}_{m,j}(n,l) \frac{\partial x_j(n-l)}{\partial \mathbf{w}_j(n)}, \tag{4.40}$$

where

$$\frac{\partial x_j(n-l)}{\partial \mathbf{w}_j(n)} \approx \phi_m(\mathbf{u}(n-l)). \tag{4.41}$$

Using (4.41) and (4.39) in (4.40), we finally obtain an expression for the gradient as,

$$\frac{\partial y_m(n)}{\partial \mathbf{w}_j(n)} = \sum_{l=-K}^{K} \tilde{h}_{m,j}(n,l) \phi_m(\mathbf{u}(n-l)). \tag{4.42}$$

Equations (4.42) and (4.37) together with (4.36) provide the LMS step for the optimization.It should be noted that, even in this case, the individual vectors $\mathbf{w}_m(0)$ are initialized as in Section 4.1.5 and the global vector $\mathbf{w}(0)$ obtained from (4.35).

- RLS Formulation The objective function to be minimized with respect to the overall predistortion coefficients vector $\mathbf{w}$ defined in (4.35) takes the form $C(\mathbf{w}(n)) = \sum_{j=1}^{M} \sum_{i=1}^{n} \lambda^{n-i} |e_j(i)|^2$ where λ is the forgetting factor. To proceed with the analysis, we introduce,

$$\mathbf{e}(n) \quad = \quad [e_1(n), \ldots, e_M(n)]^T \tag{4.43}$$

$$\frac{\partial \mathbf{y}(i)}{\partial \mathbf{w}(n)} \quad = \quad \left[\frac{\partial y_1(i)}{\partial \mathbf{w}(n)}, \ldots, \frac{\partial y_M(i)}{\partial \mathbf{w}(n)} \right] \tag{4.44}$$

where $\frac{\partial \mathbf{y}(i)}{\partial \mathbf{w}(n)}$ is $\sum_m \sum_p |\Omega_{m,p}| \times M$ matrix and $\frac{\partial y_m(i)}{\partial \mathbf{w}(n)}$ is obtained from (4.37). Notice in (4.44), as with the joint LMS formulation of Section 4.1.5, we can identify a complexity increase with respect to the individual RLS estimation in (4.29) where only terms $\{\frac{\partial y_m(n)}{\partial \mathbf{w}_m(n)}\}_{m=1}^{M}$ are required.

Towards defining the global RLS, we set,

$$-2\sum_{i=1}^{n}\lambda^{n-i}\frac{\partial \mathbf{y}(i)}{\partial \mathbf{w}(n)}\mathbf{e}^{*}(i)=\mathbf{0}. \tag{4.45}$$

Similarly to [40], we use the weak non-linearity assumption to approximate the instantaneous channel output as,

$$y_m(n)\approx\sum_{l=-K}^{K}\sum_{j=1}^{M}\tilde{h}_{m,j}(n,l)x_j(n-l). \tag{4.46}$$

Referring to Appendix A.3, the weak non-linearity approximation of (4.46), and using the definition in (4.44), we obtain for (4.45) a recursive solution:

$$\begin{aligned}\mathbf{R}(n)\mathbf{w}(n) &= \mathbf{r}(n), \qquad (4.47)\\ \mathbf{R}(n) &= \sum_{i=1}^{n}\lambda^{n-i}\left[\frac{\partial \mathbf{y}(i)}{\partial \mathbf{w}(n)}\right]^{*}\left[\frac{\partial \mathbf{y}(i)}{\partial \mathbf{w}(n)}\right]^{T}\\ \mathbf{r}(n) &= \sum_{i=1}^{n}\lambda^{n-i}\left[\frac{\partial \mathbf{y}(i)}{\partial \mathbf{w}(n)}\right]^{*}\mathbf{u}(i).\end{aligned}$$

This leads to the following recursive set of equations,

$$\mathbf{w}(n+1)=\mathbf{w}(n)+\mu\mathbf{K}(n)\mathbf{e}(n), \tag{4.48}$$

$$\begin{aligned}\mathbf{K}(n)=\lambda^{-1}\mathbf{P}(n-1)&\frac{\partial \mathbf{y}(n)}{\partial \mathbf{w}(n)}\times\\ &(\mathbf{I}+\lambda^{-1}\left[\frac{\partial \mathbf{y}(n)}{\partial \mathbf{w}(n)}\right]^{H}\mathbf{P}(n-1)\frac{\partial \mathbf{y}(n)}{\partial \mathbf{w}(n)})^{-1},\end{aligned}$$

$$\mathbf{P}(n)=\lambda^{-1}(\mathbf{P}(n-1)-\mathbf{K}(n)\left[\frac{\partial \mathbf{y}(n)}{\partial \mathbf{w}(n)}\right]^{H}\mathbf{P}(n-1)). \tag{4.49}$$

Unlike in Section 4.1.5, we now deal with a $\sum_m\sum_p|\Omega_{m,p}|\times M$ gain matrix $\mathbf{K}(n)$ in the update equations. Notice that $\mathbf{P}(0)=\mathbf{I}$ and $\mathbf{w}(0)$ is initialized as in the earlier section.

4.1.6 Simulation Results

In the following, we compare the performance of the proposed direct estimation method for a multicarrier memory polynomial predistorter with respect to the known indirect approach. Through extensive numerical simulations covering several scenarios, we evaluate the gain obtained by the proposed approach. Such an evaluation combines both power efficiency and error performance, since the two quantities are typically in conflict.

Figure of Merit

Total Degradation is a standard figure of merit for evaluating the performance over non-linear channels [6, 20]. It is defined as,

$$TD|_{@BER}=\frac{E_s}{N_0}|_{NL}-\frac{E_s}{N_0}|_{AWGN}+OBO \tag{4.50}$$

where $\frac{E_s}{N_0}|_{NL} - \frac{E_s}{N_0}|_{AWGN}$ represents the energy loss between the non-linear and linear channels for a given target bit error rate (BER). OBO is defined as the ratio in dB between the multicarrier signal output power and the saturation output power of the selected amplifier model. For the considered amplifier model we have a nominal saturation output power of 0 dB. When the amplifier is operated in high efficiency region it yields strong distortion effects increasing the needed $\frac{E_s}{N_0}|_{NL}$, while in linear operation we have a power efficiency degradation accounted by the measure of OBO. The total degradation is illustrated as a function of the OBO resulting in a convex curve whose minimum identifies the optimal amplifier operating point. Notice that (6.27) reduces to $TD|_{@BER} = OBO$ in case of perfect compensation or absence of non-linear interference and serves as a lower bound.

Set Up

Referring to Fig. 5.2, we consider two channel scenarios with three and five equally spaced carriers, respectively. Spectrally efficient modulation schemes are applied in each carrier channel. The set of channel parameters are summarized in Table 5.1. In Table 5.1, the DPD parameter estimation noise corresponds

Table 4.1: Simulation Parameters

Number of carriers	$M_c = 3,\ 5$
Symbols rate, Roll Off	$R_s = 8$ MBaud, $\rho = 0.25$
Carrier frequency spacing, $\triangle f$	1.25 R_s
Modulation, Coderate (LDPC)	16 APSK, 2/3
Target BER	10^{-5}
$\frac{E_s}{N_0}\|_{AWGN}$ @ Target BER	9.05 dB
DPD parameter estimation noise	$\frac{E_s}{N_0} = 9.05$ dB
HPA	Saleh model [23]
Channel filters IMUX /OMUX	$BW_{1dB} \approx\ M\ R_s(1+\rho)$
Oversampling factor	20

to the receiver $\frac{E_s}{N_0}$ set during the estimation of the kernel parameter for all the considered techniques. A high oversampling is needed for simulating the chain due to the spectral enlargement caused by non-linearities.

Predistortion Structure

In order to have a fair comparison among the different parameter estimation techniques, the structure and complexity of the underlying predistortion function is kept the same. Moreover 10000 training symbols are used in all the techniques. This allows us to identify the gains obtained from better parameter estimation. In particular, the memory polynomial model defined in (4.16) is used with a memory depth of three ($K_d = 1, \forall d$) and polynomial degree of three ($d = 3$). Table C.1 provides the frequency-centered intermodulation products $\Omega_{m,d}$ derived in [1] and included in the predistorter evaluation for the three and

Table 4.2: Frequancy Centered IMD [1]: (a) Three Carrier Channel In-band Terms, (b) Five Carriers Channel In-band Terms

(A)

$\Omega_{1,3}$	$\Omega_{2,3}$	$\Omega_{3,3}$
[111]	[121]	[131]
[122]	[132]	[221]
[133]	[222]	[232]
[223]	[233]	[333]

(B)

$\Omega_{1,3}$	$\Omega_{2,3}$	$\Omega_{3,3}$	$\Omega_{4,3}$	$\Omega_{5,3}$
[111]	[121]	[131]	[141]	[151]
[122]	[132]	[142]	[152]	[241]
[133]	[143]	[153]	[231]	[252]
[144]	[154]	[221]	[242]	[331]
[155]	[222]	[232]	[253]	[342]
[223]	[233]	[243]	[332]	[353]
[234]	[244]	[254]	[343]	[443]
[245]	[255]	[333]	[354]	[454]
[335]	[334]	[344]	[444]	[555]
[-]	[345]	[355]	[455]	[-]
[-]	[-]	[445]	[-]	[-]

five carriers scenarios, respectively. With the considered memory, degree and interfering carriers, it can be shown that the number of predistorter coefficients are 63 and 207 for the three and five carrier, respectively.

Convergence Performance

Central to the performance of direct estimation techniques is the determination of the adaptation parameters (μ, λ) that guarantee fast convergence. Similarly to [40,66], this is achieved by fine tuning of the adaptation parameters. In both the Individual and Joint methods, the parameters μ and λ have been tuned to provide minimal residual error. For the LMS updates of (4.23) and (4.36) we set $\mu = 0.00001$, while for the RLS updates defined in (4.32) and (4.48), we set $\mu = 0.005$ and $\lambda = 0.95$. In Figs. 4.9 and 4.10 we show the envelope of the squared error $|e_m(n)|^2$ for the individual and joint techniques, respectively. The plotted envelopes relate to the central carrier in the three carriers scenario.

These curves indicate that the simpler LMS algorithm performs poorly compared to RLS in terms of convergence performance. Hence, we focus on direct estimation techniques implemented using the described RLS algorithms. This result is consistent with [1], where the LMS and RLS techniques were developed for the estimation of the IMD in a multicarrier scenario and the suitability of RLS over LMS was also illustrated.

Total Degradation Results

We evaluate TD for the considered scenarios. For $M = 3$ equally spaced carriers, Figures 4.11 and 4.12 respectively present the TD for the central and external carriers. The results for the external carriers are symmetric and hence only one is reported.

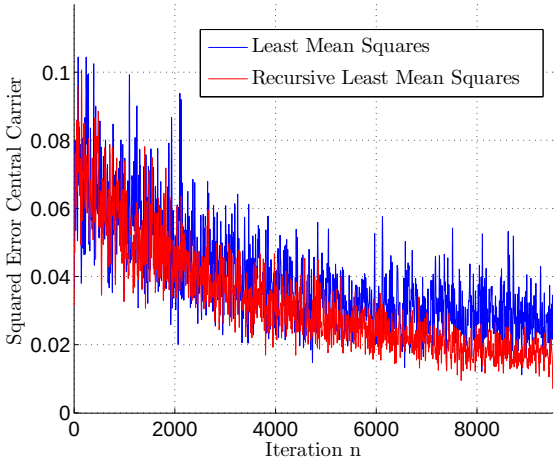

Figure 4.9: Direct Individual Method Convergence:Central Carrier with $M = 3$

As expected, significant degradation occurs in the central carrier due to the stronger ACI. Multicarrier predistortion, in general, provides significant gains (> 3 dB) with respect to a baseline scenario where no compensation applied (legend *No Compensation* in Fig. 4.11). Direct estimation of the predistorter parameters provides further gain over the indirect estimation. The joint optimization method yields the best performance providing about $0.5 - 1$dB gain over the indirect method for the same predistorter complexity and training length.

To the best of authors' knowledge, there exist no published work on multicarrier techniques for a direct comparison. A related work, that tackles a similar scenario (same HPA model, modulation, coderate, roll off and frequency spacing) but using a multicarrier equalizer (instead of predistortion) coupled with turbo decoder can be found in [1]. Further, unlike our case, [1] does not consider on-board channelization filters (IMUX and OMUX). These dissimilarities not withstanding, we consider Fig. 4 of [1] with Fig. 4.11 above. Fig. 4 in [1] depicts the BER of the central carrier for an OBO $= 2.1$ dB that corresponds to a total degradation of $2.75 - 3$ dB depending on the specific configuration in place. This value is very similar to those achieved by our joint predistortion solution ($TD \approx 3$ dB in Fig. 4.11).

TD results for a five carrier satellite channel are provided in Figs. 4.13, 4.14, 4.15 for the carriers located at center, immediate left to the center and leftmost locations. Compared to the three carrier scenario the degradation is prominent. In this very challenging configuration, the advantage of the direct optimization methods over the indirect one is still valuable providing additional $0.5 - 0.75$dB of gain.

Estimation Noise Sensitivity Analysis

We now investigate the robustness of the proposed direct estimation methods to the estimation noise. The estimation noise is defined as the ambient noise level

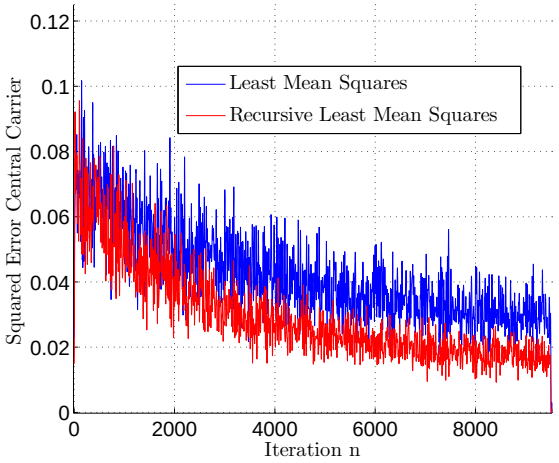

Figure 4.10: Direct Joint Method Convergence:Central Carrier with $M = 3$

at the receiver during the predistorter parameter estimation. In the considered scenario, the estimation of the predistorter parameters takes place off-line with the support of a dedicated user terminal in charge of providing feedback to the transmitting GW. The noise level at the considered receiver plays a key role in the estimation accuracy of the predistorter parameter and in determining the final system performance.

Fig. 4.16 illustrates the normalized noiseless interference level, defined as $E[|u_m(n) - y_m(n)|^2]/E[|y_m(n)|^2]$, with respect to the estimation noise level $\frac{E_s}{N_0}$ for the three carrier scenario. This result indicates that the indirect estimation is very sensitive to the noise level. On the other hand, direct estimation is robust and provides improved performance. This is consistent with the results for single carrier signal predistortion provided in [39]. Joint direct estimation is shown to guarantee the best performance independently of the estimation noise level. This allows the system designer to employ a predistorter over a wider range of $\frac{E_s}{N_0}$, thereby reducing the operational costs.

Sensitivity to Mismatched Estimation

In this section, we evaluate the sensitivity of the system performance to mismatches in scenarios: between the one prevailing during the estimation of predistortion coefficients and the one when the predistortion is in operation. Slight differences in the processing of the individual carriers, can arise out of the system components (cables/ waveguide lengths), on-ground amplifier settings, feedback delay and propagation conditions. We consider two prominent manifestations of these differences: power imbalance and timing misalignments among the carriers.

Sensitivity of different predistortion techniques to power imbalance is assessed by forcing different carrier power levels on the down link channel during the predistorter estimation; on the other hand, the performance is evaluated with identical down link power on all carriers. In Fig. 4.17 we depict the varia-

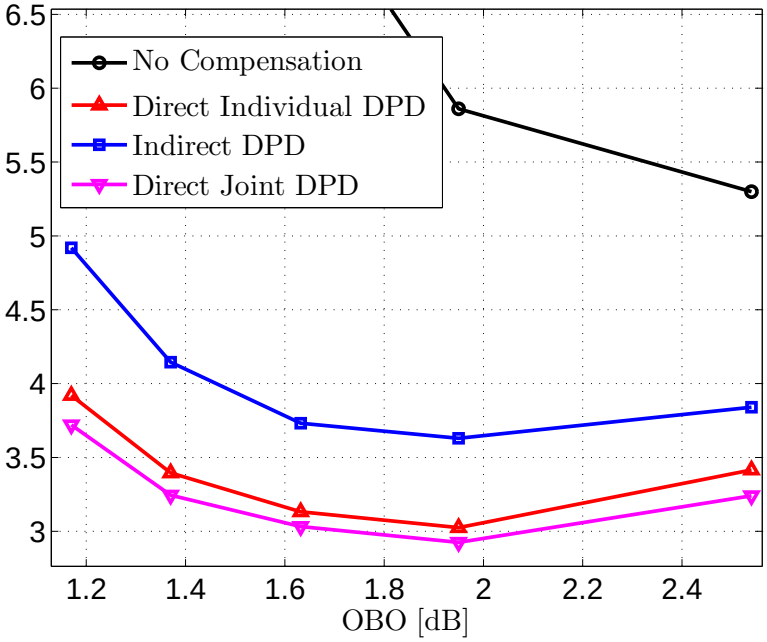

Figure 4.11: Total Degradation of the central carrier in a three carrier scenario

tion in TD with power imbalance for a three carrier scenario. In particular, the imbalance is defined as the ratio between the signal power of the external carriers (both having the identical power levels for simplicity) and the signal power of the central carrier. Performance of the central carrier is sensitive to the power imbalance only in the case of indirect estimation (about 20% variation) while only a minor degradation is observed in the cases of individual and joint direct estimation (kindly refer to Fig. 4.17). The external carriers are rather robust to power imbalance for all estimation methodologies, even exhibiting minor improvements. The minor improvement in the external carriers can be related to the magnitude of the predistortion parameters of the central carrier. In fact, due to the lower signal to noise ratio (in case of power imbalance) of the central carrier during estimation, the related predistortion parameters show a lower magnitude compared to the external ones. This magnitude imbalance in the predistortion function slightly reduces the uplink power of the central carrier, thereby lowering the corresponding ACI injected onto the external carriers.

Similar to the power imbalance case, we consider predistorter parameters estimation with some timing misalignment during uplink process, while performance is assessed in the case of perfect matching using the TD . We considered a three carrier scenario where the two external carriers are perfectly aligned, while the central carrier has a timing misalignment defined as a percentage of the symbols time T_s. The external carriers experience minor variation with respect to this misalignment while the central carrier suffers performance degradation for all considered methodologies (kindly refer to Fig 4.18). Joint estimation is shown to be less sensitive to timing errors with respect to the other techniques;

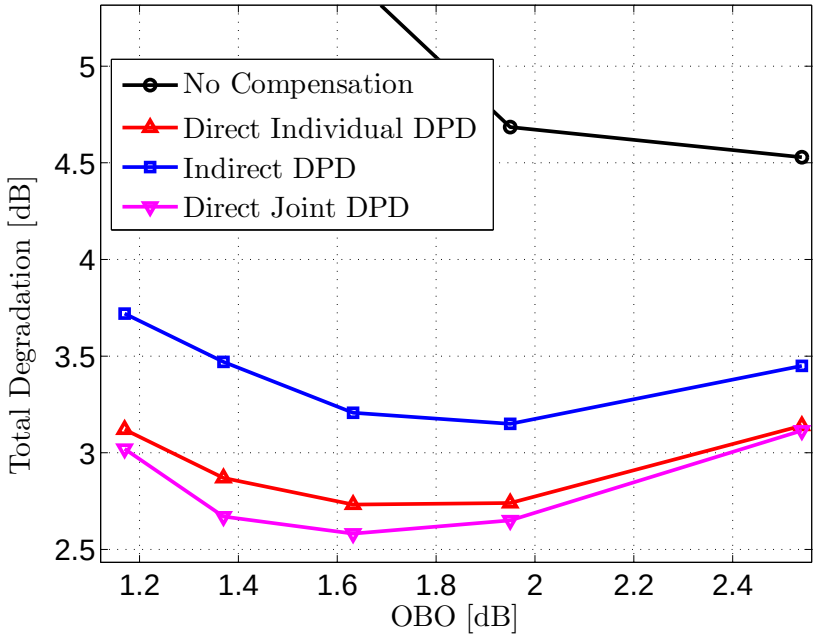

Figure 4.12: Total Degradation of the external carrier in a three carrier scenario

further direct individual estimation is more sensitive than indirect estimation. Notice in this case that direct techniques show a very minor improvement in the external carriers

Complexity Discussion

Direct estimation, while providing for increased performance, requires additional complexity compared to indirect estimation. Direct estimation relies on the knowledge of the channel parameters that need to be estimated in the adaptation loop, while indirect estimation does not require the channel parameters. This does not increase the amount of data feedback required to the gateway but the complexity of the processing. Further, individual direct estimation has a lower complexity compared to the joint one in the number of parameters computed. The complexity of individual and joint predistortion techniques can be compared considering the number of scalar differential terms of the kind $\frac{\partial y_m}{\partial w_{i,j}}$ that are computed at each iteration. This number is the same for both LMS and RLS implementations. For individual predistortion, considering all the M carriers, we require the computation of $\sum_m \sum_p (2K_p+1)|\Omega_{m,p}|$ differential terms (kindly refer to (4.23)). On the other hand for joint predistortion $M \sum_m \sum_p (2K_p + 1)|\Omega_{m,p}|$ differential terms are required (kindly refer to (4.36)).

This section proposes two novel techniques for multicarrier predistorter design in a non-linear satellite channel. Implemented through iterative first order techniques, these estimation methods, namely *Individual* and *Joint* DPD, provide optimized model parameters for a memory polynomial based predistorter. The individual DPD method optimizes the predistortier coefficients for differ-

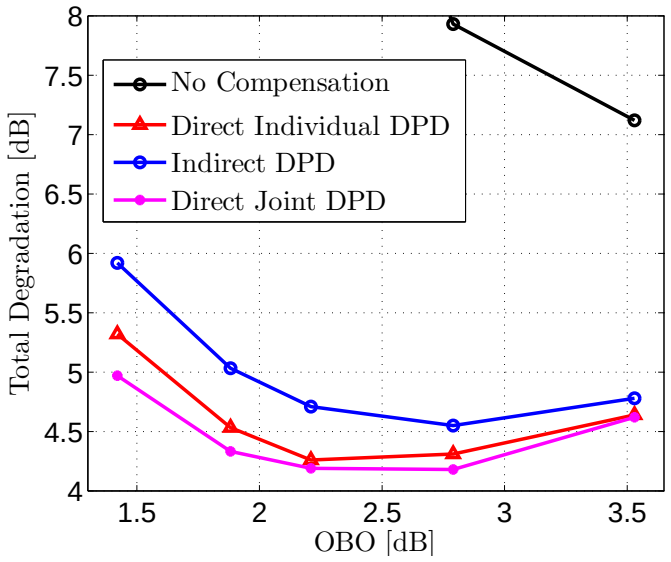

Figure 4.13: Consider Total Degradation of the center carrier in a five carriers scenario

ent carriers separately, while the joint method favors a global optimization of the coefficients at the cost of increased complexity. Through simulations we have shown that the direct estimation of parameters provides improved performance over the well-known indirect estimation method, achieving gains that are valuable in the satellite context. Direct estimation also leads to a predistorter that is robust to the level of noise present during the estimation and to channel mismatch. Depending on the complexity affordable, either the *Joint* or the *Individual* method could serve as a promising technique for the current and future satellite missions where power and spectral efficiencies play a vital role.

In the following section we consider signal predistortion for multicarrier and a novel direct learning algorithm is derived. Further, in conjunction with direct predistortion, we propose an adaptive method for PAPR reduction.

4.2 Generalized Direct Volterra Signal Predistortion with Automatic Crest Factor Reduction

4.2.1 Introduction

Communication systems are based on the assumption that the transmitter can deliver the signal to the receiver with the required level of energy. Power amplification has the key purpose of enhancing the signal power sufficient to compensate for the channel losses and impairments and achieve the target signal to noise ratio at the receiver. However, power amplification is inherently a non-linear operation that introduces distortion of the signal. This distortion is due to the natural saturation effect present in the HPA that, depending on

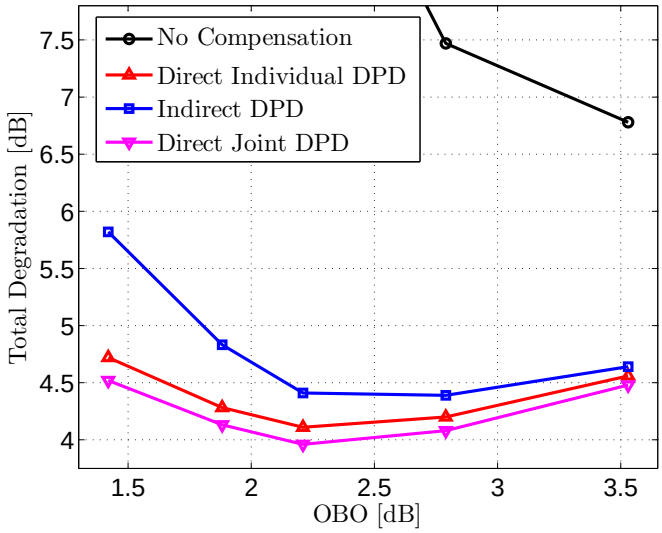

Figure 4.14: Total Degradation of the left to the center carrier in a five carrier scenario

the amplitude of input signal distribution and the required power efficiency, can generate significant distortions. Further, the severity of the interference generated is magnified when the non-linearity of the HPA is combined with channel memory effects. A simple mechanism to avoid such distortions is to operate the HPA in the linear region far from the saturation region. However, operating the amplifier in the linear region drastically reduces the power efficiency and the resulting signal output power. The back-off needed for such an operation depends on the PAPR of the input signal. PAPR refers to the ratio between the peak input power and the average input signal power. Further, the PAPR is significant for multiple carrier signals being amplified by a single HPA.

A common approach to counteract the distortion effect and still maintain the required level of output power, is to perform specific preprocessing of the signal prior to signal amplification. This technique, referred as signal predistortion is usually performed on the baseband version of the signal and it is often based on polynomial functions [16, 18, 26, 27, 38] or LUT [28, 43]. While literature mostly focuses on terrestrial applications, signal predistortion techniques are also becoming popular in satellite communications [25] partly due to the move towards amplification of multiple carriers (or multicarrier signals) in a single wideband HPA for reducing the payload mass and mission costs. Very large PAPR values, typical of multicarrier signals, force a substantial component of the signal input distribution beyond the amplifier saturation point. This effect introduces unwanted strong distortion that cannot be compensated with predistortion. Motivated by this, we pursue the study of PAPR reduction in multicarrier systems. Several PAPR reduction methods have been proposed in [45]: amongst these, clipping and filtering can provide significant PAPR reduction with minor interference generation (clipping noise) [46]. Clipping of the signal is in general referred as CFR. Further, the use of PAPR reduction

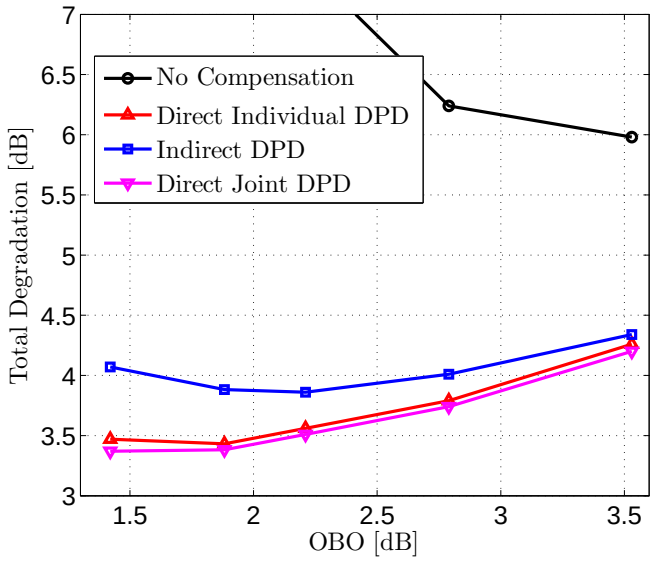

Figure 4.15: Total Degradation of the leftmost carrier in a five carriers scenario

in conjunction with signal predistortion has also been widely considered in literature. Several works propose a scheme in which PAPR reduction precedes predistortion [47, 48], while [49] proposes a scheme where predistortion is followed by PAPR reduction. A different approach was recently proposed in [50], that presents a method to include PAPR control as a constraint in the estimation of the predistortion parameters.

In this section we present our work [51] where we consider a transmitter architecture in which PAPR reduction is performed before signal predistortion. The contribution with respect to the state of the art is two fold: on one hand, we propose a novel optimization framework to automatically determine the optimal level of PAPR reduction towards maximizing system performance; on the other hand, direct estimation for predistortion proposed in [40] is reformulated to include new terms towards improving the parameter optimization and consequently the system performance. While the focus here is on signal predistortion, an optimization of the CFR reduction in presence of data predistortion [41] can be equivalently pursued.

Referring to the Fig. 4.19, we consider a general baseband multicarrier signal $u(n)$ input to the cascade of CFR and predistortion blocks prior to transmission. The channel is assumed to be a non-linear function with memory.

The general multicarrier signal, $u(n)$, is defined as,

$$u(n) = \sum_m u_m(n) e^{j2\pi\Delta f_m n}, \tag{4.51}$$

where Δf_m is the center frequency of mth channel and $u_m(n)$ is the baseband signal of the mth carrier generally defined as,

$$u_m(n) = \sum_k a_m p_m(nT_s - kT_m), \tag{4.52}$$

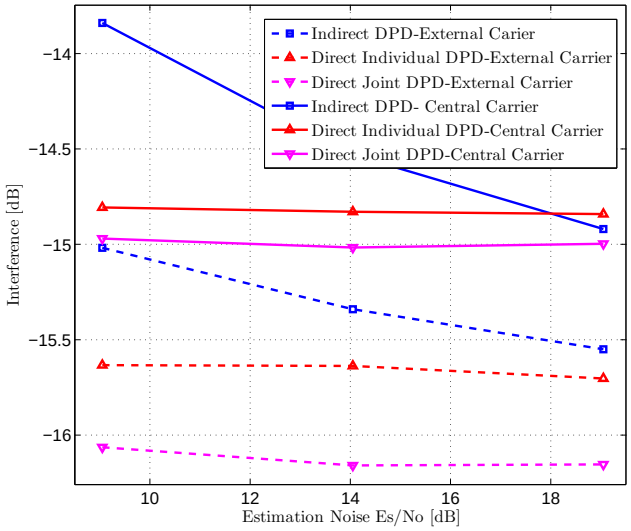

Figure 4.16: Three Carriers: Estimation noise vs Interference (OBO = 1.7 dB)

where T_m is the symbol rate of the mth channel, T_s is the oversampling period and $p_m(\cdot)$ is the pulse shaping function. Notice that the oversampling period T_s is equal for all carriers and such that $T_s >> MT_m$ where M is the total number of carriers. Referring to Fig. 4.19, $u_c(n)$ is the signal output of the CFR. The objective of the CFR is to ensure $PAPR(u_c(n)) \leq PAPR(u(n))$. Further, $x(n)$, the output of the predistortion block serves as input to the channel.

Channel Model

We consider a general baseband Volterra non-linear system with memory to model the channel [24]. Using Kronecker products, we formulate the general baseband Volterra function in a compact way and referring to Fig. 4.19, the noiseless channel output is expressed as,

$$\begin{aligned} y(n) &= \mathbf{h}_1 G_1 \mathbf{x}_{k_1}(n) \\ &+\mathbf{h}_3 G_3 \mathbf{x}_{k_3}(n) \otimes \mathbf{x}_{k_3}(n) \otimes [\mathbf{x}_{k_3}(n)]^* \\ &+\mathbf{h}_5 G_5 \mathbf{x}_{k_5}(n) \otimes \mathbf{x}_{k_5}(n) \otimes \mathbf{x}_{k_5}(n) [\mathbf{x}_{k_5}(n) \otimes \mathbf{x}_{k_5}(n)]^*, \end{aligned} \tag{4.53}$$

where $\mathbf{x}_{k_d} = [x(n-k_d), \cdots, x(n+k_d)]^T$, K_d is the single side memory relative to the dth degree and $\mathbf{h}_d$ is a row vector with L_d elements where $L_d = \prod_{a=0}^{(d-1)/2}(2k_d+1-a)\prod_{b=0}^{(d-3)/2}(2k_d+1-b)$. G_d is a $L_d \times (2k_d+1)^d$ matrix selecting the relevant product terms from the dth degree Kronecker product vector for a complete, non-redundant Volterra representation.

In particular we have $G_3 = [\mathbf{g}^T_{i_1,j_1,k_1}, \cdots, \mathbf{g}^T_{i_{L_3},j_{L_3},q_{L_3}}]^T$ where each row vector corresponds to a standard basis $\mathbf{g}_{i_s,j_s,q_s} = \mathbf{e}_p$ with $p = q_s + (j_s - 1)(2k_3+1) + (i_s-1)(2k_3+1)^2$. Further, we have $(i_s, j_s, q_s) \in \Omega_3$ where $\Omega_3 = \{(i,j,q) | \forall i \in (1, \cdots, 2k_3+1), \forall j \in (i, \cdots, 2k_3+1), \forall q \in (1, \cdots, 2k_3+1)\}$.

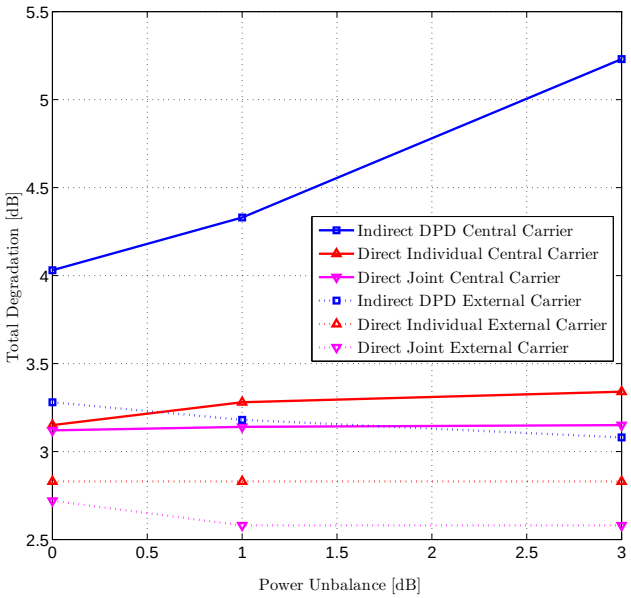

Figure 4.17: Sensitivity of TD to power imbalance of central carrier during estimation: Three carrier scenario (OBO = 1.3 dB)

Similarly, $G_5 = [\mathbf{g}^T_{i_1,j_1,q_1,a_1,b_1}, \cdots, \mathbf{g}^T_{i_{L_5},j_{L_5},q_{L_5},a_{L_5},b_{L_5}}]^T$ where each row vector corresponds to a standard basis $\mathbf{g}_{i_s,j_s,q_s,a_s,b_s} = \mathbf{e}_p$ with $p = b_s + (a_s - 1)(2k_5 + 1) + (q_s - 1)(2k_5 + 1)^2 + (j_s - 1)(2k_5 + 1)^3 + (i_s - 1)(2k_5 + 1)^4$. Further, we have $(i_s, j_s, q_s, a_s, b_s) \in \Omega_5$ where $\Omega_5 = \{(i, j, q, a, b) | \forall i \in (1, \cdots, 2k_5 + 1), \forall j \in (i, \cdots, 2k_5 + 1), \forall q \in (j, \cdots, 2k_5 + 1), \forall a \in (1, \cdots, 2k_5 + 1), \forall b \in (a, \cdots, 2k_5 + 1)\}$.

Crest Factor Reduction Model

The output of CFR is related to its input as

$$u_c(n) = \begin{cases} u(n) & \text{if } |u(n)| \leq |\gamma|^2, \\ |\gamma|^2 \; u(n)/|u(n)| & \text{if } |u(n)| > |\gamma|^2 \end{cases} \tag{4.54}$$

where γ is the clipping parameter. Notice that the CFR clipping function does not modify the phase of the complex signal, i. e. $\angle u_c(n) = \angle u(n)$. Further, the clipping function as defined here, is slightly different from the standard clipping function of [70] and involves $|\gamma|^2$ rather than γ. This choice will enable the formulation of the optimization algorithm to compute the optimal clipping value.

Predistorter Model

The predistortion function acts on the output of the clipping function to yield the channel input $x(n)$. The predistorter per-se is a non-linear function with

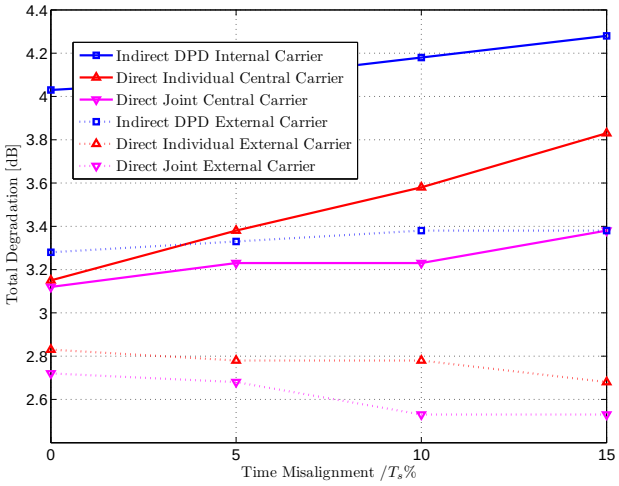

Figure 4.18: Sensitivity of TD to timing misalignment of central carrier during estimation: Three carrier scenario (OBO = 1.3 dB)

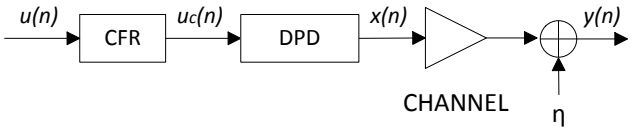

Figure 4.19: System Model Block Diagram

memory accomodating various polynomial functions including memory polynomials [16], generalized memory polynomials [38] and Volterra expansion [26]. The output of the predistorter is computed as,

$$x(n) = [\phi(n)]^T \mathbf{w} \tag{4.55}$$

where the predistorter function is explicitly expressed as a function of the parameter $m \times 1$ vector $\mathbf{w}$ and where $\phi(n)$ is a $m \times 1$ vector collecting the linear and non-linear terms generated from input signal $u_c(n)$ including linear terms $\{u(n-k)\}$ third degree terms $\{u(n-k_1)u(n-k_2)u^*(n-k_3)\}$ and so on [16,26]. The value of m depends on the degree and the associated memory depth [16,26] and is not detailed further for ease of comprehension. Central to the performance of the predistortion is the determination of the parameters $\mathbf{w}$. Well known methods for estimation of predistortion parameters are the indirect [26] and direct learning [40] approaches.

Referring to Fig. 4.19 we notice that the DPD block is between the CFR block and the channel. This means that the predistortion function is not designed to invert the channel function but rather to reduce the receiver inter-

ference. This fundamental observation suggests a direct estimation approach rather then an indirect one [39] for obtaining $\mathbf{w}$.

Peak Controlled Predistortion

Rather then pre or post clipping the predistorted signal, we can design the predistortion function to respect a specific PAPR value [50]. Referring to the indirect predistortion paradigm, we can estimate the predistortion coefficients and adding a constraint on the predistorter output PAPR value as,

$$\begin{aligned} min_{\mathbf{w}} \quad & ||\mathbf{u} - \Phi(\mathbf{y})\mathbf{w}||^2 \\ s.t. \quad & |\Phi(\mathbf{u})\mathbf{w}|^2 < A_{max}^2 \end{aligned} \tag{4.56}$$

where $\mathbf{u} = [u(0), \cdots, u(N-1)]^T$, $\mathbf{y} = [y(0), \cdots, y(N-1)]^T$, $\Phi(\mathbf{u}) = [\phi(\mathbf{u}_k(0)), \cdots, \phi(\mathbf{u}_k(N-1))]^T$, $\Phi(\mathbf{y}) = [\phi(\mathbf{y}_k(0)), \cdots, \phi(\mathbf{y}_k(N-1))]^T$, $\phi(\mathbf{v}_k(n))$ is the vector collecting linear and non linear terms from the $2K+1$ samples $\mathbf{v}_k(n) = [v(n-k), \cdots, v(n+k)]^T$, $u(n)$ predistorter input signal and $y(n)$ channel output signal and A_{max} is the desired predistorter output signal maximum amplitude. This can be set such as $PAPR = IBO$. The convex problem of (4.56) is proposed and solved in [50] and it considered herein as a baseline method for comparison.

4.2.2 Adaptive Peak Controlled Direct Predistortion

Given the crest factor reduction and predistortion techniques proposed in Sections 4.2.1 and 6.4.2, we define a transmitter architecture in which the CFR block precedes the DPD block. In this section, we derive optimization algorithms to determine the optimal CFR and predistortion parameters towards reducing the error at the receiver. Fig. 4.20 illustrates the considered transmitter architecture including the two iterative optimization processes.

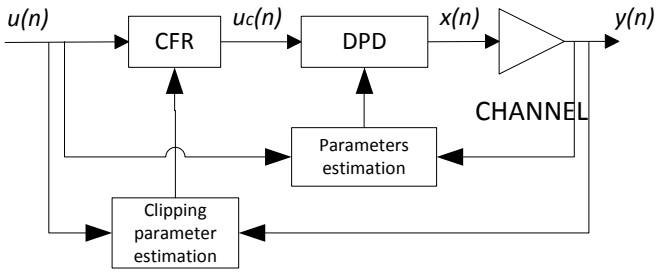

Figure 4.20: Combined Optimization Function Block Diagram.

Generalized Direct Estimation

The target of the predistortion function is to reduce the non-linear distortion at the channel output. This is achieved by optimizing the parameters $\mathbf{w}$. The general estimation paradigm is shown in Fig. 4.20.

Referring to (4.53) and (4.55), we define

$$\mathbf{x}_{k_i}(n) = \Phi_{k_i}(n)\mathbf{w}, \tag{4.57}$$
$$\Phi_{k_i} = [\phi(n-k_i), \cdots, \phi(n+k_i)]^T. \tag{4.58}$$

Combining (4.53) with (4.57) and limiting the expansion to third degree polynomial for ease of presentation, we obtain,

$$\begin{aligned} y(n) &= \mathbf{h}_1 G_1 \Phi_{k_1}(n)\mathbf{w} \\ &\quad + \mathbf{h}_3 G_3 \left[\Phi_{k_3}(n) \otimes \Phi_{k_3}(n) \otimes \Phi_{k_3}(n)^*\right] \left[\mathbf{w} \otimes \mathbf{w} \otimes \mathbf{w}^*\right]. \end{aligned} \tag{4.59}$$

Similarly to [40], we define the cost function for the optimization of the predistortion parameters as $C(\mathbf{w}) = |u(n) - y(n)|^2$ and formulate a least mean squares (LMS) algorithm for minimizing $C(\cdot)$. We can then derive the update equation for $\mathbf{w}$ as,

$$\mathbf{w}(n+1) = \mathbf{w}(n) - \mu \frac{\partial C(\mathbf{w})}{\partial \mathbf{w}} \tag{4.60}$$

where μ is the algorithm step. Using $C(\mathbf{w})$ in (4.60), we obtain

$$\mathbf{w}(n+1) = \mathbf{w}(n) + \mu(e^*(n)\frac{\partial y(n)}{\partial \mathbf{w}(n)} + e(n)\frac{\partial y^*(n)}{\partial \mathbf{w}(n)}). \tag{4.61}$$

where $e(n) = u(n) - y(n)$, and

$$\begin{aligned} \frac{\partial y(n)}{\partial \mathbf{w}} &= \mathbf{h}_1 G_1 \Phi_{k_1}(n) \\ &\quad + \mathbf{h}_3 G_3 \left[\Phi_{k_3}(n) \otimes \Phi_{k_3}(n) \otimes \Phi_{k_3}(n)^*\right] \\ &\quad \left[\mathbf{w} \otimes I_m + I_m \otimes \mathbf{w}\right] \otimes \mathbf{w}^*, \end{aligned} \tag{4.62}$$

$$\begin{aligned} \frac{\partial y^*(n)}{\partial \mathbf{w}} &= \mathbf{h}_3^* G_3^* \left[\Phi_{k_3}^*(n) \otimes \Phi_{k_3}^*(n) \otimes \Phi_{k_3}(n)\right] \\ &\quad \mathbf{w}^* \otimes \mathbf{w}^* \otimes I_m, \end{aligned} \tag{4.63}$$

where I_m is an $m \times m$ identity matrix (recall from Section 6.4.2 that the size of $\mathbf{w}$ is $m \times 1$). Notice that in the derivation of the direct estimation method in [40], the term in (4.63) is not included in the algorithm. This results in a performance degradation which is illustrated in Section 4.2.3. In order to guarantee optimal performance, the vector of predistortion parameters, $\mathbf{w}$, is initialized with the result of the offline indirect estimation [71] where CFR is assumed to be absent.

Adaptive Crest Factor Reduction

The CFR block performs clipping of the original signal before signal predistortion. The challenge of signal clipping is to understand if and to what extent it is convenient to clip the signal. In fact, clipping too much results in a loss of the signal while not clipping would naturally enhance PAPR. In particular, referring to (4.54), it is necessary to estimate the parameter γ towards improving the system performance.

The cascaded predistortion and channel blocks (kindly refer to Figs. 4.19, 4.20) result in a non-linear system with memory that can be modeled using a Volterra system as (here limited to the third degree),

$$y(n) = \sum_{k}^{K_1} q^{(1)}(k) u_c(n-k) \tag{4.64}$$
$$+ \sum_{k_1,k_2,k_3}^{K_3} q^{(3)}(k_1,k_2,k_3) u_c(n-k_1) u_c(n-k_2) u_c^*(n-k_3)$$

where K_1 quantifies the linear memory, K_3 is the third degree memory component and $\{q^{(d)}(\cdot)\}$ are the model parameters relative to the dth degree. Parameters in (4.64) can be estimated during on-line operation using standard least squares techniques [66]. Towards this, we consider the cost function $C(\gamma) = |u(n) - y(n)|^2$ and formulate a least mean squares algorithm to determine the optimal γ. We define the update equation for γ as,

$$\gamma(n+1) = \gamma(n) - \epsilon \frac{\partial C(\gamma)}{\partial \gamma} \tag{4.65}$$

where ϵ is the algorithm step. Notice that, in general, we have $\gamma \in \mathbb{C}$. From (4.65), and using the chain rule, we obtain,

$$\gamma(n+1) = \gamma(n) + \tag{4.66}$$
$$\epsilon \left[e(n)^* \frac{\partial y(n)}{\partial u_c(n)} \frac{\partial u_c(n)}{\partial \gamma} + e(n) \frac{\partial y^*(n)}{\partial u_c(n)} \frac{\partial u_c(n)}{\partial \gamma} \right]$$

where $e(n) = u(n) - y(n)$ and both $\frac{\partial y(n)}{\partial u_c(n)}$ and $\frac{\partial y^*(n)}{\partial u_c(n)}$ can be derived analytically from (4.64) using the partial differential rules provided in [67]. Notice that, in general, $\frac{\partial y^*(n)}{\partial u_c(n)} \neq [\frac{\partial y(n)}{\partial u_c(n)}]^*$. Further, we can define analytically the differential quantity

$$\frac{\partial u_c(n)}{\partial \gamma} = \begin{cases} 0 & \text{if } |u(n)| < |\gamma|^2, \\ \gamma^* e^{i \angle u(n)} & \text{if } |u(n)| > |\gamma|^2 \end{cases} \tag{4.67}$$

where we used $\frac{\partial |\gamma|^2}{\partial \gamma} = \gamma^*$ [67]. Notice that for $|u(n)| = |\gamma|^2$, the derivative of (4.67) does not exist and hence its value is set to 0 in the simulations. Further, if the algorithm is initialized such that $|\gamma_{init}|^2 > max|u(n)|$ the resulting derivative will always be zero and the algorithm will only produce $|\gamma(n)|^2 = |\gamma_{init}|^2 \ \forall n$.

Therefore, key to the convergence of the algorithm, is the choice of the initial guess γ_{init}. This can be trivially set to 0 or obtained knowing the amplifier saturation power P_{in}, the signal PAPR and the selected IBO (Input Backoff).

4.2.3 Numerical Results

In this section we numerically evaluate the performance of the algorithms for a selected case of study.

Simulation Scenario

We consider a typical satellite communication scenario where the channel includes a satellite transponder model [22]. As transponder model, we consider an input multiplexer filter (IMUX), a HPA, and an output multiplexer filter (OMUX). Typical responses for the IMUX and OMUX filter are extracted from [6] and modelled as FIR filters. On the other hand, the HPA is parameterized using the standard Saleh model with AM/AM and AM/PM functions taking the form $A(r) = \frac{2r}{1+r^2}; \Phi(r) = \frac{\pi}{6}\frac{r^2}{1+r^2}$, respectively [41].

The channel input signal $u(n)$ consists of five independent DVB-S2 [9] carriers, each employing 16APSK modulation, with identical symbol rate R_s and spaced equally in frequency with a separation of $R_s(1+\rho)$ where $\rho = 0.2$ is the pulse roll off. The resulting PAPR of the signal, without compensation, is 9.8 dB.

Algorithm Setting

Both estimation algorithms described in Sections 4.2.1 and 4.2.2 are trained over 100000 samples corresponding to 10000 symbols per carrier (oversampling factor or 10). Step parameters are determined by fine simulation tuning to be: $\epsilon = 10^{-2}$ in (4.67); $\mu = 10^{-5}$ in (4.61). Notice that, in all considered cases, training is carried out in absence of receiver noise. The channel parameters $\mathbf{h}_d$ (kindly refer to (4.53) with $k_1 = 5$, $k_3 = 3$ and $k_5 = 0$) and the parameters corresponding to the cascaded predistortion and channel function ($q^{(d)}(\cdot)$ in (4.64) with $K_1 = 3$, $K_3 = 2$ and $K_5 = 1$), are estimated on-line using standard least squares (LS) techniques [66].

The predistortion function of (4.55) implements a standard memory polynomial [16] of fifth degree with single side memory depth $k_1 = 5$, $k_3 = 3$ and $k_5 = 1$ for each degree respectively.

Further, in the case when both CFR and DPD algorithms are applied, they can be run alternately or concurrently. However, when running concurrently the final performance is slightly penalized due to the inter dependency in the target error. For the sake of performance optimization, we alternate them in three phases: we first perform a DPD estimation followed by the CFR estimation and a subsequent DPD estimation. We noticed that further iterations do not improve significantly the performance.

Performance Evaluation

- Figure of Merit: As figure of merit, we consider the signal to interference plus noise ratio (SINR) at the output of the channel with respect to the amplifier OBO (output back off). In practice, the OBO determines the operating point of the amplifier and hence determines both the useful output power and amount on non-linearities. For the current study, we focus on the impact of OBO on non-linearities; in particular, the receiver signal to noise ratio (SNR) is fixed. Further, we plot the power spectral densities at the channel output to observe and compare the spectral regrowth. Towards quantifying the spectral shaping, we also consider the normalized mean square error (NMSE) at the receiver in absence of noise as NMSE= $1/N \sum_{n=1}^{N} |u(n)-y(n)|^2 / \sum_{n=1}^{N} |y(n)|^2$ computed with respect

the channel output signal $y(n)$ with respect to the properly delayed version of the input signal $u(n)$.

- SINR Performance: Fig. 4.21 depicts the SINR versus OBO for different techniques with a set SNR= 20dB. Referring to Fig. 4.21 and focussing on the cases in which CFR is not applied, we present three sets of results: standard indirect estimation [27] (brown), conventional direct estimation [40] (red) and our novel direct estimation algorithm (green) of Section 4.2.2. Observing Fig. 4.21, we have that standard indirect predistortion and conventional direct predistortion have similar performance while the reformulated LMS algorithm of (4.61) provides additional performance gain over [40] of about $1-1.25$ dB due to inclusion of new terms. Considering the combination of CFR and DPD, we compare the peak constraint predistortion of [48] with our method. Referring to Fig. 4.21 we have a significant gain in performance of our proposed method over [48] of about 2 dB.

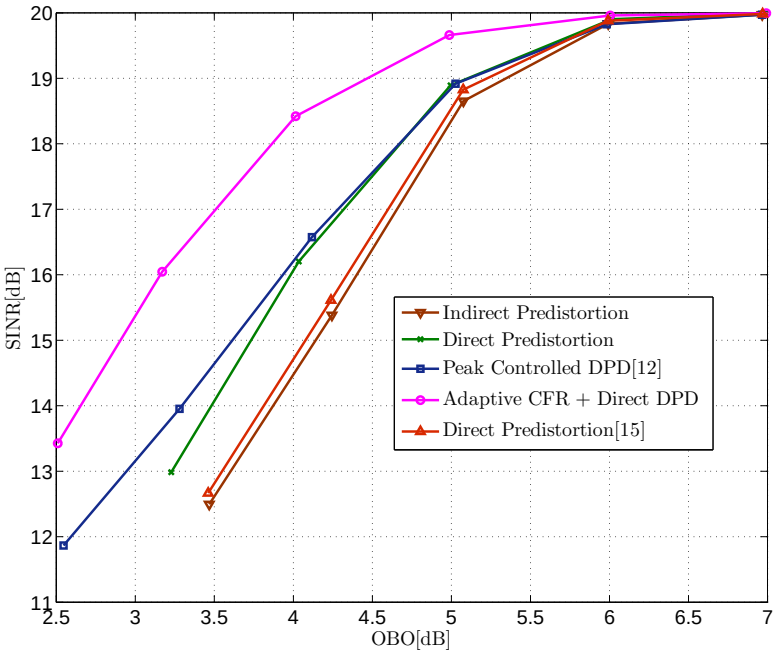

Figure 4.21: Signal to Interference plus Noise versus Output Back-Off

- Spectral Density and NMSE: At the output of the channel (output of the OMUX filter), we can observe the typical spectral regrowth of the signal due to the non-linear characteristic of the amplifier. In Fig. 4.22 we can observe the power spectral density of the multicarrier signal (only the positive part it is shown) for the different techniques considered.

  As expected, techniques with a lower NMSE also show a lower spectral regrowth.

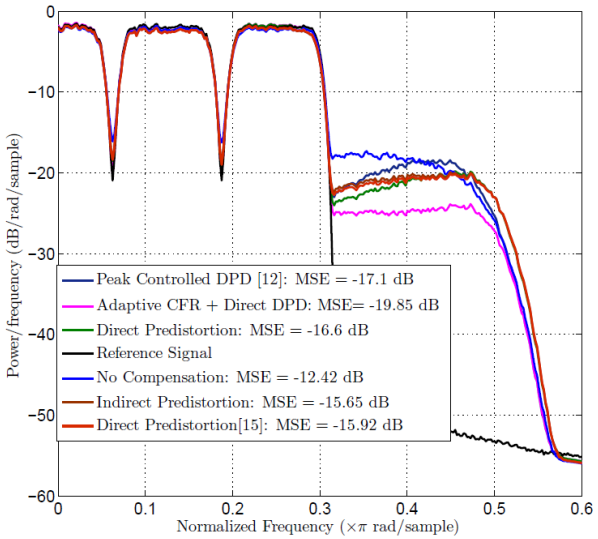

Figure 4.22: Power Spectral Density Response for Five Carriers DVB-S2 carriers at IBO=4 dB

A novel design method for combined CFR and DPD has been proposed. This includes an automatic method to determine the optimal clipping amplitude for a general non-linear channel with memory together with a reformulated and generalized direct estimation method for predistortion. While the reformulated direct estimation itself shows to provide gain with respect to the state of the art, the combination of CFR and DPD is shown to provide the best performance.

Chapter 5

Distributed Multiple Carrier Predistortion

5.1 Introduction

On-board power amplification, a key satellite operation, is inherently non-linear and can generate severe interference that limits the achievable throughput. As the amplifier is operated in its high efficiency region, the non-linear distortion effects increase, requiring a natural trade-off between power and spectral efficiency. Non-linear interference becomes even more prominent when high order modulation schemes are employed or when IMD are excited in the multicarrier operation mode. Multicarrier amplification using a single on-board HPA is an application being actively considered by the satellite community since it can reduce the payload weight and cost while providing design flexibility to the on-ground up-link GW [29].

Multicarrier operation of an HPA generates severe distortion effects including strong adjacent channel interference (ACI) and inter-symbol interference (ISI) [1]. Towards optimizing power and spectral efficiencies, several on-ground predistortion techniques have been considered in the literature for single gateway application [**?**, 25, 29, 30, 32]. Model based multicarrier data predistortion, first introduced in [29], was based on memory polynomials. The use of orthogonal memory polynomials to aid the estimation of the predistorter was discussed in [**?**] while a sensitivity analysis of the compensation techniques was reported in [30] for a DVB-S2 based system. A novel method of estimating the predistorter coefficients using the *Direct Learning* paradigm of [40] has been recently proposed in [**?**] for multicarrier satellite systems. The use of direct learning in reducing estimation error is also highlighted. On the other hand, low complexity look-up-table based multicarrier predistortion techniques have shown to be effective in reducing the receiver interference for 8, 16 and 32 APSK constellations [32]. Complimenting the data predistortion, recent works have successfully applied the traditional signal predistortion techniques to the multicarrier satellite channel without violating the limited uplink bandwidth [25].

In addition to the multicarrier operation, another system level development is the use of multiple beam satellites to exploit the various flexibilities (frequency reuse, resource allocation, routing etc) and enhance the throughput [72].

With increase in demand for offered services as well as inclusion of new ones, emerging satellite systems are being designed to handle traffic to the tune of 1 Terabit/s [73,74]. A key aspect in such scenarios is the need to employ multiple GWs to provide adequate feeder link bandwidth and/ or associated robustness. While the technology is being developed for migrating to newer bands like Q/V where multiple GWs are needed to ensure uninterrupted feeder links [75], this chapter focuses on the use of multiple GWs in existing frequency allocations to provide the needed feeder bandwidth. Further, the current work presented in this chapter aims to reduce mission costs in such a scenario by considering joint on-board amplification of carriers from different GWs using a single HPA. A typical application would be the use of a wideband amplifier to process signals from different GWs intended for different beams. While the issues of joint amplification are similar to those encountered in a single GW case, applying "centralized" countermeasures as proposed in [**?**, **?**, 25, 29, 32] is not feasible due to the distributed nature of the multi-GW scenario. The key difference amongst the scenarios is the availability of data on all the carriers at each of the GWs to estimate and implement the predistortion. These differences notwithstanding, for ease of presentation, we continue to refer to the processing of carriers in different GWs to counter the distortions due to their joint amplification as *multicarrier predistortion*.

Joint amplification of signals uplinked from different gateways on-board the satellite is seen as a next step to enhance mission efficiency in next generation high-throughput satellites. The considered distributed multi-GW scenario in which non-linear effects are accounted has not been tackled before in relevant literature, while this chapter analyses the problem and proposes novel methods to solve the related issues. The current work presented in this chapter explores three key aspects towards reaping the benefits of multicarrier operation in multiple GWs: (a) amount of side information available to effect multiple carrier predistortion at each GW, (b) robust estimation of predistortion coefficients at each GW, and (c) the effect of synchronization imperfection (amongst GWs) on the implemented predistortion mechanism. These aspects and the related contributions are detailed below:

- While the model for multiple carrier data predistortion has already been proposed in the literature [**?**, **?**, 25, 29, 32], they focus on a single gateway application that allows for joint processing. Rather than discussing the standard independent processing at each site in the multi-gateway application, the chapter proposes novel models that have been derived analytically for multiple carrier data predistortion. These methods indicate a trade-off between the data available from other gateways and the achieved performance. Such a study in valuable for the ground segment service provider to trade off the costs of providing side information at different GWs (deployment and maintenance of backbone network) with the benefits of effecting multicarrier predistortion. The different techniques can also be viewed as providing for a progressive upgradation of the backbone network.

- This chapter presents a novel robust estimation method for multiple carrier data predistortion built on the method proposed in [76] for a single carrier application. Further, the chapter presents a novel analysis on the

corresponding estimation gain (noise reduction) of the proposed method. Notice that no similar analysis was presented in the original work of [76].

- A key issue in multi-GW applications involves synchronization among the uplinked streams in terms of waveform delay and phase. This chapter analyzes the effects of imperfect synchronization on the predistorter performance and provides valuable inputs to a system designer on the selection of techniques.

5.2 Multi-gateway Satellite Channel

5.2.1 Scenario

A Ka-band multi-beam broadcasting application to fixed terminals employing a single geostationary (GEO) satellite and multiple gateways is considered. For simplicity, we assume that each GW uplinks a single carrier signal to a shared GEO satellite where the composite signal, obtained by superposition of carriers from different GWs, will be processed by a single on-board HPA. Each carrier can provide an independent service; in a typical application different carriers could be relevant to different beams. Further, in common commercial applications such as TV broadcast, each User Terminal (UT) can only decode its intended carrier. For each beam, we assume a dedicated receiver in charge of providing sporadic feedback information to the corresponding transmitting GW. Such a receiver could be operator installed having better reception capability towards reducing noise in the feedback. As depicted in Fig. 5.1, a certain level of

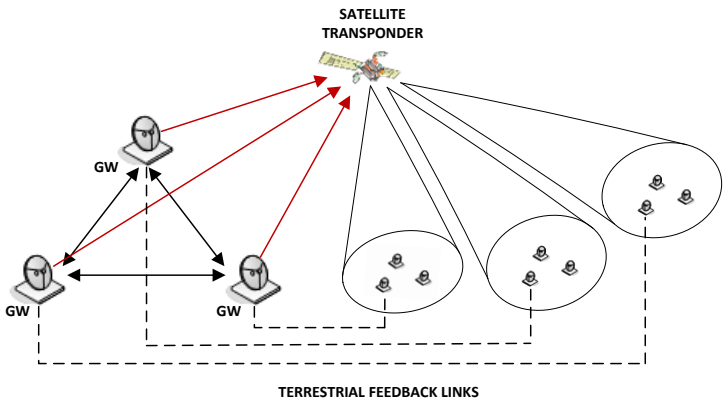

Figure 5.1: Multi-gateway, multi-beam scenario: GWs inter-connected by a terrestrial link, a shared satellite repeater and on-ground receivers

terrestrial connectivity is assumed amongst gateways for exchanging channel parameters and side information. In this chapter, side information pertains to partial knowledge of the data content uplinked by each gateway.

5.2.2 System Model

We consider a simplified multi-gateway satellite architecture abstracted in Fig 5.2 wherein each gateway uplinks, independently, a single carrier signal to the satellite transponder. We further assume that each carrier illuminates a different beam. To focus on the effects of joint amplification, we assume that the inter-beam interference is negligible.

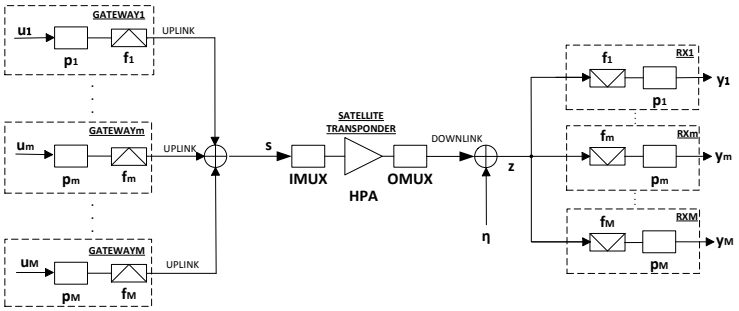

Figure 5.2: Multi-gateway system model illustrating M transmitting GWs, the satellite transponder model and M UT receivers

In Fig 5.2, the mth modulated carrier stream, u_m, is pulse shaped, upconverted to a center frequency f_m and uplinked to the satellite transponder. The composite signal at the input of the satellite transponder is

$$s(t) = \sum_m \sum_n w_m u_m(n) p_m(t - nT_s - \epsilon_m T_s) e^{j(2\pi f_m t + \phi_m)}, \tag{5.1}$$

where $u_m(n)$ is the nth symbol uplinked by the mth gateway, w_m is a real parameter modeling the power imbalance, $p_m(\dot{})$ is the pulse shaping function, T_s is the symbol period, ϵ_m is the delay relevant to the mth carrier, f_m denotes the uplink center frequency of the mth gateway and ϕ_m is the corresponding phase. The satellite transponder is modeled as a memoryless non-linear function combined with input and output filter namely IMUX and OMUX. The downlink is assumed to be an AWGN channel [1]. We consider the Saleh model to characterize the AM/AM and AM/PM function of the HPA [1]. Further, the HPA is assumed to be frequency flat for the scenarios considered [**?**, 1, 6, 29]. The carriers are assumed to have similar baudrates (R_s) and roll-off (ρ) while being equally spaced in frequency with a separation of $\Delta f = R_s(1 + \rho)$.

The on-board IMUX and OMUX filters responses are extracted from [6] and modeled as FIR (finite impulse response).

In general, the channel function relating $y_m(n)$ to $\{u_k(n)\}$ can be represented at the data level as a multivariable non-linear function with memory such that the nth received symbol on the mth carrier takes the form,

$$y_m(n) = \tilde{g}(\mathbf{u}_1(n), \ldots, \mathbf{u}_M(n)) + \eta_m(n), \tag{5.2}$$

where $\mathbf{u}_m(n) = [u_m(n - K), \ldots, u_m(n + K)]^T$, K is the single-side memory

$$
\begin{aligned}
y_m(n) &= \sum_{p}\sum_{k=0}^{K_1} g^{(1)}_{p,m}((k-\epsilon_p)T_s)u_p(n-k)e^{j(2\pi f_p nT_s+\phi_p)} + \sum_{(p_1,p_2,p_3)=1}^{M}\sum_{k_1,k_2,k_3=0}^{K_3} \\
&\quad g^{(3)}_{p_1,p_2,p_3,m}((k_1-\delta\epsilon_{m_1})T_s,(k_2-\delta\epsilon_{m_2})T_s,(k_3-\delta\epsilon_{m_3})T_s,f_{p_1}+f_{p_2}-f_{p_3}-f_m) \\
&\times\ u_{p_1}(n-k_1)u_{p_2}(n-k_2)u^*_{p_3}(n-k_3)e^{j(2\pi(f_{p_1}+f_{p_2}-f_{p_3}-f_m)nT_s+\phi_{p_1}+\phi_{p_2}-\phi_{p_3}-\phi_m)} + \eta_m(n)
\end{aligned} \tag{5.3}
$$

depth, η_m is additive white Gaussian noise and $\tilde{g}$ is a non-linear function of the M input vectors.

Motivated by the analysis presented in [1] for a multicarrier non-linear channel with memory, we limit the non-linearity to third order. We can then express the received symbols for carrier m as shown in (5.3) (kindly refer to the top of the next page). In (5.3), $g^{(i)}_{p_1,\cdots,p_i,m}(\cdot)$ is the channel kernel function corresponding to degree i, $\delta\epsilon_{m_i} = \epsilon_{m_i} - \epsilon_m$ and we identify in-band distortion terms as those for which $f_{p_1} + f_{p_2} - f_{p_3} - f_m = 0$ holds [1].

5.3 Predistortion Techniques for Multi-GW Scenarios

5.3.1 Distributed Data Predistortion

In the case of a single gateway, wherein all carriers are uplinked from a single entity, we can equivalently apply data [29] or signal predistortion techniques [25]. Such a centralized predistortion approach requires the availability of all the data or baseband waveform samples from all the carriers and it cannot be applied otherwise in a distributed scenario. Towards defining distributed multicarrier data predistortion methods, we henceforth consider the ground architecture of Fig. 5.3.

Given the distributed nature of the problem, we build on the multicarrier Volterra analysis of [1], allowing predistortion functions that could be implemented without data exchange. The multicarrier predistortion function is similar to the Volterra expansion of the multicarrier non-linear channel in (5.3) and considers data from all carriers in a centralized scenario. Further we limit the polynomials to third degree and the predistortion function takes the form,

$$
\begin{aligned}
x^{\mathrm{C}}_m(n) &= \sum_{p}\sum_{k=0}^{K_1} h^{(1)}_{p,m}(k)u_p(n-k) \\
&+ \sum_{(p_1,p_2,p_3)\in\Omega_m}\sum_{k_1,k_2,k_3=0}^{K_3} h^{(3)}_{p_1,p_2,p_3,m}(k_1,k_2,k_3) \\
&\quad u_{p_1}(n-k_1)u_{p_2}(n-k_2)u^*_{p_3}(n-k_3)e^{j2\pi(f_{p_1}+f_{p_2}-f_{p_3}-f_m)nT_s}.
\end{aligned} \tag{5.4}
$$

where $x_m(n)$ is the nth predistorted symbol of the carrier from the mth gateway, K_i is the predistorter memory depth of the ith degree polynomial and Ω_m is the set of inter-modulation terms considered for each carrier m with polynomial

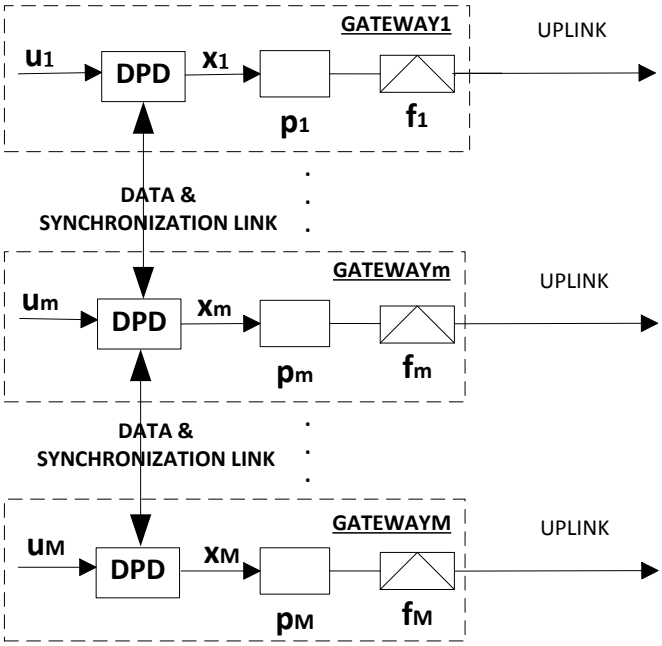

Figure 5.3: Multi-gateway data predistortion model illustrating local processing of the uplinked data at each GWs and side information exchange with the other GWs

degree three. In the sequel, we refer to the predistortion function of (5.4) as *centralized joint data predistortion* (CJDP) since it inherently requires the real-time data content from all carriers similar to a centralized (single gateway) application. This data predistortion, though easily applied in a centralized scenario, results in a high complexity distributed predistortion method where each gateway requires the instantaneous content ($u_m(n)\ \forall m, n$) from all other gateways. Further, for CJDP, baseband synchronization amongst gateways is required. Synchronization amongst gateways mandates stability of both frequency phase $\phi_m \forall m$ and delay error $\epsilon_m \forall m$ (kindly refer to (5.3)). The effects of the drift in these synchronization parameters are discussed later in the chapter.

From this fully informed solution, other predistortion functions shall be derived in the sequel to reduce the amount of data exchange amongst gateways. As described in the following subsections, the parameters of the derived predistortion functions will be a subset of the complete set of parameters of (5.4). The goal is to obtain performance benefit whilst minimizing the amount of exchanged information amongst gateways.

$$x_m^I(n) = \sum_k h_{m,m}^{(1)}(k)u_m(n-k) \tag{5.6}$$
$$+ \sum_{p\neq m}\sum_{k,k_s}[h_{m,p,p}^{(3)}(k,k_s,k_s) + h_{p,m,p}^{(3)}(k_s,k,k_s)]u_m(n-k)$$
$$+ \sum_{k_1,k_2,k_3} h_{m,m,m}^{(3)}(k_1,k_2,k_3)u_m(n-k_1)u_m(n-k_2)u_m^*(n-k_3).$$

$$x_m^A(n) = \sum_k h_{m,m}^{(1)}(k)u_m(n-k) \tag{5.7}$$
$$+ \sum_{p\neq m}\sum_{k,k_s}[h_{m,p,p}^{(3)}(k,k_s,k_s) + h_{p,m,p}^{(3)}(k_s,k,k_s)]u_m(n-k)$$
$$\times \ |u_p(n-k_s)|^2 + \sum_{k_1,k_2,k_3} h_{m,m,m}^{(3)}(k_1,k_2,k_3)u_m(n-k_1)u_m(n-k_2)u_m^*(n-k_3).$$

Independent Data Predistortion

The most efficient solution is to assume minimal communication amongst gateways for predistortion. In this case, we defined a *independent data predistortion* (IDP) method that neither requires any information exchange amongst gateways nor synchronization. Given the joint predistortion function of (5.4), we redefine the predistortion function as in (5.5) rendering it completely independent of all the other carriers,

$$x_m^{\mathrm{I}}(n) = E_{u_p(n):\forall p\neq m}\{x_m^{\mathrm{C}}(n)\}. \tag{5.5}$$

Given that $E\{u_p(n)\} = 0$, assuming $E\{u_p(n)|^2\} = 1$, and the data streams to be uncorrelated across GWs, we can rearrange the predistortion in (5.5) to the form of (5.6) (kindly refer to the top of the next page).

The formulation of (5.6) results in a single carrier predistortion function where only the carrier of interest appears explicitly ($\{u_m\}$). The key aspect is that the single carrier formulation for the predistorter has been derived for the channel operated in multicarrier model. In other words, $x_m^{\mathrm{I}}(n)$ is not equivalent to $x_m^{\mathrm{C}}(n)$ conditioned to $u_p(n) = 0\ \forall p \neq m$.

Amplitude Aware Data Predistortion

Towards improving the quality of service, we consider the case in which each GW is aware of the instantaneous amplitude of the modulated symbols uplinked from all the other gateways, i. e, $|u_m(n)|\ \forall m, n$. This assumption requires a certain amount of side information to be exchanged amongst gateways. However, the required amount of data from other gateways to implement this approach is lower then full data exchange. For example, if every GW uplinks a 16APSK signal (two ring constellation), implementing *amplitude aware predistortion* (AADP) requires a side information exchange of 1 bit per symbol among each of the GWs. Compared to this, the centralized solution requires 4 bits of exchange.

We now define the AADP function where each gateway will process its own data together with the amplitude information received from the other gateways

to reduce the non-linear effects of the channel. Noting that, given the symbol $u_p(n) = |u_p(n)|e^{j\theta_m(n)}$ and recalling the centralized predistortion function of (5.4), we redefine the AADP as in (5.8). Such a formulation is independent of the phase of symbols from other carriers.

$$x_m^{\mathrm{A}}(n) = E_{\theta_m(n):\forall p\neq m}\{x_m^{\mathrm{C}}(n)\}. \tag{5.8}$$

Rearranging (5.8), and using $E\{e^{j\theta_m(n)}\} = 0$, we obtain the new data function (equation (5.7), kindly refer to the top of the page) where only the amplitude of the symbols from other gateways ($p \neq m$) appears.

In the derivation of (5.7), we obtained only in-band distortion terms for which we have $e^{j2\pi(f_m+f_{p_i}-f_{p_i}-f_m)nT_s} = 1$. The resulting predistortion function in (5.7) includes not only symbols from the considered carrier u_m, but also amplitude terms from all the other carriers $|u_p|$ with $p \neq m$. Similar to (5.6), the parameters of (5.7) are a subset of the full set of parameters in (5.4). Differently from (5.6), however we require instantaneous amplitude data content information to be available at each gateway. This results in a certain amount of traffic in the terrestrial network connecting the gateways.

Coarse Joint Data Predistortion

Assuming that a higher connection rate can be supported amongst gateways, we consider the case in which gateways exchange, for a given uplink modulation scheme, not only the amplitude of the symbols, but also partial phase information. Given the uplinked data symbols $u_m(n)$ with phase $\theta_m(n)$, we define $Q(\theta_m(n)) = \{1, 2, 3, 4\}$ as the information about the quadrant of the nth symbol's phase. We now assume that each gateway provides instantaneous information about the quadrant of the phase along with the amplitude of the symbols to all the other gateways. Notice that the quadrant of a symbol is represented with only two bits. This would require, for a 16 APSK modulation, an exchange involving one bit for the amplitude and two additional bits to represent the coarse phase information (a total of three bits).

Recalling the centralized predistortion model of (5.4) we define,

$$x_m^{\mathrm{R}}(n) = E_{\theta_p(n):\forall p\neq m}\{x_m^{\mathrm{C}}(n)|Q(\theta_p(n)), \forall p \neq m\}. \tag{5.9}$$

The novel function referred to as the *coarse joint data predistortion* (RJDP) and indicated with the superscript R, can be formulated using (5.9) as,

$$\begin{aligned} x_m^{\mathrm{R}}(n) &= \sum_p \sum_k h_{p,m}^{(1)}(k)\tilde{u}_p(n-k) \qquad (5.10)\\ &+ \sum_{(p_1,p_2,p_3)\in\Omega_m} \sum_{k_1,k_2,k_3} h_{p_1,p_2,p_3,m}^{(3)}(k_1,k_2,k_3)\\ &\tilde{u}_{p_1}(n-k_1)\tilde{u}_{p_2}(n-k_2)\tilde{u}_{p_3}^*(n-k_3)e^{j2\pi(f_{p_1}+f_{p_2}-f_{p_3}-f_m)nT_s}, \end{aligned}$$

where $\tilde{u}_p(n) = |u_p(n)|E_{\theta_p(n)}\{e^{j\theta_p(n)}|Q(\theta_p(n))\}$ if $p \neq m$ and $\tilde{u}_m(n) = u_m(n)$ otherwise. Focussing on the well known uplink modulation schemes – QPSK, 16APSK and 32 APSK [9]– we have that,

$$E_{\theta_p(n)}\{e^{j\theta_p(n)}|Q(\theta_p(n))\} = \frac{1}{N_Q}\sum_{\theta_p\in Q} e^{j\theta_p} = \xi_Q\ e^{j[\frac{\pi}{2}(Q(\theta_p)-1)+\frac{\pi}{4}]}. \tag{5.11}$$

where N_Q is the number of symbols falling in the quadrant for the considered modulation, and $0 < \xi_Q < 1$ with the actual value depending on the considered modulation. Due to the symmetry of the considered modulation schemes, the resulting complex vector of (5.11) will always lie on the two main diagonals of the complex plane ($y = -x$ and $y = x$). Notice that the predistortion function of (5.10) applies the same predistortion parameters as those of the centralized multicarrier predistortion of (5.4).

5.3.2 Side Information to Uplink Rate Ratio

Satellite industry considers ground segment to be critical infrastructure and hence connecting the multiple GWs adds to the fixed and operational costs. Thus illustrating the trade-off between performance benefits and connectivity costs relaxes the requirements on the design and maintenance of these elements thereby rendering a positive economic impact. In fact, current established multiple gateway systems do not foresee any data exchange to improve the overall system performance. The various techniques detailed in the previous sections require different amounts of data to be exchanged and can also be considered as intermediate steps in a progressive deployment of ground connectivity. In particular, depending on the selected predistortion methodology, each gateway requires to receive a certain amount of side information from all the other GWs in order to apply the selected predistortion methodology and uplink. We now evaluate the ratio between the required side information with respect to the GW uplink transmission rate. This changes depending on the selected predistortion mechanism and with respect to the selected modulation scheme. The side information to uplink rate ratio for a generic mth GW is defined as,

$$\mu_m = \frac{\sum_{p \neq m} R_p}{T_m} \tag{5.12}$$

where R_p (in bits/second) is the side information received from the pth GW andT_m (in bits/s) is the uplink rate for GW m. Notice that μ_m varies with the predistortion technique and modulation scheme. In Fig. 5.4 we evaluate μ_m for a three GWs scenario applying different predistortion mechanism, varying the modulation scheme (assumed identical for all GWs) and assuming uncoded communication. As shown in Fig. 5.4, IDP does not require any content data exchange resulting in zero traffic amongst gateways. On the other hand, all the other techniques require some data content exchange. RJDP shows a relative decrease of required side information as the modulation order increases. However, μ_m does not show such a behaviour for AADP.

5.3.3 Robust Estimation of Predistortion Parameters

It can be easily seen from (5.6), (5.7) and (5.10) that the parameters of the derived predistortion functions can be extracted from the complete set of the parameters of the CJDP of (5.4). Towards presenting an unified framework for estimation and for ease of comprehension, in this section, we discuss parameter estimation generally referring to the centralized model from which the parameters for the other models can be obtained. However, an equivalent estimation mode wherein each GW estimates its own predistorter parameters based on

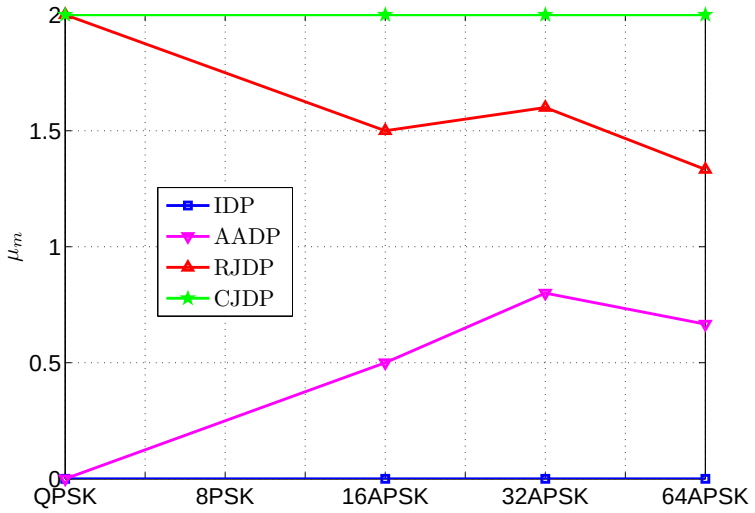

Figure 5.4: Side Information to Uplink Rate Ratio μ_m for different distributed predistortion schemes

(5.6), (5.7) or (5.10), without taking recourse to the *centralized* paradigm, will be presented at the end of the section.

The CJDP model of (5.4) is linear in the parameters $\{h_m(\cdot)\}$. The parameters can be obtained by training, using known sequences of transmitted and received symbols from all gateways. We can assume at least one dedicated receiver per beam providing sporadic feedback of received data to the corresponding transmitting gateway. Given the availability of this data, we now estimate the predistortion parameters using the indirect estimation paradigm.

In fig. 5.5 the indirect learning architecture applied to a multicarrier channel is depicted. This iterative method computes the predistortion parameters such that the predistortion function fits into a post-inverse channel function [26, 27]. However, indirect estimation can be equivalently pursued without resorting to iterative algorithm [**?**, 29, 39]. The indirect estimation approach depicted in Fig. 5.5 is very sensitive to receiver noise [39]. The receiver noise appears at the input of the non-linear predistortion function in the lower branch producing a bias in the corresponding parameter estimates [76].

Referring to Fig. 5.5, the output of the predistortion function in the lower branch results in a non-linear combination of channel output data $\{y_m\}$ and receiver noise $\{\eta_m\}$; this is shown in (5.13) at the top of the next page. As a consequence, the target error to be minimized is biased with a data dependent non-linear noise component,

$$e_m(n) = x_m(n) - [\tilde{x}_m^{\mathrm{nl}}(n) + \gamma_m(n)] \tag{5.15}$$

where $\tilde{x}_m^{\mathrm{nl}}(n)$ is the output of the feedback predistortion loop in the ideal case of zero receiver noise and $\gamma(n) = \tilde{x}_m(n) - \tilde{x}_m^{\mathrm{nl}}(n)$ is the non-linear noise which depends on the input noise and the data as shown in (5.14) at the top of the next page. This component of the noise affects the output with an average data

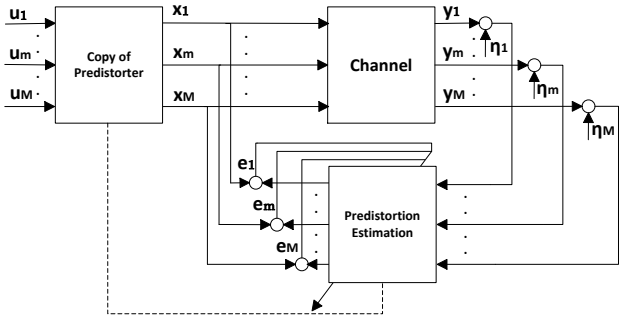

Figure 5.5: Standard indirect learning architecture for multicarrier predistortion parameter estimation

$$\begin{aligned}\tilde{x}_m(n) = &\sum_p \sum_k h^{(1)}_{p,m}(k)(y_p(n-k) \\ &+ \eta_p(n-k)) + \sum_{(p_1,p_2,p_3)\in\Omega_m} \sum_{k_1,k_2,k_3} h^{(3)}_{p_1,p_2,p_3,m}(k_1,k_2,k_3) \\ &\times [y_{p_1}(n-k_1)+\eta_{p_1}(n-k_1)]\,[y_{p_2}(n-k_2)+\eta_{p_2}(n-k_2)] \\ &\times [y_{p_3}(n-k_3)+\eta_{p_3}(n-k_3)]^* e^{j2\pi(f_{p_1}+f_{p_2}-f_{p_3}-f_m)nT_s}.\end{aligned} \tag{5.13}$$

$$\begin{aligned}\gamma_m(n) = &\sum_p \sum_k h^{(1)}_{p,m}(k)\eta_p(n-k)) + \sum_{(p_1,p_2,p_3)\in\Omega_m} \sum_{k_1,k_2,k_3} h^{(3)}_{p_1,p_2,p_3,m}(k_1,k_2,k_3) \\ &[y_{p_1}(n-k_1)y_{p_2}(n-k_2)\eta_{p_3}(n-k_3) + y_{p_1}(n-k_1)\eta_{p_2}(n-k_2)y_{p_3}(n-k_3) \\ &+ y_{p_1}(n-k_1)\eta_{p_2}(n-k_2)\eta_{p_3}(n-k_3) + \eta_{p_1}(n-k_1)y_{p_2}(n-k_2)y_{p_3}(n-k_3) \\ &+ \eta_{p_1}(n-k_1)y_{p_2}(n-k_2)\eta_{p_3}(n-k_3) + \eta_{p_1}(n-k_1)\eta_{p_2}(n-k_2)y_{p_3}(n-k_3) \\ &+ \eta_{p_1}(n-k_1)\eta_{p_2}(n-k_2)\eta_{p_3}(n-k_3))e^{j2\pi(f_{p_1}+f_{p_2}-f_{p_3}-f_m)nT_s}].\end{aligned} \tag{5.14}$$

---

dependent bias,

$$\begin{aligned}E_{\eta_{1,\ldots,M}}\{\gamma_m(n)\} = \sigma^2 \textstyle\sum_{(p_1,p_2)\in\Omega_m} \sum_{k_1,k_2} [h^{(3)}_{p_1,p_2,p_2,m}(k_1,k_2,k_2) \\ y_{p_1}(n-k_1)e^{j2\pi(f_{p_1}-f_m)nT_s} + h^{(3)}_{p_1,p_2,p_1,m}(k_1,k_2,k_1) \\ y_{p_2}(n-k_2)e^{j2\pi(f_{p_2}-f_m)nT_s}]\end{aligned} \tag{5.16}$$

where σ^2 is the noise power assumed to be equal for all carriers. Based on the approach described for single carrier in [76], we propose a robust indirect estimation method for multicarrier data predistortion that reduces the effect of the receiver noise. The estimation method is depicted in Fig. 5.6.

This approach comprises the following steps,

- First, an estimate of the channel model parameters is obtained to be used

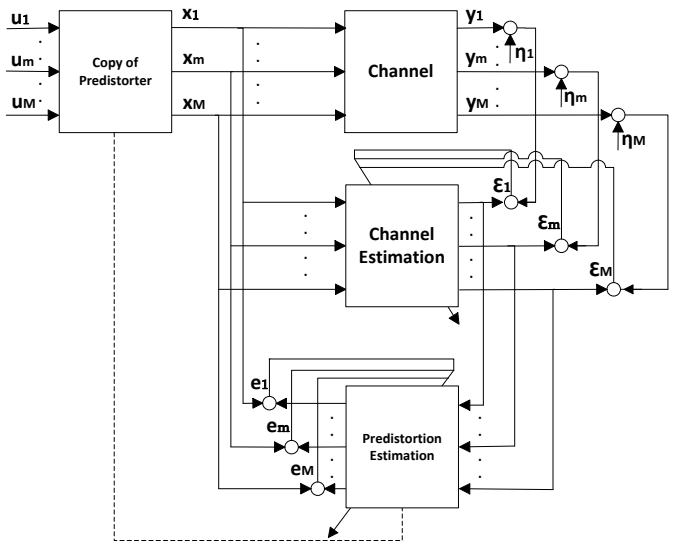

Figure 5.6: Robust Indirect Learning Architecture for Multicarrier Predistortion Parameter Estimation

for a successive predistorter parameter estimation.

- The obtained channel model then replaces the real channel during the estimation of predistortion parameters based on the indirect method. In fact, using the generated output from the channel model, we estimate the predistortion ideally eliminating the influence of receiver noise.

The key aspect is that the channel model parameters, obtained in the first step, can be estimated with high accuracy even in the presence of receiver noise [76]. This aspect is now analyzed in detail.

We consider a multicarrier Volterra model [1] to describe the channel; such a model is similar to the chosen predistortion function of (5.4). Referring to Fig 5.2 (no predistortion applied), we define $\mathbf{u}(n) = [u_1(n-K), \ldots, u_1(n+K), u_2(n-K), \ldots, u_2(n+k), \ldots, u_M(n+K)]^T$ as a column vector with $(2K+1)M$ entries collecting the input data from all carriers with memory depth K. Recalling the definition of $y_m(n)$ from (5.3) and assuming N samples of transmitted and received symbols, the channel model parameters are estimated by minimizing,

$$\sum_{n=0}^{N-1} |y_m(n) - \mathbf{g}_m^T [\psi_m(\mathbf{u}(n))]|^2 \tag{5.17}$$

where $\mathbf{g}_m = [\{g_m(\cdot)\}]$ is a column vector whose entries are the parameters of the channel model and ψ_m is a column vector stacking all the linear and non-linear combination terms of input symbols as $\psi_m(\mathbf{u}(n)) = [\{u_m(n-k)\}, \cdots, \{u_{m_1}(n-k_1)u_{m_2}(n-k_2)u_{m_3}(n-k_3)^*\}]^T$ (using this simplified notation, we have that $[\cdot]$ indicates the vector and $\{\cdot\}$ surrounding the entries indicates that undefined

indexes such as m and k are variable within some range). Towards obtaining the solution of the least squares problem, we stack these quantities to obtain,

$$\mathbf{v}_m = [y_m(0), \ldots, y_m(N-1)]^T, \tag{5.18}$$

$$\mathbf{Z}_m = \begin{bmatrix} [\psi_m(\mathbf{u}(0))]^T \\ \vdots \\ [\psi_m(\mathbf{u}(N-1))]^T \end{bmatrix}, \tag{5.19}$$

so that the minimization can be expressed as $\|\mathbf{v}_m - \mathbf{Z}_m\mathbf{g}_m\|^2$. The least squares solution for $\mathbf{g}_m$ is straightforward, leading to,

$$\hat{\mathbf{g}}_m = (\mathbf{Z}_m^H\mathbf{Z}_m)^{-1}\mathbf{Z}_m^H\mathbf{v}_m. \tag{5.20}$$

The vector collecting the received symbols $\mathbf{v}_m$ is affected by receiver noise η_m. As a consequence, the estimated kernel $\hat{\mathbf{g}}_m = \mathbf{g}_m + \eta_{\mathbf{g_m}}$ has an ideal noiseless component $\mathbf{g}_m$ and a noise component,

$$\eta_{\mathbf{g_m}} = (\mathbf{Z}_m^H\mathbf{Z}_m)^{-1}\mathbf{Z}_m^H\eta_m, \tag{5.21}$$

where $\eta_m = [\eta_m(0), \ldots, \eta_m(N-1)]^T$.

Consider the previously collected N input symbols and using the estimated channel model parameters, we generate N channel output symbols as $\tilde{y}_m(n) = \hat{\mathbf{g}}_m^T\psi_m(\mathbf{u}(n))$. These estimated channel outputs do not have an explicit noise component but they have an intrinsic noise component generated by the parameter estimation error of (5.21),

$$\tilde{\eta}_m(n) \quad = \quad \psi_m(\mathbf{u}(n))^T\eta_{\mathbf{g_m}} = [\psi_m(\mathbf{u}(n))]^T(\mathbf{Z}_m^H\mathbf{Z}_m)^{-1}\mathbf{Z}_m^H\eta_m \tag{5.22}$$

the equivalent power of the residual noise at the output of the model can be evaluated as

$$E\{|\tilde{\eta}_m(n)|^2\} = \sigma^2 \left[\psi_m(\mathbf{u}(n))\right]^T \left(\mathbf{Z}_m^H\mathbf{Z}_m\right)^{-2} \left[\psi_m(\mathbf{u}(n))\right]^* . \tag{5.23}$$

Notice that in (5.23) if $\mathbf{Z}_m$ is well conditioned, we can have $E\{|\tilde{\eta}_m(n)|^2\} << \sigma^2$. Infact, it can be proved that is $E\{|\tilde{\eta}_m(n)|^2\} < \sigma^2 || \left[\psi_m(\mathbf{u}(n))\right] ||^2 \frac{\kappa(\mathbf{Z}_m^H\mathbf{Z}_m)^2}{||(\mathbf{Z}_m^H\mathbf{Z}_m)||^2}$ where $\kappa(\cdot)$ is the condition number (kindly refer to sub-multiplicative properties of norm in [**?**]) and we used $\kappa(\mathbf{Z}_m^H\mathbf{Z}_m) = \kappa((\mathbf{Z}_m^H\mathbf{Z}_m)^{-1})$. Further, since ψ_m is a row of $\mathbf{Z}_m$, we have that $||\psi_m|| << ||\mathbf{Z}_m^H\mathbf{Z}_m||^2$. Thanks to these properties, the equivalent channel model output noise $\tilde{\eta}_m(n)$ can be drastically reduced compared to the original receiver noise $\eta_m(n)$. The resulting noise in predistorter parameters estimation follows (5.14) with $\tilde{\eta}_m$ replacing η_m. Hence the resulting bias would be smaller for the proposed method compared to standard indirect method. Using the symbols generated by the channel model, we now consider minimizing,

$$\sum_{n=0}^{N-1} |u_m(n) - \mathbf{h}_m^T \left[\psi_m(\tilde{\mathbf{y}}(n)\right] |^2, \tag{5.24}$$

where $\mathbf{h}_m = [\{h_m(\cdot)\}]$ is a column vector whose entries are the parameters of the predistortion function and $\tilde{\mathbf{y}}(n) = [\tilde{y}_1(n-K), \ldots, \tilde{y}_M(n+K)]^T$. Further, $\psi_m(\cdot)$ is a column vector stacking all the linear and non-linear combination

terms of the generated output symbols $\tilde{y}_{p_i}(n-k_i)$ and follows (5.3) (with no imperfections) . Notice that minimizing (5.24) fits the parameters $\mathbf{h}_m$ into a post-inverse channel model. The corresponding least squares problem, similar to the one derived for the channel parameter estimation, has a solution,

$$\mathbf{h}_m = (\mathbf{Q}_m^H \mathbf{Q}_m)^{-1} \mathbf{Q}_m^H \mathbf{d}_m, \tag{5.25}$$

where $\mathbf{Q}_m$ is an $N \times j$ matrix whose rows are $[\psi_m(\tilde{\mathbf{y}}(\cdot))]^T$, j being the number of parameters of $\mathbf{h}_m$ and $\mathbf{d}_m = [u_m(0), \ldots, u_m(N-1)]^T$ the column vector collecting the N input symbols. Notice that distributed estimation in the aforementioned presentation, given the parameters $\{h_m(\cdot)\}$ of the CJDP model of (5.4), each gateway will extract the required coefficients depending on the carrier m and on the selected predistortion model (kindly refer to (5.6), (5.7), (5.10)). Alternatively, given the data vectors for training, each gateway can directly estimate the parameters of the chosen predistortion model following a procedure similar to (5.25) and replacing $\psi_m(\tilde{\mathbf{y}}(\cdot))$ by a vector of linear and non-linear terms relevant to the selected predistortion method.

5.3.4 On-Ground and On-board Signal Predistortion

While the earlier discussion was related to the data predistortion, we briefly discuss the other paradigm: signal predistortion. On-ground signal predistortion has been performed on the uplinked wideband signal in [25]. The predistorter is designed in conjunction with an uplink spectral mask designed to satisfy the tight out-of-band emission restrictions.

In this centralized scenario, signal predistortion is shown to be effective even if limited by the uplink spectral mask. On one hand, uplinking of carriers from different GWs and their superposition over the air, makes the application of on-ground signal predistortion [25] infeasible. On the other hand, in a multi-gateway application, it is natural to assume that an uplink mask is assigned to each individual carrier bandwidth instead of the ensemble. As a consequence of this, signal predistortion would be limited to the carrier bandwidth resulting in single carrier predistortion and essentially being similar to data predistortion that is applied to the signal before pulse shaping (refer to fig. 5.3). This motivates us to consider on-board processing which can render gateway operation completely independent.

In general, analogue on-board processing is considered feasible and it is usually implemented in the RF domain [77], [78]. However, on-board digital processing [79] is *typically* not considered in general communication satellites, especially those in GEO orbits, due to the due to the rigid reliability requirements (related to the hostile environment, mission cost and expected satellite lifetime), power efficiency and mass limitations. In this chapter, we consider as benchmark, an on-board processing technique to compensate linear and non-linear distortion effects as depicted in Fig. 5.7.

Referring to the Saleh [23] model and based on [80], we can analytically derive the ideal memory-less on-board signal predistortion function to obtain a linearized amplifier response. The Saleh function is defined as $y = A(|x|)e^{j(\chi(|x|)+\angle(x))}$ where $A(|x|) = \frac{\alpha_a|x|}{\beta_a|x|^2+1}$ and $\chi(|x|) = \frac{\alpha_p|x|}{\beta_p|x|^2+1}$. The predistorted signal input to

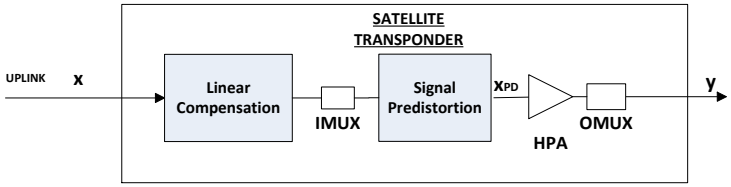

Figure 5.7: On-board digital signal predistortion scheme

the amplifier is defined as $x_{\mathrm{PD}} = xP(|x|)e^{j\Omega(|x|)}$ where,

$$P(|x|) = \begin{cases} \frac{\alpha_a - \sqrt{\alpha_a^2 - 4\beta_a|x|^2}}{2\beta_a|x|^2} & \text{if } |x| < |y|_{\mathrm{sat}}, \\ \frac{|x|_{\mathrm{sat}}}{|x|} & \text{if } |x| > |y|_{\mathrm{sat}} \end{cases}$$

where $|x|_{\mathrm{sat}} = \frac{1}{\sqrt{\beta_a}}$ and $|y|_{\mathrm{sat}} = \frac{\alpha_a}{2\sqrt{\beta_a}}$ are the amplitude saturation coordinates [80]. The predistorted phase for ideal compensation is simply defined as $\Omega(|x|) = -\chi(|x|P(|x|))$ [80]. Notice that the predistortion function $P(|x|)$, differently from [80], includes a clipping mechanism such as $|x|_{\mathrm{PD}}$ being hard limited to $|x|_{sat}$.

The obtained linearized amplifier response as shown in Fig 5.8 results is a perfectly linear characteristic in the invertible region and in a flat response in the saturation region. Phase distortion is completely compensated. Further,

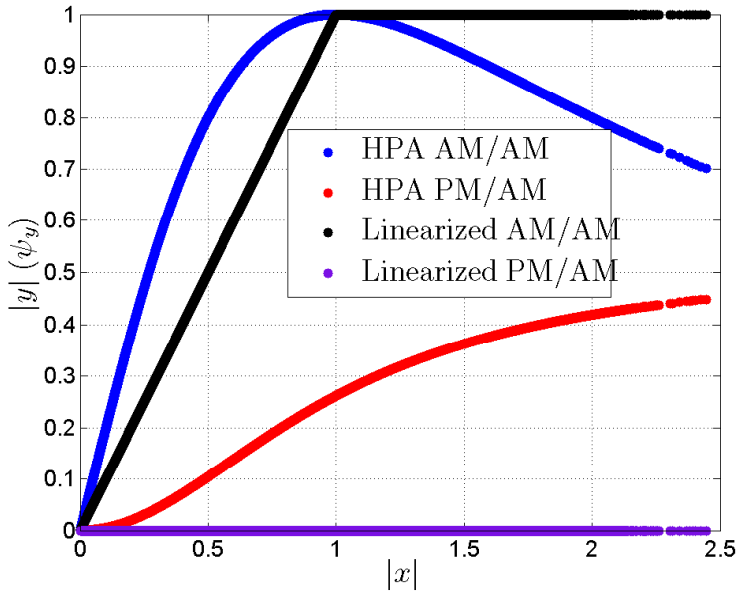

Figure 5.8: On-board HPA AM/AM and AM/PM characteristics and linearizion

in addition to the linearizion of the memory-less amplifier response, we include

digital on-board filtering to compensate for the linear distortions introduced by the IMUX and OMUX filters. This is depicted in Fig. 5.7 as *Linear Compensation* and it includes a linear filter (FIR) designed to pre-compensate the cascaded IMUX and OMUX distortion effects. The filter coefficients are estimated following a simple MMSE (least squares) design.

5.4 Simulation Results

In this section, we numerically compare the performance of the devised distributed predistortion methods. The baseline scenario includes the basic compensation of the warping distortion effects applying a one tap MMSE linear equalization. Further, we consider on-board signal predistortion as an upper bound on performance. The robustness of the proposed parameter estimation scheme with respect to noise will also be illustrate. Further, the sensitivity to imperfections in uplink synchronization will also be assessed.

5.4.1 Figure of Merit

Total Degradation (TD) is a traditional figure of merit for evaluating the performance over non-linear channels [6, 20]. It is defined as,

$$\mathrm{TD}|_{@\mathrm{BER}} = \frac{E_s}{N_0}|_{\mathrm{NL}} - \frac{E_s}{N_0}|_{\mathrm{AWGN}} + \mathrm{OBO} \tag{5.26}$$

where $\frac{E_s}{N_0}|_{\mathrm{NL}} - \frac{E_s}{N_0}|_{\mathrm{AWGN}}$ represents the energy loss between the non-linear and linear channels for a given target bit error rate (BER). Output Back Off (OBO) is defined as the ratio in dB between the multicarrier signal output power and the saturation output power of the selected amplifier model. For the considered amplifier model, we have a nominal saturation output power of 0 dB. When the amplifier is operated in the high efficiency region, it yields strong distortion effects increasing the needed $\frac{E_s}{N_0}|_{\mathrm{NL}}$, while in linear operation we have a power efficiency degradation and the same is accounted by the OBO. The total degradation when illustrated as a function of the OBO resulting in convex ; its minimum identifies the optimal amplifier operating point. Notice that (6.40) reduces to $\mathrm{TD}|_{@\mathrm{BER}} = \mathrm{OBO}$ in case of perfect compensation or absence of non-linear interference and serves as a lower bound.

5.4.2 Scenario Definition

A simulation chain has been set up for evaluating the performance of the proposed techniques. Referring to the DVB-S2 standard for satellite communication [9], we consider the signal characteristics described in Table 5.1.

Similarly to [1, 25], the choice of using higher order modulation is motivated by the challenges posed by them while achieving higher spectral efficiency. The high PAPR typical of the multi-ring constellation (such 16/32APSK) is further enhanced in case of multiple carrier signaling. Hence, such a scenario presents an ideal case to depict the applicability of the proposed algorithms to challenging settings. In Table 5.1, $\frac{E_s}{N_0}$ in the training phase corresponds the noise during predistorter parameter estimation. A high oversampling rate is needed for simulating the chain due to the spectral enlargement caused by non-linearities.The

Table 5.1: Simulation Parameters

Number of carriers/gateways	$M = 3,\ 5$
Modulation, Code Rate	32APSK, 9/10
Symbols rate , Roll Off	$R_s, \rho = 0.25$
Carrier frequency spacing, $\triangle f$	1.25 R_s
Target BER	10^{-5}
$\frac{E_s}{N_0}\vert_{AWGN}$ @ Target BER	16 dB
$\frac{E_s}{N_0}$ @ Training Phase	25 dB
HPA	Saleh model [23]

power imbalance parameters are considered to be ideal, i.e., $w_m = 1,\ \forall m$ in (5.1).

5.4.3 Predistortion Model Settings

The CJDP function of (5.4) requires the definition of parameters such as memory depth as well as the selection of the intermodulation terms to be included. Differently from previous works on multicarrier data predistortion [**?**,29] we consider not only the in-band distortion terms for which $f_{p_1} + f_{p_2} - f_{p_3} - f_m = 0$, but also the first order out-of-band terms of the model [1], for which we have $f_{p_1} + f_{p_2} - f_{p_3} - f_m = \pm\Delta f$. As shown in [1], the inclusion of these terms improves the model accuracy. The in-band and out-of-band terms are listed in Table C.1, C.2 and C.3 of Appendix C.1 for a third degree non-linear Volterra model for three and five carriers. Notice that the out-of-band terms are not included in the IDP and AADP predistortion methods but only in RJDP and CJDP.

Due to the large amount of intermodulation terms considered, and towards reducing the predistorter complexity, we selected a subset of non-linear terms that include memory effects. Referring to the CJDP model of (5.4), we considered a single side memory depth $K_1 = K_3 = 10$ for the linear and in-band non-linear terms (kindly refer to Table C.1). Further, non-linear memory is limited only to the diagonal terms such as $k_1 = k_2 = k_3$ (kindly refer to (5.4)). On the other hand, the out-of-band inter-modulation terms are considered memoryless (kindly refer to Tables C.2, C.3). This particularly chosen setting is the result of several simulation tests and fine tuning conducted with the purpose of trading off the relative performance gain and the complexity of parameter estimation.

5.4.4 Performance Evaluation

In this section we evaluate the TD of the considered methods for a three and five carriers scenarios.

Three carrier scenario

In Fig. 5.9 and 5.10 we see the TD results for a three carrier multi-gateway channel. Observing the result of the central carrier in Fig. 5.9, the performance improves as expected with the amount of side information. IDP provides a significant interference reduction compared to the case where only average warping compensation is applied of about $0.5 - 0.75$ dB. A minor gain of about $0.2 - 0.3$ dB is provided by the AADP over the IDP for the central carrier while the gain is $0.5 - 0.75$ dB for the outer carrier. On the other hand RJDP substantially improves the power efficiency and provides additionally $1 - 1.5$ dB of gain over AADP for the central carrier. CJDP provides about 0.5 dB of further improvement. The performance upper bound defined by the case of on-board signal predistortion is quite close the performance of the CJDP (about 0.3 dB) demonstrating the accuracy of the data predistortion model over signal predistortion The external carrier performance (only one carrier is shown for symmetry) is similar to the central carrier, but degrades to a lower extent.

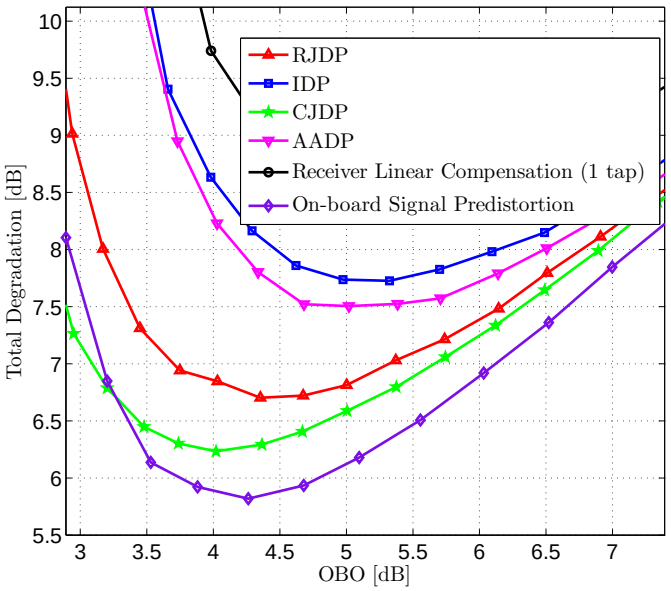

Figure 5.9: Total Degradation Performance for the Central Carrier: Three Carriers Channel

Five carrier scenario

Fig. 5.11 shows the TD for the central (innermost) carrier in a five carrier scenario. The order of performance for the different techniques is similar to the three carrier scenario, albeit, with reduced relative gains. Fig. 5.12 shows the TD result for the external (outermost) carrier in a five carrier scenario. Due to the nature of the channel [1], outer carriers are, in general, subject to lower ACI compared to inner carriers, thereby providing slightly lower TD values.

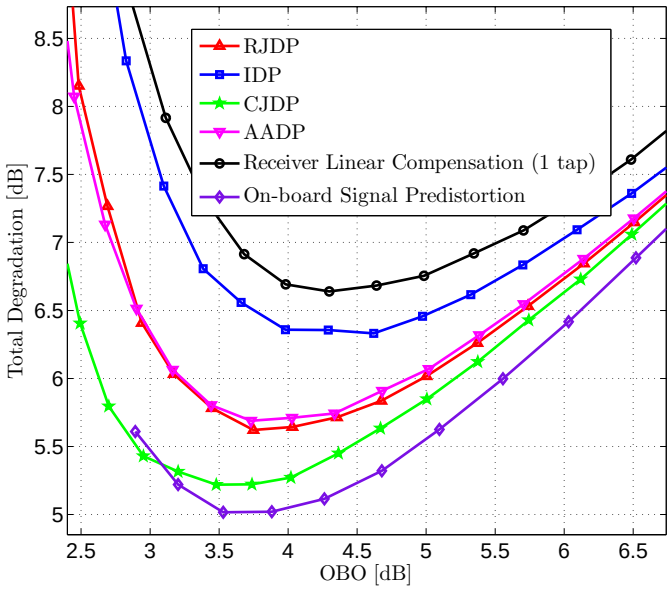

Figure 5.10: Total Degradation Performance for the Outer Carrier: Three Carriers Channel

5.4.5 Sensitivity to Estimation Noise

In this section, we evaluate the performance of the robust estimation method presented in Section 5.3.3 with respect to standard indirect estimation [29]. During the estimation phase, a certain amount of noise, specified by E_s/N_0, is applied at the receivers. Clearly, this affects the accuracy of the estimated predistortion coefficients for all the devised predistortion models. The corresponding TD is now evaluated for a given OBO in a three carrier scenario.

Fig. 5.13 and 5.14 show the variation of TD with respect to the applied estimation noise for the central and outer channel, respectively. Standard (indirect) estimation is shown to be very sensitive to the estimation noise for all the considered techniques, while robust estimation outperforms the standard method while providing a response invariant to noise level. The comparison illustrated in Fig. 5.13 and 5.14 includes also the direct estimation method proposed in [**?**] and here applied to the complete model case of CJDP. As shown in [**?**], direct learning outperforms standard indirect estimation when high noise is present during parameter estimation. On the other hand, at a lower noise regime, we have a minor loss due to the modeling errors typical of the direct estimation [39].

5.4.6 Analysis of Sensitivity to Synchronization

The devised distributed data predistortion techniques rely on the assumption that gateways are capable of sharing some data content as side information. Further, for the full predistortion model of (5.4) to hold, we require frequency and

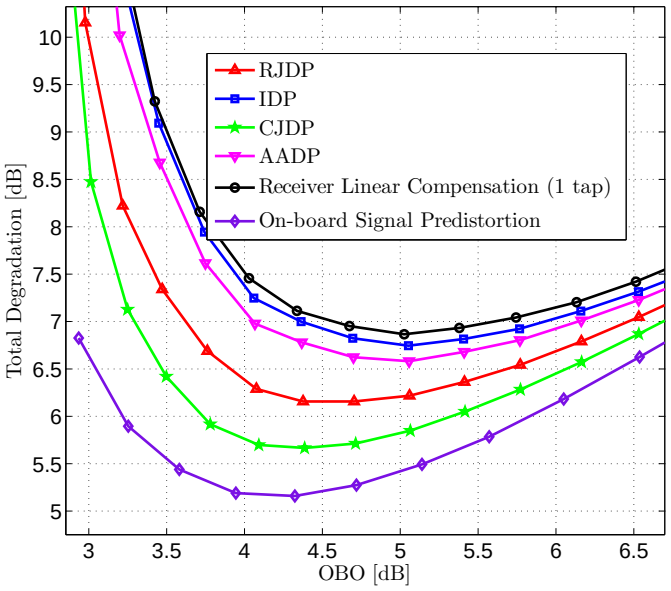

Figure 5.11: Total Degradation Performance for the Central Carrier: Five Carriers Channel

time synchronization across gateways. Assuming the availability of such a synchronization mechanism, for instance based on the GPS signal (the GPS timing signal provides accuracy in the order of 100 ns and is already used to synchronize terrestrial wireless base stations [81]), we now investigate the system sensitivity to drifts in synchronization parameters (measured with the parameters ϵ_m and ϕ_m of (5.3)). Referring to (5.3), we consider estimating the predistortion parameters for a reference case with $\epsilon_m = 0$ and $\phi_m = 0$, $\forall m$, while in a second phase, we test the system performance simulating a drift in one of the uplink synchronization parameters.

In Fig. 5.15, 5.16 we evaluate the variation of the TD at a given OBO, for the central and outer carrier, with respect to a baseband timing misalignment ϵ_2. It should be noted that the misalignment occurs only in the inner carrier while $\phi_m = 0$ $\forall m$.

Fig. 5.15 and 5.16 show that if the alignment of the baseband signals deviates from the ideal case, the system undergoes a significant performance loss for all cases except, as expected, IDP which remains invariant. On the other hand,even with 30% sync losses, having some data exchange provides better performance than IDP. The synchronization error is introduced in the inner carrier resulting in higher degradation in the inner carrier. However, observing Fig. 5.16, relative to the outer carrier, we notice a significant sensitivity to the inner carrier synchronization as well.

Similar to the previous case, in Fig 5.17 and 5.18 we consider an ideal predistortion estimation phase in which $\epsilon_m = 0$ and $\phi_m = 0$, $\forall m$ and a subsequent operational phase where only ϕ_2 undergoes a drift. In Fig. 5.17 and 5.18 we observe severe degradation in the cases of CJDP and RJDP, while IDP and

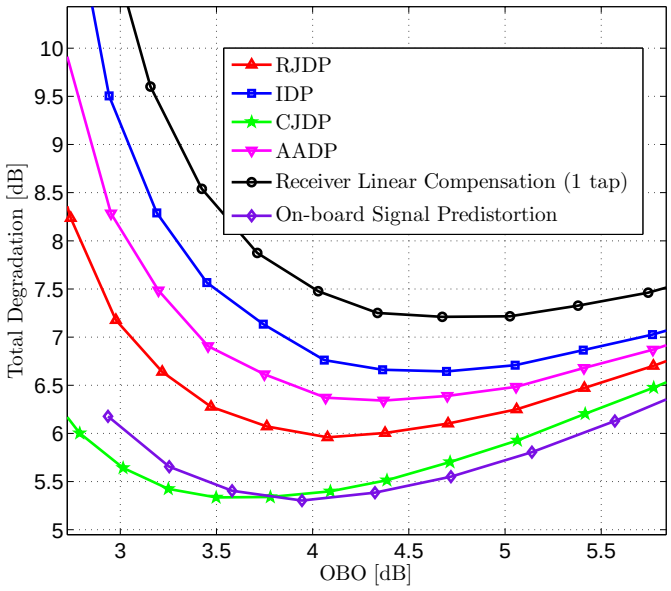

Figure 5.12: Total Degradation Performance for the Most External Carrier: Five Carriers Channel

AADP provide completely invariant performance. The invariance to phase drift of both the IDP and AADP is related to their in-band distortion nature (kindly refer to (5.6) and (5.7)). Given the in-band distortion characteristic of (5.6) and (5.7), we can easily show that the predistortion function is linear with respect to phase rotation. Essentially,

$$\begin{aligned} x_m^{\mathrm{I,\,A}}(n) &\triangleq f_{\mathrm{I,\,A}}(\mathbf{u}_1(n),\ldots,\mathbf{u}_m(n),\ldots,\mathbf{u}_M(n)) \\ e^{j\phi_m} f_{\mathrm{I,\,A}}(\ldots,\mathbf{u}_m(n),\ldots) &= f_{\mathrm{I,\,A}}(\ldots,e^{j\phi_m}\mathbf{u}_m(n),\ldots). \end{aligned} \tag{5.27}$$

Using this property, we can claim that a phase rotation applied to the predistorted symbol is equivalent to a rotation of the data $u_m(n)$ by the same amount ($x_m^{\mathrm{I,\,A}}(n) \rightarrow e^{j\phi_m} x_m^{\mathrm{I,\,A}}(n) \Rightarrow \mathbf{u}_m(n) \rightarrow e^{j\phi_m}\mathbf{u}_m(n)$). Thus the effect of phase rotation by the channel can be moved to the data allowing the receiver to compensate the same via simple equalization. This indicates the importance of the single tap MMSE equalizer. However, property (5.27) does not hold when out-of-band terms are included in the predistortion model (for example CJDP and RJDP methods). Thus the resulting mismatch cannot be compensated by the single tap equalizer.

5.5 Conclusion

In this chapter we proposed several predistortion techniques with the goal of counteracting non-linear effects in a multi-gateway non-linear satellite channel. Different on-ground distributed data predistortion algorithms have been proposed to trade-off between required information exchange amongst gateways and

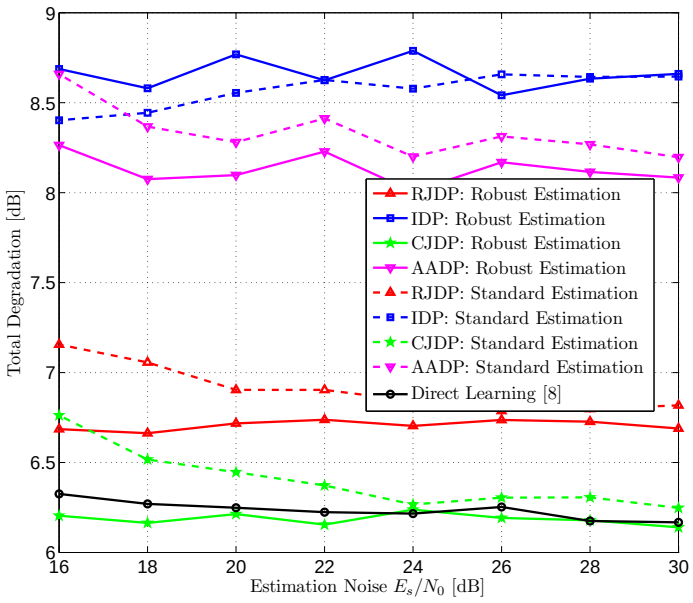

Figure 5.13: Sensitivity of TD to Estimation Noise: Central Carrier of Three Carriers Channel

system performance. A robust estimation approach has been devised for multi-carrier predistortion improving substantially the system performance. Assumptions on synchronization have been critically analyzed and investigated through extensive sensitivity simulations. AADP, amongst all the considered schemes, is the one providing the best trade-off between performance and amount of required terrestrial data traffic, as well as a stable performance with respect to uplink synchronization mismatches.

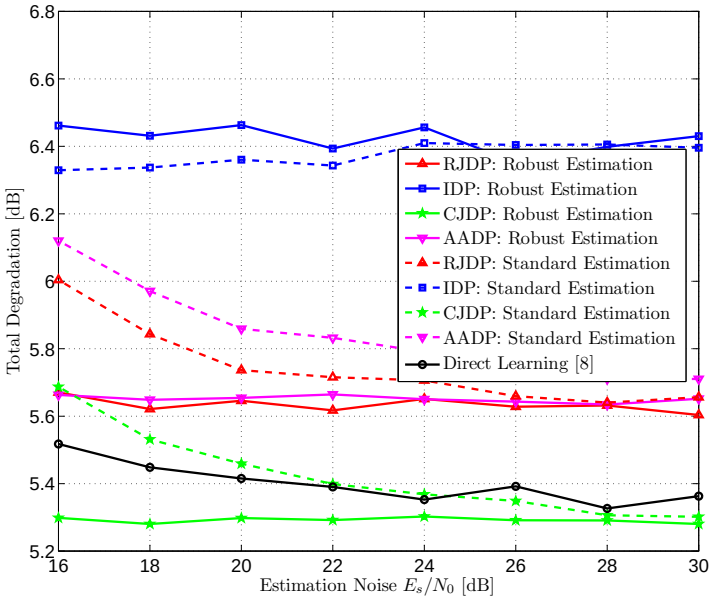

Figure 5.14: Sensitivity of TD to Estimation Noise: Outer Carrier of Three Carriers Channel

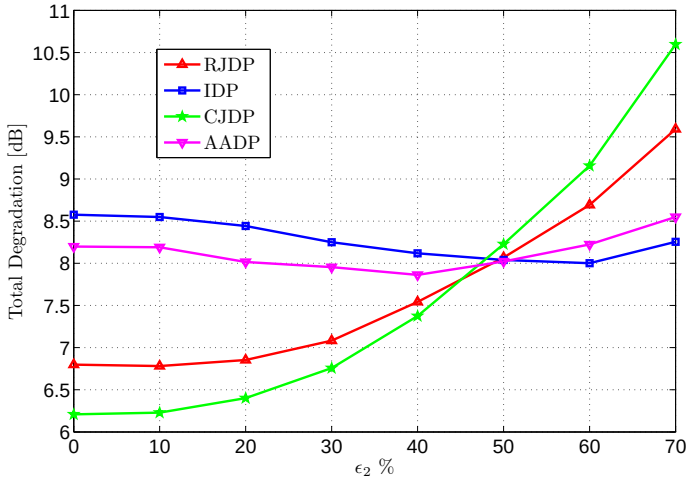

Figure 5.15: Total Degradation Sensitivity to Inner Carrier Timing Error ϵ_2 with $\epsilon_1 = \epsilon_3 = 0$: Inner Carrier

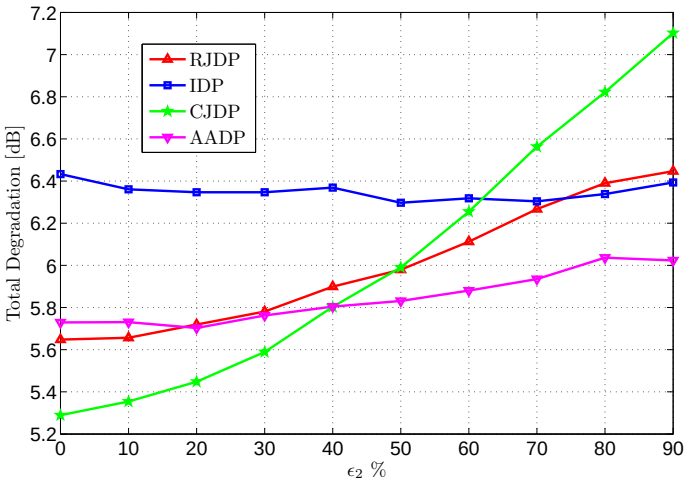

Figure 5.16: Total Degradation Sensitivity to Inner Carrier Timing Error ϵ_2 with $\epsilon_1 = \epsilon_3 = 0$: External Carrier

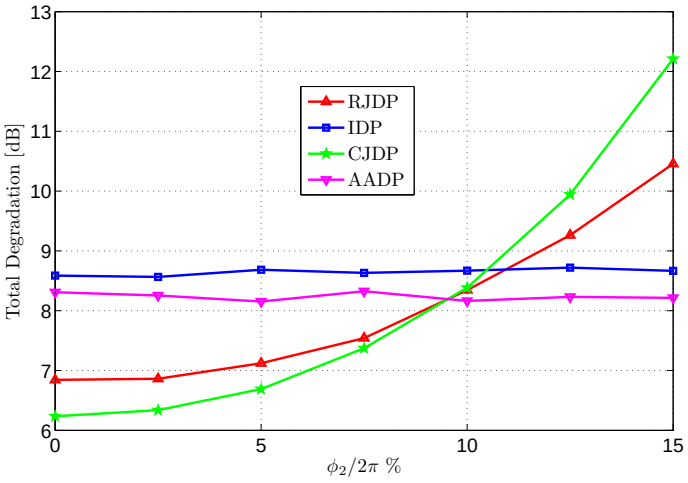

Figure 5.17: Sensitivity Inner Carrier of Three Carriers Channel to Inner Carrier Frequency Phase ϕ_2 with $\phi 1 = \phi_3 = 0$

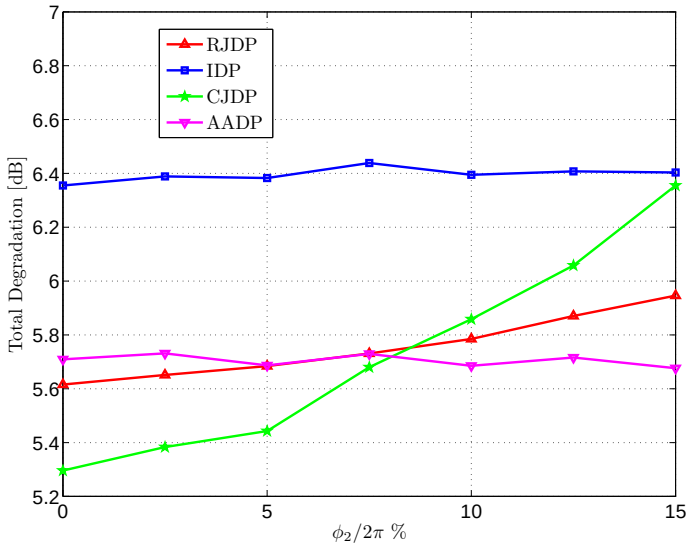

Figure 5.18: Sensitivity Inner Carrier of Three Carriers Channel to Outer Carrier Frequency Phase ϕ_2 with $\phi 1 = \phi_3 = 0$

Chapter 6

Equalization Techniques

6.1 Introduction

In this chapter we present different approaches to the equalization of a multiple carrier non-linear satellite channel. This includes different scenarios and techniques:

- UT equalization in the forward link:
  - Single carrier equalization [29, 30, 58] (presented in section 6.2)
  - Low complexity multiple carrier equalization [59](presented in section 6.3)
- Multiple carrier GW equalization [61] (presented in section 6.4)

Single carrier UT equalization techniques are considered for commercial broadcast applications. In this chapter we propose symbol and fractional space equalization and performance are evaluated in the multiple carrier scenario in combination with multiple carrier predistortion techniques discussed in chapter 3. Further, we devise a method to enhance receiver decoding performance for fine optimization over the residual distortion bias in the received constellation.

Joint equalization or multiple received carriers is considered for professional applications in the forward link. Low complexity multiple carrier joint equalization is enabled by applying specific complexity reduction techniques, generally known as Least Absolute Shrinkage and Selection Operator (LASSO), to limit the total number of model parameters. This contribution includes the comparison with an equivalent predistortion model. in the specific, our contribution refers only to the design and definition of the equalization while the LASSO algorithm and the predistortion itself are developed from the main author of [59].

Finally we consider a multiple carrier return link, in section 6.4 we propose gateway joint equalization of multiple carrier, each one representing an independent user, to improve carrier spectral efficiency.

6.2 Symbol and Fractionally Spaced Equalization

In the following we present symbol and fractionally spaced single carrier equalization for multiple carrier satellite channels. The considered scenario and channel model is the one presented in chapter 2 and is herein repeated for completeness.

6.2.1 Multiple Carrier Scenario

Figure 6.1 illustrates the addressed satellite system scenario, which refers to a multicarrier satellite channel where independent channels are uplinked to a transparent satellite. A gateway transmits a broadcast or broadband forward link carrier, typically a DVB-S2 signal, to a number of receivers. The considered frequency bands are mainly Ka-band and Ku-band frequencies for broadcast or broadband fixed satellite services (BSS/FSS) applications. On board the satellite, joint filtering and amplification takes place before the signals are downlinked to ground receivers. As described in [29], joint on board filtering and amplification of the stream of carriers allows for a significant saving in hardware complexity and weight.

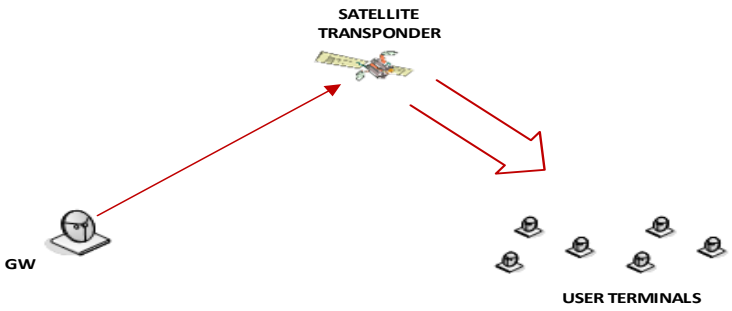

Figure 6.1: Satellite Communication System Scenario

6.2.2 Multicarrier Non-linear Satellite Channel Characteristic

The channel model is shown in Figure 2. M carriers are uplinked from a single gateway to a satellite transponder for channelization power amplification.

IMUX and OMUX filter responses are depicted in Figure 6.3 for the case of a standard 36 MHz transponder bandwidth.

On-board HPAs are implemented with TWTAs that are intrinsically non-linear, especially when operated in their high efficiency region. However, partial linearization of the TWTA amplifier can be achieved on-board by means of specific RF technology resulting in the Linearized-TWTA (L-TWTA). Further, the TWTAs used in Ku-band can be assumed to have a transfer characteristic

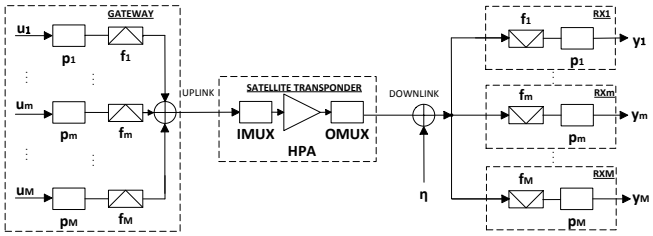

Figure 6.2: Channel Model for the considered scenario where f_m is the mth carrier center frequency and p_m is the pulse shaping function

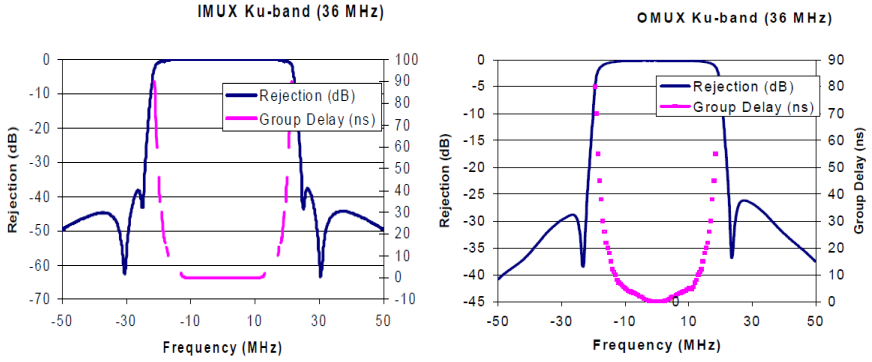

Figure 6.3: Typical IMUX and OMUX filter characteristics

largely independent of the frequency. Such memoryless amplifier functions are characterized by the AM/AM and AM/ PM curves. These curves are depicted in Figure 6.4 for a representative TWTA and L-TWTA considered in the exercise.

Since the channel is non-linear and has memory, we not only have constellation warping effects but significant ISI and ACI. Inter-symbol Interference is generated by the inherent memory combined with the non-linear characteristic of the amplifier. However, in our scenario, the dominant interference effects are the non-linear ACI excited by the intermodulation products generated by the multicarrier joint amplification.

6.2.3 Baseline On-ground Mitigation Techniques

Multicarrier data predistortion is considered at the transmitting gateway in combination with single carrier symbol rate equalization at the receiving user terminals [29].

Figure 6.5 depicts the overall baseline system model where both predistortion and equalization are applyed. As discussed in Chapter 3, data predistortion function takes the form of a multicarrier memory polynomial where each carrier is predistorted by a polynomial function with memory,

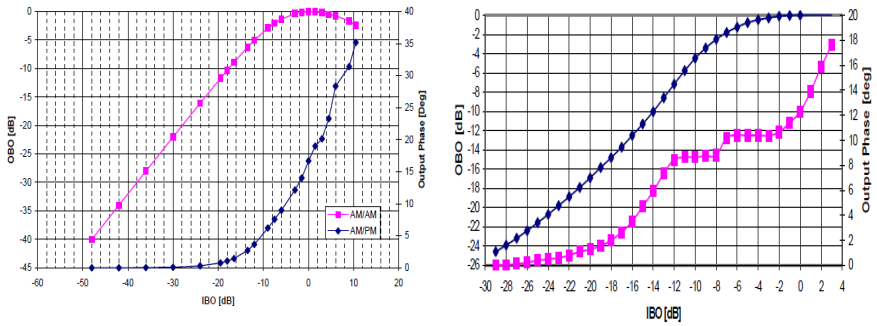

Figure 6.4: LUT based AM/AM and AM/PM characteristics TWT 197 (left) and LTWTA

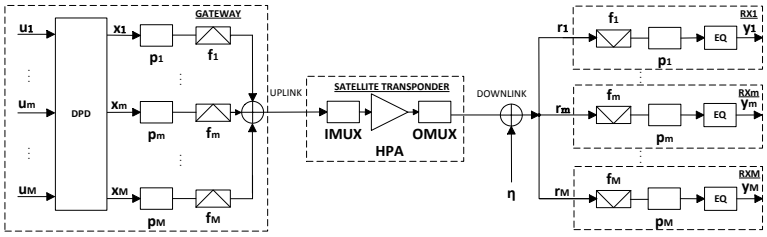

Figure 6.5: System Block Diagram

$$x_m(n) = \sum_p \sum_{k_1} h^{(1)}_{m,p}(k_1) u_p(n-k_1) + \sum_{p_1 p_2 p_3} \sum_{k_3} h^{(3)}_{m,p_1,p_2,p_3}(k_3) u_{p_1}(n-k_3) u_{p_2}(n-k_3) u_{p_3}(n-k_3)^* \tag{6.1}$$

where $u_p(n-k_p)$ is the $n-k$ th symbol of the pth carrier and $h^{(d)}_m(k)$ are the coefficients relative to the polynomial degree d. Parameters estimation is based on sporadic feedback provide by some dedicated receiver to the transmitting gateway1. Single carrier symbol rate equalization is implemented at the UT applying MMSE linear of linear symbol rate filtering,

$$y_m(n) = \sum_k h_m(k) r_{d,m}(n-k) \tag{6.2}$$

where $y_p(n-k)$ is the $n-k$ th symbol of the mth carrier and h_m are the linear coefficients. Estimation of the equalizer parameters is performed using the pilots already included in DVB-S2 standard [9].

6.2.4 Symbol Spaced Equalization for Multiplecarrier

While multicarrier digital predistortion is implemented at the transmitter side, in reality, it cannot fully compensate the distortion effects of the channel. Digital predistortion implemented in the form of a memory polynomial function is well suited to compensate for the effects of IMUX and HPA , while the remaining distortion introduced by the OMUX filter can be effectively addressed by single carrier linear equalization at the receiver side. Moreover, equalization at the receiver can be easily made adaptive capable to track fast channel variations with the aid of dedicated training symbols.

Symbol spaced equalization operated after the receiver match filter on the sampled signal (kindly refer to Fig. 6.6). The sampling rate corresponds to the symbol rate R_s.

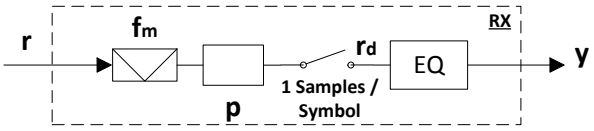

Figure 6.6: Symbol Spaced Equalization

$$y(n) = \mathbf{r}_d(n)\mathbf{h} \tag{6.3}$$

where $\mathbf{r}_d(n) = [r_d(n), \cdots r_d(n-N)]^T$, N the filter memory depth and $\mathbf{h}$ is the receiver coefficients vector.

Identification

For a given order and memory, estimation of the kernel coefficients can be formulated as a Linear Least Squares problem In this work, a standard Recursive Least Squares implementation is considered to reduce the complexity and to be able to track channel changes. In all equalization cases, RLS technique is employed to iteratively adapt the kernel coefficients to channel changes according to the following set of equations:

$$e(i) = d(i) - u(i)^T h(i-1) \tag{6.4}$$

$$g(i) = \frac{P(i-1)u(i)^*}{\gamma + u(i)^T P(i-1)u(i)^*} \tag{6.5}$$

$$P(i) = \gamma^{-1}P(i-1) - g(i)u(i)^T\gamma^{-1}P(i-1) \tag{6.6}$$

$$h(i) = h(i-1) + e(i)g(i) \tag{6.7}$$

where $u(i)$ is the vector of all the linear terms included in the equalization function (form and number of terms depend on the type of model, degree and memory depth), $h(i) = [h_1^i(0), \cdots h_1^i(K-1)]^T$, is the vector consisting of the

kernel coefficients during the ith instance, $d(i)$ is the desired symbol and γ the forgetting factor.

Each frame is assumed to have a dedicated *codeseg1* of 90 training symbols in the target modulation. This allows supporting Adaptive Code Modulation operation mode foreseen by the standard, as well as estimating the drift in channel parameters. From simulation results the forgetting factor has been set to 0.995.

6.2.5 Fractionally Spaced Equalization for Multiple carrier

The primary goal of this work is to investigate the use of FSE in a multicarrier scenario with the aim of reducing the performance degradations caused by

- Non-constant group delay of the on-board filters
- Residual non-linear distortions that are present after the use of DPD

Further, the FSE is implemented on a per carrier basis with the requirement of a low receiver complexity. In view of this, we consider a FSE working at an oversampling factor of 2 and not any higher. This receiver is based on the assumption that the group delay distortions are significant and that the DPD has well compensated for the non-linear distortions. In addition, it is also seen from earlier works that the gains in performance due to higher oversampling do not offset the increase in receiver complexity and training overhead. Hence the oversampling factor of 2 is considered henceforth.

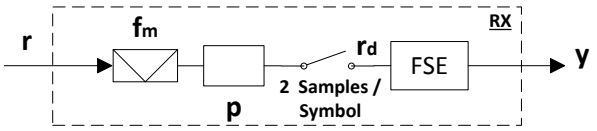

Figure 6.7: Fractionally Spaced Equalization

Given the restriction to an oversampling of 2 and referring to Figure 6.7, we consider a general equalization function with the expression,

$$y(n) = \sum_{k_1} b(k_1) v(n - k_1) \tag{6.8}$$

where $v(n-k)$ is the $n-k$ th received symbol in upsampled domain and b are the linear coefficients. Notice that in Figure 6, we consider as matched filter a standard square root raised cosine function as per DVB-S2 standard. The output of the FSE is sampled at the symbol rate. It is important to note that the bandwidth of the signal used in processing is $(1+\rho)/T_s$ where ρ is the roll-off factor and corresponds to the bandwidth of the matched filter and T_s to the symbol time. Let $y(n)$ be the output of FSE when $v(n)$ is the stream input

to the FSE. Assuming that the training consists of N pilots denoted by $u_m(n)$, the coefficients of the FSE are designed to minimize the error $\sum_{n=1}^{N} E[r(n) - u_(n)]^2$ where $r(n)$ is the response of the FSE to$v(n)$. Further $v(n)$ is the stream obtained when $u(n)$ is transmitted. The minimization is a Linear Least Squares problem (both for linear filters and kernel of non-linear filters) and can be solved using standard techniques as described in section 6.2.4.

Optimized Demapping

Demapping in the traditional sense involves generating Euclidean distance between a received (and processed) point and those in the constellation. However, since the non-linearites and memory effects are not completely compensated, a bias is, in general, added to the constellation points at the receiver. In other words, the centroids obtained from the scatter plot do not coincide with the reference constellation points. To overcome this mismatch, the decoder is tuned to compute Euclidean distance to the centroids and not the constellation points per-se. Let F_k be the cluster of points obtained corresponding to the constellation points a_k. Let c_k denotes the centroid of F_k obtained as,

$$c_k = arg\ min_c \hat{a}\text{Ą}\text{ą} \sum_{x \in F_k} |x - c|^2, k \in [1, M] \tag{6.9}$$

Instead of finding the Euclidean distance between any received point and a_k, we consider demapping to c_k. The proposed scheme differs from the âĂIJaverage constellation demappingâĂİ (ACD) where the demapping is performed to βa_k where β is obtained as,

$$\beta = arg\ min_c \frac{\sum_{k=1}^{M} \sum_{x \in F_k} |x - c|^2)}{\sum_{k=1}^{M} |a_k|^2} \tag{6.10}$$

On the other hand, the centroid based demapping (CBD) uses M variables instead of one in the average constellation demapping. Figure 6.8 show the residual bias between the estimated centroids and the standard reference constellation points.

The centroids are obtained apriori using the same training used for the estimation of the equalizer coefficients. Once the centroids are obtained, implementing the centroid based decoding is trivial. Note that a serial processing paradigm is used: equalizer coefficients are derived first based on constellation points and then the centroids are found using the equalizer output (after equalization is applied). This method is straightforward (if not optimal) and allows for a simpler decoder implementation.

6.2.6 Performance Evaluation

Figure of Merit

Performance of each channel is evaluated by means of the Total Degradation (TD) [6] defined as,

$$TD|_{BER} = \frac{E_s}{N_0}_{NL} - \frac{E_s}{N_0}_{AWGN} + OBO \tag{6.11}$$

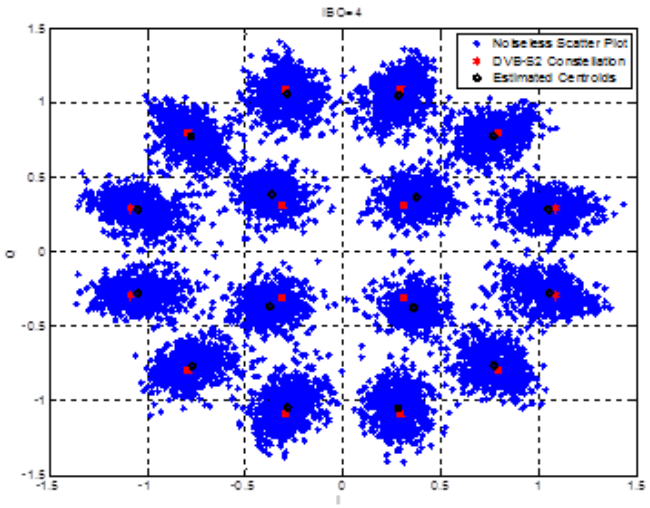

Figure 6.8: Noiseless Receiver Scatter Plot with Centroids for a Three Carriers Satellite Channel

Here, $\frac{E_s}{N_0}_{NL}$ is the signal to noise ratio needed in the considered non-linear (NL) channel to achieve the target bit error rate (BER) for the specific modulation and code scheme, while $\frac{E_s}{N_0}_{AWGN}$ is the signal to noise ratio achieving the same target BER with an identical transmission scheme but with a linear AWGN single carrier channel and, finally, OBO is a measure of the on-board HPA power efficiency. The total degradation results in a convex function of the output back-off providing for the optimal amplifier operating point.

Numerical Results

Figure 6.9 shows the performance evaluation for symbol spaced equalization for a three carrier channel with multiple carrier data predistortion applied at the transmitter.

Symbol spaced equalization can provide about 0.2 dB of extra gain at the top of multple carrier multiple carrier predistortion (kindly refer to Fig. 6.9). Additional gain can be achieved applying fractionally spaced equalization and optimized receiver decoding (kindly refer to Figures 6.10,6.11).

Results show that FSE is capable of improving performance over symbol spaced equalization. Further, centroid decoding provides an additional performance gain compensating the residual warping effects for an optimal decoding process.

6.2.7 Robustness to Sampling Error

In this section, we assess the sensitivity of FSE and standard equalization with respect to receiver sampling error. The sensitivity is investigated by computing

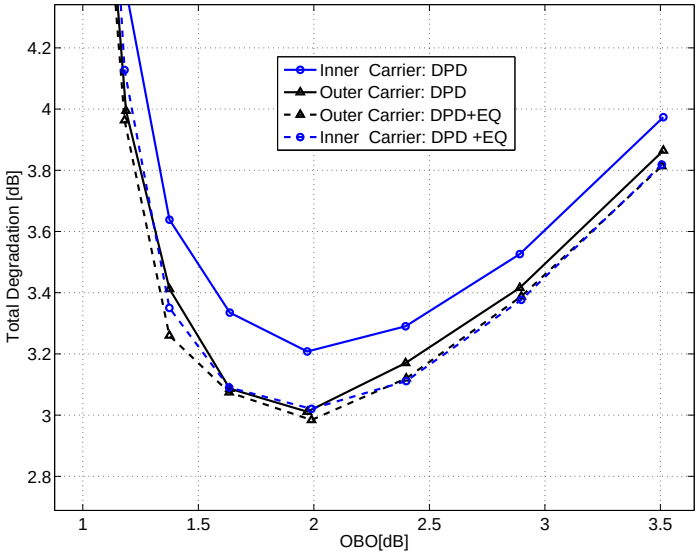

Figure 6.9: Symbol Spaced Equalization Performance For Three Carrier With 10 Mbaud (16 APSK 3/4), Roll-Off = 0.2, Interpolated LUT For TWTA No Overlap Among Carriers

the system bit error rate when the receiver sampling is intentionally moved from the ideal sampling instant. The bit error rate results for the inner channel in a three carriers scenario is depicted in Figure 6.12 for different sampling errors. FSE equalization can substantially compensate for the receiver sampling error even when considering very large error. On the other hand, symbol rate equalization is very sensitive to sampling error and can generate severe performance degradation.

The section studied the use of Symbol and Fractionally Spaced equalization techniques for multiple carrier non-linear satellite channels. Multicarrier data predistortion is considered as baseline at the uplink GW while FSE equalization techniques are evaluated at the UTs for different scenarios. Towards improving decoding performance, optimized symbols demapping is implemented after FSE to compensate for the residual distortion bias. FSE is shown to provide 0.1 - 0.2 dB of TD gain. The combination of FSE with the optimized symbols demapping method provides an addition 0.1-0.3 dB of TD reduction. Further, also in this specific scenario, it is shown that FSE is very robust to the receiver sampling error. In conclusion FSE is shown to provide improved performance and robustness with very low complexity impact in the UT architecture motivating its use in future satellite systems.

In the following section we consider multiple carrier joint equalization at the user terminal for improved performance in professional applications.

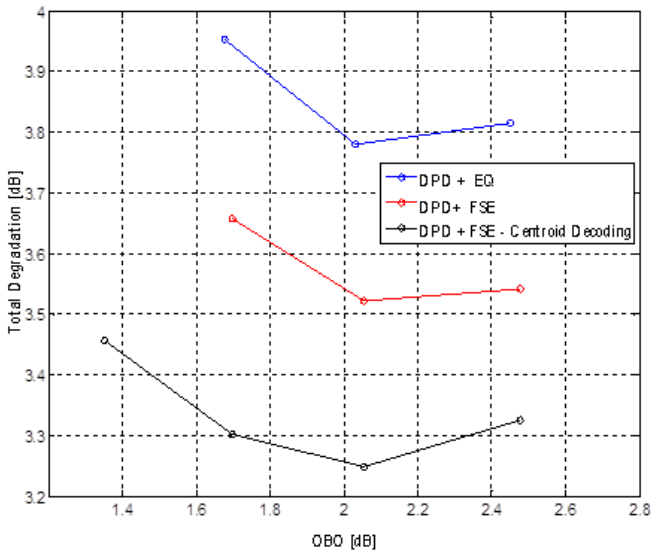

Figure 6.10: Comparison of FSE With Centroid Based Demapping And Average Constellation Demapping For Dual Carrier With 16.36 Mbaud (16 APSK 3/4), Roll-Off = 0.2, Interpolated LUT For TWTA No Overlap Among Carriers

6.3 Joint Multiple Carrier Equalization Forward Link

6.3.1 Introduction

In common broadcast applications involving multicarrier systems, the GW has access to all carriers while the UT can decode only one carrier. This scenario allows joint processing of all carriers only at the GW which enables multicarrier DPD [29] for interference mitigation. However, in the next generations of satellite systems, joint processing of all carriers can still be envisaged enabling the use of multicarrier EQ techniques as described in [1, 20]. Such scenarios include professional receivers on the forward link having enhanced capability or GW processing of multiple carriers on the reverse link with carriers originating from different users. The latter scenario arises since the return link comprises elements similar to forward link described earlier [20] and it excludes the possibility of a joint DPD.

In this section, we present low complexity mitigation techniques for multicarrier nonlinear satellite channels working at the symbol rate (data-level). We compare two distinct scenarios: the first one where only joint processing is applicable at the GW employing DPD [29], secondly, we consider a scenario where joint processing of all carriers can be performed at the receiver employing equalization [20]. Building on the works of multicarrier data DPD [29] and equalization [1], we provide a solution that minimizes the complexity of the

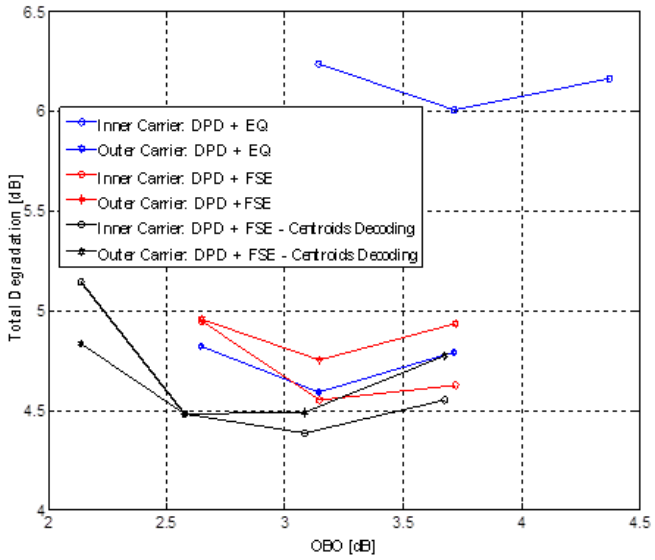

Figure 6.11: Comparison of FSE With Average Constellation Demapping And Centroid Based Demapping For 3 Carrier With 32 APSK 4/5, Roll-Off = 0.2, Interpolated LUT For TWTA, No Overlap Among Carriers

implementation with minor performance degradation. Complexity reduction is obtained by systematically reducing the MIMO Volterra basis function set using the LASSO, algorithm [60] in a basis pursuit approach. The solution obtained by such an algorithm is sparse, producing an efficient basis representation of the system. While, a similar algorithm has been applied to reduce complexity in Volterra models [82], to the best of the authors' knowledge this is the first time a LASSO algorithm is used in a multicarrier framework. The multicarrier scenario deals with a much larger bases set compared to the single carrier system, thereby strongly motivating the application of our approach. In this section we also trade-off the predistorter and equalizer for performance, complexity and ease of implementation, with emphasis on parameter identification in time-varying channels.

6.3.2 Multiple Carrier Transmission : System Overview

Scenario

The system considered involves broadcast transmission from a single gateway to many receivers through a transparent satellite transponder wherein only filtering to remove out-of-band noise, amplification and channelization of the streams are assumed to occur.

The satellite transponder is formed by a cascade of IMUX, HPA and the OMUX. The bandpass filters (IMUX/OMUX) are modeled as finite impulse response (FIR) digital filters. The HPA is characterized by the amplitude and

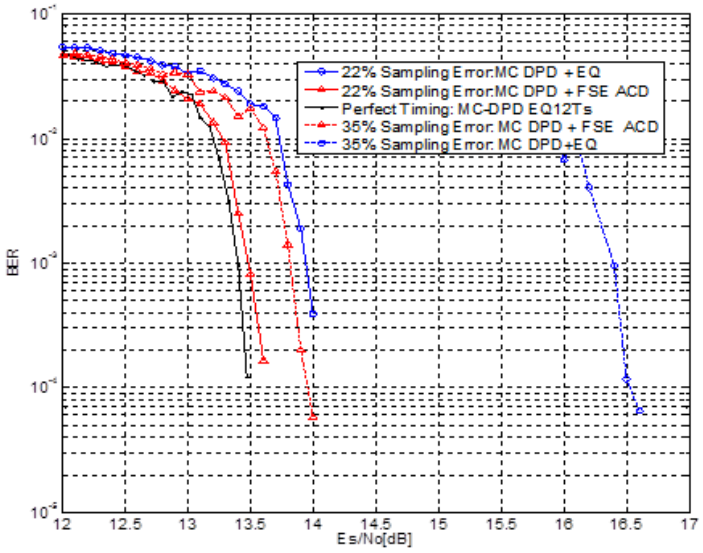

Figure 6.12: Sensitivity of equalization schemes to timing error, central carrier of a three carrier per HPA channel, 16 APSK, Roll Off=0.2, IBO=4 dB, LDPC with Code Rate=3/4

phase distortion curves, known as AM/AM and AM/PM curves, and are modeled by the well-known Saleh model [23]. The model is described in (6.12) and the parameters of the model for a typical DVB-S2 application can be obtained by curve-fitting to the experimental data in [9],

$$\begin{aligned} A(z) &= \frac{\alpha_0 z}{1+\alpha_1 z^2}, \\ \Gamma(z) &= \frac{\beta_0 z^2}{1+\beta_1 z^2} \end{aligned} \tag{6.12}$$

with z denoting the magnitude of the complex-valued base-band signal at the input of the HPA, and A, Γ representing its AM/AM and AM/PM conversion, respectively.

Based on the HPA and IMUX/OMUX described above, the satellite transponder can be modeled as a nonlinear system with memory. The memoryless nonlinearity causes constellation warping and ACI while the ISI is caused by the filters *per se* and their *coupling* with the nonlinearity. While ISI and constellation warping are present in a single carrier system [6], multicarrier systems are further affected by ACI and IMD that severely distort the received symbols [1].

The output of the transponder is received at the terminals perturbed by additive white Gaussian noise (AWGN). After matched filtering made to the shaping pulse (square root raised cosine with roll-off factor ρ) in accordance to the DVB-S2 standard [9], and sampling (assuming coherent receiver), the

received signal on the i-th branch takes the form,

$$y_i(n) = g_i(\{\{u_i(n-l)\}_{l=0}\}_{i=1}^{K}) + \eta_i(n) \tag{6.13}$$

where $g_i(\cdot)$ models the transponder effect on the i-th carrier and $\eta_i(n)$ is the AWGN. Note that, the i-th received signal y_i is a function of all carrier sequences through $g_i(\cdot)$.

Volterra Analysis

As discussed in chapter 2, the multiple carrier satellite channel can be modeled as a multiple carrier baseband Volterra system as,

$$\begin{aligned}
y_i(n) &= y_i^{(1)}(n) + y_i^{(3)}(n) + y_i^{(5)}(n) + \dots \\
y_i^{(1)}(n) &= \sum_{k_1=1}^{K} \sum_{m_1=0}^{\infty} h_{k_1}(m_1) u_{k_1}(n-m_1), \\
y_i^{(3)}(n) &= \sum_{k_1,k_2,k_3=1}^{K} \sum_{m_1,m_2,m_3=0}^{\infty} h_{k_1,k_2,k_3}(m_1,m_2,m_3)\dots \\
&\quad u_{k_1}(n-m_1) u_{k_2}(n-m_2) u_{k_3}^*(n-m_3), \\
y_i^{(5)}(n) &= \sum_{k_1,\dots,k_5=1}^{K} \sum_{m_1,\dots,m_5=0}^{\infty} h_{k_1,\dots,k_5}(m_1,\dots,m_5)\dots \\
&\quad u_{k_1}(n-m_1) u_{k_2}(n-m_2) u_{k_3}(n-m_3)\dots \\
&\quad u_{k_4}^*(n-m_4) u_{k_5}^*(n-m_5),
\end{aligned} \tag{6.14}$$

where $i = 1, \dots, K$. $u_i(n)$ and $y_i(n)$, respectively, denote the transmitted and received symbols on the i-th carrier at n-th instance. Further, the signal $y_i^{(p)}(n)$ represents the contribution of the p-th nonlinear order at the i-th received carrier, and $\{h_{k_1,\dots}(m_1,\dots)\}$ are the Volterra kernels [24]. Note that (6.14) only includes odd nonlinear orders since those are responsible for the in-band distortion encountered at the output of the nonlinear channel [1, 83]. For complexity reasons to be discussed below and for fostering a hardware implementation, the series in (6.14) is truncated to a certain memory depth and nonlinear order.

Assuming that the series (6.14) is truncated to P-th nonlinear order with M_p being the memory depth for the $(2p-1)$-th nonlinear order, the number of parameters in (6.14) corresponds to $\sum_{p=1}^{\frac{P+1}{2}} K^{2p-1}(M_p+1)^{2p-1}$. This number exponentially increases with nonlinear order and memory depth and further motivates the truncation. Fig. 6.13 illustrates this relationship using $M_p = 2$ for all nonlinear orders. The number of terms grows with the nonlinear order (P), memory depth (M_p), and the number of carriers (K). Notice that the number of parameters for the MIMO system are orders of magnitude larger than for the SISO system. Even with a modest nonlinear order of 3, a 5×5 MIMO system increases the number of parameters by two orders of magnitude compared to a SISO system. The large number of parameters in the latter is a well-known problem and has given rise to large research efforts in finding more parameter efficient models [84]. There is a certain level of redundancy in the formulation due to the permutations of the terms that can lead to identical contribution, such as, $x_i x_j x_z^* = x_j x_i x_z^*$, referred as symmetry [85]. The general

trends are, however, the same as presented in Fig. 6.13 even if redundancy is considered.

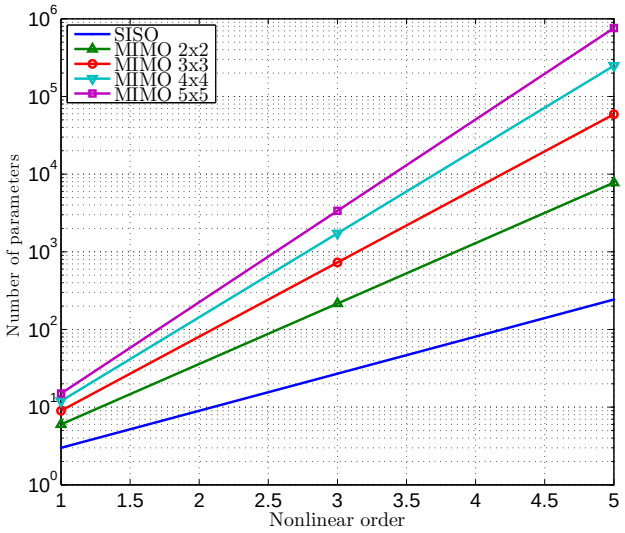

Figure 6.13: Number of parameters versus the nonlinear order in the Volterra series using 2 memory depth for all nonlinear orders. Single (SISO) and multiple input/ output (MIMO) channels are reported. Redundancy due to the symmetry was not considered

The Volterra model in (6.14) describes the impairments in the received carrier symbols; for every nonlinear order p. These terms can be further identified as IMD, ISI and ACI that limit the achievable throughput. Enhancing the throughput in such situations is taken up next.

6.3.3 Nonlinear Mitigation Techniques

In this section, we describe the two designed countermeasures for multicarrier nonlinear channels: DPD and EQ. The parameter identification method applied to both techniques is presented, and, subsequently we provide the method for complexity reduction based on a basis pursuit approach.

Multicarrier Data Pre-distortion

Digital pre-distortion (DPD), introduced at the GW, aims to mitigate the channel interference and to increase power efficiency. Joint processing of carriers allows pre-cancellation of the relevant interference generated by the IMD products. Further, processing is performed at data level (at symbol rate), prior to pulse shaping, in order to avoid signal spectral regrowth on the uplink channel and to reduce the GW hardware requirements [86] (cf. Fig. 6.14).

The pre-distorter function is designed to approximate the inverse channel, which is also nonlinear and dynamic, and hence can be described by Volterra series. As a consequence, the predistorter output for the i-th carrier, $q_i(n), 1 \leq$

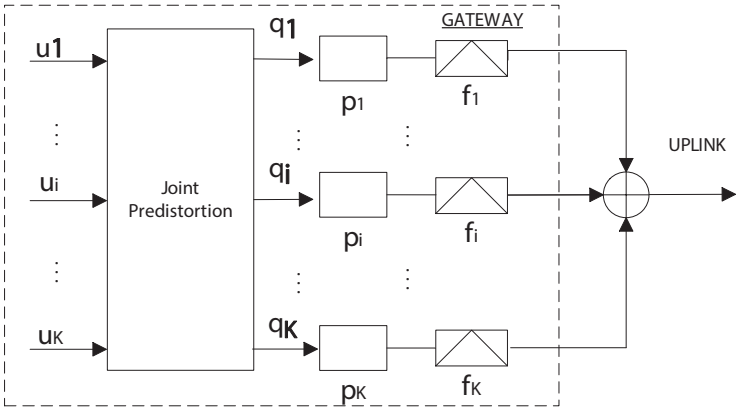

Figure 6.14: Multicarrier predistortion (DPD) architecture: K carriers are simultaneously processed at the GW

$i \leq K$ can be described as,

$$q_i(n) = [\phi_i(\mathbf{u}_M(n))]^T \mathbf{w}_i, \tag{6.15}$$

where $q_i(n)$ denotes the predistorted symbols and $\mathbf{w}_i$ is the $\sum_{p=1}^{\frac{P+1}{2}} K^{2p-1}(M_p + 1)^{2p-1} \times 1$ vector of the predistorter parameters which are the coefficients of the Volterra series. Thus, the number of parameters in $\mathbf{w}_i$ corresponds to the number of basis functions of the MIMO Volterra series. $\phi_i()$ is the vector comprising the nonlinear input combinations. In particular, we define,

$$\mathbf{u}(n) = [u_1(n), \ldots, u_K(n)]^T, \tag{6.16}$$

$$\mathbf{u}_M(n) = [\mathbf{u}^T(n-M), \ldots \mathbf{u}^T(n+M)]^T. \tag{6.17}$$

Further, the entries of the $\sum_{p=1}^{\frac{P+1}{2}} K^{2p-1}(M_p + 1)^{2p-1} \times 1$ vector $\phi_i()$ are the Volterra basis $\phi^{\{d\}}_{k_1,\ldots,k_d/m_1,\ldots,m_d}$ defined as [83],

$$\begin{aligned} \phi^{\{d\}}_{k_1,\ldots,k_d/m_1,\ldots,m_d}(\mathbf{u}(n)) &= \prod_{j=1}^{(d+1)/2} u_{k_j}(n-m_j)\ldots \\ &\quad \prod_{j=(d+1)/2+1}^{d} u^*_{k_j}(n-m_j). \end{aligned} \tag{6.18}$$

For each nonlinear order d, we stack terms relative to all carrier combinations together with memory combinations in the $K^{2d-1}(M_d+1)^{2d-1} \times 1$ vector

$$\phi^{\{d\}}_i(\mathbf{u}_{M_d}(n)) = [\{\phi^{\{d\}}_{k_1,\ldots,k_d/m_1,\ldots,m_d}(\mathbf{u}(n))\}], \tag{6.19}$$

with $k_j \in (1, K)$, $m_j \in (-M_d, M_d)$ and d denoting the nonlinear order considered. Finally, we augment vectors of different nonlinear orders obtaining,

$$\phi_i(\mathbf{u}_M(n)) = [\{\phi^{\{d\}}_i(\mathbf{u}_{M_d}(n))\}], \tag{6.20}$$

with $d \in (1, P)$, $\phi_i(\mathbf{u}_M(n))$ being a $\sum_{p=1}^{\frac{P+1}{2}} K^{2p-1}(2M_p+1)^{2p-1} \times 1$ vector. Identification of the parameters $\mathbf{w}_i$ is performed such that the predistorter function approximates the channel post-inverse. This can be achieved using the indirect learning architecture [63] where the inverse is estimated from the input and output signals. A detailed description of the parameter identification method is provided in the sequel. The number of basis functions becomes very high, as described previously; we therefore reduce their number while retaining the model performance as described below.

Multicarrier Data Equalization

From a system point of view, a completely different approach would be to compensate for the nonlinear interference at the receiver side. Joint processing of multicarrier signals at the user terminals can be envisaged in broadcast applications where the receiver can decode more than one carrier (professional application, for example). Such receivers are expensive with the complexity and cost compared to user receivers being dictated by the market. Another application of multicarrier equalization is on the return link. However, the return link in consumer applications is usually large which makes equalization complex. The set-up is dual of the considered scenario, where different users uplink carriers that are simultaneously amplified by the onboard HPA and processed jointly at the GW. Complexity and cost of the user receivers is also tightly limited by the market.

Multicarrier equalization for non linear satellite channels was first introduced in [20] for a dual carrier channel. In [20] the authors designed and compared two different kinds of equalization techniques: a Volterra equalizer implementing the channel inverse function and an interference canceler based on the channel function identification. Results show that the interference canceler slightly outperforms the channel inversion approach. In [1] the interference cancellation method is further extended to a Turbo Volterra architecture designed for an arbitrary number of carriers. In this work, we extend the dual carrier Volterra equalizer implementing the channel inverse [20] to an arbitrary number of carriers. The goal of our exercise is to reduce the receiver architecture complexity compared to [1] with minor performance degradation.

The considered equalization architecture is illustrated in Fig. 6.15, and is described by,

$$r_i(n) = [\phi_i(\mathbf{y}_M(n))]^T \mathbf{w}_i, \tag{6.21}$$

where $r_i(n)$ denotes the equalized symbols and $\phi_i()$ is defined similarly to (6.15) taking $\{y_k(n)\}_{k=1}^K$ as inputs. Following [20], we estimate the equalizer parameters $\mathbf{w}_i$ to implement the channel post-inverse function. In the following section, we provide the general formulation for channel post-inverse parameter identification that is valid for both DPD and EQ design.

Identification of Channel Inverse

For the equalizer design, referring to Fig. 6.15, the aim is to estimate $\mathbf{w}_i$ such that $E\{||u_i(n) - r_i(n)||_2\}$ is minimized for each $i \in (1, \ldots, K)$. The operator $\|\cdot\|_2$ denotes the ℓ_2 norm. For the predistorter design, referring to Fig. 6.14, the aim is to minimize $E\{||u_i(n) - y_i(n)||_2\}$. The coefficients $\mathbf{w}_i$ are used to denote both the equalizer and the predistorter weights. While the aforementioned

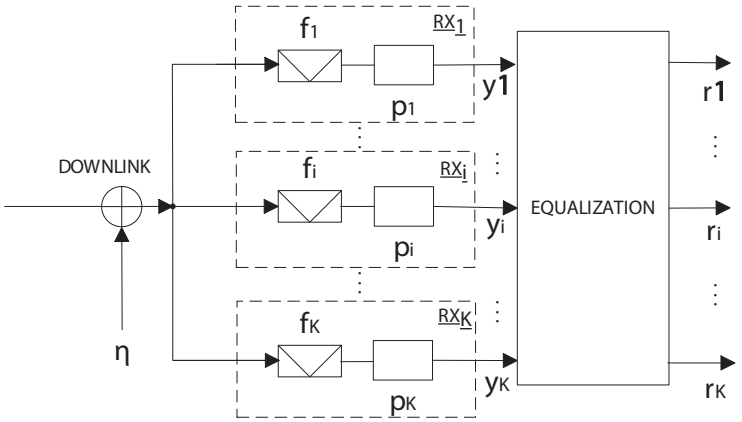

Figure 6.15: Multicarrier equalization (EQ) architecture: K carriers are simultaneously processed at the receiver.

minimization is formulated in a straightforward manner for equalizer based on (6.21), it relates to the indirect learning architecture [63] for predistorter design. In the indirect learning architecture, the predistorter weigths are obtained using the post-inverse (equalization) solution. In particular, we consider,

$$u_i(n) = [\phi_i(\mathbf{y}(n))]^T \mathbf{w}_i. \tag{6.22}$$

Given a dedicated training sequence providing N samples of transmitter and received symbols, $\{u_i(n)\}_{i=1}^K$ and $\mathbf{y}(n) = [y_1(n), \ldots, y_K(n)]^T$, respectively, we can stack the quantities to obtain,

$$\mathbf{s}_i = [u_i(0) \ldots u_i(N-1)]^T, \tag{6.23}$$

$$\mathbf{\Phi}_i = \begin{bmatrix} {\phi_i}^T(\mathbf{y}(0)) \\ \vdots \\ {\phi_i}^T(\mathbf{y}(N-1)) \end{bmatrix}. \tag{6.24}$$

From (6.22), using (6.23) and (6.24), it follows that $\mathbf{s}_i = \mathbf{\Phi}_i \mathbf{w}_i$. The least squares solution for $\mathbf{w}_i$ can then be readily obtained from [64] as,

$$\mathbf{w}_i = (\mathbf{\Phi}_i^H \mathbf{\Phi}_i)^{-1} \mathbf{\Phi}_i^H \mathbf{s}_i, \tag{6.25}$$

where H denotes the Hermitian transpose operator. The identified parameters can be equivalently used for DPD and EQ architectures. The large number of parameters in $\mathbf{w}_i$ makes the implementation of these techniques difficult and computationally expensive in practical applications. In the following section we describe a method for substantially reducing the complexity of the model.

Complexity Reduction

The parameters $\mathbf{w}_i$, representing the predistorter or equalizer coefficients (cf. (6.25)), are basis functions of a Volterra series in which the input and output have been interchanged to describe the postdistorter function. The parameters

$\mathbf{w}_i$ are commonly estimated using least squares identification methods. A system modeled by the Volterra series can be represented in multiple forms. Thus, different identification methods provide different system representations. Least square methods yield *dense* system representations, that is, most of the coefficients have significant weight in the model output. Hence, an implementation of the Volterra series becomes complex and its analysis cumbersome. A different approach followed by compressed sensing methods allows to reduce the number of coefficients while retaining the modeling properties. Such an approach is known as LASSO [60], in the view of the principle of parsimony [87], such sparse model representations must be preferred. These techniques have been used successfully in SISO Volterra basis selection and polynomial models [82, 88, 89].

The large number of coefficients of the predistorter or equalizer limits its applicability to only low nonlinear orders, short memory depth and a few carriers. It is therefore, in practice, necessary to reduce the complexity by selecting the basis functions (coefficients) that are the most significant when reducing the model error. We use a form of the LASSO technique [60] similar to [90] to select the significant coefficients of the system. The LASSO solves a least squares problem constraining the model to be sparse; such a constraint is usually represented as a sum of the magnitude of the model parameters,

$$\begin{aligned} \underset{\{\mathbf{w}_i\}_i}{\text{minimize}} \quad & \frac{1}{N}\sum_{i=1}^{K} \left\|\mathbf{s}_i - \mathbf{\Phi}_i \mathbf{w}_i\right\|_2, \\ \text{subject to} \quad & \sum_{n=1} R_{i,n}|w_i(n)| \leq \gamma_i, \qquad i = 1, \ldots, K. \end{aligned} \tag{6.26}$$

Here N is the total number of symbols used, $w_i(n)$ is the n-th coefficient of the $\mathbf{w}_i$ vector

$$\mathbf{w}_i = \left[w_i(1), w_i(2), \ldots, w_i(\sum_{p=1}^{\frac{P+1}{2}} K^{2p-1}(M_p+1)^{2p-1}) \right]^T. \tag{6.27}$$

$R_{i,n}$ is a scalar normalizing factor required since the coefficients in the predistorter and equalizer have different scales of magnitude provided by distinct nonlinear orders. $R_{i,n}$ is set as the sample variance of the n-th column of the regression matrix $\mathbf{\Phi}_i$ or equivalently as the energy of the n-th base function,

$$R_{i,n} = \frac{1}{N} {\varphi_{\mathbf{n}}}^H \varphi_{\mathbf{n}}, \tag{6.28}$$

where $\varphi_{\mathbf{n}}$ denotes the n-th column of the matrix $\mathbf{\Phi}_i$. Such a normalization is recommended for basis selection [91]. Despite (6.26) is formulated similarly to the weighted LASSO [90], it does not compute the Ridge vector required for the constraint in the weighted LASSO.

In contrast to identification techniques using only the error square as a loss function, the solution of (6.26) produces sparse solutions forcing some of the coefficients in $\mathbf{w}_i$ to reduce to zero and hence providing an efficient basis representation for the channel inverse. Note that, the weight of each basis function is given by the corresponding coefficient in $\mathbf{w}_i$ and the estimated $\mathbf{w}_i$ is sparse. Hence, basis functions which corresponding coefficient is zero can be eliminated without sacrificing performance. The reduction in complexity from the use this technique is shown in the next section.

6.3.4 Simulations

Figures of merit

The total degradation (TD) is used to evaluate the performance in coded satellite links. TD accounts for the nonlinear distortion while penalizing the loss in HPA power efficiency (measured as output power back-off (OBO)) [92],

$$TD_i = \frac{E_s}{N_0\, i}^{NL} - \frac{E_s}{N_0\, i}^{L} + OBO, \tag{6.29}$$

where $\frac{E_s}{N_0\, i}^{NL}$ and $\frac{E_s}{N_0\, i}^{L}$ are the average symbol energy to noise ratios required to achieve a target bit error rate (BER) in the nonlinear channel and the ideal linear channel (AWGN), respectively, for the i-th carrier. While $\frac{E_s}{N_o}$ is a single carrier metric, the OBO depends on the combined signal and not on individual carriers (aggregate OBO). In all our simulations, we consider a target BER of 10^{-5}. In contrast to equalization, the DPD will cause a change in the operating OBO of the satellite transponder due to the change in the signal statistics exciting the HPA. The OBO change, due to the use of DPD, is then included in the TD.

Simulation Settings

The satellite transponder was simulated as the cascade of three systems: an IMUX filter, a TWTA and an OMUX filter. The IMUX and OMUX filters were modeled by FIR structures using 51 and 41 taps, respectively that operate at the simulation rate. The TWTA was modeled by the static nonlinear Saleh model in (6.12) with $\alpha_0 = 2$, $\alpha_1 = 1$, $\beta_0 = \frac{\pi}{6}$, and $\beta_1 = 1$. Table 6.1 summarizes the settings used in the simulations.

Table 6.1: Simulation settings

		3 Carrier
Signal	Modulation format	8 PSK, 16 / 32 APSK
	Symbol rate (T_r)	7 M Baud
	Carrier Spacing	1.25 T_r
	Coding scheme	LDPC $\frac{3}{4}, \frac{4}{5}, \frac{5}{6}, \frac{8}{9}, \frac{9}{10}$
Channel	Pulse-shaping filter	SRRC $\rho = 0.25$
	IMUX bandwidth	26 MHz
	OMUX bandwidth	32 MHz
	Simulation rate	20
	HPA	Saleh's model

The Simulation rate referred in Table 6.1 indicates the amount of upsampling used in the carrier signals. The upsampling is required to accurately represent the nonlinear effects. These effects cause the signal bandwidth to expand and is commonly referred as spectral regrowth. The LDPC coding scheme [93] in Table 6.1 is representative of the state of art in satellite communications [9].

Basis selection results

The system depicted was simulated with the settings in Table 6.1 exploiting the built-in libraries for modulation and coding that are compliant with DVB-S2 [9].

The problem in (6.26) was solved using convex solvers [94, 95].

The constraints γ_i in (6.26) must be adjusted properly to produce sparse / relevant basis functions. This can be addressed by plotting the Pareto optimal boundary for the problem, as depicted in Fig. 6.16 [96, Chapter 6]. It is suggested to choose γ_i at the knee point of the curve; this point provides a trade-off between number of basis functions and the goodness of fit of the model.

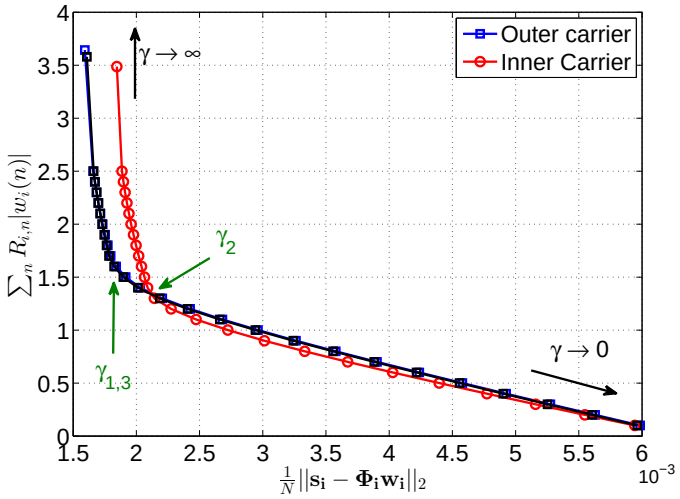

Figure 6.16: Weighted sum of the magnitude of the parameters versus the model error in a three-carrier simulation. The curves are obtained by sweeping γ_i

Note that in Fig 6.16, there is a region to the left in the figure where the model error (on the horizontal axis) is insensitive to variations of $\sum_n R_{i,n}|w_i(n)|$ (on the vertical axis). Since $\sum_n R_{i,n}|w_i(n)|$ is a metric for the model sparsity, by selecting γ_i as suggested, it is possible to promote the model sparsity without compromising for the model error.

We test the Volterra model of (6.14) for a $K = 3$ carrier case with the LASSO algorithm to distinguish the relevant bases for the system inverse. The simulated system with the parameters indicated in Table 6.1, using 16 APSK symbols in every carrier, and the transponder aggregate OBO was set to 2 dB. Fig. 6.17 shows the magnitude of the MIMO Volterra parameters render by the LASSO solver. The predistorters are shown in colors for each carrier. Fig. 6.17 indicates some basis functions corresponding to the predistorter of carrier three. The LASSO technique in (6.26) does not produce coefficients with values equal to zero, instead very small values are rendered [97], as noted in Fig. 6.17. Hence, we retained the basis functions with coefficient $\mathbf{w}_i$ larger than 10^{-4} in the model, and the rest were eliminated. Noted that, From Fig. 6.17 the amplitude variations of the vector $\mathbf{w}_i$ is of several orders of magnitude. Thus, altering the threshold level of 10^{-4}, used for discriminating the basis functions, did not change the basis selection results.

The Volterra basis model for the channel inverse was truncated to nonlinear order 5 and memory depths $M_1 = 5$, $M_2 = 3$ and $M_3 = 1$ (5 for the linear, 3 and 1 for the third and fifth nonlinear orders, respectively). This original set

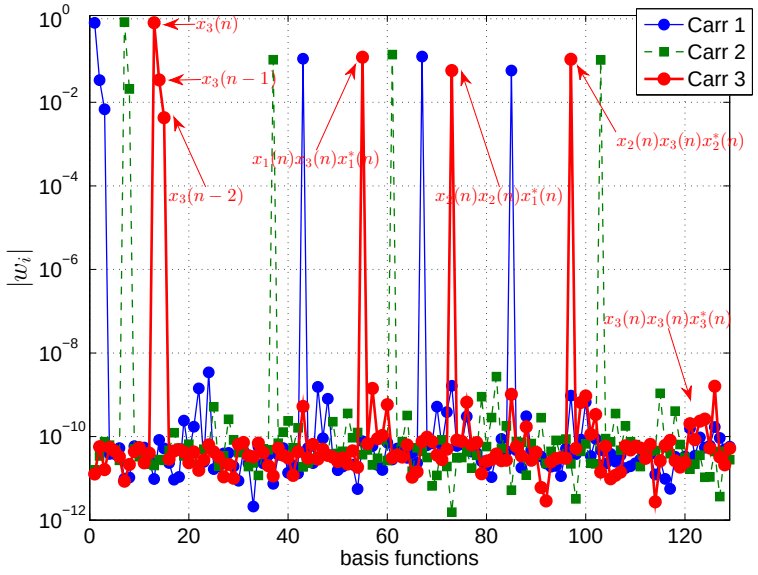

Figure 6.17: Magnitude of the parameters in the MIMO Volterra series when using the proposed LASSO solver.

of bases is redundant when considering the compensation of distortion channel effects, as can be seen in the left part of Fig. 6.16. The 'knee' shape in Fig. 6.16 indicates possible parsimonious system representation for which no degradation of the model error is observed. The total number of tested basis functions is 1458 when considering symmetric representation of (6.14), from which only 17 basis functions are finally selected and reported in Table 6.2.

Table 6.2: Selected basis functions for the system inverse in a 3-carrier satellite link

Carrier 1	Carrier 2	Carrier 3
$x_1(n)$	$x_2(n)$	$x_3(n)$
$x_1(n-1)$	$x_2(n-1)$	$x_3(n-1)$
$x_1(n-2)$	-	$x_3(n-2)$
$x_2(n)x_2(n)x_3^*(n)$	$x_1(n)x_2(n)x_1^*(n)$	$x_1(n)x_3(n)x_1^*(n)$
$x_1(n)x_3(n)x_3^*(n)$	$x_1(n)x_3(n)x_2^*(n)$	$x_2(n)x_2(n)x_1^*(n)$
$x_1(n)x_2(n)x_2^*(n)$	$x_2(n)x_3(n)x_3^*(n)$	$x_2(n)x_3(n)x_2^*(n)$

Thus, only 17 basis are required for the mitigation technique, which is formed as a linear combination of the basis indicated in Table 6.2. This number of basis functions could be compared to the result for a multicarrier equalizer in [1], where at least 30 basis functions were selected by using a different approach that resorts to enumerating the contribution at certain frequencies.

The basis selection test was repeated for different aggregate OBOs and different modulation formats; despite the varied settings, the basis selection give the same result as reported in Table 6.2. These tests were however repeated

under the following conditions:

- The carriers have the same frequency locations.
- The relative power between carrier signals is kept constant.
- The carriers have the same bandwidth (symbol rate T_r is fixed).
- The IBO is varied only in the region where significant amount of nonlinear distortion is produced.

Obtaining the same basis representation, despite of the varied settings, suggests that a parsimonious system representation can be found at data domain (symbol level) which is the cause of the observed behavior. From Table 6.2, larger memory is required for the outer carriers than the inner (central) carrier, as they are affected more by the IMUX, OMUX filters. Secondly, no memory is required for the third nonlinear order terms, and finally, that all fifth order terms were ruled out from the selected basis functions.

Link Performance

Fig. 6.18 shows the TD of the 3-carrier satellite link as a function of OBO in the HPA, for 16 APSK using a $\frac{3}{4}$ code rate, the outer and inner carriers are presented in Fig. 6.18a) and Fig. 6.18b), respectively. In this comparison solely data mitigation techniques are presented. The TD of only one outer carrier is shown due to symmetry. In Fig. 6.18, the benefit of applying nonlinear mitigation techniques can be observed. Fig. 6.18 includes single carrier data DPD for comparison [6]. Since single carrier predistortion does not include intermodulation products, it is ineffective at combating nonlinear distortions appearing in the multicarrier scenario; consequently it has poorer performance compared to proposed multicarrier data predistortion (cf. Fig. 6.18). The proposed data equalizer is compared with the multicarrier interference canceler of [1]. It can be observed from Fig. 6.18 that the proposed EQ scheme has some losses compared to the reference receiver technique of [1]. In fact, the multiple carrier turbo Volterra equalizer proposed in [20] relies on the powerful, but highly complex, iterative interference cancellation and decoding paradigm. On the other hand, our proposed low complexity equalization does not include any data decoding nor interference cancellation. Further, the proposed EQ has the same complexity of the proposed DPD technique, which is dual for the gateway. The complexity of the DPD is further discussed in the following sections. As seen fig. 6.18, the TD performance depends on the carrier location, as the inner carrier exhibits significantly more degradation than the outer ones. While the benefit of applying multicarrier over single carrier mitigation techniques is evident at the inner carrier, the performance gain is lower in the outer carriers where memory effects (ISI) dominates over ACI.

The investigated multicarrier mitigation techniques show different performance in Fig. 6.18. The differences are due to the effects of the receiver noise, both in the identification stage as well as during operation. While the DPD uses a dedicated receiver that can be designed to have low noise, the equalization has to operate *on-the-fly* at the receiver with higher levels of noise as in standard operation mode. Note that the equalizer has to operate on received signals which are corrupted by AWGN. Since the equalization operation is nonlinear

in the received symbols, the subsequent elements of the chain are affected by a nonlinear function of the front-end noise. This aspect is missing in the DPD and hence it provides further performance enhancement (cf. Fig. 6.18).

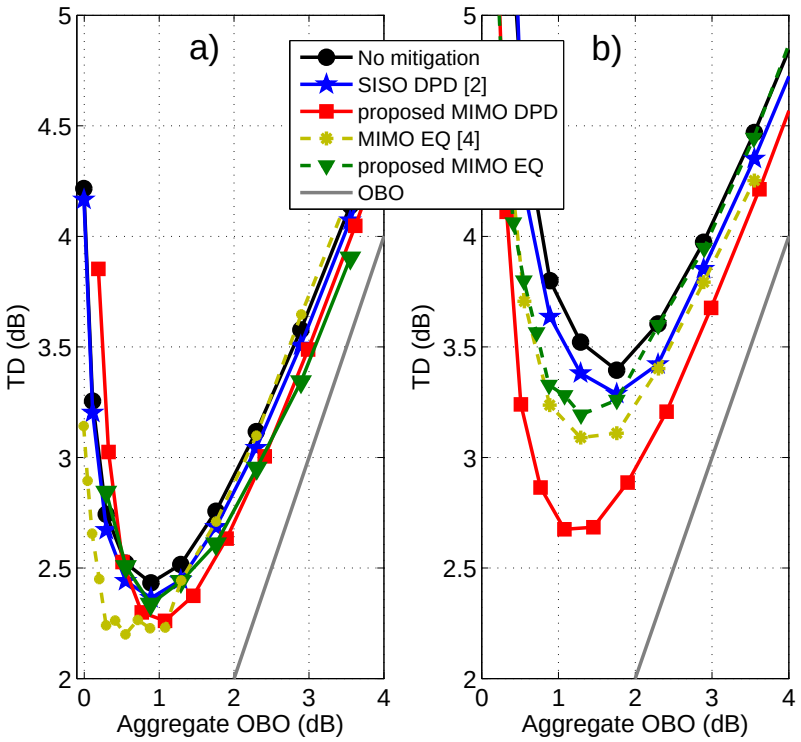

Figure 6.18: Performance comparison in TD versus aggregate OBO for data mitigation techniques. The system simulated is a three-carrier satellite link using 16 APSK $\frac{3}{4}$ in every carrier. a) Outer carrier. b) Inner carrier. Both proposed multicarrier DPD and EQ use the basis functions indicated in table 6.2.

This section studied the use of nonlinear mitigation techniques to the situation where multiple carriers were amplified by a single HPA in a satellite transponder. The mitigation techniques, predistortion (DPD) and equalization (EQ), are described in the framework of MIMO Volterra series. However, the large number of coefficients required in the mitigation techniques limit their practical applicability. In this work, a basis pursuit approach is employed using the LASSO algorithm to reduce the complexity of the mitigation technique yielding models with fewer number of coefficients that keep limited modeling error. The model complexity, for the inverse system mitigating the channel effects, grows with increasing number of carriers and hence the need for complexity reduction is exacerbated in the DPD/EQ models. Although the LASSO method described in this paper has been applied in a three carrier scenario, it can still be used for larger number of carriers. The LASSO approach would also

be of benefit in terrestrial applications where signal DPD is used for concurrent multiband HPAs.

The proposed DPD mitigation scheme reduces the complexity of multicarrier memory polynomial models by a factor of ten while achieving nearly the same TD performance. Multiple carrier data predistortion gives better performance than equalization in terms of TD. The explanation of this difference is in the level of noise in the received signals. in fact, while DPD is estimated using the received data from a reference receiver, which is designed to be low noise, EQ is evaluated at higher noise levels, from standard receivers. Thus, the deployment of a reference receiver, is beneficial from the system perspective. Moreover, the DPD operates on nearly noiseless data from the transmitter, while the EQ operates on the received noisy data. This implies that in the EQ, the noise at the receiver propagates through a nonlinear compensation scheme, which is missing in the DPD and explaining the different gains in performance.

In the following section we consider joint multiple carrier gateway equalization in the return link for an interactive satellite service.

6.4 Carrier Rate Optimization on the Return Link: UT Predistortion and GW Multicarrier Equalization

Interactive satellite services for mobile applications targeting vehicular, maritime and portable devices is an emerging market [98]. Satellite interactive services are enabled by a return link that provides the UT with the capability to transmit a narrow-band signal with service request information. Each user terminal has a specific frequency band allocated to transmit information back to the gateway through the satellite channel. Several narrow-band carriers are packed together and share the same satellite return link bandwidth. For such transmissions, certain regulations need to be adhered to guarantee negligible ACI at the gateway. On the other hand, mobile user terminals employ low cost Solid State Power Amplifier (SSPA)s that are required to work in high efficiency regime. Such amplifiers generate non linear distortion causing in-band and out-of band interference, especially when driven in high efficiency region (close to saturation). Out-of-band interference arises due to spectral regrowth and such spurious emissions have to be controlled in order to meet the regulations on ACI. Also, the in-band distortion needs to be reduced for enhanced performance. UT predistortion can reduce the non-linear distortions by manipulating the signal to be amplified using a function approximating the inverse of the SSPA non-linearity.

While the SSPA non-linearity is addressed using a predistorter at the UT, an interesting issue that needs additional processing is the optimization of the user rate on the return link given the available transponder bandwidth. Such an optimization arises from a demand for increased return link capacity fueled by a number of interactive applications over the internet. A straightforward way towards this objective seems to be the use of carriers with enhanced baudrate (increased bandwidth). However, due to the limited transponder bandwidth, such carriers result in ACI at the gateway and the exercise is futile if the interference is not mitigated. Effective mitigation of ACI requires joint processing

of carriers; this requires additional processing at the gateway since the UTs do not co-operate and predisotortion is not effective. The individual processing of carriers at UT followed by a joint processing at gateway motivates the current work. Since these techniques aim to minimize the ACI and enhance the throughput, the regulations on the ACI are inherently taken care of. In particular, we relax the constraints imposed by the regulations on the spectral occupation (the spectral mask and the inter-carrier guard band suggested in the standard [98]) and aim to achieve throughputs higher than [98] by the user of predistortion and equalization. As an added benefit, higher power efficiency at the user terminal is also aimed at.

It is apparent that the equalizer plays a central role towards achieving the said objectives. Equalization of non-linear satellite channel has been covered by several works in the literature [13–15]. However, joint equalization of multi-user channel is relatively less explored. Multi-carrier equalization for non linear channel has been introduced in [20] for a dual carrier channel and generalized in [1] for a general multicarrier channel. In [20] the authors design two different multicarrier receiver techniques for a dual carriers non-linear satellite channel : A MMSE Volterra equalizer and an iterative interference canceler. Further, in [1] the interference cancellation method is generalized to an arbitrary number of carriers. However, differently from the scenario in [1, 20], we do not have the generation of inter-modulation products among carrier products. This allows the definition of a simplified multi-carrier non-linear equalizer. Further, another simplification is implemented to the equalizer model leading to a memory polynomial form for reduced complexity implementation.

6.4.1 System Model and Problem Formulation

The system under consideration is presented in Fig. 6.19. It describes a typical return link of an interactive satellite system and includes a certain number of user terminals, a satellite channel and a receiving gateway. Such a system is similar to the return link of the Broadband Global Area Network (BGAN) system [98] which provides mobile telephony and broadband internet access via satellite. Similar to the BGAN system, we assume the satellite to be in a geostationary orbit and the L band ($1626.5 - 1660.5$ MHz) transmissions occur in the burst mode (MF-TDMA) on the return link. Towards formulating the problem, the different blocks in Fig. 6.19 are now detailed.

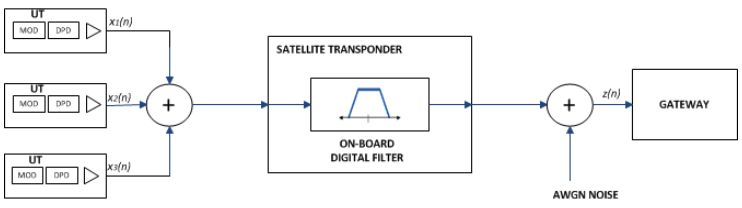

Figure 6.19: System model of the considered satellite return channel

User Terminal Transmitter

The user terminal essentially includes a Forward Error Correction (FEC) encoder, a modulator supporting QPSK and 16QAM constellation mappings [98], a pulse shaper modelled as Root Raised Cosine (RRC) filter with a roll-off factor of 0.25 and a SSPA. The AM/AM and AM/PM characteristics for the SSPA model obtained from experimental data are illustrated in Fig. 6.20 and Fig. 6.21 respectively. These characteristics of the SSPA are assumed to be independent of the frequency (memoryless). The AM/AM characteristic of the

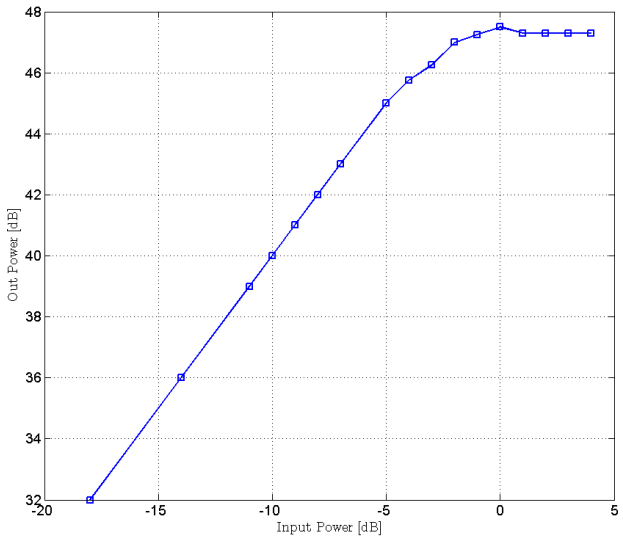

Figure 6.20: AM/AM characteristics of the SSPA

user terminal SSPA can be modelled using the Rapp model [99] which takes the form,

$$A(r) = r/(1 + ((|r|)/\alpha)^{2P})^{1/2P} \tag{6.30}$$

where r in the input Voltage, $A(r)$ is the corresponding signal output amplitude, P is the smoothing factor and α is the value of input at saturation. Typical values of P are 2 or 3. While the Rapp model is suited for representing AM/AM characteristics, there is no known accurate model for the AM/PM function. Hence, we employ a linear interpolation of the AM/PM data provided in Fig 6.21.

Further, the input back-off (IBO) is defined as $IBO = -10\log\left(\frac{<|v_{in}(t)|^2>}{P_{ref}^{in}}\right)$, where $< |v_{in}(t)|^2 >$ is the average input power to the amplifier and P_{ref}^{in} is the input power corresponding to the -1dB compression point. Similarly the output back-off (OBO) is defined as $OBO = -10\log\left(\frac{<|v_{out}(t)|^2>}{P_{ref}^{out}}\right)$, with $|v_{out}(t)|^2$ being the average output power of the amplifier and P_{ref}^{out} is the output power when IBO$= 0$. Notice that P_{ref}^{out} depends on amplifier characteristics and the input signal distribution.

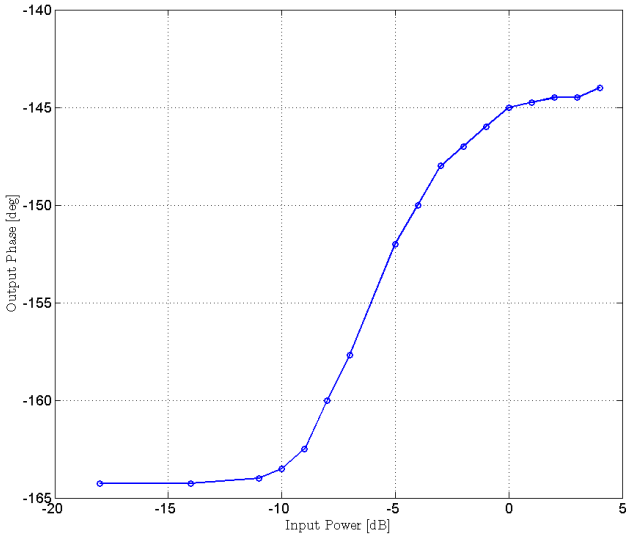

Figure 6.21: AM/PM curve for the SSPA

Satellite Channel

The uplink channel is assumed ideal and an equivalent AWGN channel is considered on the downlink. A typical transponder model includes IMUX and OMUX filters modelled as linear systems and the on-board power amplifier. For ease of analysis, we assume the operation of the amplifier to be in the linear region and model the satellite transponder as a linear filter. Referring to Fig.6.19, the satellite transponder is modelled using a 200kHz filter whose characteristic is illustrated in Fig. 6.22 [98]. Carriers from a number of users (typically three, details in Section 6.4.1) are filtered by Fig. 6.22. The linear filter is designed to ensure that the downlink spectrum adheres to the assigned frequency slot. Linear distortions manifest in ISI mainly in the carriers lying at the edge of the filter passband due to the frequency selectivity. On the other hand, the internal carriers experience a frequency non-selective gain and a linear phase shift. Hence they do not suffer from ISI, but can be subject to ACI from both external carriers as will be explained below.

Receiving Gateway

The multi-carrier signal at the output of the transponder is down-linked to the gateway for further processing. The typical gateway set up on the return link would involve a single user architecture where each carrier passing through the 200kHz transponder filter is decoded independently. This includes an equalizer to mitigate distortions, a demodulator and a decoder. An iterative detection and decoding can also be considered instead. On the other hand, since all the carriers are processed at the gateway, it is possible to envisage a multi-user architecture where all carriers through a 200kHz transponder filter are decoded jointly. The details of the equalizer design are deferred to Section 6.4.3. Further,

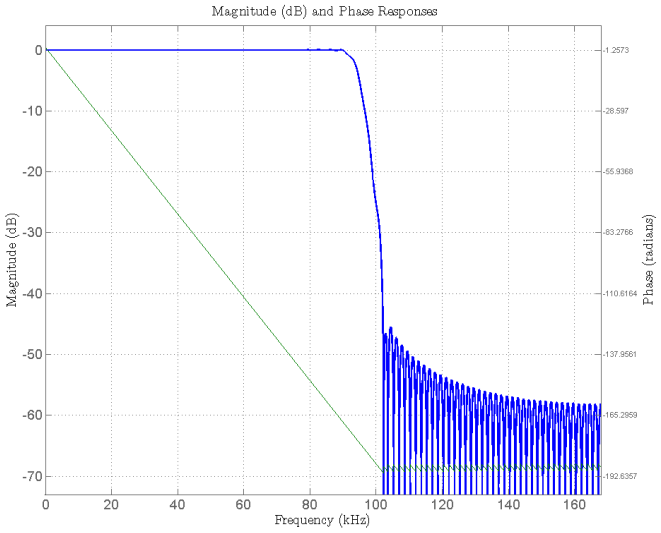

Figure 6.22: On-board Filter response

in the case of joint processing of the user carriers, we assume, for simplicity, that different carriers are synchronized at the gateway. Efforts towards synchronizing the multiple users are currently being pursued, for e.g. [100].

Problem Formulation

Based on the demand from the user terminal, several transmission configurations (carrier rates, burst size and MODCODs) can be set on the return link [98]. As a reference scenario, we select the case where each user terminal employs a $R_{ref} = 33.6$ kBaud carrier [98]. While the return link supports multiple users, we focus on three such users whose carriers have a frequency spacing of $1.3R_{ref}$ and can be accommodated in 200kHz transponder filter. For the typical roll-off factors $(0.1 - 0.3)$, such a configuration neither results in carrier overlap and nor in spectrum broadening on linear channels. The carrier configuration described above is illustrated in Fig. 6.23. In the current work, we increase the carrier bandwidths with the aim to increase the throughput. However, to reflect on the fixed system bandwidth, we assume that the three carriers continue to be filtered by the 200kHz transponder. With their carrier spacing fixed, such a bandwidth enhancement invariably causes ACI; additional ACI is generated by the spectral regrowth resulting from the terminal amplifer characteristics. These manifestations are depicted in Fig. 6.24. Thus, the increase in bandwidth reduces the Signal to Interference Ratio (SINR) at the gateway, resulting in lower throughput. The aim of this work is to minimize the ACI using suitable on-ground processing, thereby allowing the exploitation of higher bandwidth to yield higher throughputs. We consider a carrier spacing of 1.3 R_{ref} throughout; however the results can be extended to other spacing, as well.

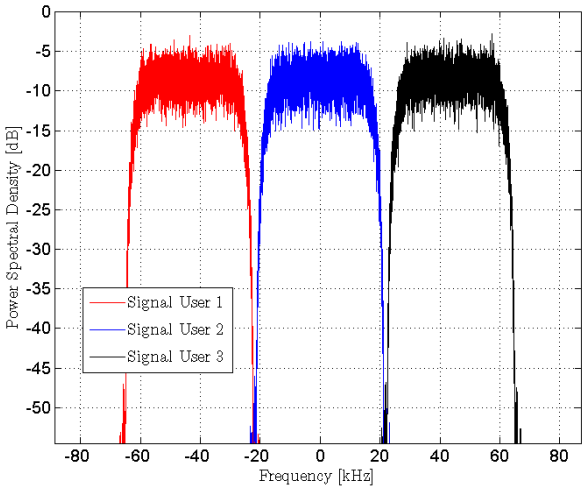

Figure 6.23: Baseline Scenario with no ACI

6.4.2 User Terminal Predistortion

While several classes of predistorters exist [22], we consider the signal digital predistortion (DPD) in the current context and a scheme involving the predistorter is provided in Fig 6.25. Unlike a data predistorter operating on the constellation set, the signal predistorter has flexibility with regards to the spectrum of its output signal. Further, since the predistorter and the SSPA are co-located, the issues of spectral regrowth on the uplinked signal have negligible impact unlike in the forward link [52]. Motivated by prior-works [16] [101], we further consider a model based predistorter based on the Volterra series [26]. Since the SSPA is memoryless, to the best of authors' knowledge, no simplification of the Volterra series, apart from truncation, is found in literature. In particular, we consider predistorter whose output, $x(n)$, takes the form,

$$x(n) = \sum_{m=0}^{(D-1)/2} w_m s(n)|s(n)|^{2m} \tag{6.31}$$

where $s(n)$ is the complex baseband sample at instance n, D is the degree of the predistorter and w_m are termed as the kernel co-efficients. The predistorter is completely defined by these coefficients.

While D is a user supplied parameter based on operational constraints, w_m need to be estimated. Note that the predistorter output is linear in these parameters and can be rearranged as $x(n) = \mathbf{w}^T \mathbf{\Phi}(s(n))$ where $\mathbf{\Phi}(s(n)) = [s(n), s(n)|s(n)|^2, \ldots, s(n)|s(n)|^{D-1}]^T$ is column vector of non linear terms and $\mathbf{w} = [w_0, \ldots, w_{(D-1)/2}]^T$ column vector of the predistorter coefficients. It is further assumed that a feedback loop is available from the output of the HPA to aid the predistorter training and adaption (kindly refer to Fig. 6.25. While such a feedback loop provides amplitude information with high fidelity, the phase information is perturbed with phase noise with characteristic depicted in Fig 6.26.

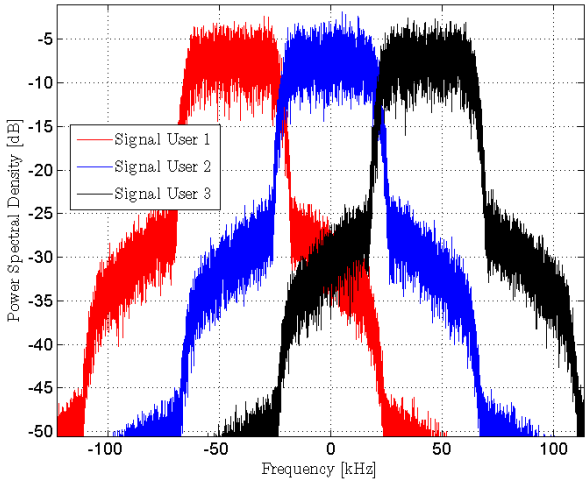

Figure 6.24: Scenario with ACI arising out of increased carrier bandwidth and terminal non-linearity

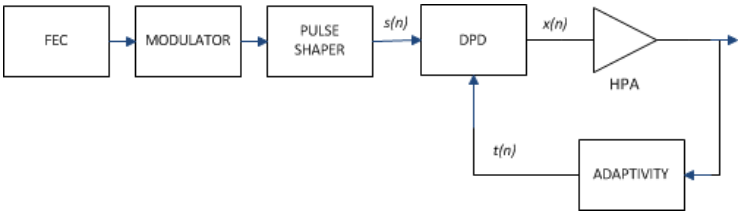

Figure 6.25: On-board Filter response

With this in mind, we denote the signal fed back as $t(n)$. Parameter estimation is based on the philosophy of finding the post-inverse for the SSPA and using it as the pre-inverse (Indirect Learning [39]). In other words, without the predistorter in place, a non-linear function that inverts the SSPA (obtaining $s(n)$ from $t(n)$) is implemented. Since this non-linear function models the post-inverse of the SSPA, it is also used as a predistorter (pre-inverse). In particular, the non-linear post-inverse function takes the form,

$$s(n) = \sum_{m=0}^{(D-1)/2} w_m t(n)|t(n)|^{2m} \tag{6.32}$$

where w_m are the kernel coefficients in (6.31). Now, since $s(n)$ and $t(n)$ are known ($s(n)$ is known by virtue of being generated and $t(n)$ is obtained from feedback), one could solve (6.32) to obtain $\mathbf{w}$. Collecting N number of $s(n)$ and $t(n)$, we can obtain $\mathbf{w}$ as a linear least squares problem,

$$\mathbf{w} = \mathbf{\Phi}^{\dagger}\mathbf{s} \tag{6.33}$$

where $\mathbf{s} = [s_0, \ldots, s_{N-1}]^T$ is the vector of known inputs, $\mathbf{\Phi} = [\mathbf{\Phi}(t(0))^T, \mathbf{\Phi}(t(1))^T, \ldots, \mathbf{\Phi}(t(N-1))^T]^T$ is $N \times (D-1)/2$ matrix with (p, q) element being $t(p)|t(p)|^{2(q-1)}$ and

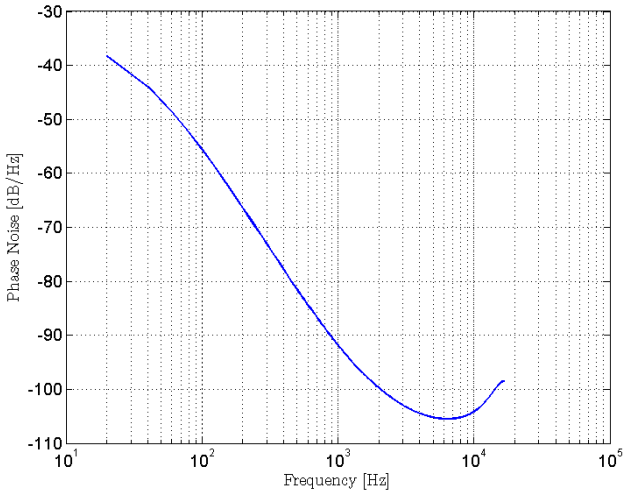

Figure 6.26: DPD Feedback Phase Noise Mask

$\mathbf{\Phi}^{\dagger}$ is its pseudo-inverse. Parameter estimation can be easily implemented adaptively using a standard recursive least squares (RLS) algorithm to track possible SSPA parameters drift. The update rate is a design parameter.

6.4.3 Joint Equalization at the Gateway

In this work, we assume that the carriers are decoded separately subsequent to joint equalization. The other architecture would be a multicarrier turbo decoder as described in [1]. Further, the equalization *per-se* could either be linear (a simple filter) or involve non-linear operations. In either of the cases, the receiver needs the return channel state information for enhanced performance. In the current work, we assume training sequences of appropriate length to estimate the channel. We now briefly describe the single and multicarrier equalizer functions and describe the methodology for determining their parameters.

Let $y_m(n)$ denote the signal at the output of the satellite transponder corresponding to carrier m at instance n. The received multi-carrier signal at instance n can then be expressed as,

$$z(n) = \sum_{k} \sum_{m} f_{m,k} y_m(n-k) + \sum_{m} I_m(n) + \eta_q(n) \tag{6.34}$$

where the first term denotes linear ISI and ACI, modelled as output of the filters $\{f_{m,k}\}$, the second term $(I_m(n))$ collects all the residual non-linear terms caused by carrier q and $\eta_q(n)$ denotes the receiver noise for carrier q. Notice that, in absence of interference, y_m is recovered at the receiver by matched filtering and sampling. The interference perceived at the receiver is frequency selective due to the carrier configuration and the innate property of the spectral regrowth. Thus the equalization at the gateway needs to cater to such an interference and can be performed individually or jointly on the received data. Individual equalization of each user-carrier is a low complexity solution that

does not require synchronization among the users. For this case, we consider the simple linear MMSE function,

$$r_q(n) = \sum_{k=-K}^{K} h_k z_q(n-k) \tag{6.35}$$

where K is the two-sided memory depth, $\{h_k\}$ are the equalizer parameters, $z_q(n)$ is the received signal corresponding to the qth user and $r_q(n)$ the corresponding equalized output.

On the other hand, joint equalization is expected to provide better performance due to the correlation among signals and ACI. Since (6.34) suggests a non-linear system with memory, a multi-carrier memory polynomial equalization model is applied in the case of joint processing. A complete Volterra multicarrier model as in [1] would result in a large number of coefficients thereby increasing the complexity. Further, the non-linear terms in (6.34) do not contain inter-modulation products. Hence, we omit the inter-modulation terms as well as the cross memory terms from the Volterra representation to obtain a reduced complexity solution. The obtained multicarrrier function results in a special case of the general multicarrier Volterra formulation proposed in [1] Each equalized carrier $r_q(n)$ is now expressed as,

$$r_q(k) = \sum_{q=1}^{Q} \sum_{m=0}^{(D-1)/2} \sum_{k=-K}^{K} h_{m,k,q} z_q(n-k)|z_q(n-k)|^{2m} \tag{6.36}$$

where $f_{m,k,q}$ are the kernel co-effiicents, Q is the total number of users jointly equalized, D denotes the polynomial degree, K is two sided memory depth and $z_q(n)$ received signal corresponding to the qth carrier.

Identification of the equalizer parameters is a standard linear least squares problem having a similar formulation for both the two equalizer solutions of (6.35) and (6.36). Given a sequence of N transmitted and received symbols, $\{a_i(n)\}$ and $\mathbf{z}(n) = [z_1(n), \ldots, z_Q(n)]^T$ respectively, we obtain the following quantities after stacking

$$\mathbf{a}_i = [a_i(0) \ldots a_i(N-1)]^T \tag{6.37}$$

$$\mathbf{\Psi}_i = \begin{bmatrix} {\psi_i}^T(\mathbf{z}(0)) \\ \vdots \\ {\psi_i}^T(\mathbf{z}(N-1)) \end{bmatrix} \tag{6.38}$$

where ψ_i correpond to the non-linear function with memory that models the equalizer in (6.36) for user-carrier i. We then obtain $\mathbf{a}_i \approx \mathbf{\Psi}_i \mathbf{h}_i$ with $\mathbf{h}_i$ column vector (appropriately stacked $\{h_{m,k,q}\}$) of model parameters to be estimated. The least squares solution for $\mathbf{h}_i$

$$\mathbf{h}_i = \mathbf{\Psi}_i^{\dagger} \mathbf{s}_i. \tag{6.39}$$

6.4.4 Results

In this section we present the numerical results for a simulated scenario with characteristic defined in Table B.1.

Table 6.3: Simulation parameters

Parameter	Value
Coding	Turbo Coding
Coding Rate	$r = \{0.51, 0.70, 0.82\}$
Packet Size	2560 bits
TX/RX filters	SRRC, roll-off : $\rho = 0.25$
Carrier Spacing	1.3×33.6 KHz
Modulation	16 QAM
Predistorter Degree D	5

Performance of Predistortion and Equalization Schemes

In this exercise, we consider the benefits of on-ground compensation schemes in mitigating linear and non-linear ACI. The throughput optimization, to be presented in next section, will draw heavily from this study. In course of this experiment, we consider carriers of different bandwidth while keeping the signal power from the satellite. Hence carriers with higher bandwidths have a lower signal to noise ratio (SNR). Towards quantifying the performance of the mitigation techniques, we evaluate the achieved Total Degradation (TD) [6] for different carrier bandwidths to determine the achievable spectral efficiency. Since the focus is on ACI, we confine the evaluations to the central carrier. The TD is defined as,

$$TD|_{@PER} = \frac{E_s}{N_0}|_{NL} - \frac{E_s}{N_0}|_{AWGN} + OBO, \tag{6.40}$$

where $\frac{E_s}{N_0}|_{NL}$ is the needed SNR in the considered non-linear (NL) channel to achieve the target packet error rate (PER) of 10^{-3} for the specific modulation and code scheme, $\frac{E_s}{N_0}|_{AWGN}$ is the SNR achieving the same target PER with an identical transmission scheme on a linear AWGN single carrier channel and, finally, the OBO, as defined in Section 6.4.1, is a measure of the SSPA power efficiency. Total degradation shows a minimum corresponding to the optimum OBO. The position and the value of this minimum depends on the channel settings and the applied technique.

In the current activity, TD performance is evaluated for the following configurations,

- A baseline case without any compensation technique applied (referred to as the *No compensation*)
- With equalization only
  - Single carrier linear MMSE with $K = 2$;
  - Non-linear multicarrier equalizer with $K = 2$ and $D = 3$.
- User terminal predistortion only with $D = 5$
- User terminal predistortion combined with equalization

The TD results for the central carrier are presented in Figs. 6.27, 6.28, 6.29 for carrier rates (R_s) of 33.6, 37.3 and 42 kBaud respectively. For each configuration we evaluate the relevant information rate in [bit/s] as $R_s C_R \log_2(M)$, where M is the modulation order and C_R is the code rate. Towards analyzing these results,

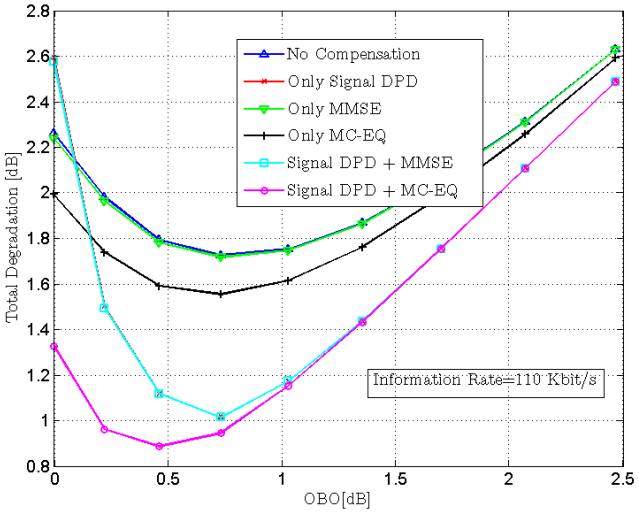

Figure 6.27: Standard R_s 33.6 kBaud, Coding Rate 0.82

it is necessary to understand the nature of the interference. The degradation has the following components,

- ACI due to overlap of the different carriers due to their increased bandwidth (linear ACI)
- ACI due to spectral regrowth caused by SSPA non-linearity (non-linear ACI)
- In-band distortions due to non-linearity and channel filters (non-linear ISI)

Therefore, it can be expected that the TD increases with increasing carrier rate and the same is evident from Figs. 6.27, 6.28, 6.29. The role of UT predistortion to reduce the TD is through minimizing the spectral regrowth and the in-band distortions. On the other hand, the multiple carrier equalizer can compensate for the linear and non-linear ACI in addition to the in-band distortions. Thus, predistortion and equalization techniques improve TD on their own [1]. However, it should be noted that the predistorter is effective in reducing the non-linear distortions compared to the equalizer; this can be attributed to the near-optimality of signal DPD and higher noise in the receiver estimation process. This is illustrated in Figs. 6.27, 6.28, where there is a limited overlap among the carriers and the ACI is predominantly due to the spectral regrowth. The conclusions change as the level of linear ACI increases

[1] the plot for signal DPD overlaps with that of signal DPD + MMSE in Figs. 6.27, 6.28

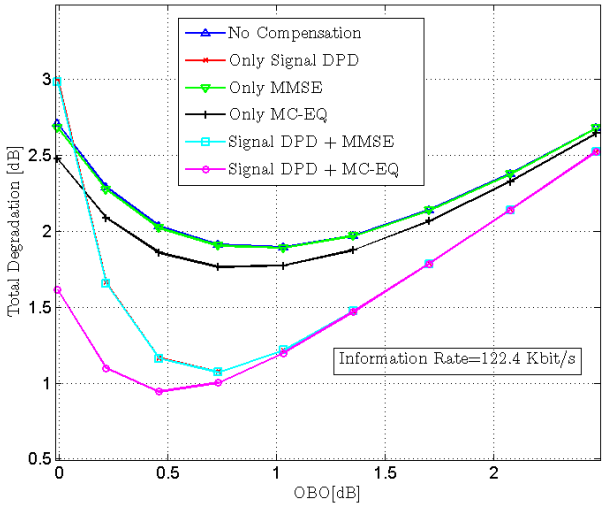

Figure 6.28: 10% excess R_s : 37.3 kBaud, Coding Rate 0.82

and the equalization provides significant gains. Such a trend can be seen in Fig. 6.29 where the carrier overlap is significant compared to those in Figs. 6.27, 6.28. Further, it is clear that non-linear joint equalization performs better than linear MMSE. The MMSE filter only aims to reduce linear ACI and hence provides gains in Figs. 6.29. Finally, the joint use of predistortion and non-linear equalization performs the best.

To obtain further insight, we evaluate the performance in presence of very strong ACI. In Fig. 6.30, we consider the 48kBaud carrier, where we have overlapping of the nominal signal bandwidth even without the spectral regrowth. This combined with the non-linear spectrum broadening effects, results in strong linear and some non-linear ACI. In such an adverse scenario, ACI is dominant and receiver equalization becomes effective in eliminating the introduced interference. On the other hand predistortion alone does not provide significant gain since the interference is mainly due to the overlap of the signal spectrum; in fact, meaningful decoding is not possible with either *no compensation* or with only predistortion. As a further indicator of the level of interference, a stronger code rate of 0.51 has been applied in this case. As ACI level increases, it has been noticed that MMSE receiver results in narrow-band filter that tries to filter out the injected ACI components lying in the external region of the signal bandwidth. Observing cases of Figure 6.29 and 6.30, we notice a degradation in performance independent on the OBO generating an offset such as TD is always greater then OBO and depend on the applied countermeasures techniques (please refer to the plot area with high OBO). This is the result of the linear component of the adjacent channel interference that is independent on the non-linear effects.

Carrier Rate Optimization

Towards finding the optimal setting for carrier rate optimization, we present the achieved spectral efficiency as a function of the required P_{sat}/N value

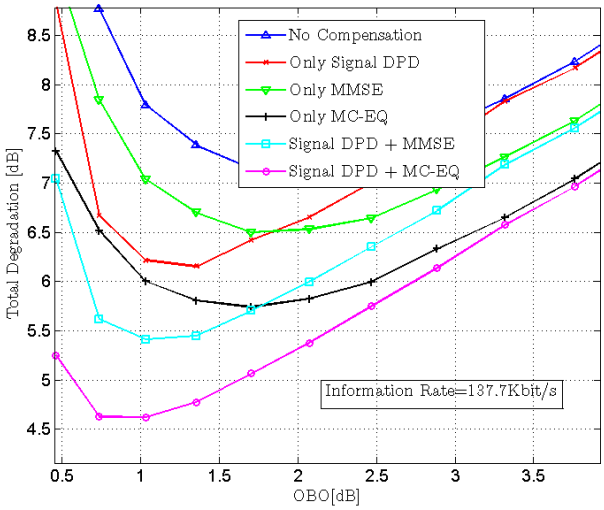

Figure 6.29: 20% excess R_s : 42 kBaud, Coding Rate 0.82

for a target PER= 10^{-3} [102]. The spectral efficiency is computed as $\mu = r\log_2(M)R_s/W_{ref}$, where r is the code rate, M the modulation order, R_s the symbol rate and $W_{ref} = 33.6(1+\rho)$kHz defined as reference bandwidth. On the other hand, P_{sat}/N is defined as [102],

$$\frac{P_{sat}}{N}|_{PER} = \frac{E_b}{N_0}\ \mu\ OBO, \tag{6.41}$$

where μ is the spectral efficiency, OBO the HPA power efficiency at the specific minimum TD and $\frac{E_b}{N_0}$ is the corresponding SNR required to achieve the target PER [102].

In Fig. 6.31 we plot the spectral efficiency for different symbol rates as a function of the required P_{sat}/N.

For each carrier rate, we identify for each code rate the required P_{sat}/N. We only consider 16QAM modulation here. This corresponds to finding the optimal total degradation for the specific applied technique in the given scenario. Referring to Fig. 6.31, we observe about 10% improvement in spectral efficiency between the existing scenario and the output of the carrier optimization. The spectral efficiency improves with the incorporations of the compensation techniques. Further, the spectral efficiency increases with the baud rate (from 33.6 $\rightarrow$ 37.3) and then decreases (from 37.3 $\rightarrow$ 42) . While the increase is a natural consequence of the higher rate, the decrease is due to the enhanced ACI. The compensation techniques reduce the loss by mitigating the ACI to a large extend. Further, relative gains of the compensation techniques increase as the coding rate is increased. This is the result of the fact that strong coding schemes mask the mitigation effect of the techniques, translating the channel to a noise limited regime. An attempt at enhancing the throughput on the return link of an interactive mobile satellite network by optimizing carrier rate for a given system bandwidth is considered. Central to the realization of throughput gains are on-ground compensation techniques, predistortion and equalization, which

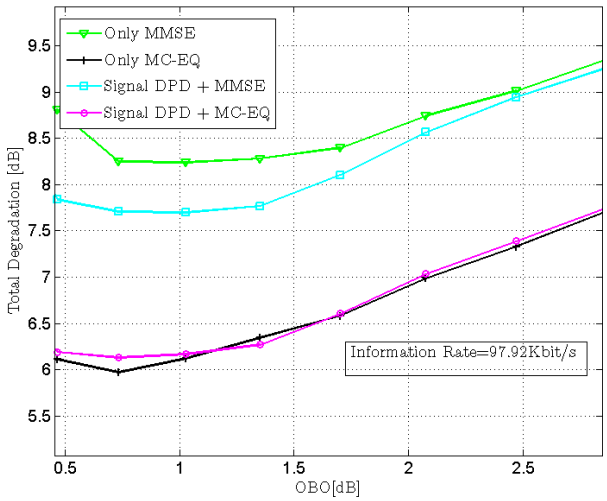

Figure 6.30: User bandwidth increased of 30 %: Bandwidth 48 KHz, Coding Rate 0.51

mitigate the linear and non-linear adjacent channel interference. Predistortion is effective in minimizing the in-band distortions and the spectral regrowth caused by the user terminal amplifier. On the other hand, ACI cannot be handled by predistortion and a multicarrier equalizer is needed. While several configurations of these techniques have been tested, the combination of predistortion and multicarrier equalization provides for the best performance. This performance improvement is exploited towards achieving higher throughput for a given power and bandwidth requirement.

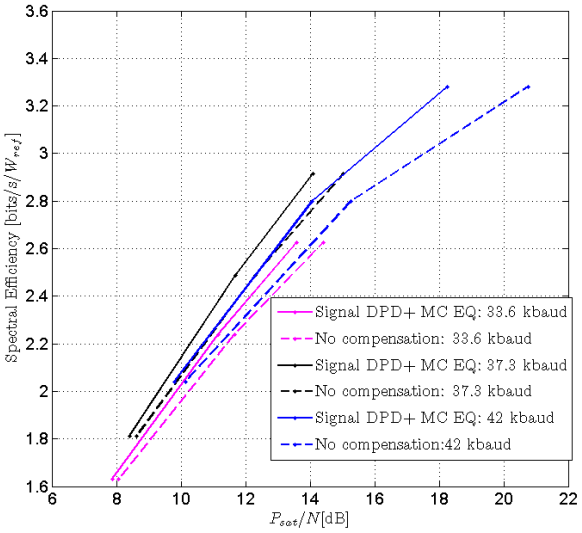

Figure 6.31: Spectral efficiency comparison for different symbol rates

Chapter 7

Thesis Conclusion

This thesis considers the problem of non-linear distortion effects in a multiple carrier satellite channel. The objective was to compensate these distortion effects enabling higher spectral and power efficiency. Two approaches are considered in this thesis namely *Predistortion* at the transmitter and *Equalization* at the receiver. As predistortion we define any signal processing technique applied at the transmitter aimed to reduce the generated non-linear interference at the output of the non-linear channel. On the other hand, equalization is a receiver technique for post interference mitigation.

Amongst all the promising proposed approached to predistortion, we identified multiple carrier data predistortion based on memory polynomial functions to provide excellent performance gain and a good compromise between complexity and adaptivity (kindly refer to section 3.4). For this predistortion model, we proposed novel multiple carrier parameter estimation methods to improve robustness to noise and to increase system performance. Further, based on the same model, we also derived novel predistortion solution applicable to a distributed scenario where multiple gateways shares the satellite transponder.

As receiver techniques, we considered different approaches including multiple carrier and single carrier methods. Amongst them FSE combined with centroid decoding emerged as promising techniques (kindly refer to section 6.2). This single carrier method guarantees the minimum impact on the receiver architecture, adaptivity and good performance gain.

Further, as tangible outcome of this Ph.D work we have recently filed a patent with the support of SES [2]:

- R. Piazza, S. Bhavani, B. Ottersten,"*Methods, devices, and computer programs for compensating nonlinearities of a communication channel*". International Patent Application PCT/EP2014/064311.

This patent is strictly related to the contribution presented in section 4.1 and this work is considered valuable for possible future technological development.

7.1 Future Work

There are a number of aspects that have significant research potential but were not investigated in this work.

- On-board signal predistortion: As discussed throughout this thesis, traditional satellite transponder architectures do not allow the installation of on-board complex digital systems to perform signal processing. However, recently emerging transponder technologies suggest this constraint is being relaxed enabling the definition of efficient on-board signal predistortion techniques. In particular on-board digital processing is being considered for basic signal processing operations such as routing and filtering while demodulation and decoding are still not considered. On-board processing would take advantage of its beneficial position in between the IMUX filter and the HPA eliminating the performance limiting constraint on the predistortion signal bandwidth. A simple initial approach ,fitting the currently available platforms, would be to implement a memory-less signal predistortion function based on LUT technology and operating directly on the multiple carrier signal input to the on-board HPA.

- PAPR reduction for multiple carrier satellite channels: Given a set of independent carriers to be uplinked, the definition of a method to reduce the resulting PAPR remains open. The definition of the method should account for the characteristic system constraints of a satellite channel including the efficient usage of the transponder bandwidth and guaranteeing the independent decoding at the user terminals.

- Joint Precoding & Predistortion: The multiple carrier data predistortion function proposed in this work can be seen as generalization of the linear precoding discussed in [69]. This aspect should be investigate to obtain a joint design of the data predistorter and the precoder to cancel the co-channel beam interference.

Appendix A

A.1 Partial Derivates Formulation

As proposed in [67], we assume x and x^* to be independent variables while differentiating a complex polynomial. Based on this, we can derive some basic differentiation rules for multicarrier complex polynomial functions as,

$$\frac{\partial(x_m|x_m|^{2P})}{\partial x_m} = (P+1)|x_m|^{2P} \tag{A.1}$$

$$\frac{\partial(x_j|x_m|^{2P})}{\partial x_j} = |x_m|^{2P} \tag{A.2}$$

$$\frac{\partial(x_j|x_m|^{2P})}{\partial x_m} = Px_jx_m^*|x_m|^{2(P-1)} \tag{A.3}$$

Since the entries of $\phi_m(\mathbf{x}(i))$ take the form in (6.18), we can exploit the aforementioned rules to generate quantities of the form $\frac{\partial\phi_m(\mathbf{x}(n))}{\partial x_m(n-l)}$.

A.2 RLS Derivation for Individual Predistorter Design

Similar to [40], we approximate $e_m(i)$ exploiting the differentiability of the channel. Using the the weak non-linearity approximation of (4.30) and recalling $x_m(i-l) \approx [\phi_m(\mathbf{u}(i-l))]^T \mathbf{w}_m(n)$ from Section 4.1.5 we have,

$$y_m(i) \approx \left(\sum_{l=-K}^{K} \tilde{h}_m(i,l)\phi_m(\mathbf{u}(i-l))\right)^T \mathbf{w}_m(n). \tag{A.4}$$

Using (A.4) and recalling (4.25), (4.28), we can express the error as,

$$e_m(i) \approx u_m(i) - \left[\frac{\partial y_m(i)}{\partial \mathbf{w}_m(n)}\right]^T \mathbf{w}_m(n) \tag{A.5}$$

This simplified expression (A.5) can be used in (4.29) to transform the problem to standard RLS formulation.

A.3 RLS Derivation for Joint Predistorter Design

Similarly to the derivation carried out in the earlier section, we use the weak nonlinearity approximation of (4.46) and recalling $x_m(i-l) \approx [\phi_m(\mathbf{u}(i-l))]^T \mathbf{w}_m(n)$ to derive,

$$y_j(i) \approx \left(\sum_{m=1}^{M} \sum_{l=-K}^{K} \tilde{h}_{j,m}(n,l) \left[\phi_m(\mathbf{u}(i-l))\right] \right)^T \mathbf{w}_m(n).$$

Using (A.6) and recalling (4.25), (4.42) we can express the error as

$$e_j(i) \approx u_j(i) - \left[\frac{\partial y_j(i)}{\partial \mathbf{w}(n)} \right]^T \mathbf{w}(n) \tag{A.6}$$

This simplified expression (A.6) can be used in (4.45) to transform the problem in a standard RLS problem.

Appendix B

B.1 Non-parametric Data Predistortion for Non-linear channels with memory

In this appendix we present the contribution of [52] that does not completely fit into the scope of this Thesis. In [52] we propose novel numerical methods for single carrier data predistortion with memory. The contribution includes a high complex solution that requires on-line complex processing and a reduced complexity LUT-based solution providing minor performance loss compared to the full complexity solution. Both approaches are shown to outperform the known techniques data predistortion techniques.

B.1.1 Introduction

Signal power amplification is necessary to achieve the desired SNR at the receiver. However the process is hardly linear due to the inherent characteristics of the amplifier which includes the saturation effect [23]. This non-linear amplification results in inter-symbol interfere (ISI) at the receiver thereby causing degradation [6]. On the other hand, efficient power amplification requires the amplifier to be operated very close to its saturation region where non-linear effects are stronger. Towards exploiting higher power gain, mitigating the non-linear effects of power amplification has been given a priority in both satellite [22] and terrestrial communications [26]. With the increasing and widespread use of high order modulation schemes towards achieving higher throughput, the mitigation of the non-linear interference generated by the power amplifier has become even more challenging. Multilevel modulation schemes are spectrally efficient but excite severe non-linear distortions due to the inherent high peak to average power ratio (PAPR) typical of the non-constant envelope signals (e.g. QAM and APSK). Proper countermeasures need to be put in place to guarantee the required throughput and the power efficiency. In most applications, it is often more desirable to counteract the generated non-linear interferences at the transmitter side with specific signal pre-processing technique generally known as predistortion. Such a processing does not entail a change in the existing user terminals, thereby making it market attractive.

One of the most consolidated approaches defines the predistortion as a nonlinear function that approximates the equivalent channel inverse function. Such an approach is paraterized by a certain number of kernel coefficients. A large number of techniques belong to this channel inverse predistortion function

category, for e.g., analytic channel inverse function [103], Volterra series [26], memory polynomials [16, 35, 40] and orthogonal polynomials [17, 18]. The non-parametric approaches for predistortion elaborated in literature, rely on iterative numerical optimization techniques and do not exploit directly any channel information [6, 19].

In this section we propose a novel non-parametric data predistortion method based on the point-wise solution of the non-linear channel equation. The new technique does not suffer of the typical inaccuracies of the channel inverse based predistortion techniques [103]- [18], exploits channel model information in a better way compared to [6, 19] and provides significant gain in performance. A variation of the method suitable for reduced complexity implementation is also developed showing negligible performance loss.

System Model

A general communication chain consisting of a non-linear channel with memory is represented in Fig. B.1. The constellation symbols, $\{a_n\}$, drawn from a M-

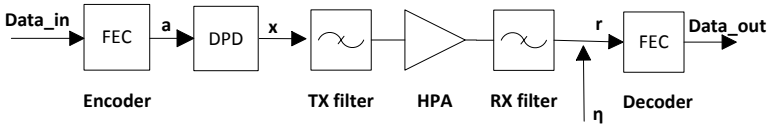

Figure B.1: Non-linear Channel: DPD denotes Digital Predistortion block

sized constellation set S_M are pre-distorted to obtain the transmitted symbols $\{x_n\}$. The non-linear channel contains linear transmit and receive filters (pulse shaping filter or Input/Ouptut multiplexing filters) and a non-linear amplifier. Denoting $H_{nl}(\cdot)$ as the channel non linear function, μ_n as the noise and $X_{n,K} = [x_n, \ldots, x_{n-K}]$ as a stacking of transmitted symbols, the received symbol at nth instance, r_n, can be expressed as

$$r_n = H_{nl}(X_{n,\infty}) + \mu_n \tag{B.1}$$

$H_{nl}(\cdot)$ can be expressed using the Volterra expansion [24] as

$$\sum_{p=0}^{\infty} \sum_{(k_0,\ldots,k_{2p})=0}^{\infty} h^{(p)}_{k_0,\ldots,k_{2p}} \prod_{j=0}^{p} x_{n-k_j} \prod_{i=p+1}^{2p} [x_{n-k_i}]^*. \tag{B.2}$$

Here $h^{(p)}_{k_0,\ldots,k_{2p}}$ denotes the Volterra kernel coefficients. The full Volterra model is a highly complex representation of the channel function due to the presence of all cross terms $\{k_{2l}\}$. A reduced complexity version of $H_{nl}(\cdot)$ is the memory polynomial that does not include all the cross terms [84]

$$H_{nl}(X_{n,\infty}) \approx \sum_{\substack{p=0 \\ (even)}}^{\infty} \sum_{k=0}^{\infty} h^{(p)}_k x_{n-k} |x_{n-k}|^p. \tag{B.3}$$

In general, both models ((B.2) and (B.3)) include only odd polynomial terms in x_n generating the relevant *in-band* distortion. Concerning channel estimation, polynomial channel models of (B.2) and (B.3) are linear equations in their kernel parameters $h^{(p)}_{k_0,\ldots,k_{2p}}$. Because of this linear relation, the estimation of $h^{(p)}_{k_0,\ldots,k_{2p}}$ is a linear least-square (LS) problem that can be solved using standard training based techniques [84]. To focus on the predistortion technique, we assume the channel model parameters to be fixed and that they have been computed *off-line*.

B.1.2 Non-parametric Predistortion based on channel model

Towards a low-complexity implementation, we use the simplified channel model of (B.3) limiting channel model degree to $D+1$ and memory to K in (B.3). We henceforth consider

$$H_{nl}(X_{n,K}) = \sum_{\substack{p=0 \\ (even)}}^{D} \sum_{k=0}^{K} h_k^{(p)} x_{n-k}|x_{n-k}|^p. \tag{B.4}$$

The ideal predistortion function would guarantee the minimization of the error between the received symbols r_n (B.1) and the intended transmitted symbols a_n. Such a symbol level approach is not feasible since the transmitter is not privy to the received symbols. Instead, we consider,

$$x_n = \underset{x_n, 0<|x_n|^2<P_x}{\arg\min} \{|H_{nl}(X_{n,K}) - a_n|^2\}. \tag{B.5}$$

The power constraint in (B.5) arises from the power constraint served by the transmitter. It also helps to avoid infeasible solutions arising due to the finite degree channel model approximation.

Clearly the minima of (B.5) is obtained when $H_{nl}(X_{n,K}) = a_n$ if the resulting solution satisfies $0 < |x_n|^2 < P_x$. Towards solving $H_{nl}(X_{n,K}) = a_n$ using (B.4), we obtain,

$$a_n = \sum_{\substack{p=0 \\ (even)}}^{D} \sum_{k=0}^{K} h_k^{(p)} x_{n-k}|x_{n-k}|^p. \tag{B.6}$$

Equation (B.6) is non-linear with memory in the complex variable x_n that can be transformed in two distinct equations in real variables: a polynomial equation for the amplitude of x_n and a linear equation for the phase. These two equations will be derived in the following.

Amplitude of the Predistorted Symbol

Equation (B.6) can be rewritten as:

$$\tilde{a}_n = \sum_{\substack{p=0 \\ (even)}}^{D} h_0^{(p)} x_n|x_n|^p \tag{B.7}$$

$$\tilde{a}_n = a_n - \sum_{\substack{p=0 \\ (even)}}^{D} \sum_{k=1}^{K} h_k^{(p)} x_{n-k}|x_{n-k}|^p \tag{B.8}$$

Applying the magnitude operator on both sides of (B.7), we obtain a $(D+1)$th degree real polynomial equation in $|x_n|^2$:

$$\sum_{\substack{p_1=0 \\ (even)}}^{D} \sum_{\substack{p_2=0 \\ (even)}}^{D} h_0^{(p_1)} [h_0^{(p_2)}]^* |x_n|^{2+p_1+p_2} = |\tilde{a}_n|^2. \tag{B.9}$$

Assuming $\tilde{a}_n$ to be known, we can find the optimal $|x_n|^2$ as the *positive* solution of (B.9). In order to obtain a solution we need to find the roots of a real polynomial of degree $(D+1)$. Closed form polynomial solutions are derived up to the third degree and numerical evaluation is applied for higher degrees. If no valid solutions to (B.9) exist or the resulting solution does not satisfy $0 < |x_n|^2 < P_x$, we redefine the amplitude $|x_n|^2$ as a solution of (B.9)

$$|x_n|^2 = \underset{0<|x_n|^2<P_x}{\arg\min} \{(f(|x_n|^2) - |\tilde{a}_n|^2)^2\} \tag{B.10}$$

$$f(|x_n|^2) = \sum_{\substack{p_1=0 \\ (even)}}^{D} \sum_{\substack{p_2=0 \\ (even)}}^{D} h_0^{(p_1)} [h_0^{(p_2)}]^* |x_n|^{2+p_1+p_2}. \tag{B.11}$$

The problem defined in (B.10) can be solved finding the local maximum of the polynomial function $f(|x_n|^2)$ under the condition $0 < |x_n|^2 < P_x$ using first and second order derivatives. Alternatively, a purely numerical approach would require a search for the minimum of $(f(|x_n|^2) - |\tilde{a}_n|^2)^2$ in the closed interval $0 < |x_n|^2 < P_x$.

Phase of the Predistorted Symbol

Once we obtain a valid solution for (B.9), we can derive the phase of x_n by using the phase relations of (B.7) as,

$$\angle x_n = \angle \tilde{a}_n - \angle \sum_{\substack{p=0 \\ (even)}}^{D} h_0^{(p)} |x_n|^p. \tag{B.12}$$

The above process generates a predistorted symbol solving (B.12) and (B.9) [or (B.10)]. This requires information about $\tilde{a}_n$, which in turn, depends on previous predistorted symbols. As a result, x_n needs to be computed for each n and the complexity of such a process is very high. We now consider a reduced complexity approach that allows for *off-line* calculation of x_n and use it as a Look Up Table (LUT).

B.1.3 Reduced Complexity Implementation

The information about the previous symbols is the cause of increased complexity. Towards implementing the process as a low complexity LUT, we choose to approximate x_{n-k} by their centroids in (B.8). Centroids of the predistorted symbols are defined as the solution of

$$\mathbb{E}[\tilde{a}_n | a_n] = \sum_{\substack{p=0 \\ (even)}}^{D} h_0^{(p)} \bar{x}_n |\bar{x}_n|^p, \tag{B.13}$$

where the averaging is performed over the previous transmitted symbols ($\{x_{n-k}\}$ or equivalently $\{a_{n-k}\}$) and $\bar{x}_n$ is defined as the centroid of x_n. For obtaining $\mathbb{E}[\tilde{a}_n|a_n]$, we take recourse to the numerically observed fact that $\mathbb{E}[\sum_{\substack{p=0\\(even)}}^{D}\sum_{k=1}^{K} h_k^{(p)} x_{n-k}|x_{n-k}|^p|a_n] \approx 0$. Using this and (B.8) leads to,

$$\mathbb{E}[\tilde{a}_n|a_n] \approx a_n \tag{B.14}$$

This approximation allows us to define centroids as a solution of an auxiliary $(D+1)$th degree equation in (B.15) that can be solved as described in Section 3

$$a_n = \sum_{\substack{p=0\\(even)}}^{D} h_0^{(p)} \bar{x}_n|\bar{x}_n|^p. \tag{B.15}$$

Solving (B.15) allows to map, *off-line*, each constellation symbol with the corresponding centroid. For a finite channel memory K, knowing $\{a_{n-k}\}$, we compute $\{\bar{x}_{n-k}\}$ and use these centroids to approximate $\tilde{a}_n$ as

$$\tilde{a}_n \approx a_n - \sum_{\substack{p=0\\(even)}}^{D}\sum_{k=1}^{K} h_k^{(p)} \bar{x}_{n-k}|\bar{x}_{n-k}|^p. \tag{B.16}$$

The value of $\tilde{a}_n$ evaluated in (B.16) can be used in (B.7) and the resulting equation solved to get an approximation of x_n. Notice that in (B.16) we obtained an approximation of $\tilde{a}_n$ as an implicit function of $[a_{n-K}, \ldots, a_{n-1}]$ using only the estimated centroids of the predistorted symbols and a_n. Since the centroid and channel computations are off-line, hence x_n can be obtained off-line entirely and a LUT generated. Such a LUT maps $[a_{n-K}, \ldots, a_n]$ to $[\tilde{x}_n]$ and has a dimension of M^{K+1}.

B.1.4 Numerical Results

In this section we compare the predistortion techniques designed in Sections 3 and 4 against standard memory polynomial predistortion [16]. To this end we simulated the channel of Fig B.1 and Table B.1 details the simulation parameters. The Saleh model is a memoryless non-linearity with AM/AM AM/PM

Table B.1: Simulation parameters

Parameter	Value
HPA model	Saleh Model [23]
TX/RX filters	Square Root Raised Cosine, roll-off=0.25
Modulation	32APSK
Coding	LDPC 3/4

characteristics: $A(r) = \frac{\alpha_1 r}{1+\alpha_2 r^2}$, $\Phi(r) = \frac{\beta_1 r^2}{1+\beta_2 r^2}$ with parameters [$\alpha_1 = 1$, $\alpha_2 = 0.25$, $\beta_1 = 0.26$, $\beta_2 = 0.25$]. The predistortion technique based on real-time roots computation (refer to Section 3) has been implemented assuming the

channel model in (B.4), with a memory depth $K = 1$ and polynomial degree $D + 1 = 5$. For the same channel characteristics, we also implemented the reduced complexity predistortion method described in Section 4 generating a LUT with $M^{K+1} = 32^2$ entries addressed with $(K + 1)\log_2(M) = 10$ bits. In either case the channel estimation is based on 15000 training symbols and the linear LS minimization [84]. For the matter of comparison, we devised a memory polynomial predistorter as in [16]. This memory polynomial predistorter function has a memory depth of $K = 1$, polynomial degree of $D + 1 = 5$ and is estimated using the indirect learning method [39] with 15000 training symbols.

As metric for HPA power efficiency we use the OBO (Out Back Off) as $OBO = 10\log\frac{P_{out}}{P_{out}^{SAT}}$ where P_{out} and P_{out}^{SAT} are the output and saturated powers of the HPA, respectively. The OBO defines the working point of the HPA and controls the level of non-linear effects as well as the overall signal power level. Non linear interferences are stronger close to the saturation region (OBO$\approx$ 0 dB) while they tend to disappear moving to the linear region (OBO$\rightarrow \infty$). However, the overall signal power decreases when OBO increases, resulting in a degradation of the effective SNR for a fixed level of noise power at the receiver.

Performance can be evaluated in absence of noise by means of the Normalized Mean Square Error (NMSE) defined as $\mathbb{E}[|r_n - a_n|^2/|r_n|^2]$. Fig B.2 shows

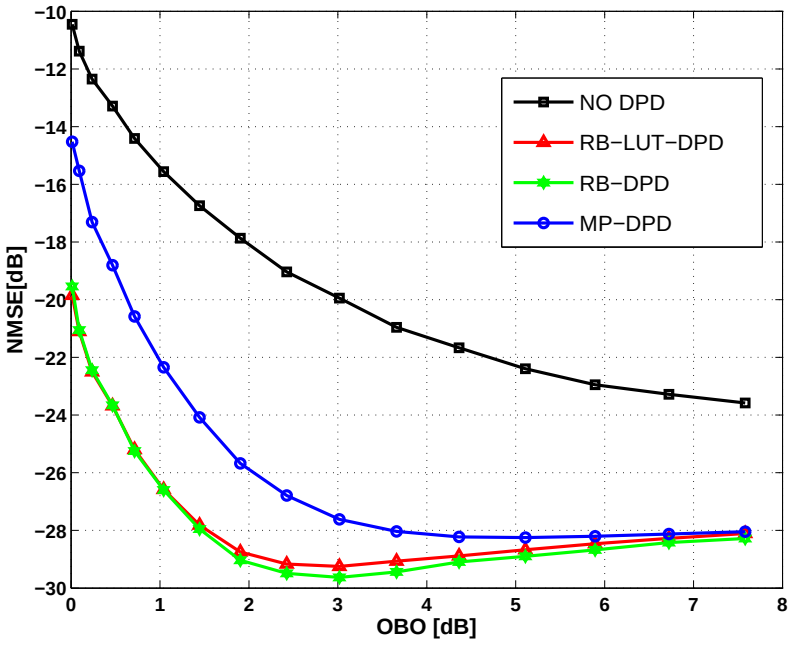

Figure B.2: NMSE vs OBO (Noiseless)

how the NMSE varies with respect to the OBO. We can notice a dramatic reduction in the interference level (here measured as NMSE) for the new techniques (legends RB-DPD and RB-LUT-DPD for techniques described in Section 3 and 4, respectively) compared to the standard memory polynomial predistor-

tion (MP-DPD). Moreover, the performance loss between the real time roots computation (RB-DPD) and its complexity reduced version (RB-LUT-DPD) is almost negligible. The slight increase in NMSE for the predistortion techniques at high OBO can be attributed to the channel mismatch.

Having demonstrated a significant NMSE gain in the non-linear region for the noiseless case, we evaluate the BER trend (see Fig B.3) with the amplifier operating very close to saturation (OBO = 1 dB). Fig. B.3 provides a measure

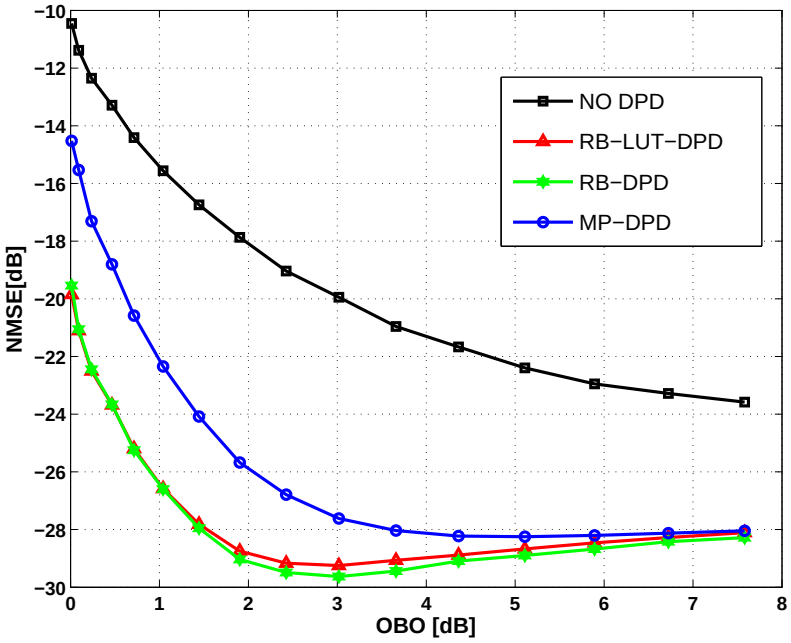

Figure B.3: BER performance of predistortion techniques for OBO=1dB

of the Es/N_0 gain of the new method over the standard memory polynomial technique and the negligible loss in performance due to approximations is also illustrated. In order to investigate BER behavior with respect to the OBO, we set a fixed noise level at the receiver of $N_o = 15dB + E_s^{(SAT)}$ where ${E_s}^{(SAT)}$ is the average signal energy received when the amplifier is in saturation (OBO = 0 dB).

Fig. B.4 illustrates the variations in BER due to OBO. Close to the saturation region, the BER is influenced by the strong non-linear interferences, while moving toward the linear region of the amplifier, the BER rises again due to the reduction in the received SNR. For the chosen settings, it can be seen that the devised techniques provide a range of OBO in which the BER is negligible. This is due to the enhanced mitigation offered by the proposed techniques that allow for the optimal performance of LDPC. On the other hand, for the MP-DPD, an increase in Es/N_0 is needed to obtain improved BER.

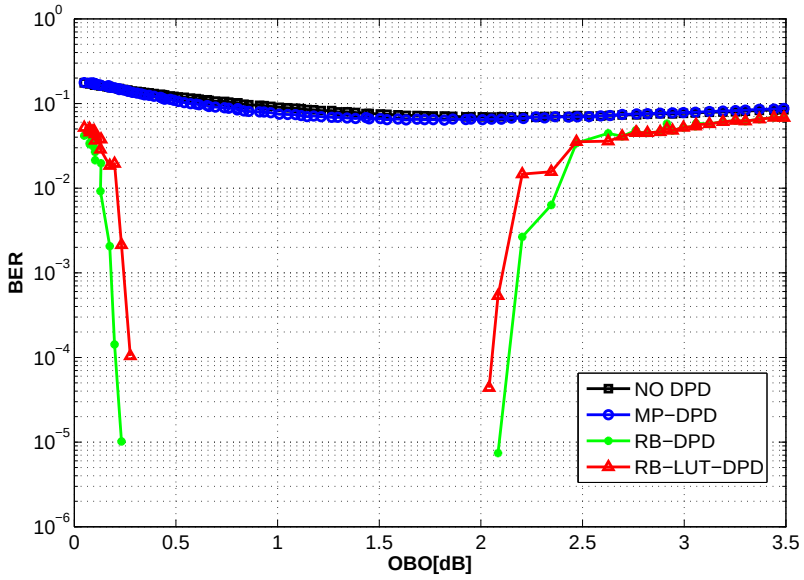

Figure B.4: Impact of OBO on BER of different predistortion techniques

B.1.5 Conclusion and Future work

A novel transmitter based technique for the mitigation of the impairments generated by a non-linear channel was designed. Exploiting the transmission of finite constellation symbols, this method provided significant gain over the most commonly applied predistortion techniques. A reduced complexity implementation yielding a LUT was also provided. Such a LUT based technique is a promising candidate for incorporation in next generation terrestrial as well as satellite systems towards improving power and spectral efficiencies. Future research will target the complexity reduction of the LUT as well as the possible extension to the multicarrier scenario.

Appendix C

C.1 Inter Modulation Distortion Terms

Table C.1: Frequency Centered IMD [1]: (a) Three Carrier Channel In-band Terms, (b) Five Carriers Channel In-band Terms

(A)

$\Omega_{1,3}$	$\Omega_{2,3}$	$\Omega_{3,3}$
[111]	[121]	[131]
[122]	[132]	[221]
[133]	[222]	[232]
[223]	[233]	[333]

(B)

$\Omega_{1,3}$	$\Omega_{2,3}$	$\Omega_{3,3}$	$\Omega_{4,3}$	$\Omega_{5,3}$
[111]	[121]	[131]	[141]	[151]
[122]	[132]	[142]	[152]	[241]
[133]	[143]	[153]	[231]	[252]
[144]	[154]	[221]	[242]	[331]
[155]	[222]	[232]	[253]	[342]
[223]	[233]	[243]	[332]	[353]
[234]	[244]	[254]	[343]	[443]
[245]	[255]	[333]	[354]	[454]
[335]	[334]	[344]	[444]	[555]
[-]	[345]	[355]	[455]	[-]
[-]	[-]	[445]	[-]	[-]

Table C.2: Out-of-band IMD terms with $f_{p_1} + f_{p_2} - f_{p_3} - f_m = \Delta f$ [1]: (a) Three Carrier Channel Terms, (b) Five Carriers Channel Terms

(A)

$\Omega_{1,3}$	$\Omega_{2,3}$	$\Omega_{3,3}$
[121]	[131]	[231]
[132]	[221]	[332]
[222]	[232]	[-]
[233]	[333]	[-]

(B)

$\Omega_{1,3}$	$\Omega_{2,3}$	$\Omega_{3,3}$	$\Omega_{4,3}$	$\Omega_{5,3}$
[121]	[131]	[141]	[151]	[251]
[132]	[142]	[152]	[241]	[341]
[143]	[153]	[231]	[252]	[352]
[154]	[221]	[242]	[331]	[442]
[222]	[232]	[253]	[342]	[453]
[233]	[243]	[332]	[353]	[554]
[244]	[254]	[343]	[443]	[-]
[255]	[333]	[354]	[454]	[-]
[334]	[344]	[444]	[555]	[-]
[345]	[355]	[455]	[-]	[-]
[-]	[445]	[-]	[-]	[-]

Table C.3: Out-of-band IMD terms with $f_{p_1} + f_{p_2} - f_{p_3} - f_m = -\Delta f$ [1]: (a) Three Carrier Channel Terms, (b) Five Carriers Channel Terms

(A)

$\Omega_{1,3}$	$\Omega_{2,3}$	$\Omega_{3,3}$
[112]	[111]	[121]
[123]	[122]	[132]
[-]	[133]	[222]
[-]	[223]	[233]

(B)

$\Omega_{1,3}$	$\Omega_{2,3}$	$\Omega_{3,3}$	$\Omega_{4,3}$	$\Omega_{5,3}$
[112]	[111]	[121]	[131]	[141]
[123]	[122]	[132]	[142]	[152]
[134]	[133]	[143]	[153]	[231]
[145]	[144]	[154]	[221]	[242]
[224]	[155]	[222]	[232]	[253]
[235]	[223]	[233]	[243]	[332]
[-]	[234]	[244]	[254]	[343]
[-]	[245]	[255]	[333]	[354]
[-]	[335]	[334]	[344]	[444]
[-]	[-]	[345]	[355]	[455]
[-]	[-]	[-]	[445]	[-]

Bibliography

[1] B. F. Beidas, "Intermodulation distortion in multicarrier satellite systems: Analysis and turbo Volterra equalization," *IEEE Trans. Commun.*, vol. 59, no. 6, pp. 1580 –1590, June 2011.

[2] "SES." [Online]. Available: http://www.ses.com/4232583/en

[3] "Digital agenda for europe." [Online]. Available: http://ec.europa.eu/digital-agenda/

[4] [Online]. Available: www.viasat.com/files/assets/web/datasheets/ViaSat-1MissionOverviewr3.pdf

[5] M. B. G. Maral, *Satellite Communication Systems : Systems, Techniques and Technologies*. Wiley Eastern, 2009.

[6] E. Casini, R. De Gaudenzi, and A. Ginesi, "DVB- S2 modem algorithms design and performance over typical satellite channels," *Intern. J.on Satellite Commun. and Networking*, vol. 22, pp. 281–318, 2004.

[7] M. Singer, "Economic and social benefits of broadband." [Online]. Available: https://www.google.lu/#q=societal+benefits+of+broadband+connectivity&safe=off

[8] [Online]. Available: www.eutelsat.com/files/contributed/news/media_library/brochures/ka-sat-professional-services.pdf

[9] "Digital video broadcasting (DVB); second generation framing structure, channel coding and modulation systems for broadcasting, interactive services, news gathering and other broadband satellite applications (DVB-S2)," 2012.

[10] "Digital video broadcasting (DVB);second generation framing structure, channel coding and modulation systems for broadcasting, interactive services, news gathering and other broadband satellite applications," 2014.

[11] A. Modenini, G. Colavolpe, and N. Alagha, "How to significantly improve the spectral efficiency of linear modulations through time-frequency packing and advanced processing," in *Communications (ICC), 2012 IEEE International Conference on*, June 2012, pp. 3260–3264.

[12] A. Piemontese, A. Modenini, G. Colavolpe, and N. Alagha, "Improving the spectral efficiency of nonlinear satellite systems through time-frequency packing and advanced receiver processing," *Communications, IEEE Transactions on*, vol. 61, no. 8, pp. 3404–3412, August 2013.

[13] S. Benedetto and E. Biglieri, "Nonlinear equalization of digital satellite channels," *IEEE J. Sel. Areas Commun.*, vol. 1, pp. 57 –62, Jan. 1983.

[14] G. Colavolpe and A. Piemontese, "Novel SISO detection algorithms for nonlinear satellite channels," in *Proc. IEEE Global Telecommun. Conf.e*, Houston, USA, Dec. 2011.

[15] L. Giugno, M. Luise, and V. Lottici, "Adaptive pre and post-compensation of nonlinear distortions for high-level data modulations," *IEEE Trans. Wireless Commun.*, vol. 3, pp. 1490 –1495, 2004.

[16] L. Ding, G. T. Zhou, D. R. Morgan, Z. Ma, J. S. Kenney, J. Kim, and C. R. Giardina, "A robust digital baseband predistorter constructed using memory polynomials," *IEEE Trans. Commun.*, vol. 52, no. 1, pp. 159 – 165, Jan. 2004.

[17] D. Ronnow and M. Isaksson, "Digital predistortion of radio frequency power amplifiers using Kautz-Volterra model," *Electronics Letters*, vol. 42, no. 13, pp. 780 – 782, June 2006.

[18] R. Raich, H. Qian, and G. Zhou, "Orthogonal polynomials for power amplifier modeling and predistorter design," *IEEE Trans. Veh. Technol.*, vol. 53, no. 5, pp. 1468 – 1479, Sept. 2004.

[19] G. Karam and H. Sari, "A data predistortion technique with memory for QAM radio systems," *IEEE Trans. Commun.*, vol. 39, no. 2, pp. 336 –344, Feb 1991.

[20] B. F. Beidas and R. Seshadri, "Analysis and compensation for nonlinear interference of two high-order modulation carriers over satellite link," *IEEE Trans. Commun.*, vol. 58, no. 6, pp. 1824 –1833, June 2010.

[21] S. Bassam, M. Helaoui, and F. Ghannouchi, "2-D digital predistortion (2-D-DPD) architecture for concurrent dual-band transmitters," *Microw. Theory and Techniques, IEEE Trans. on*, vol. 59, no. 10, pp. 2547 –2553, Oct. 2011.

[22] G. E. Corazza, *Digital Satellite Communications, Chapter 8.* Springer, 2007.

[23] A. Saleh, "Frequency-independent and frequency-dependent nonlinear models of TWT amplifiers," *IEEE Trans. Commun.*, vol. COM-29, no. 11, pp. 1715–1720, Nov. 1981.

[24] M. Schetzen, *The Volterra and Wiener Theories of Nonlinear Systems.* John Wiley & Sons, Apr. 1980. [Online]. Available: http://www.worldcat.org/isbn/0471044555

[25] T. J. B. Noel Kelly, Anding Zhu, "Digital predistortion feasibility studies for multicarrier satelite communication systems," in *Proc. 31th AIAA Intern.Commun. Satellite Syst. Conference (ICSSC)*, Florence, Italy, Oct. 2013.

[26] C. Eun and E. Powers, "A new Volterra predistorter based on the indirect learning architecture," *Signal Processing, IEEE Trans. on*, vol. 45, no. 1, pp. 223 –227, Jan 1997.

[27] L. Ding, R. Raich, and G. T. Zhou, "A Hammerstein predistortion linearization design based on the indirect learning architecture," in *Acoustics, Speech, and Signal Processing (ICASSP), 2002 IEEE International Conference on*, vol. 3, May 2002, pp. III–2689 –III–2692.

[28] K. Muhonen, M. Kavehrad, and R. Krishnamoorthy, "Look-up table techniques for adaptive digital predistortion: a development and comparison," *Vehicular Technology, IEEE Transactions on*, vol. 49, no. 5, pp. 1995–2002, Sep 2000.

[29] R. Piazza, E. Zenteno, B. Shankar, D. Ronnow, J. Grotz, F. Zimmer, F. Heckmann, and S. Cioni, "Multicarrier digital pre-distortion/ equalization techniques for non-linear satellite channels," in *Proc. 30th AIAA Intern.Commun. Satellite Syst. Conference (ICSSC)*, Ottawa, Canada, Sep. 2012. [Online]. Available: http://publications.uni.lu/record/10106/files/

[30] R. Piazza, E. Zenteno, B. Shankar, D. Ronnow, K. Liolis, F. Zimmer, F. Berheide, and S. Cioni, "Sensitivity analysis of multicarrier digital predistortion/ equalization techniques for non-linear satellite channels," in *Proc. 31th AIAA Intern.Commun. Satellite Syst. Conference (ICSSC)*, Florence, Italy, Oct. 2013.

[31] R. Piazza, B. Shankar, and B. Ottersten, "Data predistortion for multicarrier satellite channels using orthogonal memory polynomials," in *Signal Processing Advances for Wireless Communications (SPAWC), 2013 IEEE International Workshop on*, June 2013. [Online]. Available: http://orbilu.uni.lu/handle/10993/4861

[32] ——, "Multicarrier LUT-based data predistortion for non-linear satellite channels," in *Communications (ICC), 2013 IEEE International Conference on*, June 2014.

[33] ——, "Multi-gateway data predistortion for non-linear satellite channels," *submitted to Communication, IEEE Transactions on*, July 2014.

[34] S. A. Bassam, W. Chen, M. Helaoui, F. M. Ghannouchi, and Z. Feng, "Linearization of concurrent dual-band power amplifier based on 2D-DPD technique," *IEEE Microw. Wireless Compon. Lett.*, vol. 21, no. 12, pp. 685 –687, Dec. 2011.

[35] C. Sheng, "An efficient predistorter design for compensating nonlinear memory high power amplifiers," *IEEE Trans. Broadcast.*, vol. 57, no. 4, pp. 856 –865, Dec. 2011.

[36] C. Yu, L. Guan, E. Zhu, and A. Zhu, "Band-limited volterra series-based digital predistortion for wideband rf power amplifiers," *Microwave Theory and Techniques, IEEE Transactions on*, vol. 60, no. 12, pp. 4198–4208, Dec 2012.

[37] S. Bassam, M. Helaoui, and F. Ghannouchi, "Crossover digital predistorter for the compensation of crosstalk and nonlinearity in MIMO transmitters," *Microwave Theory and Techniques, IEEE Transactions on*, vol. 57, no. 5, pp. 1119–1128, May 2009.

[38] D. Morgan, Z. Ma, J. Kim, M. Zierdt, and J. Pastalan, "A generalized memory polynomial model for digital predistortion of RF power amplifiers," *Signal Processing, IEEE Transactions on*, vol. 54, no. 10, pp. 3852–3860, Oct 2006.

[39] M. Abi Hussein, V. A. Bohara, and O. Venard, "On the system level convergence of ILA and DLA for digital predistortion," in *Wireless Communication Systems (ISWCS), 2012 International Symposium on*, Aug 2012, pp. 870 –874.

[40] D. Zhou and V. E. DeBrunner, "Novel adaptive nonlinear predistorters based on the direct learning algorithm," *Signal Processing, IEEE Transactions on*, vol. 55, no. 1, pp. 120 –133, Jan. 2007.

[41] R. Piazza, B. Shankar, and B. Ottersten, "Data predistortion for multicarrier satellite channels based on direct learning," *submitted to Signal Processing, IEEE Transactions on*, Oct. 2013.

[42] P. Jardin and G. Baudoin, "Filter lookup table method for power amplifier linearization," *Vehicular Technology, IEEE Transactions on*, vol. 56, no. 3, pp. 1076–1087, May 2007.

[43] B. Ai, Z. Yang, C. Pan, S. Tang, and T. Zhang, "Analysis on LUT based predistortion method for HPA with memory," *Broadcasting, IEEE Transactions on*, vol. 53, no. 1, pp. 127–131, March 2007.

[44] H. Zhi-yong, G. Jian-hua, G. Shu-jian, and W. Gang, "An improved look-up table predistortion technique for HPA with memory effects in OFDM systems," *Broadcasting, IEEE Transactions on*, vol. 52, no. 1, pp. 87–91, March 2006.

[45] S. H. Han and J. H. Lee, "An overview of peak-to-average power ratio reduction techniques for multicarrier transmission," *Wireless Communications, IEEE*, vol. 12, no. 2, pp. 56–65, April 2005.

[46] D. Kim and G. Stuber, "Clipping noise mitigation for OFDM by decision-aided reconstruction," *Communications Letters, IEEE*, vol. 3, no. 1, pp. 4–6, Jan 1999.

[47] O. Gouba and Y. Louet, "Joint study of PAPR reduction and digital predistortion," in *General Assembly and Scientific Symposium, 2011 XXXth URSI*, Aug 2011, pp. 1–4.

[48] C. Nader, P. Landin, W. Van Moer, N. Bjorsell, P. Handel, and D. Ronnow, "Peak-power controlling technique for enhancing digital predistortion of RF power amplifiers," *Microwave Theory and Techniques, IEEE Transactions on*, vol. 60, no. 11, pp. 3571–3581, Nov 2012.

[49] R. Braithwaite, "A combined approach to digital predistortion and crest factor reduction for the linearization of an RF power amplifier," *Microwave Theory and Techniques, IEEE Transactions on*, vol. 61, no. 1, pp. 291–302, Jan 2013.

[50] P. Landin, W. Van Moer, M. Isaksson, and P. Handel, "Peak-power controlled digital predistorters for RF power amplifiers," *Microwave Theory and Techniques, IEEE Transactions on*, vol. 60, no. 11, pp. 3582–3590, Nov 2012.

[51] R. Piazza, B. Shankar, and B. Ottersten, "Generalized direct volterra predistortion with adaptive crest factor reduction control," in *Acoustics, Speech, and Signal Processing (ICASSP), 2015 IEEE International Conference on*.

[52] ——, "Non-parametric data predistortion for non-linear channels with memory," in *Acoustics, Speech, and Signal Processing (ICASSP), 2013 IEEE International Conference on*. [Online]. Available: http://orbilu.uni.lu/handle/10993/4862

[53] G. Colavolpe, A. Modenini, and F. Rusek, "Channel shortening for nonlinear satellite channels," *Communications Letters, IEEE*, vol. 16, no. 12, pp. 1929–1932, December 2012.

[54] S. W. R.D Gitlin, "Fractionally spaced equalization:an improved digital transversal equalizer," *Bell Systems Technical Journal*, Feb 1981.

[55] W. Mattis, "A hybrid fractionally spaced digitally controlled equalizer for satellite systems," in *Communications, Computers and Signal Processing, 1989. Conference Proceeding., IEEE Pacific Rim Conference on*, June 1989, pp. 482–486.

[56] A. Gutierrez and W. Ryan, "Performance of volterra and mlsd receivers for nonlinear band-limited satellite systems," *Communications, IEEE Transactions on*, vol. 48, no. 7, pp. 1171–1177, Jul 2000.

[57] S. Cioni, C. Ernst, A. Ginesi, and G. Colavolpe, "Bandwidth optimization for satellite digital broadcasting scenarios," in *Proc. 31th AIAA Intern.Commun. Satellite Syst. Conference (ICSSC)*, Florence, Italy, Oct. 2013.

[58] R. Piazza, E. Zenteno, B. Shankar, D. Ronnow, K. Liolis, F. Zimmer, F. Berheide, and S. Cioni, "Performance analysis of fractionally spaced equalization in non-linear multicarrier satellite channels," in *Proc. 32th AIAA Intern.Commun. Satellite Syst. Conference (ICSSC)*, San Diego, U.S., 2014.

[59] R. Piazza and R. D. Zenteno, Shankar B., "Low complexity predistortion and equalization in nonlinear multicarrier satellite communications," in *Submitted to EURASIP*.

[60] R. Tibshirani, "Regression shrinkage and selection via the LASSO," *J. R. Statist. Soc. B*, vol. 58, no. 1, pp. 267–288, 1994.

[61] R. Piazza, B. Shankar, and B. Ottersten, "Carrier rate optimization on the return link of interactive mobile satellite networks," in *European Wireless*, Barcelona, Spain, May 2014.

[62] S. Benedetto, E. Biglieri, and R. Daffara, "Modeling and performance evaluation of nonlinear satellite links-a volterra series approach," *Aerospace and Electronic Systems, IEEE Transactions on*, vol. AES-15, no. 4, pp. 494–507, July 1979.

[63] C. Eun and E. Powers, "A new Volterra predistorter based on the indirect learning architecture," *IEEE Trans. Signal Process.*, vol. 45, no. 1, pp. 223 –227, Jan. 1997.

[64] S. M. Kay, *Fundamentals of statistical signal processing: Estimation theory.* Upper Saddle River, NJ, USA: Prentice-Hall, Inc., 1993.

[65] A. Bjorck, "Solving linear least-squares problems by Gram-Schmidt orthogonalization," *BIT Numerical Mathematics*, vol. 7, pp. 1–21, 1967.

[66] V. J. Mathews, *Polynomial Signal Processing.* New York: Wiley, 2000.

[67] M. H. Hayes, *Statistical Digital Signal Processing and Modeling.* New York:Wiley, 1998.

[68] A. Z. N. K. Thomas J. Brazil, Anding Zhu, "Project final report: Advanced digital predistortion techniques for satellite communications," in *ESA Contract No.: 4000106470/12/NL/CBi*, 2014.

[69] G. Z. Christopoulos Dimitrios, S. Chatzinotas and B. Ottersten, "Joint precoding with flexible power constraints in multibeam satellite systems," in *Global Telecommunication Conference (GLOBECOM)*, Houston, Texas, USA, December 2011.

[70] J. Armstrong, "Peak-to-average power reduction for OFDM by repeated clipping and frequency domain filtering," *Electronics Letters*, vol. 38, no. 5, pp. 246–247, Feb 2002.

[71] M. Borkar, F. Mujica, and G. Copeland, "Method and system for calculating the pre-inverse of a nonlinear system," Jun. 8 2010, US Patent 7,733,177. [Online]. Available: http://www.google.com/patents/US7733177

[72] A. Kyrgiazos, B. Evans, P. Thompson, and N. Jeannin, "Gateway diversity scheme for a future broadband satellite system," in *Advanced Satellite Multimedia Systems Conference (ASMS) and 12th Signal Processing for Space Communications Workshop (SPSC), 2012 6th*, 2012, pp. 363–370.

[73] O. Vidal, G. Verelst, J. Lacan, E. Alberty, J. Radzik, and M. Bousquet, "Next generation high throughput satellite system," in *IEEE First AESS European Conference on Satellite Telecommunications (ESTEL*, 2012, pp. 1–7.

[74] D. Mignolo, E. Re, A. Ginesi, A. B. Alamanac, P. Angeletti, and M. Harverson, "Approaching terabit/s satellite: a system analysis," in *17th Ka and Broadband Communications Conference*, Palermo, Italy, 2011.

[75] P.-D. Arapoglou, M. R. B. Shankar, A. Panagopoulos, and B. Ottersten, "Gateway diversity strategies in Q/V band feeder links," in *17th Ka and Broadband Communications Conference, Palermo, Italy*, 2011.

[76] D. Morgan, Z. Ma, and L. Ding, "Reducing measurement noise effects in digital predistortion of rf power amplifiers," in *Communications, 2003. ICC '03. IEEE International Conference on*, vol. 4, May 2003, pp. 2436–2439 vol.4.

[77] A. Katz, R. Gray, and R. Dorval, "Wide/multi-band linearized TWTAs," in *Vacuum Electronics Conference, 2007. IVEC '07. IEEE International*, May 2007, pp. 1–2.

[78] K. Mahesh, J. Whartenby, and H. J. Wolkstein, "Predistortion linearize using GaAs dual-gate MESFET for TWTA and SSPA used in satellite transponders," *Microwave Theory and Techniques, IEEE Transactions on*, vol. 33, no. 12, pp. 1479–1488, Dec 1985.

[79] A. Kondrashov, "Digital predistortion in on-board satellite system power amplifiers," in *Embedded Computing (MECO), 2012 Mediterranean Conference on*, June 2012, pp. 200–203.

[80] S. Chen, "An efficient predistorter design for compensating nonlinear memory high power amplifiers," *Broadcasting, IEEE Transactions on*, vol. 57, no. 4, pp. 856–865, Dec 2011.

[81] "Official U.S. government information about the global positioning system (GPS) and related topics: Timing application." [Online]. Available: http://www.gps.gov/applications/timing/

[82] V. Kekatos and G. Giannakis, "Sparse volterra and polynomial regression models: Recoverability and estimation," *IEEE Trans. Signal Process.*, vol. 59, no. 12, pp. 5907–5920, 2011.

[83] D. Hummels and R. Gitchell, "Equivalent low-pass representations for bandpass volterra systems," *IEEE Trans. Commun.*, vol. 28, no. 1, pp. 140–142, 1980.

[84] M. Isaksson, D. Wisell, and D. Ronnow, "A comparative analysis of behavioral models for rf power amplifiers," *Microwave Theory and Techniques, IEEE Transactions on*, vol. 54, no. 1, pp. 348 –359, jan. 2006.

[85] A. K. Swain and S. A. Billings, "Generalized frequency response function matrix for MIMO non-linear systems," *Int. J. Control*, vol. 74, no. 8, pp. 829–844, 2001.

[86] J. Kim, P. Roblin, D. Chaillot, and Z. Xie, "A generalized architecture for the frequency- selective digital predistortion linearization technique," *IEEE Trans. Microw. Theory Tech.*, vol. 61, no. 1, pp. 596–605, 2013.

[87] P. Stoica, B. Friedlaner, and T. Söderström, "On the parsimony principle," *Int. J. Control*, vol. 36, no. 3, pp. 409–418, 1982.

[88] K. Shi and P. Shi, "Adaptive sparse volterra system identification with ℓ_0-norm penalty," *Signal Processing*, vol. 91, no. 10, pp. 2432 – 2436, 2011.

[89] N. Kalouptsidis, G. Mileounis, B. Babadi, and V. Tarokh, "Adaptive algorithms for sparse system identification," *Signal Processing*, vol. 91, no. 8, pp. 1910 – 1919, 2011.

[90] H. Zou, "The adaptive LASSO and its Oracle properties," *J. Amer. Statist. Assoc.*, vol. 101, no. 476, pp. 1418–1429, 2006.

[91] J. Huang, P. Breheny, and S. Ma, "A selective review of group selection in high-dimensional models," *Statist. Science*, vol. 27, no. 4, pp. 481 –499, Apr. 2012.

[92] M. Aloisio, E. Casini, and A. Ginesi, "Evolution of space traveling-wave tube amplifier requirements and specifications for modern communication satellites," *IEEE Trans. Electron Devices*, vol. 54, no. 7, pp. 1587–1596, 2007.

[93] R. Gallager, "Low density parity-check codes," Ph.D. dissertation, MIT Press, Cambridge MA, 1963.

[94] M. Grant and S. Boyd, "Graph implementations for nonsmooth convex programs," pp. 95–110, 2008.

[95] I. CVX Research, "CVX: Matlab software for disciplined convex programming, version 2.0," Aug 2012.

[96] D. Luenberger, *Microeconomic theory.* New York: McGraw-Hill, 1995.

[97] A. Wächter and L. T. Biegler, "On the implementation of an interior-point filter line-search algorithm for large-scale nonlinear programming," *Mathematical Programming*, vol. 106, no. 1, pp. 25–57, 2006.

[98] "Satellite component of umts (s-umts); family sl satellite radio interface;part 2: Physical layer specifications; sub-part 1: Physical layer interface," in *ETSI TS 102 744-2-1, V0.0.9.*

[99] C. Rapp, "Effects of hpa-nonlinearity on a d-dpsk/ofdm-signal for a digital sound broadcasting system," in *Proceedings of 2nd European Conference on Satellite Communications*, October 1991, pp. 179–184.

[100] D. C. P.-D. A. Z. Abu-Shaban, B. Shankar, "Timing and frequency synchronisation for multiuser detection on the return link of interactive mobile satellite networks," in *Proc. 31th AIAA Intern.Commun. Satellite Syst. Conference (ICSSC)*, Florence, Italy, Oct. 2014.

[101] G. Colavolpe and A. Piemontese, "Novel siso detection algorithms for nonlinear satellite channels," *Wireless Communications Letters, IEEE*, vol. 1, no. 1, pp. 22–25, February 2012.

[102] A. G. G. C. S. Cioni, C. Ernst, "Bandwidth optimization for satellite digital broadcasting," in *Proc. 31th AIAA Intern.Commun. Satellite Syst. Conference (ICSSC)*, Florence, Italy, Oct. 2014.

[103] J. Kim and K. Konstantinou, "Digital predistortion of wideband signals based on power amplifier model with memory," *Electronics Letters*, vol. 37, no. 23, pp. 1417 –1418, Nov 2001.